Tese de Doutorado

Inatel
Instituto Nacional de Telecomunicações

Sistema FiWi 6G Baseado em FSO, RoF e VLC

CELSO HENRIQUE DE SOUZA LOPES

DEZEMBRO/2023

SISTEMA FIWI 6G BASEADO EM FSO, ROF E VLC

CELSO HENRIQUE DE SOUZA LOPES

Tese de Doutorado apresentada ao Instituto Nacional de Telecomunicações (Inatel), como parte dos requisitos para obtenção do título de Doutor em Engenharia de Telecomunicações.

ORIENTADOR: Prof. Dr. Arismar Cerqueira Sodré Junior.

Santa Rita do Sapucaí

2023

Lopes, Celso Henrique de Souza
L864s
Sistema FiWi 6G Baseado em FSO, RoF e VLC / Celso Henrique de Souza Lopes. – Santa Rita do Sapucaí, 2023.
184 p.

Orientadores: Prof. Arismar Cerqueira Sodré Junior.
Tese de Doutorado em Telecomunicações – Instituto Nacional de Telecomunicações – INATEL.
Inclui Bibliografia e anexo.

1. 5G 2. 5G New Radio 3. 6G 4 Ondas Milimétricas 5. Comunicação óptica sem fio 6. Doutorado em Telecomunicações. I. Sodré Junior, Arismar Cerqueira . II. Instituto Nacional de Telecomunicações – INATEL. III. Título.

CDU 621.39

Ficha Catalográfica elaborada pelo Bibliotecário da Instituição
CRB6-2718 – Paulo Eduardo de Almeida

FORMULÁRIO DE APROVAÇÃO

Tese de Doutorado defendida e aprovada em 11/ 12/ 2023, pela comissão julgadora:

Prof. Dr. Arismar Cerqueira Sodré Junior
Instituto Nacional de Telecomunicações (INATEL)

Prof. Dr. Evandro Conforti
Universidade Estadual de Campinas (UNICAMP)

Prof. Dr. Antônio Marcos Alberti
(INATEL)

Prof. Dr. Danilo Henrique Spadoti
Universidade Federal de Itajubá (UNIFEI)

Profa. Dra. Victoria Dala Pegorara Souto
(INATEL)

Coordenador de Pós Graduação (Inatel)
Prof. Dr. José Marcos Camara Brito

“Se caíres sete vezes, levanta-te oito.”

Provérbio Japonês

Dedico este trabalho a minha família.

Agradecimentos

Agradeço imensamente aos meus pais e irmãos pelo apoio incondicional ao longo deste período.

Sou grato ao Professor Arismar por disponibilizar a infraestrutura do laboratório WOCA, que foi fundamental para a implementação prática das minhas ideias.

Também agradeço ao Inatel por fornecer uma excelente infraestrutura que possibilitou a realização deste trabalho.

Meus sinceros agradecimentos aos colegas do laboratório WOCA pelas experiências compartilhadas durante esta etapa da minha vida.

Gostaria de expressar minha gratidão a todas as pessoas que estiveram envolvidas direta e indiretamente na conclusão deste trabalho.

Por fim, gostaria de expressar meu profundo agradecimento ao apoio financeiro da RNP, com recursos do MCTIC, processo No 01245.020548/2021-07, no âmbito do projeto Brasil 6G do Centro de Referência em Radiocomunicações (CRR) do Instituto Nacional de Telecomunicações - Inatel, Brasil, e da Huawei, no âmbito do projeto Formação Avançada em Redes e Sistemas de Telecomunicações. Além disso, também agradeço o apoio financeiro do CNPq, da CAPES, da FINEP, da FAPEMIG e da FAPESP.

Celso Henrique de Souza Lopes

Índice

Lista de Publicações

Os seguintes artigos originais fundamentam esta Tese de Doutorado:

- **[1]: C. H. S. Lopes**, T. P. V. Andrade, L. A. M. Pereira, E. Conforti, and Arismar Cerqueira. S. Jr, " Implementation of HetNet Architectures Based on FSO, VLC, RoF and Photonics RF Generation Towards 6G Applications", *Journal of Optical Communications and Networking* (JOCN), Submetido em 2024.
- **[2]: C. H. de Souza Lopes**, T. P. V. Andrade, L. A. M. Pereira, A. Bogoni, E. Conforti and A. C. Sodré, "Implementation of a Hybrid FiWi System Using FSO, VLC and mm-Waves Toward 6G Applications", in IEEE Photonics Technology Letters, vol. 35, no. 24, pp. 1403-1406, 15 Dec.15, 2023, doi: 10.1109/LPT.2023.3327210.
- **[3]: C. H. S. Lopes**, L. C. Souza, T. P. V. Andrade, E. Conforti and A. C. S.,"60-GHz 5G-NR Optical Fronthauls Based on CS-DSB Technique,"2023 International Conference on Optical MEMS and Nanophotonics (OMN) and SBFoton International Optics and Photonics Conference (SBFoton IOPC), Campinas, Brazil, 2023, pp. 01-02, doi: 10.1109/OMN/SBFotonIOPC58971.2023.10230932.
- **[4]: C. H. S. Lopes;** L. A. M. Pereira ; T. P. Villena ; E. Conforti ; Arismar Cerqueira S. Jr. " Implementação de um Sistema Híbrido FiWi utilizando FSO, VLC e Ondas Milimétricas para Aplicações 6G. In: Simpósio Brasileiro de Telecomunicações, 2023, São José dos Campos. Anais do SBrT 2023, 2023.

Outros artigos publicados durante o período do Doutorado:

- [5] H. R. D. Filgueiras, E. S. Lima, M. S. B. Cunha, **C. H. S. Lopes**, L. C. de Souza, R. M. Borges, L. A. M. Pereira, T. H. Brandao, T. P. V. Andrade, L. C. Alexandre, G. Neto, A. Linhares, L. L. Mendes, M. A. Romero and Arismar Cerqueira S. Jr., "Wireless and Optical Convergent Access Technologies Toward 6G," IEEE Access, vol. 11, pp. 9232-9259, 2023, doi: 10.1109/ACCESS.2023.3239807.
- [6] L. C. Souza, **C.H. S. Lopes**, R. C. C. Santos, A. C. S. Júnior and Luciano Leonel.,"A Study on Propagation Models for 60 GHz Signals in Indoor Environments" Frontiers in Communications and Networks, vol. 2, 2022
- [7] **C. H. d. S. Lopes** et al., " Non-Standalone 5G NR Fiber-Wireless System Using FSO and Fiber-Optics Fronthauls", in Journal of Lightwave Technology, vol. 39, no. 2, pp. 406-417, 15 Jan.15, 2021, doi: 10.1109/JLT.2020.3029500.
- [8] Borges, R.M.; **de Souza Lopes, C.H.**; Lima, E.S.; de Oliveira, M.A.; Cunha, M.S.B.; Alexandre, L.C.; da Silva, L.G.; Pereira, L.A.M.; Spadoti, D.H.; Romero, M.A.; et al. "Integrating Optical and Wireless Techniques towards Novel Fronthaul and Access Architectures in a 5G NR Framework". Appl. Sci. 2021, 11, 5048. https://doi.org/10.3390/app11115048
- [9] L.A.M. Pereira, **C.H.S. Lopes**, R.M. Borges, E.S. Lima, A.C. Ferreira, M. Abreu, L.L. Mendes, Arismar Cerqueira S., "Implementation of a multiband 5G NR fiber-wireless system using analog radio over fiber technology", Optics Communications, Volume 474, 2020, https://doi.org/10.1016/j.optcom.2020.126112.
- [10] **C. H. de Souza Lopes**, E. S. Lima, L. A. Melo Pereira and A. C. Sodré, "Peaceful Coexistence Between 5G NR and LTE-A Over a RoF-Based Fronthaul,"2021 SBFoton International Optics and Photonics Conference (SBFoton IOPC), Sao Carlos, Brazil, 2021, pp. 1-4, doi: 10.1109/SBFotonIOPC50774.2021.9461959.
- [11] **C. H. de Souza Lopes**, E. Saia Lima and A. C. Sodré Junior, "RoF/FSO-based Fronthaul for 5G Systems and Beyond,"2021 SBMO/IEEE MTT-S International Microwave and Optoelectronics Conference (IMOC), Fortaleza, Brazil,

2021, pp. 1-3, doi: 10.1109/IMOC53012.2021.9624921.

- [12] **LOPES, C.H.S.**; LIMA, E.S. ; CERQUEIRA S., ARISMAR ; MENDES, L.L. . "Sistema Híbrido RoF/FSO para Redes 5G. In: 19º SBMO - Simpósio Brasileiro de Micro-ondas e Optoeletrônica e 14º CBMAG - Congresso Brasileiro de Eletromagnetismo (MOMAG), 2020, Niterói. MOMAG, 2020.
- [13] **C.H.S.Lopes**; LIMA, E.S. ; CERQUEIRA S., ARISMAR ; MENDES, L.L. " Coexistência entre LTE-A e 5G NR em Fronthaul Móvel". In: 19º SBMO - Simpósio Brasileiro de Micro-ondas e Optoeletrônica e 14º CBMAG - Congresso Brasileiro de Eletromagnetismo (MOMAG), 2020, Niterói. MOMAG, 2020.
- [14] **LOPES, C.H.S.**; PEREIRA, L.A.M. ; CERQUEIRA S., ARISMAR. " Coexistência entre 5G NR e LTE-A em Sistemas Fiber/Wireless". In: Simpósio Brasileiro de Telecomunicações e Processamento de Sinais (SBrT), 2020, Florianópolis. SBrT, 2020.

Premiações:

Lista de Figuras

Lista de Abreviações e Acrônimos

3GPP	3rd Generation Partnership Project
5G	fifth generation of mobile network
5G NR	5G New Radio
6G	sixth generation of mobile network
A-RoF	analog radio over fiber
ADC	analog-to-digital conversion
BBU	baseband unit
BPF	band-pass filter
C-RAN	centralized radio access network
CA	carrier aggregation
CAPEX	capital expenditure
CD	chromatic dispersion
CMOS	complementary metal–oxide–semiconductor
CO	central office
CP-OFDM	cyclic prefix based orthogonal frequency division multiplex
CPE	common phase error
CPRI	common public radio interface
CW	continuous wave
D-RAN	distributed radio access network
D-RoF	digital radio over fiber

DAC	digital-to-analog conversion
DBR-LD	distributed Bragg reflector laser
DD-MZM	dual-drive Mach Zehnder modulator
DFB	distributed feedback
DMRS	demodulation reference signal
DWDM	dense wavelength division multiplexing
E/O	electrical-to-optical
eCPRI	enhanced common public radio interface
EDFA	Erbium-doped fiber amplifier
eMBB	enhanced mobile broadband
EPC	evolved packet core
ERB	estação radio base
ESA	electrical spectrum analyzer
EVM	error vector magnitude
EVM_{RMS}	root mean square error vector magnitude
FiWi	fiber-wireless
FR	frequency range
FSO	free-space optics
FWM	four-wave mixing
GPIO	general purpose input/output
HetNet	heterogeneous network
HNLF	highly nonlinear fiber
IIoT	industrial Internet of things
IMT	International Mobile Telecommunications
IMWP	integrated microwave photonics
Inatel	National Institute of Telecommunications

InP	Indium Phosphide
ITU	International Telecommunication Union
KPI	key performance indicators
LD	laser diode
LIDAR	light detection and ranging
LTE	long-term evolution
MATP	maximum transmission point
MITP	minimum transmission point
MLL	mode-locked laser
mm-wave	millimeter-wave
MMI	multimode interference
mMIMO	massive multiple input multiple output
mMTC	massive machine-type communications
MWP	microwave photonics
MWT	multi-wavelength transmitter
MZM	Mach Zehnder modulator
NSA	non-standalone
O/E	optical-to-electrical
OBSAI	open base station architecture initiative
OFC	optical frequency comb
OFDM	orthogonal frequency-division multiplexing
OFM	optical frequency multiplication
OIL	optical injection locking
OIPLL	optical injection phase-lock loop
OOK	on–off keying
OPEX	operational expenditure

OPLL	optical phase-lock loop
ORI	open radio equipment interface
OSA	optical spectrum analyzer
OSNR	optical signal-to-noise ratio
PBCH	physical broadcast channel
PCB	printed circuit board
PCF	photonic-crystal fiber
PD	photodetector
PDSCH	physical data shared channel
PIC	photonic integrated circuits
PM	phase modulator
PS	phase shifter
PSS	primary synchronization signals
PTRS	phase tracking reference signal
QAM	quadrature amplitude modulation
QP	quadrature point
QPSK	quadrature phase-shift keying
RAN	radio access network
RB	resource block
RBW	resolution bandwidth
RF	radiofrequency
RoF	radio over fiber
RRU	remote radio unit
SA	standalone
SCS	subcarrier spacing
SD-MZM	single-drive Mach Zehnder modulator

SDN	software-defined networks
SFDR	spurious-free dynamic range
SFP	small form-factor pluggable transceiver
SMF	single-mode fiber
SMSR	side-mode suppression ratio
SNR	signal-to-noise ratio
SOA	semiconductor optical amplifier
SOFCG	self-oscillating optical frequency comb generator
SSC	spot-size converter
SSS	secondary synchronization signals
SWaPC	size, weight and power consumption, and cost
URLLC	ultra-reliable and low-latency communications
V2X	vehicle to everything
VBW	video bandwidth

Resumo

Este trabalho apresenta soluções de arquiteturas híbridas de redes ópticas para serem empregadas em redes sem fio de quinta (5G, *fifth-generation*) e sexta (6G, *sixth-generation*) geração. Ao adotar o padrão 5G *New Radio* (NR), juntamente com técnicas fotônicas para multiplicação de frequência, infraestrutura de fibra óptica, comunicações em faixas de ondas milimétricas, transmissão óptica em espaço livre (FSO, *free space optics*) e comunicação através de luz visível (VLC, *visible light communication*), conseguimos efetuar uma implementação experimental da referida proposta de rede e avaliamos o desempenho das arquiteturas com base nas especificações da versão 18 do 3GPP (*3rd Generation Partnership Project*).

A primeira contribuição consiste na aplicação da técnica fotônica (CS-DSB, *carrier supressed double side band*) em sistemas de rede passiva com multiplexação por divisão de comprimento de onda (WDM-PON, *wavelength-division multiplexing passive optical network*) para a transmissão de sinais 5G NR na frequência de 60 GHz. Através do uso de moduladores eletro-ópticos em cascata, foi possível gerar e transmitir o sinal 5G NR na banda V, proposta pela versão 18 do 3GPP, atingindo uma vazão de dados de 11,8 Gbit/s.

A segunda contribuição aborda um sistema híbrido que combina rádio analógico sobre fibra (A-RoF, *analog radio over fiber*) e FSO para aprimorar o *fronthaul* da rede, enquanto que uma proposta de acesso duplo que utiliza comunicações por VLC e ondas milimétricas foi implementada. Essa arquitetura foi concebida para satisfazer as demandas de comunicações móvel tanto em ambientes internos quanto externos, com capacidade de alcançar velocidades de até 4,92 Gbit/s.

Em síntese, este estudo ilustra a enorme potencialidade das redes ópticas híbridas

na amplificação da comunicação sem fio em redes celulares de última geração. As contribuições oferecidas não somente demonstram a viabilidade dessas abordagens, mas também prometem aplicabilidade em uma diversidade de cenários, abrangendo ambientes *indoor* e *outdoor*.

***Palavras Chave*:** 5G, 5G *New Radio*, 6G, Ondas Milimétricas, *Comunicação óptica sem Fio*, FSO e VLC.

Abstract

This work presents solutions of hybrid optical network architectures to be employed in fifth (5G, *fifth-generation*) and sixth (6G, *sixth-generation*) generation wireless networks. By adopting the 5G New Radio (NR) standard, along with photonic techniques for frequency multiplication, optical fiber infrastructure, millimeter wave communications, free-space optical transmission (FSO), and visible light communication (VLC), we were able to experimentally implement the proposed network and evaluate the performance of the architectures based on the specifications of the 3rd Generation Partnership Project (3GPP) Release 18.

The first contribution consists of applying the photonic technique (CS-DSB, *carrier suppressed double side band*) in passive network systems with wavelength-division multiplexing (WDM-PON, *wavelength-division multiplexing passive optical network*) for transmitting 5G NR signals at a frequency of 60 GHz. Through the use of cascaded electro-optic modulators, it was possible to generate and transmit the 5G NR signal in the V band, proposed by 3GPP Release 18, achieving a data throughput of 11.8 Gbit/s.

The second contribution addresses a hybrid system that combines analog radio over fiber (A-RoF) and FSO to enhance the fronthaul of the network, while a dual access proposal using VLC and millimeter waves was implemented. This architecture was designed to meet the demands of mobile communications in both indoor and outdoor environments, with the ability to achieve speeds of up to 4.92 Gbit/s.

In summary, this study illustrates the enormous potential of hybrid optical networks in amplifying wireless communication in state-of-the-art cellular networks. The contributions offered not only demonstrate the feasibility of these approaches but also promise applicability in a variety of scenarios, covering indoor and outdoor environ-

ments.

***Keyords*:** 5G, 5G *New Radio*, 6G, Millimeter Wave, *Optical Wireless Communication*, FSO e VLC.

Capítulo 1

Introdução

Este capítulo fornece uma visão geral da pesquisa acadêmica realizada. A Seção 1.1 apresenta o contexto e a motivação por trás do desenvolvimento deste trabalho. A Seção 1.2 aborda a revisão bibliográfica sobre o tema de estudo, enquanto a Seção 1.3 destaca o objetivo principal e as contribuições do trabalho.

1.1 Contextualização e Motivação

Ao longo da história, os seres humanos evoluíram e aprimoraram técnicas de transmissão de informações por diferentes meios. Jornais, televisão, telégrafo ou sinais de fumaça são alguns exemplos de métodos para transmitir informações [1]. Mais especificamente, as tecnologias de telecomunicação desempenham e têm desempenhado um papel fundamental na evolução da humanidade [2]. No meio do século XX, a era da informação teve início com o desenvolvimento do transistor, permitindo a digitalização da informação [3]. Dessa forma, a informação pode ser transmitida de maneira eficiente, replicável e segura por meio da rede. Como resultado, a globalização acelerou drasticamente, induzindo alguns dos crescimentos tecnológicos e econômicos mais rápidos da história humana [2].

Na década de 1980, as comunicações móveis começaram com a implantação da primeira geração (1G, *first generation*). No entanto, os serviços de 1G eram acessíveis apenas a alguns nichos de mercado [4]. Com as gerações seguintes de redes móveis,

2G, 3G e 4G ou *Long-Term Evolution* (LTE), os serviços móveis se tornaram mais acessíveis e, portanto, contribuíram para um impacto significativo na sociedade, cultura, economia, meio ambiente e indústria [5, 6]. Por exemplo, em 2018, mais de 3,6 bilhões de dispositivos móveis conectados à rede LTE foram registrados em todo o mundo, seguindo o crescimento exponencial da última década [7]. Esse aumento drástico anual no número de dispositivos conectados à rede móvel impulsiona o rápido crescimento do tráfego de dados móveis [7]. Por esse motivo, é crucial atualizar e aprimorar constantemente a rede móvel, sendo a quinta geração de redes móveis (5G, *fifth-generation of mobile networks*) a geração atualmente sendo implantada e o (6G, *sixth-generation of mobile networks*) que está em fase de pesquisa e desenvolvimento.

O setor de radiocomunicações da união internacional de telecomunicações (ITU-R, *international telecommunication union radiocommunication sector*) identificou três principais cenários para o 5G, de acordo com o *international mobile telecommunications*-2020 (IMT). Esses cenários são [8, 9]:

- Comunicação de banda larga móvel aprimorada (eMBB, *enhanced mobile broadband*): esse cenário tem como objetivo aumentar as taxas de dados para os usuários finais, proporcionando uma experiência de banda larga móvel mais rápida e eficiente.
- Comunicação massiva do tipo máquina (mMTC, *massive machine-type communications*): esse cenário visa conectar um grande número de dispositivos à rede central. Ele é projetado para atender às necessidades de comunicação de dispositivos IoT e outras aplicações que exigem conectividade em larga escala.
- Comunicação ultra-confiável de baixa latência (URLLC, *ultra-reliable and low-latency communications*): este cenário tem como objetivo reduzir o tempo de resposta da rede, garantindo uma comunicação extremamente confiável e de baixa latência. É adequado para aplicações que exigem alta confiabilidade e tempo de resposta rápido, como comunicações críticas, saúde digital e automação industrial.

Esses diferentes cenários impõem requisitos rigorosos, contrastantes e desafiadores na camada física (PHY, *physical layer*) da rede 5G. A camada PHY precisa ser flexível

o suficiente para atender aos requisitos específicos de cada cenário de uso definido, garantindo o desempenho e a eficiência necessários para cada tipo de comunicação. Soluções técnicas como o novo padrão de rádio 5G (5G NR, *new radio*), utilização de espectro na faixa de ondas milimétricas (mm-wave, *millimeter waves*), RANs heterogêneas e centralizadas (C-RAN, *centralized*-RAN) e comunicação óptica sem fio (OWC, *optical wireless communication*) estão sendo propostas e implementadas para atender as demandas iminentes dos cenários citados [10, 11].

No que diz respeito ao espectro de frequências, o projeto de parceria da terceira geração (3GPP, 3rd *Generation Partnership Project*) definiu duas faixas de frequências (FR, *frequency range*) [12] para o padrão 5G NR. A primeira faixa de frequência (FR1) abrange de 0,410 a 7,125 GHz, suportando largura de banda (BW, *bandwidht*) de até 100 MHz. A segunda faixa de frequência (FR2-1) cobre ondas milimétricas (mm-waves) na faixa de 24,5 a 52,6 GHz, com BW de até 400 MHz. Por fim, a terceira faixa de frequência (FR2-2) abrange frequências de 52,6 a 71 GHz, proporcionando BW de até 2 GHz. No entanto, sabe-se que o método convencional de geração e distribuição de frequências na faixa de ondas milimétricas é complexo e apresenta desafios, especialmente quando se trabalha no domínio elétrico. Isso muitas vezes pode não ser economicamente viável devido à necessidade de componentes elétricos de alta velocidade, o que acaba limitando a velocidade geral alcançável dos sinais de ondas milimétricas gerados [13, 14].

Nesse contexto, a fotônica de micro-ondas (MWP, *microwave photonics*) desempenha um papel importante no suporte às novas gerações de tecnologia sem fio, permitindo a convergência óptico-sem fio desejada e oferecendo soluções atrativas para geração e distribuição de ondas milimétricas por meio de tecnologia óptica [15, 16]. O transporte eficiente de sinais de ondas milimétricas em links de fibra óptica é realizado usando a tecnologia de rádio sobre fibra (RoF, *radio over fiber*), que é considerada uma abordagem promissora para alcançar a convergência óptico-sem fio em redes 5G e 6G. Essa abordagem simplifica o controle, gerenciamento e compartilhamento de recursos [17].

Basicamente, os enlaces *fronthaul* ópticos baseados na tecnologia RoF são utiliza-

dos para transportar sinais digitais ou analógicos, conhecidos como rádio digital sobre fibra (D-RoF, *digital radio over fiber*) e rádio analógico sobre fibra (A-RoF, *analog radio over fiber*), respectivamente [18, 19]. Os esquemas D-RoF digitalizam sinais analógicos para transmiti-los pelo link óptico, enquanto os esquemas A-RoF transmitem sinais de rádio frequência (RF, *radio frequency*) diretamente através da fibra óptica, ou seja, a distribuição ocorre na própria frequência do canal. Uma solução híbrida combina D-RoF e A-RoF para aproveitar as vantagens de ambas as técnicas em um único sistema [20]. Por outro lado, a tecnologia de comunicação baseado em óptica de espaço livre (FSO, *free space optics*) têm demonstrado potencial como uma alternativa para a rede de transporte de ondas milimétricas. Os links FSO podem oferecer um desempenho semelhante ao da fibra óptica. No entanto, é importante destacar que fenômenos atmosféricos como chuva, neblina e poeira podem afetar negativamente a qualidade do link óptico [21, 22]. Para lidar com esses desafios, os enlaces FSO têm sido implementados em conjunto com enlaces de RF como *backup* e combinados com a tecnologia RoF. Isso permite ter um link duplo e/ou aplicações de última milha quando há restrições para a instalação de fibras ópticas. Assim, é possível alcançar um sistema mais flexível [23].

Quando se trata de técnicas baseadas em fotônica para gerar ondas milimétricas, o principal método para gerar sinais elétricos de forma óptica é a detecção heteródina. Essa técnica requer uma alta correlação de fase entre as portadoras ópticas para produzir sinais com baixo ruído de fase. A detecção heteródina explora a interferência de duas portadoras ópticas no fotodetector (PD, *photodetector*), resultando em um sinal elétrico com frequência igual à diferença de frequência entre as duas portadoras originais [16]. No entanto, embora essa técnica seja relativamente simples, o uso de portadoras ópticas não correlacionadas em fase resulta em sinais de RF com ruído de fase proibitivamente alto. Por essa razão, são necessárias técnicas e dispositivos adicionais para garantir a correlação de fase e, assim, gerar sinais de ondas milimétricas com baixo ruído de fase usando a abordagem heteródina. Alguns desses dispositivos incluem a (OIL, *optical injection locking*) [25], o (OPLL, *optical phase lock loop*) [26] e o (OIPLL, *optical injection phase-lock loop*) [27]. Esses dispositivos adicionais são utilizados para garantir a correlação de fase necessária e, assim, obter sinais de ondas

milimétricas com baixo ruído de fase.

Uma segunda metodologia para gerar sinais ópticos refere-se à multiplicação de frequência óptica (OFM, *optical frequency multiplication*), geralmente baseada em técnicas de modulação externa. Nesse caso, a correlação de fase entre as portadoras, mais especificamente, as modulações das bandas laterais, é assegurada durante o processo de conversão elétrico-óptico (E/O). Essa estratégia utiliza um fator de multiplicação de frequência, como 2, 4, 6, 8, 10 ou 12, dependendo da configuração aplicada [28, 29], para realizar a conversão de RF para ondas milimétricas.

A configuração típica é composta por moduladores eletro-ópticos em cascata, polarizados em pontos de operação distintos, como o ponto mínimo de transmissão (MITP, *minimum point*) e o ponto máximo de transmissão (MATP, *maximum transmission point*), dependendo do fator de multiplicação desejado. Com a OFM, é possível alcançar alta pureza espectral e baixo ruído de fase, porém o número de elementos em cascata aumenta à medida que o fator de multiplicação aumenta [30].

Com o avanço da tecnologia em direção ao 6G, a densificação de células torna-se necessária. Se o objetivo for alcançar taxa de dados ultra-rápidos uma possível solução é dividir uma macrocélula em zonas menores possibilitando assim a reutilização espacial dos recursos de rádio [38]. No entanto, a implantação densa de células pequenas representa desafios em termos de custos de instalação e consumo de energia, que geralmente representam uma preocupação principal dos operadores de redes móveis (MNOs, *mobile network operators*) [38, 39]. Neste contexto, a arquitetura C-RAN surge como proposta para atender economicamente a densificação das RANs, onde as funcionalidades avançadas de processamento de sinal será realizada em uma unidade centralizada (CU, *central unit*) com objetivo de atender as várias unidades de rádio remotas (RRUs, *remote radio units*) [38]. No C-RAN, a CU pode conectar a RRU usando um link físico conhecido como *fronthaul* (FH), ou empregando um *midhaul* (MH) óptico até uma unidade de distribuição (DU, *distribution unit*) seguida pelo FH, que pode ser óptico ou sem fio. As redes de transporte *fronthaul* e *midhaul* compõem então a interface fronthaul de próxima geração (NGFI, *next generation fronthaul interface*), na qual a estação base 5G também é chamada de gNodeB e pode incluir

entidades RRU, DU e CU [39].

O NGFI faz parte da visão 5G X-haul, conforme ilustrado na Fig 1.1. Ele integra as funções de *backhaul* (BH) e *fronthaul* em uma arquitetura física comum, proporcionando suporte para transporte e acesso, bem como flexibilidade na divisão funcional [39, 40]. Isso significa que o 5G pode se beneficiar de uma comunicação rápida entre as unidades de banda base que estão co-localizadas, resultando em um gerenciamento eficiente e economia de energia, custos de implantação viáveis, escalabilidade e tempo de implantação ágil. Vale ressaltar que tanto o RoF quanto o FSO têm sido reconhecidos como promissores para a implantação dos *fronthauls* ópticos na tecnologia 5G.

Na rede 6G, espera-se que surjam novos cenários de utilização, abrangendo telepresença, comunicação onipresente, utilização de robôs em diferentes áreas do cotidiano, biossensores e potenciais aplicações ainda não identificadas [41]. Dentre algumas soluções técnicas que estão sendo propostas para o 6G incluem: o uso de comunicações na faixa de Terahertz (THz), inteligência artificial e aprendizado de máquina para atender redes autônomas e superfícies refletoras inteligentes [41, 42].

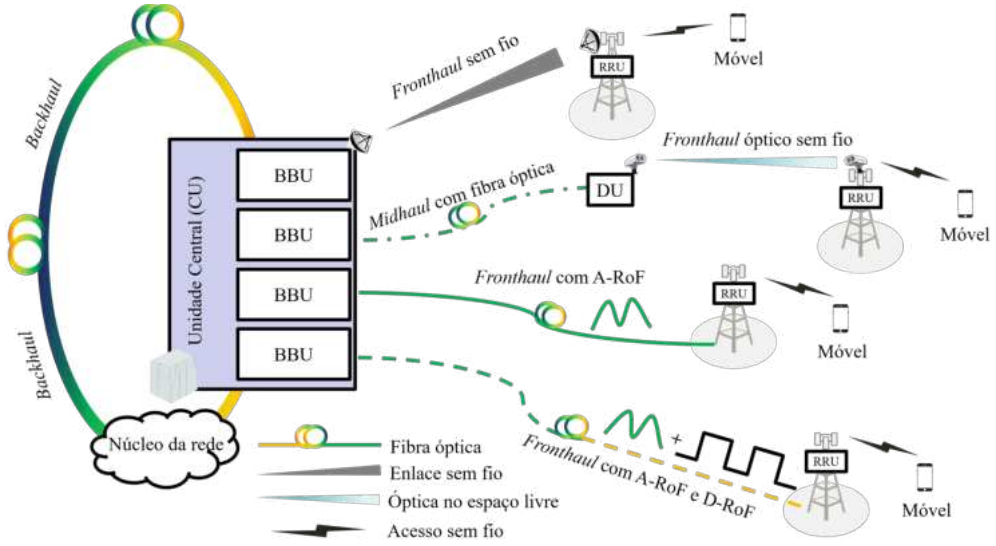

Figura 1.1: *Rede de acesso de rádio centralizada, apta a suportar transporte e acesso de dados em uma arquitetura chamada Xhaul.*

1.2 Revisão da Literatura

A academia e a indústria têm atuado intensamente nos últimos anos no desenvolvimento de soluções que atendam as redes 5G. Diversas abordagens baseadas na utilização de técnicas fotônicas para geração de ondas milimétricas têm sido propostas para atender aos requisitos dos cenários propostos. Em [43], por exemplo, demonstrou-se experimentalmente duas abordagens distintas para gerar sinais na frequência de 60,25 GHz. Aplicando dois estágios de modulação externa em cascata e utilizando variações das técnicas OSSB e CS-DSB, transmitiu-se o sinal em um *fronthaul* baseado em A-RoF para aplicações 5G. Foi relatado em [44] a integração e avaliação de desempenho experimental de um transceptor 5G baseado em multiplexação por divisão de frequência generalizada (GFDM, *generalized frequency division multiplexing*) em uma rede GPON. Enquanto que em [45] foi demonstrado que a utilização de técnicas como a geração de pente de frequência autooscilante (SOFCG, *selfoscillating frequency comb generation*) para geração de ondas milimétricas em sistemas RoF é uma solução atraente em termos de baixo ruído de fase do sinal. Com objetivo de avaliar o desempenho das técnicas DSB e CS-DSB, duas configurações experimentais utilizando um *link* hibrido de fibra óptica e FSO para atender aplicações que operam na banda de 25 GHz foram demonstradas em [46]. A avaliação de desempenho experimental de um sistema FiWi baseado em processamento digital de sinais foi aplicado para transmissão de sinais 5G com objetivo de atender aplicações eMBB. A solução de *fronthaul* proposta emprega uma infraestrutura WDM-PON, para permitir a operação em diferentes faixas de frequência [47]. Em [48], os autores propuseram uma solução baseada na técnica DSB para transmitir sinais M-QAM na frequência de 60 GHz. No entanto, a distância do *fronthaul* óptico foi limitada a 1 km, o que pode ser considerado relativamente curto para *fronthauls* ópticos aplicados em redes 5G.

Esquemas de geração de ondas milimétricas utilizando a técnica CS-DSB para configurações locais e remotos da rede são avaliados teórica e validados experimentalmente [49]. Com objetivo de comparar ambas as abordagens para implantações práticas, experimentos foram realizados e a configuração remota demonstrou um desempenho superior em ambas avaliações para *links* ópticos de até 25 km. Lopes *et.*

al [50] relatam a implementação e investigação experimental de duas arquiteturas de rede para aplicações 5G NR. Com o objetivo de atender às demandas 5G a primeira implementação aplica modulação e detecção direta para transmissão de sinais 4G e 5G em um *link* FiWi. A segunda arquitetura proposta baseia-se em uma nova e eficiente rede óptica heterogênea 5G utilizando fibra óptica e FSO para compor o transporte da rede, enquanto que, o acesso é realizado por um link sem fio de 10 m. Em [51], a transmissão de sinais 5G NR foi investigada utilizando as técnicas DSB e CS-DSB em um link híbrido combinando A-RoF e FSO. Já em [52] o impacto da distorção harmônica e de intermodulação foi avaliado na recepção de um sinal em 40 GHz gerado utilizando a técnica CS-DSB. Shiet et.al [53] propuseram um *link* RoF baseado nas técnicas DSB e OSSB para transmissão de sinais 5G na frequência de 3.5 GHz e 28 GHz respectivamente.

Com objetivo de atender aplicações 5G que exigem o uso intensivo de largura de banda, uma arquitetura FiWi é proposta em [55]. Esta solução suporta a coexistência de links digitais e analógicos na mesma arquitetura de rede. Os autores em [55] implementaram uma solução de *fronthaul* baseado em FSO para aplicações *Ethernet full-duplex*. Uma demonstração experimental utilizando a técnica OFC para geração de sinais de ondas milimétricas 5G NR foi apresentada em [56]. A abordagem proposta emprega um filtro passa-faixa elétrico para isolar o ruído de fase da portadora em 26 GHz, aumentando assim a eficiência espectral do sistema. O trabalho relatado em [57] descreve a implementação de uma prova de conceito em um *link* A-RoF com *fronthaul* de 12,5 km seguido por um *link* de VLC de 1,2 m para aplicações internas. A prova de conceito inicial alcançou uma taxa de transferência de dados de 60 Mbit/s. Por fim em [58], uma transmissão de vídeo 4K a 60 GHz foi demonstrada usando a tecnologia FiWi em uma infraestrutura de rede de transporte X-Haul. A Tabela 1.1 fornece um resumo dos trabalhos implementados experimentalmente abordando as demandas emergentes de 5G e 6G.

A partir desta revisão bibliográfica foi possível identificar algumas áreas chaves de estudo referentes a implementação de novas soluções para atender demandas do pós 5G. Desta forma, soluções que utilizam técnicas fotônicas para geração de ondas milimétricas aplicadas a tecnologia A-RoF e soluções híbridas utilizando FSO e VLC

Tabela 1.1: Estado-da-arte em arquiteturas de redes para sistemas 5G e 6G.

[Ref] Ano	Tecnologia Utilizada	Aplicação ou Arquitetura	Frequência Transmitida	Técnica Fotônica	Vazão de dados
[43] 2017	A-RoF	Fronthaul	60,25 GHz	CS-DSB OSSB	5 Gbit/s
[44] 2018	A-RoF	GPON	735 MHz 26 GHz	DSB	1,1 Gbit/s
[45] 2018	A-RoF	Fronthaul	94,8 GHz	SOFCG	120 Mbit/s
[46] 2019	A-RoF FSO	WDM	25 GHz	CS-DSB	300 Mbit/s
[47] 2020	FiWi	WDM-PON	788 MHz 3,5 e 26 GHz	DSB	4,41 Gbit/s
[48] 2020	A-RoF	GPON	60 GHz	DSB	1,4 Gbit/s
[49] 2021	A-RoF	Fronthaul	40 GHz	CS-DSB	500 Mbit/s
[50] 2021	FiWi FSO	Fronthaul	788 MHz 3,5 e 26 GHz	DSB	3 Gbit/s
[51] 2021	A-RoF FSO	Fronthaul	3,5 GHz 27 e 39 GHz	DSB CS-DSB	1,4 Gbit/s
[52] 2022	A-RoF	Fronthaul	40 GHz	CS-DSB	100 Mbit/s
[53] 2022	A-RoF	Fronthaul	3,5 e 28 GHz	DSB OSSB	240 Mbit/s
[54] 2022	D-RoF A-RoF	WDM-PON	10 e 60 GHz	DSB	40 Gbit/s
[55] 2022	D-RoF FSO	GPON	Baseband	DSB	600 Mbit/s
[56] 2022	FiWi FSO	X-HAUL	26 GHz	E/O OFC	4 Gbit/s
[57] 2023	A-RoF VLC	Fronthaul	25 MHz	DSB	60 Mbit/s
[58] 2023	FiWi	X-HAUL	1,5 and 60 GHz	DSB	408 Mbit/s
Este Trabalho	**A-RoF FiWi FSO VLC**	**WDM-PON X-Haul**	**Baseband 550 MHz 39 GHz 60 GHz**	**CS-DSB DSB**	**4,92 Gbit/s 11,8 Gbit/s**

foram investigadas e propostas para atender diferentes cenários.

1.3 Objetivo e Contribuições da Pesquisa

Esta pesquisa tem como objetivo apresentar soluções ópticas para aplicar em arquiteturas de redes propostas para atender redes 5G e 6G. Para isso, realizamos demonstrações experimentais abordando técnicas fotônicas para a geração e transmissão de sinais 5G NR em ondas milimétricas, seguindo o conceito C-RAN. Exploramos a capilaridade da rede PON como meio de transporte para diversos sinais de RF. Além disso,

utilizamos soluções baseadas em RoF e FSO para a camada de transporte da rede, assim como *links* VLC para o acesso. As principais contribuições deste trabalho são:

- Utilização da técnica fotônica CS-DSB para gerar um sinal padrão 5G NR em 60 GHz com largura de banda de 400 MHz;
- Implementar um *link* A-RoF para transmissão do sinal 5G NR em 60 GHz em uma arquitetura WDM-PON, atingindo uma vazão de dados total de 11,8 Gbit/s.
- A implementação experimental e investigação de um X-Haul baseado em A-RoF, FSO, ondas milimétricas e VLC, operando em 39 GHz e 550 MHz para aplicações 6G.
- Propomos uma abordagem de acesso duplo e simultâneo para comunicações de alta capacidade em ambientes urbanos densos, utilizando a frequência de 39 GHz ao ar livre e uma conexão VLC de 550 MHz em ambientes internos.
- A solução proposta permite maior flexibilidade na densificação de células operando em ondas milimétricas, aplicando novas tecnologias em redes ópticas existentes.

1.4 Estrutura da Tese

Esta Tese de Doutorado possui quatro capítulos distintos. O Capítulo 2 aborda a base teórica utilizada neste estudo. O Capítulo 3 destaca os principais resultados alcançados, os quais foram apresentados sob a forma de artigos originais. Por fim, o Capítulo 4 contém as conclusões e sugestões para pesquisas futuras.

Capítulo 2

Fundamentos Teóricos

Este capítulo está dividido em cinco seções principais. A Seção 2.1 apresenta o novo padrão de rádio 5G, conhecido como *New Radio*. A Seção 2.2 aborda as redes de acesso rádio distribuídas e centralizadas. A Seção 2.3 trata dos sistemas *fiber-wireless*. A Seção 2.4 descreve soluções fotônicas aplicadas nas redes 5G e 6G. Por fim, a Seção 2.5 discute sistemas de comunicações ópticos sem fio.

2.1 5G *New Radio*

Esta subseção tem como objetivo fornecer uma visão geral dos fundamentos relacionados às características da camada física do 5G, também conhecido como 5G NR, que foi padronizado pelo 3GPP. O 3GPP é uma parceria entre sete organizações de telecomunicações que trabalham em conjunto para governar e supervisionar novas tecnologias e protocolos de redes sem fio. Suas soluções técnicas geralmente seguem as diretrizes e requisitos estabelecidos pela União Internacional de Telecomunicações (UIT, *International Telecommunication Union*), uma organização que regula o uso global das comunicações móveis [8].

A UIT também é responsável por desenvolver e aprovar as especificações relacionadas às faixas de RF para o (IMT, *International Mobile Telecommunications*). Existem três principais padrões de IMT estabelecidos pela UIT: IMT-2000, IMT-Advanced e IMT-2020 (5G). Em 2015, a UIT publicou a recomendação M.2083, chamada de

”Visão IMT - estrutura e objetivos gerais do desenvolvimento futuro do IMT para 2020 e posterior”, que estabeleceu os objetivos globais para as redes de telecomunicações móveis. Esse documento destacou vários indicadores-chave de desempenho (KPI, *key performance indicator*) importantes, como taxa de dados de pico, latência, mobilidade, densidade de conexões, eficiência energética e capacidade de dados por área [59]. Esses KPIs serviram como referência para o desenvolvimento do 5G e para garantir que as metas globais de desempenho fossem atingidas.

Para atingir os KPIs definidos, o 5G foi padronizado pela primeira vez na versão 15 em 2019 [9]. Sua primeira versão focou principalmente na cobertura do cenário eMBB ao aumentar a eficiência espectral do sistema, utilizando novas faixas de frequência e novas topologias de rede. As soluções de eficiência espectral estão relacionadas a novas formas de onda, alocação de recursos, duplexação e técnicas de acesso múltiplo. Em relação às novas faixas de frequência, a faixa de ondas milimétricas permite uma taxa de transferência de Gbit/s devido à largura de banda disponível, suportando o cenário eMBB. Por fim, as novas topologias de rede concentram-se em soluções para reduzir a latência e aprimorar o gerenciamento e a orquestração da rede por meio do uso de redes definidas por software (SDN, *software-defined networks*), virtualização e segmentação da rede. Além disso, a versão 16 foi publicada em 2020 para complementar a versão 15, introduzindo novos recursos de núcleo, RAN, aplicativos e casos de uso. As principais características da versão 16 incluem Internet das Coisas Industrial (IIoT, *industrial Internet of things*), URLLC, mMTC e veículo para tudo (V2X, *vehicle to everything*) [60]. O lançamento da versão 17, o terceiro padrão 5G, propõe melhorias adicionais no desempenho do sistema com objetivo de expandir para novas aplicações, tais como: serviços de *multicast* e *Broadcast*, redes não terrestres (NTN, *Non-terrestrial networks*), redes privadas autônomas (SNPN, *Standalone Non-public networks*), geoposicionamento dentre outros [61]. O lançamento 18 do 3GPP é chamado de 5G *Advanced* devido às suas melhorias significativas, pois incluirá aprimoramentos importantes nas áreas de inteligência artificial (IA, *artificial intelligence*) e realidade estendida (XR, *extended reality*). Isso possibilitará soluções de rede altamente inteligentes que podem suportar uma variedade ainda maior de aplicações [61]. O documento completo do padrão 5G NR compila uma variedade de versões com

várias especificações técnicas e relatórios. Portanto, a descrição a seguir aborda apenas os principais aspectos do 5G NR necessários para entender as contribuições de pesquisa, ou seja, os modos de operação do 5G, faixa de frequência e largura de banda, numerologia, alocação de recursos e magnitude do vetor de erro (EVM, *error vector magnitude*).

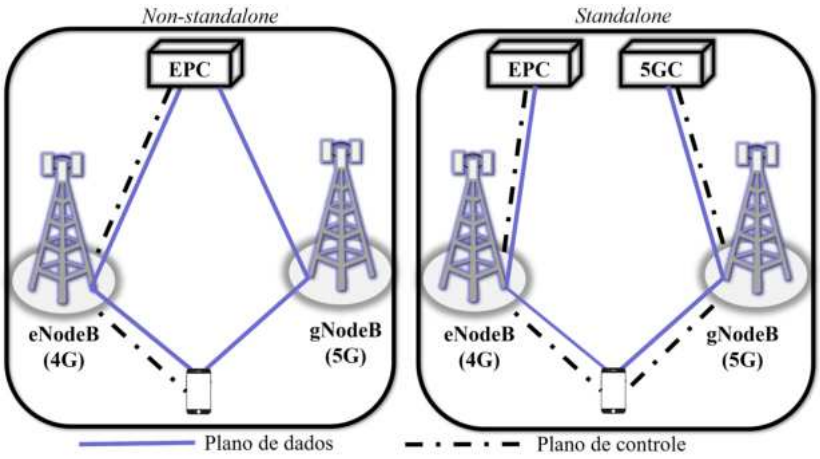

Figura 2.1: *Estrutura simplificada dos modos de operação non-standalone e standalone do 5G NR.*

Embora o 5G comercial já esteja sendo implantado globalmente, a implementação de novos *softwares* e componentes de *hardware* 5G é necessária para habilitar todas as funcionalidades da rede. O 3GPP especificou dois modos de operação distintos para permitir uma transição suave desde o início da implantação do 5G até a versão completa. O primeiro modo é chamado de não autônomo (NSA, *non-standalone*), no qual a sinalização de controle das redes 5G é ancorada no núcleo de pacotes evoluído (EPC, *evolved packet core*) do LTE, utilizando a infraestrutura de rede existente sem substituí-la, como mostrado na Fig 2.1. A principal vantagem do modo NSA é a implantação rápida do 5G, no entanto, essa abordagem não permite explorar completamente o potencial das funcionalidades do que se propõe o 5G. Por outro lado, o modo autônomo (SA, *standalone*) conecta diretamente os planos de dados e controle do rádio 5G à rede central 5G (5GC), eliminando a dependência do núcleo 4G existente. Toda a infraestrutura, incluindo unidades de rádio remotas, redes centrais e links de *fronthaul* e *backhaul*, é dedicada ao 5G. Portanto, o modo NSA pode ser visto como uma etapa temporária em direção a uma implantação completa do 5G, simplificando a transição do LTE para o 5G, enquanto somente o modo SA é capaz de fornecer todas as capaci-

dades das redes 5G [62].

Em relação às frequências de operação do 5G NR, O espectro suportado é classificado em dois intervalos de frequência (FR, *frequency range*): FR1 e FR2. O FR1 abrange de 410 MHz a 7,125 GHz, enquanto o FR2 é subdividido em FR2-1 e FR2-2, abrangendo de 24,25 GHz a 52,6 GHz e de 52,6 GHz a 71 GHz, respectivamente [12]. Além disso, o 3GPP também especificou uma diversidade de alocações de largura de banda do 5G NR com o objetivo de atender à pluralidade de cenários do 5G, permitindo flexibilidade e gerenciamento de *throughput*. A Tabela 2.1 resume a alocação de largura de banda especificada para ambas as faixas de frequência. Pode-se observar que, mesmo para a FR1, são possíveis larguras de banda de até 100 MHz sem agregação de portadora (CA, *carrier agregation*), cinco vezes maior em comparação com a versão atual do LTE. Além disso, a FR2-2 apresenta uma largura de banda sem precedentes de até 2000 MHz por usuário, visando aplicações de alto *throughput*.

Tabela 2.1: *Larguras de banda alocadas para o padrão 5G NR.*

	FR1	**FR2-1**	**FR2-2**
Frequência	410 MHz - 7125 MHz	24250 MHz - 52600 MHz	52600 MHz - 71000 MHz
Largura de banda (MHz)	5, 10, 15, 20, 25, 30, 35, 40, 45, 50, 60, 70, 80, 90 e 100	50, 100, 200, 300 e 400	100, 400, 800, 1600 e 2000

As frequências operando na faixa de ondas milimétricas são uma abordagem promissora para aumentar significativamente a capacidade dos sistemas 5G. No entanto, sistemas que operam nessa faixa de frequência enfrentam perdas severas de propagação em comparação com a faixa abaixo de 6 GHz. Consequentemente, a utilização de técnicas como: *beamforming*, múltiplas entradas e múltiplas saídas em massa (mMIMO, *massive*-MIMO) e técnicas de codificação robustas devem ser empregadas para lidar com esse problema. Além disso, os pontos de acesso que operam na banda de ondas milimétricas sofrem de ruído de fase, que é tipicamente causado e aumentado por componentes ativos, especialmente osciladores de RF. Um dos principais problemas causados pelo ruído de fase em um sinal OFDM é a rotação de fase de todas as subportadoras, denominada erro de fase comum (CPE, *common phase error*). Consequentemente, o sinal de referência de rastreamento de fase (PTRS, *phase tracking*

reference signal) foi implementado em sistemas 5G NR com objetivo de rastrear a fase, reduzindo seu impacto no desempenho do sistema [63]. Portanto, sinais de ondas milimétricas com alta pureza espectral e baixo ruído de fase desde a geração são obrigatórios para aplicações 5G. Normalmente, geradores de RF sintetizados eletronicamente são usados como fontes, que podem ser volumosas e caras, especialmente na faixa de ondas milimétricas. Alternativamente, a fotônica de micro-ondas tem sido considerada uma técnica promissora para gerar e distribuir sinais de RF com baixo ruído de fase [63], que é um tópico abordado mais adiante nesta Tese.

O 5G NR utiliza multiplexação por divisão de frequência ortogonal baseada em prefixo cíclico (CP-OFDM, *cyclic prefix-based orthogonal frequency division multiplexing*) nas direções de downlink e uplink [9]. A tecnologia 5G NR também introduziu o conceito de numerologia μ, permitindo configurar o espaçamento entre subportadoras (SCS, *subcarrier spacing*) de 60 kHz até 960 kHz nas faixas FR1 e FR2, respectivamente, uma vez que o LTE utiliza um espaçamento fixo de 15 kHz entre subportadoras adjacentes [64]. Portanto, aumentar o SCS permite o uso de maiores larguras de banda em cada subportadora e, consequentemente, atinge maior vazão de dados. O SCS resultante depende do valor de μ utilizado e é dado por:

$$\text{SCS} = 2^{\mu}(15 \times 10^{3}), \tag{2.1}$$

em que μ assume valores de 0, 1 ou 2 na faixa FR1, resultando em SCS de 15, 30 ou 60 kHz, respectivamente, enquanto na faixa FR2-1 é possível utilizar 2 ou 3 resultando em SCS de 60 ou 120 kHz, e por fim μ quando assume valor de 3; 5 e 6 resulta e SCS equivalente a 120 kHz, 480 e 960 kHz, respectivamente.

A Fig 2.2 apresenta a estrutura de domínio temporal do 5G NR. Um bloco de recurso (RB, *resource block*) é definido como a unidade mínima de alocação de recursos disponível para um usuário, sendo composto por uma matriz de tempo e frequência com as informações. No domínio temporal, o RB é composto por um período de quadro de 10 ms dividido em dez subquadros de 1 ms. Os slots de tempo são compostos por 14 símbolos OFDM, independentemente do valor de μ [65]. Consequentemente, aumentar o valor de μ resulta em uma duração de slot mais curta e fragmentação

do subquadro seguindo o fator 2^{μ}. Por exemplo, μ = 0, 1, 2 e 3 resulta em slots com duração de 1, 0,5, 0,25 e 0,125 ms, respectivamente, conforme mostrado na Fig 2.2. Portanto, aumentar o valor de μ implica em transmitir mais símbolos no mesmo período, o que corrobora com a flexibilidade do sistema proposta pela estrutura de quadro do 5G NR. Além disso, o padrão também propôs dividir o slot de tempo em dois, criando slots de tempo com 7 símbolos OFDM visando aplicações de baixa latência, uma vez que o processamento do sistema está diretamente relacionado ao slot de tempo [66].

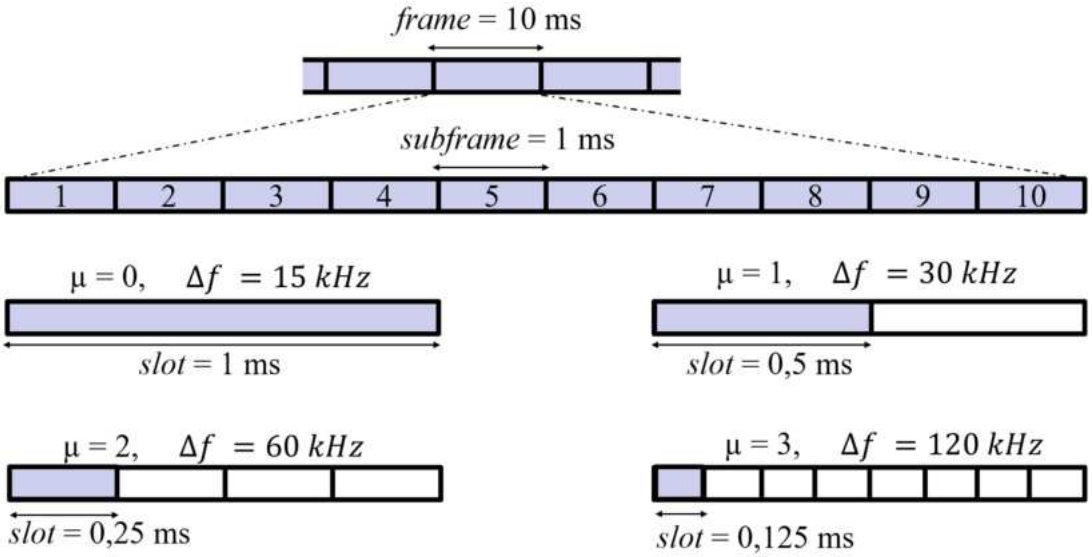

Figura 2.2: *Estrutura no domínio do tempo 5G NR.*

A estrutura do 5G NR também é organizada em canais de dados, nomeadamente: físicos, de transporte e lógicos. Os canais físicos são responsáveis pela comunicação entre o sistema 5G e os dispositivos de equipamento do usuário. Já os canais de transporte funcionam entre a camada (MAC, *media access control*) e a camada física. Os canais lógicos são utilizados para a transmissão de informações de controle e configuração entre as camadas de (RLC, *radio-link control*) e MAC. A Fig 2.3 apresenta uma geração prática do padrão 5G NR, incluindo a alocação de recursos e canais de dados mencionados anteriormente. Os sinais de sincronização primária (PSS, *primary synchronization signals*), sinais de sincronização secundária (SSS, *secondary synchronization signals*) e o canal de transmissão física (PBCH, *physical broadcast channel*) foram alocados para permitir que o equipamento do usuário adquira o sincro-

nismo do quadro e a identificação da célula. O canal físico compartilhado de dados 5G NR (PDSCH, *physical data shared channel*) é responsável por transportar os dados do usuário, configurado em particular com modulação 16 e 64-QAM. O sinal de referência de demodulação (DMRS, *demodulation reference signal*) é específico para o usuário final e utilizado para estimar o canal sem fio [67].

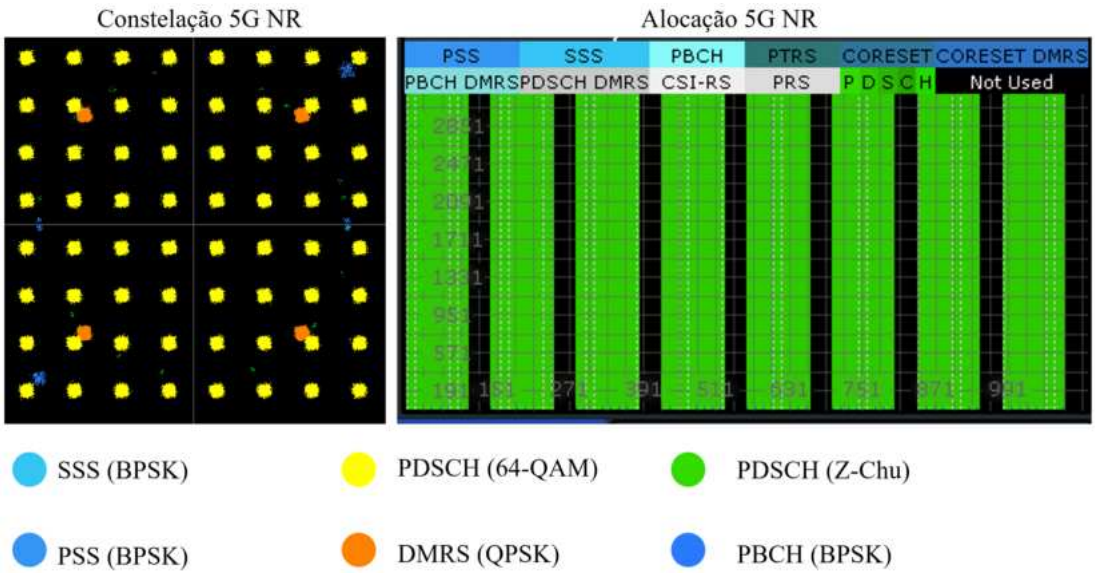

Figura 2.3: *Exemplo de descrição e alocação de símbolos/canais de dados 5G NR.*

Em relação à qualidade do sinal do 5G NR, a medida de EVM é proposta e utilizada para avaliar o desempenho do sistema, como ilustrado na Fig 2.4. Um vetor de erro é um vetor no plano I-Q entre o símbolo ideal da constelação e o símbolo recebido, ou seja, a distância entre os símbolos recebidos e os símbolos ideais. Portanto, o EVM total é a raiz quadrada média de todas as magnitudes dos vetores de erro entre os símbolos recebidos e a localização ideal mais próxima na constelação [68]. O 3GPP padronizou a magnitude máxima do erro quadrático médio do vetor (EVM_{RMS}) para o sinal 5G NR, como uma função da ordem de modulação, especificamente: 3,5%, 8,0%, 12,5% e 17,5% para 256-, 64-, 16-QAM e modulação de deslocamento de fase em quadratura (QPSK, *quadrature phase shift keying*), respectivamente.

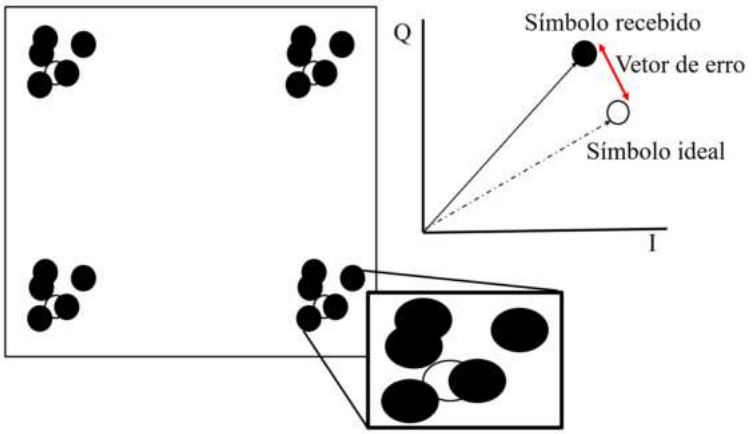

Ordem de Modulação	EVM_{RMS} máximo
QPSK	17.5%
16-QAM	12.5%
64-QAM	8%
256-QAM	3.5%

Figura 2.4: *Representação do EVM e os valores máximos permitidos para sinais 5G NR.*

2.2 *Radio Access Network* (RAN)

A rede de acesso por rádio (RAN, *radio acces network*) representa a ponte entre os usuários móveis e a rede central, sendo composta por cabos coaxiais e/ou fibras ópticas, além das antenas e elementos da estação base (BS, *base station*). Estes últimos são principalmente a unidade de banda base (BBU, *baseband unit*), responsável pelo processamento completo do sinal de banda base, incluindo o controle de recursos, e a unidade de rádio (RU, *radio unit*), que realiza tarefas de processamento de radio frequência, como filtragem de frequência e amplificação. De acordo com a topologia, a RAN pode ser classificada como uma rede de acesso por rádio distribuída (D-RAN, *distributed*-RAN) e uma rede de acesso por rádio centralizada (C-RAN, *centralized*-RAN) [69, 70].

2.2.1 *Distributed*-RAN (D-RAN)

A arquitetura distribuída da RAN localiza fisicamente a unidade de banda base juntamente com a unidade de rádio nos sites das células das redes móveis. A Fig 2.5 (a) mostra que, inicialmente, as funções de processamento de rádio e banda base são integradas na estação base, de modo que a eletrônica funcional é colocada na base da torre e conectada às antenas usando cabos coaxiais. Assim, todas as funcionalidades são processadas no site da célula, conectado à rede central por meio do *gateway* e do link físico de *backhaul*. Essa estrutura de D-RAN foi implementada principalmente para a segunda geração de redes móveis [70].

Num segundo momento, a unidade de banda base e a unidade de rádio são separadas uma da outra, conforme ilustrado na Fig 2.5(b). A unidade de rádio é posicionada próxima às antenas e é chamada de cabeçote de rádio remoto (RRH, *remote radio head*) ou unidade de rádio remota, enquanto a unidade de banda base permanece no gabinete. O RRH e a BBU são conectados utilizando fibra óptica, o que possibilita a redução de peso, volume e atenuação em comparação com o cabo coaxial. Essa solução de D-RAN também permite o uso de cabos coaxiais curtos para conectar as antenas setoriais, reduzindo assim as perdas de RF [69].

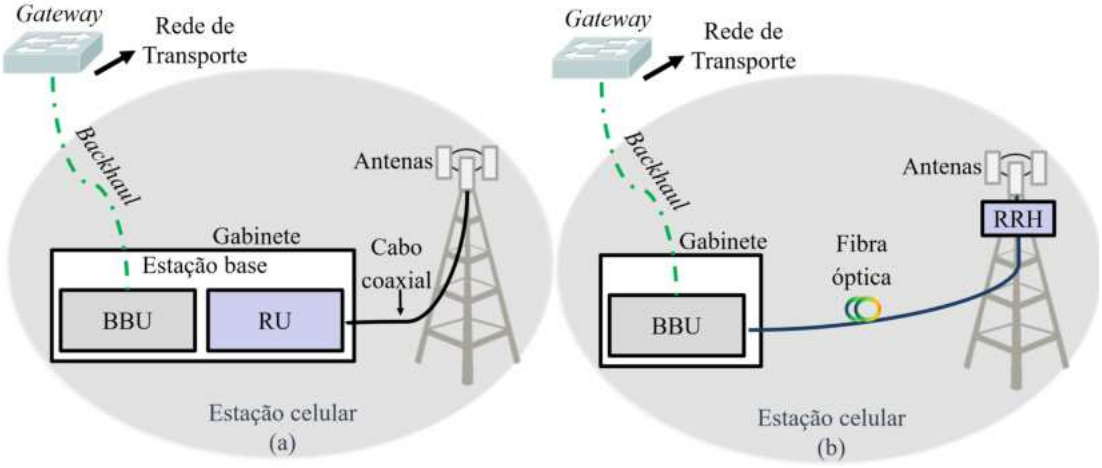

Figura 2.5: *Rede de Acesso por Rádio Distribuída: (a) Unidade de Banda Base (BBU) e Unidade de Rádio (RU) integradas na estação base; (b) BBU no gabinete e Unidade Remota de Rádio (RRH) próxima às antenas.*

A segunda fase da D-RAN supriu as demandas do (UMTS, *universal mobile telecommunications system*) e do 4G, porém não é escalável nem eficiente o suficiente para oferecer os serviços de alta largura de banda e baixa latência esperados pelo 5G. Além disso, os gastos operacionais (OPEX, *operational expenditure*) e de capital (CAPEX, *capital expenditure*) da D-RAN aumentam significativamente quando mais estações base (chamadas de NodeB) são implementadas, pois cada novo local requer uma infraestrutura completa de energia e refrigeração, além de uma área física relevante. O CAPEX cobre os custos necessários para a construção da rede, incluindo aquisição do local, hardware de RF, licenças de software, instalação, entre outros, enquanto o OPEX refere-se aos custos relacionados à operação da rede, como eletricidade, aluguel do local, manutenção e atualização. Esses gastos são uma questão importante para as futuras gerações sem fio devido ao aumento previsto no número de locais de células.

Portanto, a D-RAN não tem sido considerada uma solução de RAN competitiva para o 5G [70, 71].

2.2.2 *Centralized*-RAN(C-RAN)

A RAN centralizada, ilustrada na Fig 2.6, surgiu como uma alternativa à arquitetura distribuída. A C-RAN mantém o RRH próximo à antena remota e centraliza as funções de processamento de banda base de várias BBUs no mesmo local, geralmente na unidade central. Esta última é uma sala de equipamentos única que abriga o chamado pool de BBUs, que pode estar a quilômetros de distância (até 20 km) dos RRHs. O *backhaul* conecta o pool de BBUs à rede central, enquanto as ligações de *fronthaul* conectam o pool de BBUs a diversos RRHs. O *fronthaul* é baseado principalmente em fibra óptica, embora também possa ser sem fio. A solução de RAN em discussão tem se mostrado atrativa em termos de economia de custos e tem sido amplamente implementada em redes comerciais 4G [39, 72].

A Fig 2.6 também ilustra a arquitetura C-RAN de acordo com o conceito de interface de *fronthaul* da próxima geração, proposto pela China Mobile em 2014 para o 5G. Essa arquitetura introduz a unidade de distribuição como um novo elemento da estação base, a fim de permitir uma divisão funcional entre as funções de banda base. A divisão funcional consiste em remover algumas funções da BBU e atribuí-las à DU ou ao local da antena, que geralmente realizam tarefas de processamento rápido. As funções de controle complexas continuam centralizadas na CU. O *fronthaul* é utilizado para conectar a DU e o RRH, enquanto o *midhaul* surge como o segmento de conectividade entre a unidade central (CU, *central unit*) e a unidade de distribuição (DU, *distributed unit*). Essa solução de RAN resulta em uma estrutura de estação base chamada de gNodeB [39].

As principais vantagens do C-RAN que o tornam promissor para o 5G podem ser listadas da seguinte forma:

- Economia de custos em CAPEX e OPEX: A centralização das BBUs e dos equipamentos de suporte em um único local permite o compartilhamento de instalações, como energia, ar-condicionado e infraestrutura civil. Além disso,

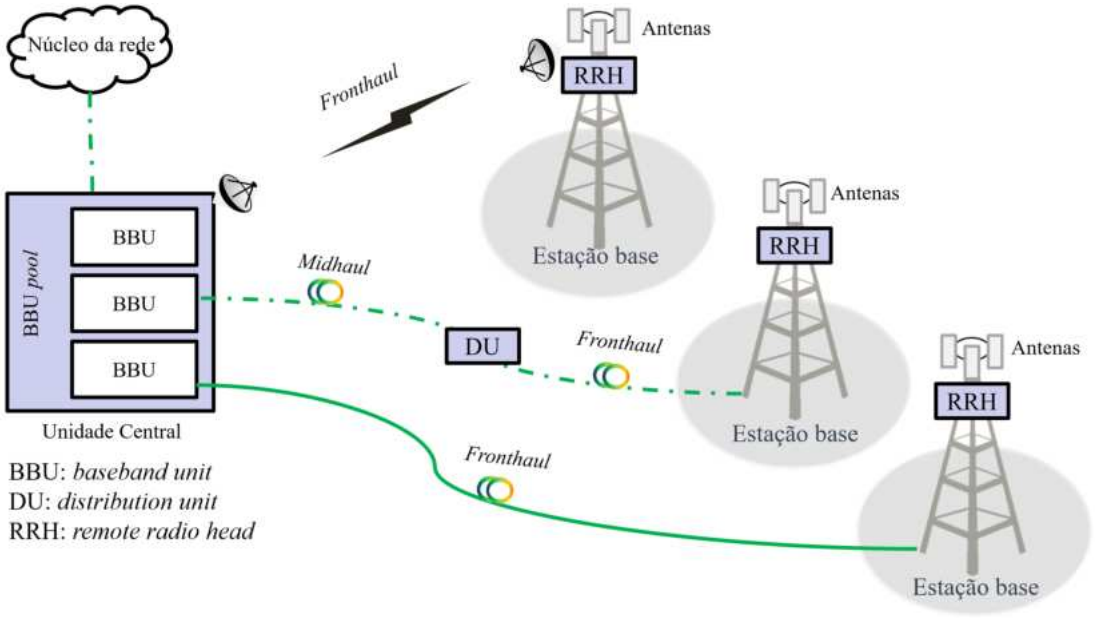

Figura 2.6: *Rede de acesso por rádio centralizada.*

a centralização permite simplificar o site da estação base, que tem tamanho e consumo de energia reduzidos, uma vez que acomoda apenas o RRH e nenhum gabinete de equipamento de banda base. O RRH pode até ser instalado em postes com taxa mínima de aluguel de site e requisitos mínimos de suporte. O gerenciamento e a manutenção da rede se tornam mais fáceis e viáveis, assumindo um grande número de estações base [70,73]. Em um dos testes de campo do C-RAN relatados na literatura, foi observado que o CAPEX e o OPEX para novos sites de células podem ser reduzidos em 30% e 5%, respectivamente, em comparação com o método de implantação de RAN distribuído [72].

- Aceleração da implantação da rede: Isso é alcançado com a simplificação do site remoto e o agrupamento de *hardware* na CU. Em números, o ciclo de construção da RAN pode ser reduzido de aproximadamente 77 dias para cerca de 30 dias ao utilizar a arquitetura centralizada [72].
- Escalabilidade e flexibilidade: Além da simplificação do site remoto, a unidade central é projetada para utilizar hardware geral, que pode ser facilmente estendido e/ou atualizado para conectar um número de DUs ou RRHs conforme a demanda. Além disso, a CU e a DU podem ser implantadas independentemente, de acordo com as capacidades de hardware, o que proporciona flexibilidade [39].

- Melhoria de desempenho: A comunicação ágil entre as BBUs co-localizadas contribui para a redução da latência e pode facilitar mecanismos de cooperação, como o (CoMP, *Coordenate Multi-Point*), já introduzido no LTE-Advanced. Algoritmos de CoMP no C-RAN se beneficiam da rápida interação entre as BBUs e podem favorecer, por exemplo, o aumento da taxa de dados na borda da célula [70, 71].
- Virtualização/cloudificação: Como os recursos computacionais são agregados no pool de BBUs, eles podem ser consolidados usando servidores padrão do setor localizados em data centers. Essa característica permite uma alocação flexível e sob demanda de recursos [39].
- Eficiência energética em direção a uma rede sustentável: O C-RAN oferece economia de energia devido a fatores como a centralização, que permite o compartilhamento de instalações, e a virtualização, que reduz os requisitos de hardware. Além disso, os recursos de processamento podem ser seletivamente desligados quando uma estação base virtual está ociosa, por exemplo, durante a noite, reduzindo o consumo de energia. De acordo com a literatura, a economia de energia no C-RAN chega a cerca de 40% em relação ao D-RAN devido à infraestrutura [39] de resfriamento compartilhada, e pode exceder 70% dependendo do nível de centralização das funções de banda base e da escala de implantação (número de células que um pool de BBUs cobre) [70, 73].

  De fato, o C-RAN traz várias vantagens que estimulam sua implantação comercial para o 5G, mas uma série de desafios precisam ser enfrentados. Por exemplo, é necessário ter disponibilidade de redes de transporte de alta largura de banda, abordagens de cooperação entre BBUs são exigidas e técnicas de virtualização do pool de BBUs precisam ser consolidadas. As soluções que serão propostas neste trabalho estão relacionadas ao elo de *fronthaul* da arquitetura C-RAN.

2.3 Sistemas *fiber-wireless* (FiWi)

Os sistemas de comunicações modernos empregam uma variedade de tecnologias para transportar e transmitir sinais entre os usuários e o núcleo da rede. Os sistemas FiWi estão entre essas tecnologias, combinando as vantagens dos sistemas ópticos e sem fio. Isso se tornou possível devido ao aprimoramento das fontes de luz e das fibras ópticas de baixa perda, juntamente com a evolução das comunicações sem fio, que contribuem para a implementação de enlaces de longa distância e alta taxa de transferência de dados. No entanto, para atingir altas taxas de transmissão no núcleo da rede, é necessário aumentar as frequências de operação. Por outro lado, isso resulta em uma diminuição na área de cobertura devido às perdas de propagação mais elevadas.

Neste contexto, a tecnologia de MWP surge como solução para convergir as comunicações ópticas e sem fio em um único sistema [15, 16]. Os sistemas FiWi, baseados na tecnologia de RoF, são utilizados em sistemas 5G, visando a transmissão simultânea de múltiplos sinais de RF entre uma unidade centralizada e o RRH [40, 74]. Essa aplicabilidade permite aproveitar a infraestrutura óptica existente, assim como sua ampla cobertura, para criar uma rede de distribuição de RF de banda larga. Para isso, o sinal de RF é modulado em uma fonte de luz com comprimentos de onda (λ) diferentes daqueles padronizados para aplicações como o GPON [75].

Uma fonte luminosa é baseada na emissão espontânea ou estimulada, que ocorre quando um átomo excitado retorna ao seu estado de energia fundamental [76]. As principais fontes ópticas utilizadas em sistemas ópticos são os LEDs (*Light-Emitting Diodes*) e os Lasers (*Light Amplification by Stimulated Emission of Radiation*). Na emissão espontânea, os fótons são gerados de forma aleatória, sem coerência de fase ou direção entre eles. Por outro lado, na emissão estimulada, um fóton existente inicia o processo, transmitindo características bem definidas, como direção de propagação, energia e fase. Essas características são replicadas nos fótons subsequentes, resultando em uma emissão de luz estimulada e coerente. Nos sistemas ópticos modernos, é necessário utilizar fontes luminosas com larguras espectrais estreitas para alcançar modulações de alta taxa de bits e baixa dispersão. Nesse contexto, os lasers são mais eficientes do que os LEDs no cumprimento dessas exigências e, portanto, são ampla-

mente utilizados em sistemas RoF.

As soluções RoF são empregadas em sistemas FiWi 5G, seguindo a arquitetura C-RAN, para o transporte de sinais analógicos (A-RoF) ou digitais (D-RoF), conforme ilustrado na Fig 2.7 [77]. Em resumo, a técnica RoF realiza a E/O (*Electrical-to-Optical Conversion*) e O/E (*Optical-to-Electrical Conversion*), adaptando o sinal ao canal de transmissão.

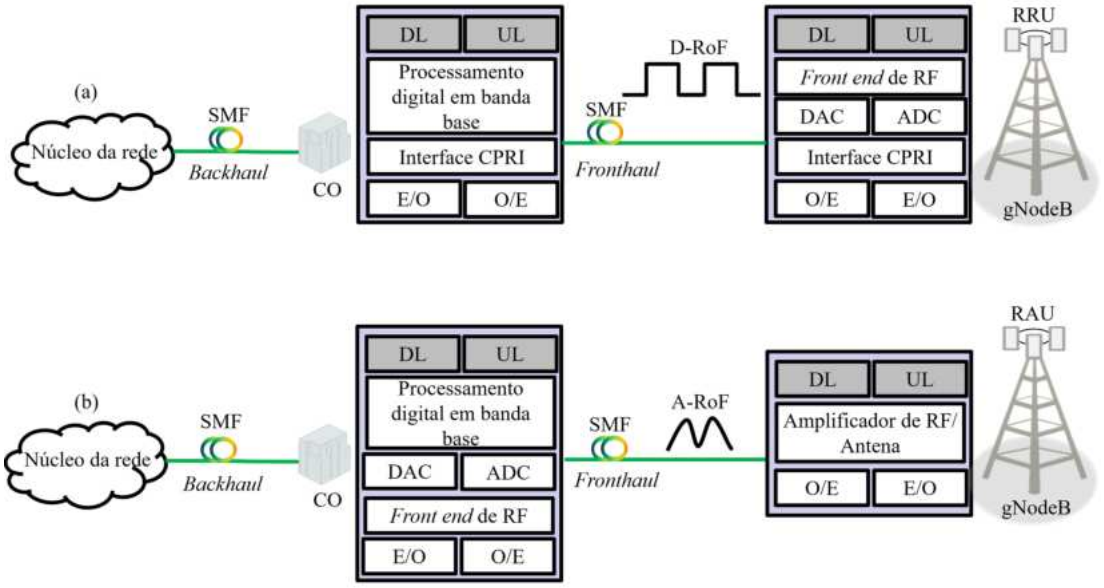

Figura 2.7: *Sistemas FiWi 5G baseados em radio sobre fibra digital (a) e analógico (b).*

Grande parte dos enlaces fronthaul modernos utiliza a tecnologia D-RoF com o padrão CPRI (*Common Public Radio Interface*). Nessa solução, o processamento digital de banda base do sinal é realizado, juntamente com o encapsulamento CPRI e a conversão E/O na *Central Office* (CO). A CO e a *Remote Radio Unit* (RRU) são conectadas por meio de fibras monomodo (SMFs), nas quais são transportadas amostras digitalizadas do sinal. Na unidade remota de radio (RRU), ocorre a conversão O/E, o desencapsulamento CPRI e a conversão do sinal digital para o domínio analógico. Em seguida, o *front-end* de RF realiza a amplificação, a conversão de frequência e a transmissão do sinal, que será recebido pelos usuários finais.

Nas transmissões na faixa de ondas milimétricas, a amostragem do sinal se torna um fator crítico devido à necessidade de utilizar conversores analógico-digital (ADC, *Analog-to-digital Converter*) e digital-analógico (DAC, *Digital-to-analog Converter*) com altas frequências de amostragem e largura de banda, o que resulta em um alto

custo. Embora os sistemas D-RoF sejam amplamente utilizados em enlaces *fronthaul*, é evidente a necessidade de melhorias para tornar essa solução viável em redes móveis de quinta geração. Isso está relacionado à baixa eficiência de transmissão de bits do padrão CPRI, que utiliza a maior parte da banda disponível para transmitir as amostras do sinal digitalizado [78, 79].

Os sistemas A-RoF surgem como uma alternativa promissora aos sistemas D-RoF, permitindo maximizar a eficiência espectral, reduzir custos e simplificar as RRUs. A simplificação ocorre devido ao deslocamento do *front-end* de RF para a CO e a eliminação dos conversores ADC e DAC nas RRUs [80]. Essa divisão levou ao surgimento de uma nova terminologia, na qual a RRU passou a ser chamada de (RAU, *Remote Access Unit*). Outras nomenclaturas que surgiram com a técnica A-RoF estão relacionadas à frequência da portadora utilizada.

Os sistemas A-RoF podem ser divididos em três categorias: RFoF (*Radiofrequency-over-fiber*), IFoF (*Intermediate Frequency-over-fiber*) e BBoF (*Baseband-over-fiber*) [81]. Ao contrário do IFoF, os sistemas RFoF transportam sinais nas frequências de radiação das redes de acesso, eliminando a necessidade de osciladores na BTS (*Base Transceiver Stations*) para multiplicação em frequência. No entanto, essa abordagem apresenta maior susceptibilidade a dispersões cromáticas e distorções em comparação com as outras técnicas A-RoF [82]. Nos sistemas BBoF, os sinais são transportados em banda base até a estação rádio base para detecção óptica. Após a detecção óptica, o sinal de informação modula uma portadora de RF de acordo com a frequência de operação da rede de acesso. É importante ressaltar que os sistemas A-RoF realizam a conversão elétro-óptica por meio de técnicas de modulação direta ou externa, em contraste com os sistemas D-RoF, que raramente empregam modulação externa [76, 83].

A Fig 2.8 ilustra o esquema fundamental de um sistema A-RoF com técnicas de modulação direta (Fig 2.8 (a)) e externa (Fig 2.8 (b)). Na modulação direta, o sinal modulante de RF, contendo as informações a serem transmitidas, é diretamente aplicado à corrente de alimentação do laser. As variações no sinal modulante alteram a intensidade da luz, resultando em uma modulação de intensidade na portadora óptica.

Consequentemente, o sinal óptico na saída do laser assume a mesma forma do sinal elétrico modulante. A modulação direta é mais econômica em comparação com a modulação externa, o que a torna atraente especialmente para aplicações com taxas de transmissão de até 10 Gbit/s [76]. Entretanto, essa abordagem é limitada principalmente pelo tempo de resposta do laser e pelo chirp, que são causados por variações de fase da portadora óptica ao longo do tempo. Para superar esses problemas, são empregados moduladores eletro-ópticos. Esses dispositivos externos possibilitam maior controle e eficiência na modulação do sinal óptico, permitindo taxas de transmissão mais elevadas e melhor desempenho do sistema A-RoF.

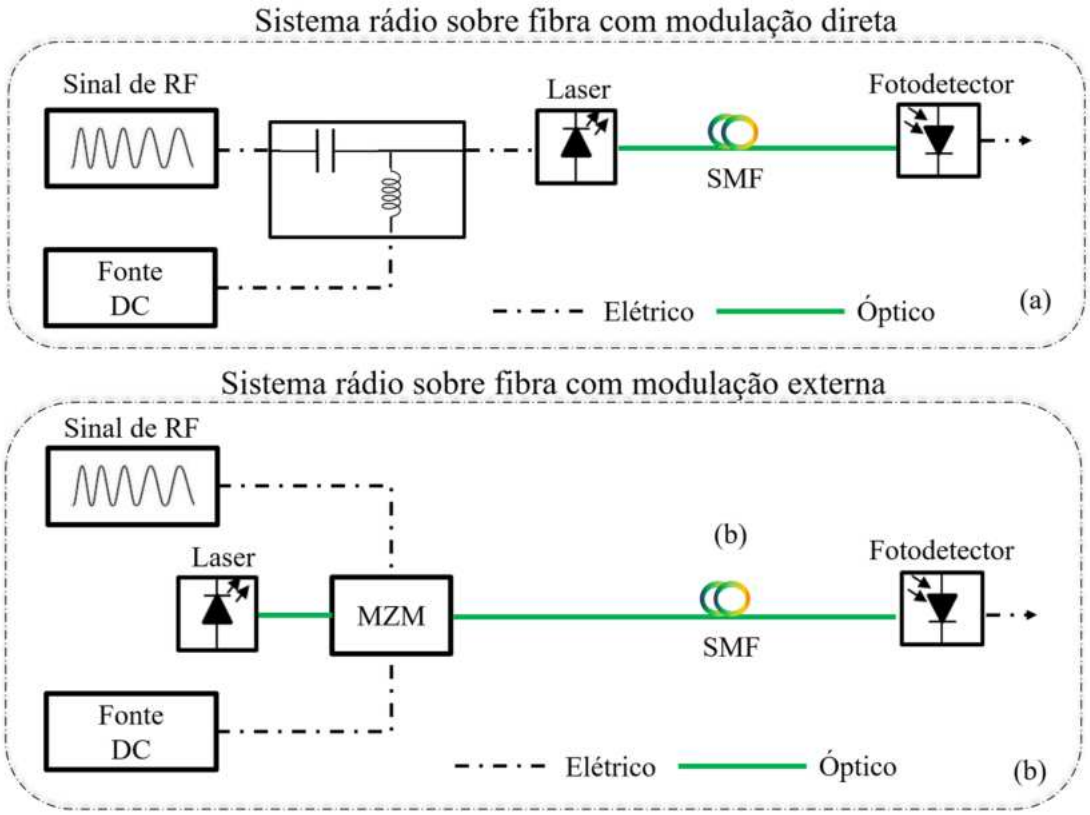

Figura 2.8: *Esquema básico do rádio sobre fibra: (a) Modulação direta; (b) Modulação externa.*

Na técnica de modulação externa, geralmente é utilizado um modulador óptico com guias de onda de Niobato de Lítio (LiNbO3) Fig 2.9. Ao aplicar uma tensão de polarização (V_{bias}), o índice modal efetivo do guia é modificado, resultando em uma variação de fase do sinal de entrada. Existem três tipos de moduladores Mach-Zehnder e estão amplamente disponíveis, como ilustrado na Fig 2.9. Eles diferem principalmente em relação ao número de entradas elétricas, mantendo o mesmo princípio ope-

racional. O modulador Mach-Zehnder (SD-MZM, *Single drive-MZM*) Fig 2.9 (a) possui uma única porta de entrada de sinal de radiofrequência (RF_{in}) e um único controle de polarização (V_{bias}). Por outro lado, o modulador Mach-Zehnder (DD-MZM, *Dual drive - MZM*) Fig 2.9 (b) possibilita duas portas de RF independentes, com controles de polarização individuais (V_{bias1} e V_{bias2}) nos braços superior e inferior do dispositivo. O modulador Mach-Zehnder (DP-MZM, *dual-parallel*) Fig 2.9 (c) combina dois moduladores SD-MZM e adiciona a possibilidade de um terceiro controle de polarização (V_{bias3}) antes da junção Y final. Vale destacar que cada um desses tipos de MZM pode ser adequadamente utilizado para aplicações específicas. O SD-MZM é geralmente empregado em modulação externa e processamento fotônico de um único sinal RF [16]. O DD-MZM é conhecido por sua aplicação em modulação óptica de banda lateral única (OSSB, *optical single side band*) [84], enquanto o DP-MZM é reconhecido por suas funções em modulação IQ [28, 85].

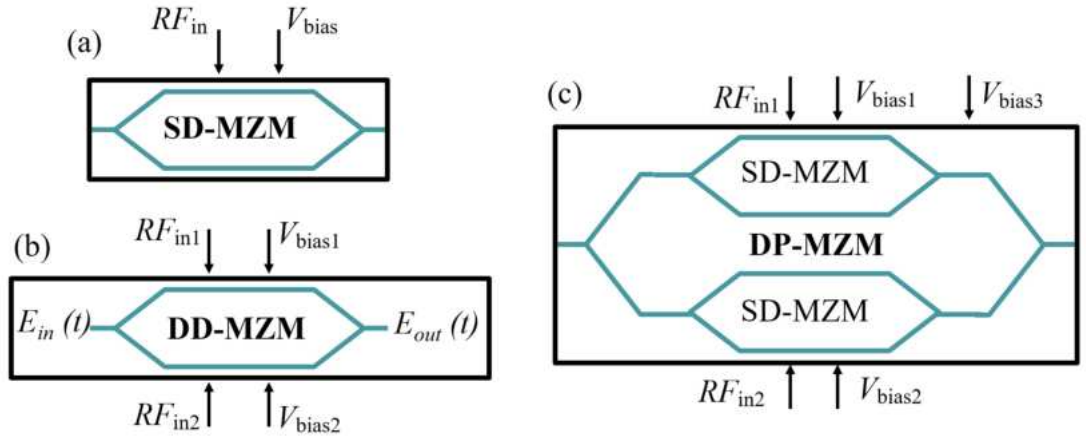

Figura 2.9: *Modulador Mach-Zehnder: (a) Single-drive; (b) Dual-drive; (c) Dual-parallel.*

Como exemplo, utilizando o DD-MZM visto na Fig 2.9 (b) a intensidade do campo elétrico da portadora óptica de entrada $(E_{\text{in}}(t))$ é igualmente distribuída em potência entre os braços do modulador. O campo elétrico da portadora óptica na saída do dispositivo $(E_{\text{out}}(t))$ varia de acordo com a tensão de polarização aplicada ao guia Fig 2.10, e essa variação pode ser descrita conforme [86].

$$E_{\text{out}}(t) = \frac{E_{\text{in}}(t)}{2}\left(e^{-i\phi_1} + e^{-i\phi_2}\right), \tag{2.2}$$

em que ϕ_1 e ϕ_2 representam as fases resultantes da aplicação das tensões de polarização

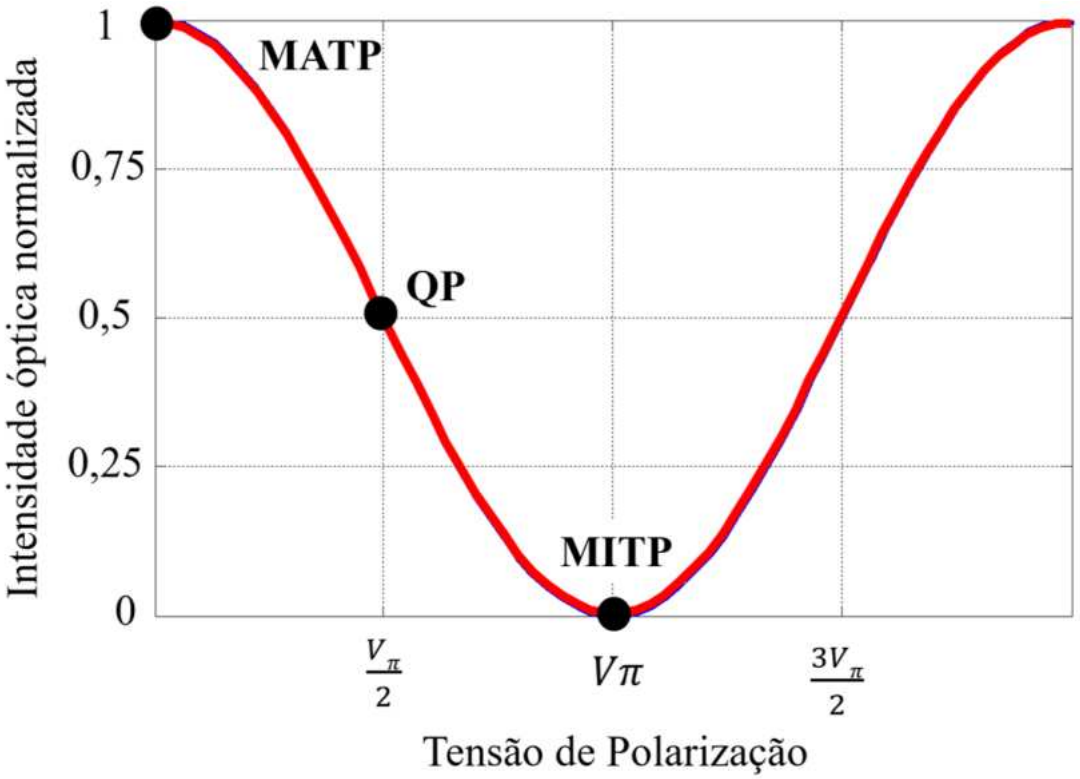

Figura 2.10: *Função de transferência do MZM.*

V_{bias1} e V_{bias2}, respectivamente, e podem ser expressas por:

$$\phi_1 = \frac{\pi}{2V_\pi} V_{e1}, \qquad \phi_2 = \frac{\pi}{2V_\pi} V_{e2}, \tag{2.3}$$

considerando V_π como a tensão de meia onda do modulador e V_{e1} e V_{e2} como as tensões de modulação aplicadas aos eletrodos dos braços superiores e inferiores, respectivamente, a relação entre essas grandezas e os sinais RF_{in1} E RF_{in2}, juntamente com as tensões de polarização, pode ser expressa da seguinte maneira:

$$V_{e1} = V_{m1}\cos(\omega_{RFin1}t) + V_{\text{bias1}}, \qquad V_{e2} = V_{m2}\cos(\omega_{RFin2}t) + V_{\text{bias2}}. \tag{2.4}$$

Finalmente, ao substituir as equações 2.3 e 2.4 na equação 2.2, obtêm-se [86]

$$E_{\text{out}}(t) = \frac{E_{\text{in}}(t)}{2}\left[e^{-i\frac{\pi}{2V_\pi}(V_{m1}\cos(\omega_{RFin1}t)+V_{\text{bias1}})} + e^{-i\frac{\pi}{2V_\pi}(V_{m2}\cos(\omega_{RFin2}t)+V_{\text{bias2}})}\right], \tag{2.5}$$

onde V_{m1}, V_{m2}, $\omega_{\mathrm{RF_{in1}}}$ e $\omega_{\mathrm{RF_{in2}}}$ representam as amplitudes e frequências angulares dos sinais de entrada do modulador (RF_{in1} e RF_{in2}), respectivamente. Na equação 2.5, observa-se que a intensidade do campo elétrico da portadora óptica varia em função da tensão aplicada aos eletrodos.

Os principais pontos de operação do modulador óptico são conhecidos como MATP (*Maximum Transmission Point*), MITP (*Minimum Transmission Point*) e QP (*Quadrature Point*). Na ausência da tensão de polarização, os campos elétricos da portadora óptica nos dois braços sofrem deslocamentos de fase iguais, sendo combinados construtivamente na saída do dispositivo, caracterizando o MATP. Quando uma tensão V_{π} é aplicada, obtemos o MITP, onde é introduzido um desvio de fase de 180 graus entre os braços do modulador. Nesse ponto, a combinação resultante é destrutiva, levando a uma atenuação do sinal de RF na frequência de interesse. É importante ressaltar que existem várias combinações de fase entre os braços do modulador, dependendo do ponto de operação escolhido ao longo da função de transferência.

Com relação as fibras ópticas aplicadas em redes de telecomunicações, são classificadas de acordo com o número de modos que se propagam pelo núcleo: a MMF (*Multi-mode Fiber*) e a SMF (*Single-mode Fiber*). Os modos referem-se às diferentes distribuições do campo eletromagnético guiado ao longo do comprimento das fibras.

Fibras monomodo permitem a transmissão de feixes ópticos modulados com taxas de bits mais elevadas, uma vez que apenas uma distribuição de campo é confinada ao núcleo, resultando em uma redução na dispersão total [83]. Após percorrer a extensão da fibra, o feixe óptico modulado é convertido de volta ao domínio elétrico por meio de um fotodetector. Essa conversão permite a recuperação dos dados transmitidos para posterior processamento e utilização.

Essencialmente, o processo de fotodetecção envolve a geração de uma corrente elétrica quando um feixe de luz incide sobre um detector. Portanto, é necessário estabelecer uma relação entre a corrente fotodetectada e as características do feixe de luz que chega ao detector. Quando a energia do feixe óptico é suficiente para liberar elétrons no material semicondutor, ocorre a transferência desses elétrons da banda de valência para a banda de condução.

Em uma situação ideal, a incidência de uma determinada quantidade de fótons por segundo resultaria na liberação de uma quantidade igual de elétrons por segundo. No entanto, na prática, o número de elétrons liberados por segundo (N_e) é menor do que o número de fótons incidentes por segundo (N_f). A relação entre esses dois valores define a eficiência quântica do dispositivo. Essa eficiência quântica indica a capacidade do detector de converter a luz incidente em corrente elétrica e é um parâmetro fundamental para a caracterização e desempenho do fotodetector, que é dada por [76]:

$$\eta_q = \frac{N_e}{N_f}, \tag{2.6}$$

esse parâmetro é influenciado pelo comprimento de onda, e cada material apresenta seu valor máximo em torno de um comprimento de onda específico. Além disso, existe um comprimento de onda de corte acima do qual não ocorre mais transferência de elétrons para a banda de condução, uma vez que o fóton não possui energia suficiente para realizar essa ação.

Ao multiplicar tanto o numerador quanto o denominador da equação 2.6 pela carga do elétron e pela energia do fóton, é possível relacionar a corrente resultante com a quantidade de elétrons por segundo e a potência do feixe óptico incidente. Esse processo leva à seguinte expressão [76]

$$\eta_q = \frac{N_e q_e hf}{N_f q_e hf} = \frac{I_p hf}{N_f hf q_e} = \frac{I_p hf}{P_{in} q_e}, \tag{2.7}$$

nesta expressão, I_p representa a fotocorrente gerada pelo deslocamento de elétrons e lacunas no semicondutor, h é a constante de Planck ($h = 6,63 \times 10^{-34}\,\mathrm{J}\cdot\mathrm{seg}$), f é a frequência do feixe óptico e P_{in} é a potência resultante do produto do número de fótons incidentes por unidade de tempo pela energia do fóton. Isolando a fotocorrente, temos:

$$I_p = \eta_q \frac{q_e}{hf} P_{in} = \eta_q \frac{q_e \lambda}{he} P_{in} = R P_{in}, \tag{2.8}$$

a responsividade do fotodetector, representada por R, é um parâmetro que combina

diferentes fatores da equação e é expressa em Amperes por Watt (A/W). O valor de R engloba a eficiência quântica, a carga do elétron, o comprimento de onda do feixe óptico, a constante de Planck e a velocidade da luz no vácuo. Sendo todos esses valores invariáveis, a responsividade é constante para um dado comprimento de onda.

Portanto, conclui-se que a fotocorrente é diretamente proporcional à potência óptica incidente [76]. Por essa razão, a fotocorrente acompanha as variações de potência do feixe óptico, permitindo reproduzir no domínio elétrico a mesma forma de onda que está modulando a onda portadora no domínio óptico. Isso torna o fotodetector uma ferramenta valiosa para converter informações ópticas em sinais elétricos, possibilitando a transmissão e processamento eficiente de dados em sistemas de comunicação óptica.

2.4 Soluções Fotônicas aplicadas em sistemas 5G

A MWP pode ser definida como uma abordagem interdisciplinar que integra as áreas de ondas milimétricas e óptica, utilizando dispositivos optoeletrônicos para transmitir, gerar e processar sinais ópticos e elétricos [16, 87]. Essa abordagem tem diversas aplicações, como redes de acesso sem fio de banda larga, redes de sensores, radar, comunicações via satélite, instrumentação, sistemas de guerra, espectroscopia, além de radioastronomia, entre outras [16, 87].

A geração de sinais de alta frequência, como os sinais de mm-wave que operam na faixa de 30-300 GHz, é um desafio significativo na área de RF. Os esquemas eletrônicos convencionais apresentam limitações devido às restrições de frequência dos dispositivos e equipamentos eletrônicos. Tradicionalmente, os sinais mm-wave são gerados por osciladores que utilizam dispositivos de dois ou três terminais, como diodos, ressonadores de cristal ou transistores. No entanto, a geração de alta frequência requer múltiplos estágios elétricos, o que aumenta o custo e a complexidade. Essas abordagens são adequadas para muitas aplicações, mas não são suficientes para as aplicações emergentes que demandam sinais de frequências mais alta. Além disso, a distribuição de sinais de alta frequência no domínio elétrico apresenta limitações devido às altas perdas associadas às linhas de transmissão elétrica, como cabos coaxiais ou guias de onda, bem como nas comunicações sem fio. Por outro lado, abordagens que utili-

zam a geração fotônica de sinais mm-wave são altamente compatíveis com técnicas de distribuição de sinal fotônico, como os esquemas RoF ou FSO.

2.4.1 Geração de sinais em ondas milimétricas utilizando técnicas fotônicas

A geração de sinais de ondas milimétricas utilizando fotônica é altamente desejável devido à sua capacidade de produzir sinais de alta frequência, inclusive na faixa de terahertz (THz), limitada apenas pela largura de banda do fotodetector. Essa abordagem apresenta baixo ruído de fase, alta capacidade de ajuste de frequência e é menos suscetível a interferências eletromagnéticas em comparação com as técnicas tradicionais no domínio elétrico [16, 87].

A heterodinação óptica é o esquema mais simples de geração de sinais de ondas milimétricas [16, 88]. Conforme ilustrado na Fig 2.11, ela é baseada no batimento entre dois campos ópticos em diferentes comprimentos de onda no fotodetector, com um espaçamento de comprimento de onda igual à frequência desejada do mm-wave, tal como:

$$\begin{aligned} E_1(t) &= E_{01} e^{j(\omega_1 t + \phi_1(t))} \\ E_2(t) &= E_{02} e^{j(\omega_2 t + \phi_2(t))}, \end{aligned} \tag{2.9}$$

onde E_{01} e E_{02} representam a amplitude, ω_1 e ω_2 são a frequência angular, e ϕ_1 e ϕ_2 são a fase dos campos elétricos.

O fotodetector realiza a conversão optoeletrônica, onde a corrente elétrica detectada pelo fotodiodo pode ser calculada como [89]:

$$i_{\text{PD}}(t) = R \cdot P(t) = R \cdot |E(t) \cdot E^*(t)|^2, \tag{2.10}$$

onde R é a responsividade do fotodiodo dado em (A/W) , $P(t)$ é a potência óptica detectada e $E(t)$ é a amplitude do campo eletromagnético na entrada do fotodiodo. Após a conversão optoeletrônica, a corrente na saída do fotodiodo é obtida e expressa da seguinte forma [16, 88]:

$$i_{\mathrm{PD}}(t) = R \cdot \left\{ E_{01}^2 + E_{02}^2 + 2E_{01}E_{02} \cos\left[(\omega_1 - \omega_2)t + \phi_1(t) - \phi_2(t)\right] \right\}. \quad (2.11)$$

Os dois primeiros termos representam a componente de (DC, *direct current*) e o terceiro é o sinal de RF gerado na frequência dada pela sua diferença, ou seja, $\omega_1 - \omega_2$. Esta técnica é capaz de gerar sinais com frequência até a faixa de THz, limitada apenas pela largura de banda do fotodetector.

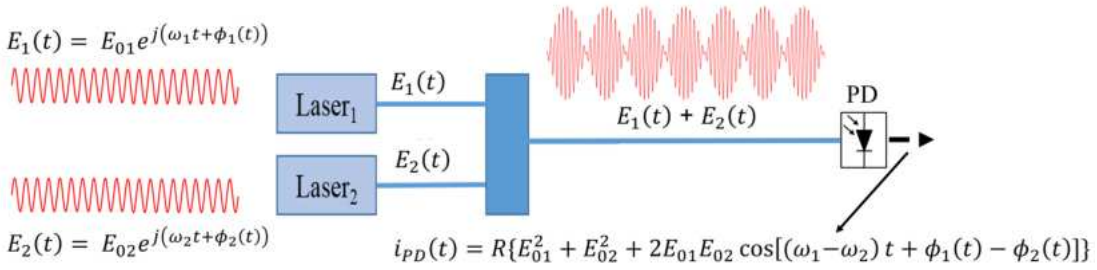

Figura 2.11: *Representação do processo de detecção heteródina de sinal A-RoF [16].*

No entanto, devido à falta de correlação nos termos de fase das duas ondas ópticas provenientes de fontes de laser independentes em funcionamento livre, o sinal gerado de onda milimétrica teria um alto nível de ruído de fase. Isso ocorre porque o processo de heterodinação transfere as flutuações de fase relativas entre as duas ondas ópticas para o sinal gerado. Para melhorar a qualidade desse sinal gerado, é necessário eliminar as flutuações relativas de fase óptica, correlacionando os termos de fase entre as fontes de laser ou comprimentos de onda. Nos últimos anos, várias técnicas fotônicas foram propostas para gerar sinais de ondas milimétricas com baixo ruído de fase. As principais técnicas utilizadas na literatura podem ser classificadas em quatro categorias: 1) (OIL, *optical injection locking*), 2) (OPLL, *Optical phase-lock loop*), uma solução híbrida que combina OIL e OPLL denominada (OIPLL, *Optical injection phase-lock loop*) e por fim 4) Geração de ondas milimétricas usando modulação externa.

(OIL, *Optical injection locking*)

A técnica OIL é baseada na utilização de dois ou mais lasers, geralmente chamado de esquema mestre-escravo, onde um laser escravo em funcionamento livre é injetado com luz coerente proveniente de um laser mestre (ML, *master laser*). Dessa forma,

o laser escravo (SL, *slave laser*) segue a fase do laser mestre. A Fig 2.12 ilustra um esquema OIL composto por um laser mestre e dois lasers escravos. Conforme amplamente conhecido, a modulação de frequência gera diferentes ordens de bandas laterais ópticas com um espaçamento de frequência angular ω_{RF}. O sinal óptico de saída do laser mestre é então direcionado para os lasers escravos. Os lasers escravos operam de modos independentes entre si, onde seus comprimentos de onda estão próximos das segundas bandas laterais do laser mestre, ou seja, $\pm 2^{nd}$. Dessa forma, os comprimentos de onda dos lasers escravos são bloqueados nas bandas laterais de segunda ordem, alcançando o bloqueio por injeção óptica. Nesse esquema, os comprimentos de onda na saída dos lasers escravos estão correlacionados em fase, resultando em um sinal de onda milimétrica gerado com ruído de fase reduzido na saída do PD.

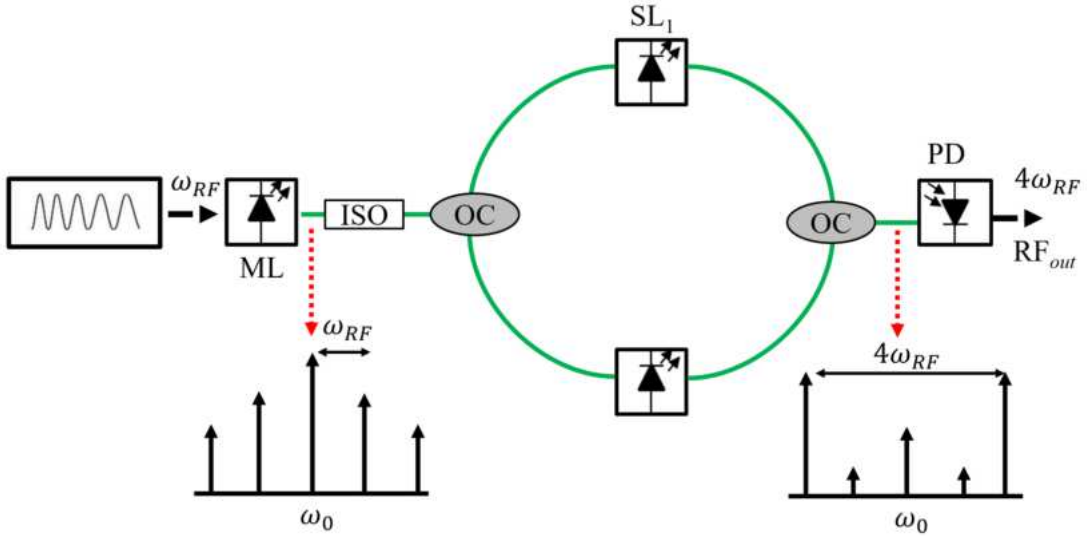

Figura 2.12: *Bloqueio por injeção óptica (OIL, Optical injection locking) de dois lasers escravos.*

Foram realizados diversos experimentos documentados na literatura. Por exemplo, foi gerado um sinal em 64 GHz com baixo ruído de fase, e espectros ópticos com largura de linha inferior a 1 Hz foram obtidos com sucesso [17]. Em um estudo posterior, os lasers escravos foram substituídos por um laser Fabry-Perot [90]. Além disso, pesquisas recentes têm demonstrado a geração fotônica de sinais de ondas milimétricas para comunicações 5G em esquemas full-duplex [91, 92]. No entanto, a principal desvantagem dessas abordagens é a necessidade de pelo menos dois lasers e outros componentes ópticos (como isoladores, circuladores, acopladores ópticos, entre outros), o que aumenta a complexidade e o custo do sistema.

(OPLP, *Optical phase-lock loop*)

Nesta técnica, denominada (OPLL, *optical phase lock loop*), um circuito de retroalimentação possibilita o controle eletrônico da fase de uma determinada fonte óptica [93]. Conforme ilustrado na Fig 2.13, a fase do sinal elétrico gerado após o batimento da onda óptica no fotodetector é comparada com a referência de RF em um misturador, seguido por um filtro de loop de baixa frequência. A diferença de fase entre o sinal e a referência de RF produz uma tensão de erro que controla a fase de uma das fontes do laser, alterando a corrente de injeção. Dessa forma, a fase de um laser é ativamente ajustada para sincronizar com a de um segundo laser.

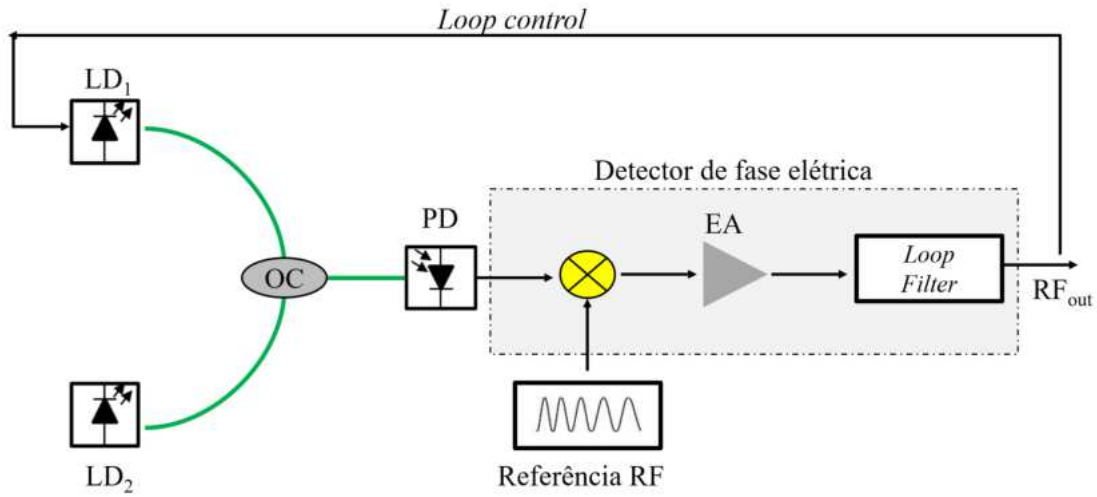

Figura 2.13: *Esquema com loop de bloqueio de fase óptica (OPLL, optical phase lock loop).*

A técnica OPLL apresenta uma limitação devido à largura de linha dos lasers, o que restringe o tempo de atraso e a largura de banda do loop OPLL [93,94]. São necessários lasers de largura de linha estreita para retroalimentações curtas [16]. No entanto, para reduzir a frequência de retroalimentação, propõe-se e demonstra-se em [95] um OPLL que incorpora um módulo de conversão de frequência para baixo. Esse módulo permite o uso de componentes de baixa frequência no loop de controle de fase, o que permite que o loop de retroalimentação controle a fase de ambas as fontes de laser.

Vários trabalhos demonstraram na literatura, como em [96], que sinais de 6 a 34 GHz com uma largura de linha inferior a 1 MHz foram gerados. Em [97], é relatada uma comparação de fase do sinal gerado em 20.5 GHz entre um modulador MZM de supressão de portadora (CS, *carrier supressed*) e esquemas OPLL.

(OIPLL, *Optical injection phase-lock loop*)

As técnicas descritas anteriormente, OIL e OPLL, podem ser combinadas em um único sistema de bloqueio denominado (OIPL, *optical injection phase locking*), conforme ilustrado na Fig 2.14. Nesse sistema, o feixe de luz emitido pelo laser mestre é dividido por um acoplador em dois caminhos de fibra óptica. Em um dos caminhos, a luz é direcionada para o modulador antes de ser injetada no laser escravo, e esse último é bloqueado em uma das bandas laterais do sinal modulado através da técnica OIL. No outro caminho, o feixe é combinado com a saída do laser escravo em um segundo acoplador e é misturado em um PD. O sinal gerado na saída do PD é então comparado com a referência de RF por um detector de fase, que controla a fase do laser escravo para atingir o bloqueio de fase.

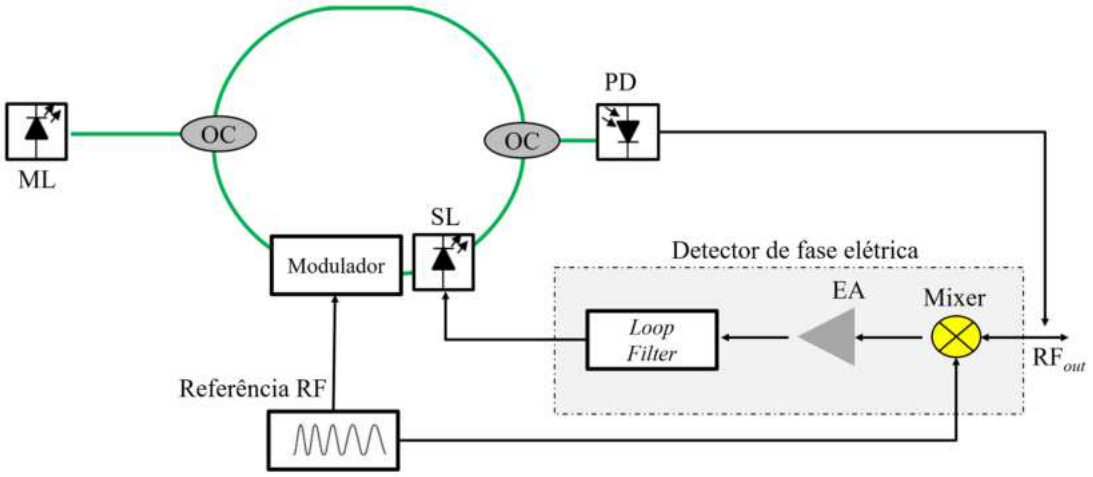

Figura 2.14: *Esquema de um sistema de bloqueio por injeção óptica e bloqueio de fase óptica.*

Conforme relatado na literatura, o OIPL apresenta menor ruído de fase em comparação com as técnicas OIL ou OPLL individualmente. Além disso, o OIPL demonstra ampla sintonização de frequência, abrangendo a faixa de 4 a 60 GHz, bem como uma ampla faixa de bloqueio de 30 GHz e baixo ruído de fase de 93 dBc/Hz a 10 kHz de afastamento em 36 GHz do sinal portador gerado [98]. No entanto, é importante destacar que o OIPL também herda as desvantagens associadas ao OIL e ao OPLL, como complexidade, custo, limitação da largura de linha do laser e a necessidade de utilização de componentes de alta frequência no loop de retroalimentação.

Modulação externa utilizando moduladores Mach-Zehnder (MZM)

Testando meu novo latex. A geração fotônica de sinais de micro-ondas ou ondas milimétricas pode ser realizada por meio da técnica de modulação externa. Essa abordagem envolve a multiplicação da frequência de um sinal de baixa frequência para uma frequência mais alta, utilizando a multiplicação de frequência no domínio óptico.

Os esquemas para geração de sinais de ondas milimétricas com base no ponto de polarização linear de um modulador Mach-Zehnder (MZM) resultam em espectros com todos os subtons ópticos, incluindo a portadora óptica. É necessário um filtro para selecionar faixas com espaçamento adequado. Na nossa abordagem, o MZM é polarizado em uma região não linear, mais especificamente, utilizamos a técnica de supressão de portadora (CS-DSB, *carrier supressed double side band*) como uma solução excelente para gerar sinais de ondas milimétricas com o dobro da frequência de rádio, ou seja, $f_{\text{mm-wave}} = 2f_{\text{RF}}$. Nesse caso, apenas os subtons de ordem ± 1 são os sinais ópticos desejados.

Assumindo que uma portadora óptica na entrada do modulador pode ser formulada como:

$$E_{\text{in}}(t) = E_0 \cdot e^{j(\omega_0 t + \phi_0(t))}, \tag{2.12}$$

onde E_0 é a amplitude constante, ω_0 é a frequência angular, e $\phi_0(t)$ é a fase do sinal óptico. O MZM, ilustrado na Figura 2.9 (b), é acionado por um sinal $v(t)$ composto por um sinal senoidal elétrico, definido como:

$$v(t) = V_{\text{bias}} + V_{\text{RF}} \cos(\omega_{\text{RF}} t + \phi_{\text{RF}}(t)), \tag{2.13}$$

onde V_{bias} é a tensão de polarização contínua, V_{RF}, ω_{RF} e $\phi_{\text{RF}}(t)$ são a amplitude, frequência angular e fase do sinal de RF de acionamento, respectivamente. Combinando as equações (2.12) e (2.13), o campo elétrico de saída após a modulação pode ser expresso como [99]:

$$E_{\text{out}}(t) = E_{\text{in}}(t)\cdot\{\cos(b)\cos(m\cos(\omega_{\text{RF}}t + \phi_{\text{RF}}(t))) - \sin(b)\sin(m\cos(\omega_{\text{RF}}t + \phi_{\text{RF}}(t)))\}\,, \tag{2.14}$$

onde $b = \frac{V_{\text{bias}}}{2V_\pi}\pi$ é o deslocamento de fase constante induzido pela tensão de polarização contínua, e $m = \frac{V_{\text{RF}}}{2V_\pi}\pi$ é o índice de modulação de fase. Combinando as equações (2.12) e (2.14) com a expansão de Jacobi-Anger e as funções de Bessel, a saída do MZM é dada por:

$$\begin{aligned} E_{\text{out}}(t) = {} & E_0\cos(b)J_0(m)\cos(\omega_0 t + \phi_0(t)) \\ & + E_0\sum_{n=1}^{\infty}[(-1)^n\cos(b)J_{2n}(m)\cos([\omega_0 + 2n\omega_{\text{RF}}]t + 2n\phi_{\text{RF}}(t) + \phi_0(t) - n\pi)] \\ & + E_0\sum_{n=1}^{\infty}[(-1)^n\sin(b)J_{2n-1}(m)\cos(\omega_0 + (2n-1)\omega_{\text{RF}}t + (2n-1)\phi_{\text{RF}}(t) + \phi_0(t) - n\pi)] \\ & + \cos(\omega_0 - (2n-1)\omega_{\text{RF}}t - (2n-1)\phi_{\text{RF}}(t) + \phi_0(t) + n\pi)\,, \end{aligned} \tag{2.15}$$

onde $J_n(.)$ é a função de Bessel de ordem n. A Figura 2.15 ilustra as típicas bandas laterais ópticas de um MZM. Conforme pode ser observado, a amplitude das bandas laterais ópticas corresponde às funções de Bessel associadas. Note que as bandas laterais ópticas de $\pm1^{\text{a}}$ e $\pm2^{\text{a}}$ exibem um deslocamento de fase de 180° em relação ao portador, de acordo com a equação (2.15).

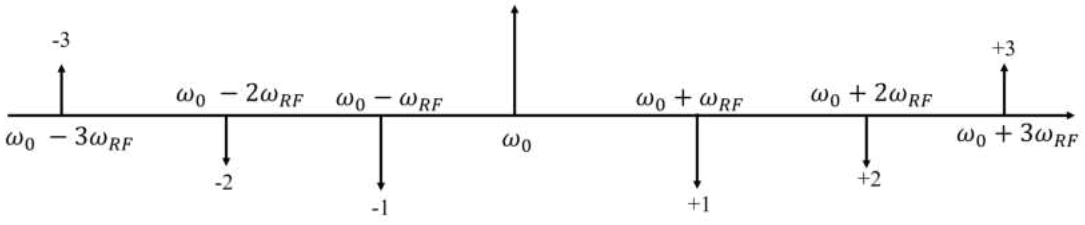

Figura 2.15: *Diagrama das bandas laterais ópticas geradas por um MZM.*

Assumindo um sinal de condução e óptico com fase nula, $\phi_{\text{RF}}(t) = 0$ e $\phi_0(t) = 0$, a modulação CS-DSB pode ser configurada em $V_{\text{bias}} = V_\pi$, ou seja, $\cos(b) = 0$ e $\sin(b) = 1$, o que leva à seguinte expressão para o campo óptico de saída:

$$E_{\text{out}}(t) = E_0 \sum_{n=1}^{\infty} [(-1)^n J_{2n-1}(m) \cos([\omega_0 + (2n-1)\omega_{\text{RF}}]t - n\pi) + \cos([\omega_0 - (2n-1)\omega_{\text{RF}}]t + n\pi)]. \tag{2.16}$$

As amplitudes das subfaixas geradas são proporcionais às funções de Bessel ímpares associadas correspondentes, $J_{2n-1}(m)$, com o índice de modulação de fase m. Quando o índice de modulação de fase é suficientemente alto, as ordens mais altas das subfaixas ópticas podem ser ignoradas. Se $V_{\text{RF}} = V_\pi$, o índice máximo de modulação de fase é $\frac{\pi}{2}$, e o argumento das funções de Bessel é $0 < m < \frac{\pi}{2}$. As bandas de ordem superior podem ser ignoradas de acordo com as funções de Bessel, e a saída do MZM pode ser simplificada como [100]:

$$E_{\text{out}}(t) = -J_1(m)E_0 [\cos([\omega_0 + \omega_{\text{RF}}]t) + \cos([\omega_0 - \omega_{\text{RF}}]t)]. \tag{2.17}$$

Essa abordagem demonstra a vantagem da robustez do sistema em relação às penalidades de potência de RF induzidas pela dispersão da fibra [101], bem como os requisitos reduzidos de largura de banda eletrônica no transmissor. No entanto, devido ao ponto de polarização não linear, é necessária uma alta potência de acionamento RF para obter uma profundidade de modulação desejável [102]. Nesta tese, a modulação externa CS-DSB é utilizada para a geração de sinais de ondas milimétricas na faixa de 60 GHz.

2.5 Comunicações Ópticas sem Fio

Uma alternativa promissora para enfrentar as restrições das tecnologias sem fio baseadas em radiofrequência é a comunicação óptica sem fio (OWC, *optical wireless communication*). A OWC oferece uma largura de banda quase ilimitada de até 400 THz e inclui subfaixas nos espectros infravermelho (IR, *infrared*), visível (VL, *visible light*) e ultravioleta (UV, *ultraviolet*), conforme ilustrado na Fig 2.16 [103]. Em comparação com as tecnologias de RF, a OWC demonstra características supe-

riores, como largura de banda ultra alta, resistência à interferência eletromagnética, capacidade de reutilização quase ilimitada de frequências (ou comprimentos de onda) e segurança física inerente [103, 104].

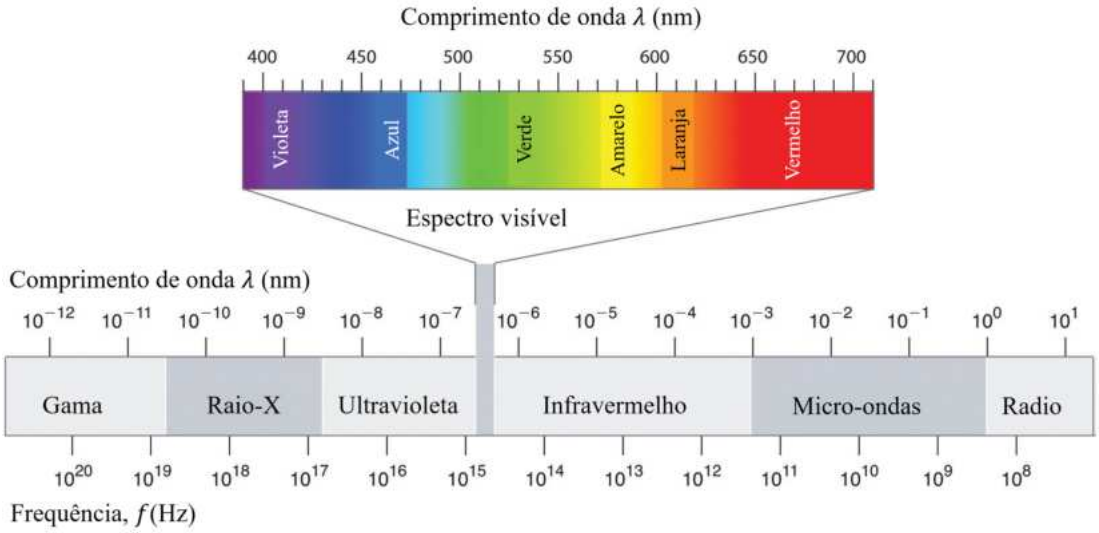

Figura 2.16: *Espectro eletromagnético.*

Além disso, as tecnologias OWC podem operar em faixas de espectro não regulamentadas, dispensando a necessidade de licenciamento, o que representa uma solução econômica para diversas aplicações [105]. O termo OWC refere-se a qualquer transmissão óptica em um meio não guiado, embora suas variações baseadas no comprimento de onda de operação (frequência) possam ter usos diferentes. Sistemas OWC operando na faixa visível (350-750 nm) são comumente conhecidos como comunicação VLC. Os sistemas VLC aproveitam tanto diodos laser (LD, *laser diodes*) quanto LEDs, que podem ser ligados e desligados em altíssima velocidade sem efeitos perceptíveis na iluminação ou no olho humano [103]. O uso múltiplo de LEDs visíveis para iluminação, comunicação de dados e localização em ambientes indoor apresenta-se como uma abordagem sustentável e energeticamente eficiente, com potencial para revolucionar como utilizaremos a iluminação no futuro. A comunicação VLC pode ser aplicada em diversas áreas, incluindo pontos de acesso sem fio, redes locais sem fio, redes pessoais sem fio e redes veiculares, transmissões sub-aquáticas entre outros [103, 105].

Por outro lado, os sistemas OWC ponto a ponto terrestres, também conhecidos como sistemas ópticos de espaço livre (FSO, *free space optical*), operam em frequências

próximas ao IR [106]. Esses sistemas normalmente utilizam transmissores a laser e oferecem uma conexão com protocolo transparente com elevadas taxas de dados, ou seja, 10 Gbps por comprimento de onda, apresentando-se como uma potencial solução para gargalos de *backhaul* e *fronthaul* [107]. Em aplicações externas, semelhantes à tecnologia RF, as ligações FSO enfrentam desafios relacionados às condições atmosféricas adversas como neblina, chuva, poeira e ao movimento de edifícios, o que afeta a disponibilidade da conexão em todos os momentos. No entanto, esses problemas podem ser superados pela utilização de ligações híbridas FSO e RF [108]. Apesar de ser predominantemente uma tecnologia externa com várias aplicações práticas, o FSO também pode ser utilizado em ambientes internos para fornecer conectividade de alta largura de banda em cenários de múltiplos pontos. Isso representa uma ótima solução para conectar vários pontos dentro de grandes áreas sem a necessidade de adaptações extensas na infraestrutura. Nesse sentido, o FSO pode oferecer as melhores soluções para substituição e implantação de sistemas de fibra óptica em edifícios modernos. Além disso, pode desempenhar um papel significativo em uma crescente tendência de pesquisa em comunicação de rádio via FSO, apresentando muitas semelhanças com os sistemas estabelecidos de rádio sobre fibra.

Também houve crescente interesse na comunicação ultravioleta devido ao progresso recente em fontes/detectores ópticos de estado sólido operando no espectro UV (200-280 nm) [103, 104]. Nessa chamada banda profunda de UV, a radiação solar é desprezível ao nível do solo, o que possibilita o projeto de detectores de contagem de fótons com receptores de amplo campo de visão, aumentando a energia recebida com pouco ruído de fundo adicional. Tais projetos são particularmente úteis para configurações sem linha de visada direta em ambientes externos, apoiando a comunicação UVC de curto alcance e baixa potência, como em redes de sensores sem fio [109].

Este trabalho propôs a utilização da comunicação via FSO para compor o *fronthaul* da rede óptica, enquanto que, concentrou esforços para propor e implementar uma solução no acesso utilizando tecnologia VLC. A seguir será apresentado uma visão geral sobre essas duas tecnologias.

2.5.1 Sistemas *Free Space Optics* (FSO)

A tecnologia FSO é considerada uma potencial habilitadora para as redes 5G e 6G [106]. Trata-se de uma tecnologia de comunicação óptica que transmite sinais ópticos sem fio através de um meio de transmissão não guiado. Seu conceito remonta às civilizações antigas, que utilizavam sinais de fogo ou fumaça para se comunicarem. A primeira comunicação óptica no espaço livre, baseada na luz solar, foi realizada por Alexander Graham Bell em 1880 [110]. Nos sistemas FSO atuais, feixes de laser extremamente estreitos, na faixa de comprimento de onda infravermelho, são transmitidos através do ar como meio de transmissão, dispensando a necessidade de fibra óptica ou qualquer outro sistema óptico que guie a luz.

O FSO enfrenta concorrência de tecnologias como a fibra óptica, comunicações sem fio via RF e cabos coaxiais. No entanto, apresenta algumas vantagens, como maior segurança, baixo custo de instalação de rede e facilidade de manutenção e atualização. Além disso, emprega o comprimento de onda que opera no infravermelho, o que confere capacidades de largura de banda de transmissão comparáveis às da fibra óptica, possibilitando elevada vazão de dados. As perdas do FSO são consideravelmente menores em comparação com as perdas do RF devido à sua alta direcionalidade do feixe óptico. Por exemplo, a atenuação atmosférica para a janela de transmissão de 1520-1600 nm é inferior a 0,2 dB/km em condições de boa visibilidade [111], enquanto as perdas de RF dependem fortemente da frequência utilizada. O sistema FSO é uma excelente alternativa em áreas onde a instalação de fibra óptica não é viável, sendo uma solução ideal para links sem fio de alta capacidade, como o link de *fronthaul*. Além disso, a portadora óptica operando em frequências na ordem de THz ainda não é licenciado, o que significa que o uso do FSO não requer taxas de licenciamento.

A transmissão FSO tem sido objeto de extensos estudos na literatura científica. Por exemplo, foi realizado um experimento onde uma taxa de transmissão de 40 Gbit/s foi alcançada ao longo de uma distância de 20 metros utilizando a tecnologia FSO [112]. Em outra pesquisa, foram realizados experimentos em ambiente externo, entre dois edifícios, nos quais a modulação de amplitude por pulso (PAM, *pulse-amplitude modulation*) foi utilizada para alcançar uma taxa de transmissão de 200 Gbit/s [113].

Um sistema de FSO consiste essencialmente em três subsistemas: transmissor, canal e receptor, conforme ilustrado na Fig 2.17 [106]. O transmissor, que geralmente incorpora uma fonte óptica e um modulador, emite um sinal elétrico modulado sobre um portador óptico. Para possibilitar a transmissão de feixes extremamente estreitos, é comum utilizar uma lente colimadora e um estágio de alinhamento mecânico. O canal FSO corresponde à atmosfera, que é sujeita a turbulência atmosférica, desalinhamento dinâmico e perdas atmosféricas durante a propagação do sinal óptico. Por fim, o receptor tem a responsabilidade de coletar o feixe óptico transmitido e recuperar o sinal elétrico de dados. Em geral, um receptor típico é composto por uma lente de focalização, um estágio de alinhamento mecânico para captar o sinal óptico e um PD que converte a potência óptica em uma corrente de saída.

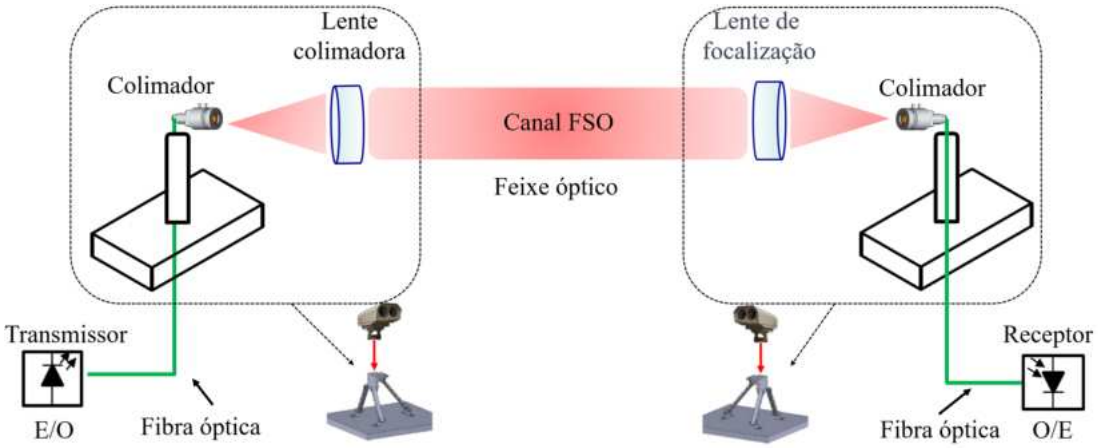

Figura 2.17: *Esquemático do sistema FSO.*

Os sistemas FSO apresentam algumas limitações devido ao meio de transmissão e às características físicas do local de instalação. Os principais efeitos que impactam o desempenho do sistema são obstruções na linha de visada direta, atenuação atmosférica, desalinhamentos, divergência do feixe e turbulência atmosférica [114, 115].

O sinal óptico transmitido pelo canal FSO sofre atenuação atmosférica devido ao processo de absorção e espalhamento [106]. A atenuação atmosférica total é determinada pelo coeficiente de atenuação atmosférica, α_{atm}, o qual é expresso como uma combinação da absorção e espalhamento da luz.

A absorção atmosférica é fortemente dependente do comprimento de onda, como ilustrado na Fig 2.18 (a) [111]. A absorção ocorre principalmente em resposta às

partículas de água (ou seja, umidade), dióxido de carbono e ozônio. No entanto, existem algumas janelas de transmissão com baixa atenuação, por exemplo, entre 780–850 nm e 1520–1600 nm. A atenuação das faixas de comprimento de onda do infravermelho é inferior a 0,2 dB/km em uma atmosfera limpa. Além disso, a maioria dos componentes ópticos disponíveis é projetada para funcionar no comprimento de onda de 1550 nm.

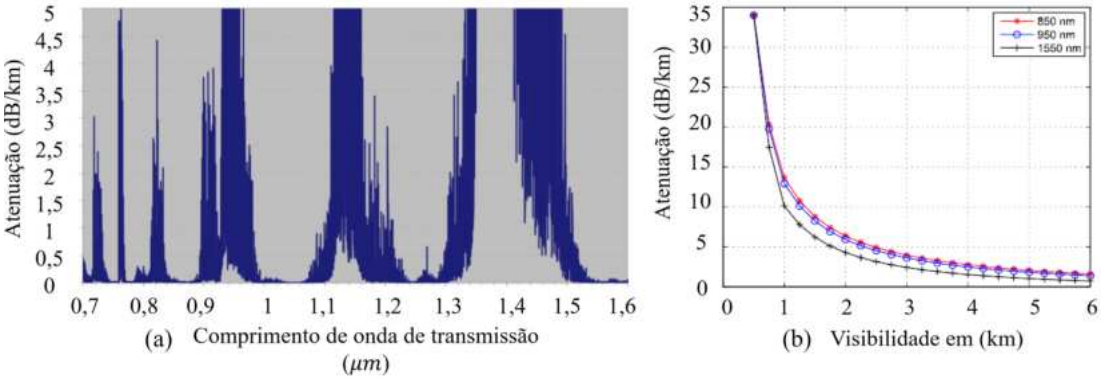

Figura 2.18: *(a) Atenuação do comprimento de onda em condições de tempo limpo devido à absorção [111]. (b) Atenuação versus visibilidade durante uma densa neblina [116].*

Condições climáticas, como nuvens, neblina, chuva ou neve, também desempenham um papel fundamental devido ao espalhamento dos sinais ópticos, fortemente dependente do comprimento de onda. Se o tamanho das partículas atmosféricas é comparável ao comprimento de onda óptico, ocorre o espalhamento de Mie [111], que é dominante na faixa de comprimento de onda do infravermelho. Por exemplo, a Fig 2.18 (b) exibe a atenuação específica em relação à faixa de visibilidade durante uma densa neblina, mostrando que o coeficiente de atenuação é superior a 30 dB/km com uma faixa de visibilidade inferior a 1 km.

As perdas geométricas causadas pela divergência do feixe óptico entre o transmissor e o receptor devem ser consideradas, principalmente em links FSO de longo alcance em ambiente externo [117, 118]. A Fig 2.19 ilustra os subsistemas do transmissor e receptor, juntamente com o canal de espaço livre. O feixe transmitido se espalha pelo canal devido à difração. Quando a abertura do receptor não é capaz de coletar todo o feixe transmitido, ocorrem perdas de potência.

A atenuação devido às perdas por divergência do feixe FSO, α_{FSO}, pode ser determinada de acordo com [111, 119].

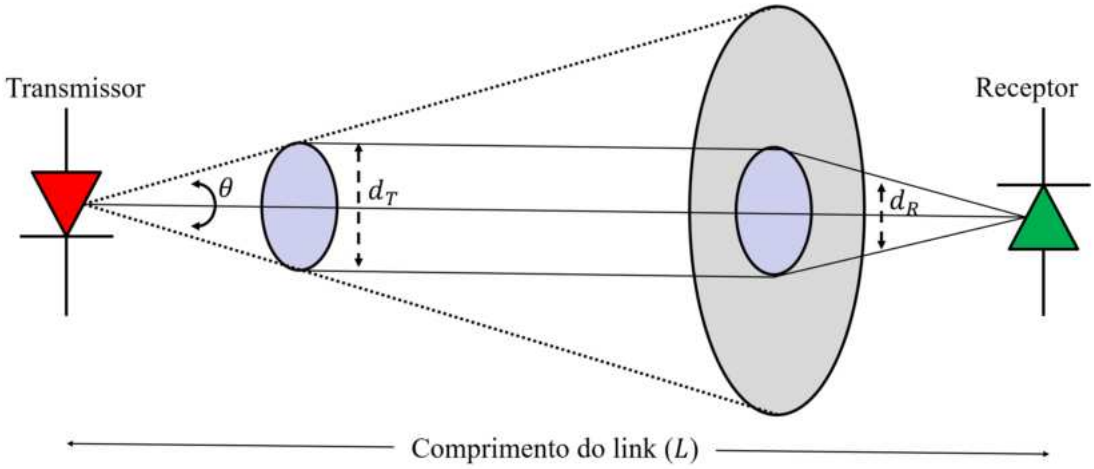

Figura 2.19: *Esquema geral de um link FSO.*

$$\alpha_{FSO} = \frac{P_{Rx}}{P_{Tx}} = \frac{d_R^2}{(d_T + \theta L)^2} \times 10^{-\frac{\alpha_{atm} L}{10}}, \tag{2.18}$$

onde d_R e d_T são os diâmetros das aberturas do receptor e do transmissor, respectivamente, θ (mrad) é a divergência do feixe, L (km) é o alcance do link FSO e α_{atm} (dB/km) é a atenuação atmosférica, conforme mencionado acima.

Além disso, o FSO é afetado pela turbulência atmosférica criada por distribuições térmicas, ao longo do link FSO, onde múltiplas fontes térmicas, como sistemas de ar condicionado, rios, fábricas, etc., podem estar envolvidas. Nesse caso, a cintilação é causada quase inteiramente por pequenas variações de temperatura, resultando em flutuações do índice de refração que contribuem para a degradação do sinal. Esse fenômeno pode ser descrito por vários modelos estatísticos, como o modelo lognormal, o modelo exponencial e, mais recentemente, o modelo Gamma-Gamma, que é adequado tanto para turbulência fraca quanto forte [120].

A cintilação é caracterizada de acordo com o modelo de turbulência atmosférica Gamma-Gamma [120], através da variância do logaritmo da amplitude, conhecida como variância de Rytov (σ_R^2). Essa variância pode ser calculada para um parâmetro de estrutura de índice refrativo uniforme C_n^2 da seguinte maneira:

$$\sigma_R^2 = 1.23 \cdot k^{7/6} \cdot C_n^2 \cdot L^{11/6}, \tag{2.19}$$

onde $K = 2\pi/\lambda$ e L é a distância horizontal percorrida pelo campo óptico. O parâmetro

C_n^2, que determina a intensidade da turbulência, é especificado por:

$$C_n^2 = \left(79 \cdot 10^{-6} \cdot \frac{P_a}{T^2}\right)^2 \cdot C_T^2, \tag{2.20}$$

onde P_a é a pressão atmosférica em milibares, T é a temperatura absoluta em Kelvin e C_T^2 é o parâmetro de estrutura de temperatura, definido como:

$$C_T^2 = \frac{(T_1 - T_2)^2}{L_P^{2/3}}, \tag{2.21}$$

onde T_1 e T_2 estão separadas por uma distância L_P.

Assim, a probabilidade de uma determinada potência óptica após a transmissão em um link FSO, denotada por $Prob(P_{FSO})$, é expressa pela seguinte distribuição:

$$Prob(P_{FSO}) = \frac{2(\alpha\beta)^{\frac{\alpha+\beta}{2-1}}}{\Gamma(\alpha)\Gamma(\beta)} K_{\alpha-\beta}(2\sqrt{\alpha\beta}P_{FSO}), \tag{2.22}$$

onde Γ é a função gama, $K_{\alpha-\beta}$ é a função de Bessel modificada e $1/\alpha$ e $1/\beta$ são as variâncias de turbulência de pequenas e grandes escalas, que são calculadas a partir da variância de Rytov da seguinte forma:

$$\begin{aligned} \alpha &= \exp\left[\frac{0.49\sigma_R^2}{(1 + 1.11\sigma_R^{\frac{12}{5}})^{\frac{5}{6}}}\right] - 1, \\ \beta &= \exp\left[\frac{0.51\sigma_R^2}{(1 + 0.69\sigma_R^{\frac{12}{5}})^{\frac{5}{6}}}\right] - 1. \end{aligned} \tag{2.23}$$

Finalmente, as flutuações de intensidade são caracterizadas pela distribuição de probabilidade, que é classificada como turbulência fraca ($\sigma_R^2 < 1$), turbulência moderada ($\sigma_R^2 \approx 1$) e turbulência forte ($\sigma_R^2 > 1$).

As vantagens da utilização de links FSO possibilita uma ampla variedade de usos, como mencionado em [121, 122]. O FSO pode ser empregado em distâncias de até 15 km para conectar usuários em aplicações como acesso sem fio, conectividade de última milha, conectividade empresarial e links ponto a ponto. Além disso, é uma solução viável em cenários onde a implantação de fibras ópticas é inviável ou exces-

sivamente custosa, como em travessias ferroviárias, rodoviárias ou fluviais. O FSO é um complemento eficiente para enlaces tradicionais de rádio e de fibra óptica, devido a sua capacidade de transmitir uma elevada vazão de dados.

2.5.2 Sistemas *Visible Light Communication* (VLC)

A comunicação por luz visível (VLC, *visible light communicatio*) denota o conjunto de sistemas onde a transmissão de dados ocorre por meio da modulação das ondas luminosas no espectro visível do campo eletromagnético, ou seja, mediante a utilização da porção espectral que abrange comprimentos de onda entre 380 nm e 780 nm [103]. Qualquer informação que é transmitida neste intervalo de comprimento de ondas pode ser considerada um tipo de comunicação baseado em sistemas VLC.

O espectro da luz visível abre uma série de oportunidades para estudos. Diferentemente da transmissão por radiofrequência, o espectro da luz visível não requer licenciamento, permitindo que dispositivos transmitam em qualquer frequência sem a necessidade de uma autorização [123]. Enquanto o espectro de ondas de rádio varia de 3 kHz a 300 GHz, as frequências no espectro visível estão na ordem dos THz, ou seja, mil vezes maiores [124]. Adicionalmente, ao contrário do infravermelho e do ultravioleta, os sistemas VLC possui a capacidade de oferecer simultaneamente iluminação e comunicação em sistemas aplicados para ambientes *indoor*. Além disso, essa tecnologia se beneficia da acessibilidade econômica dos dispositivos utilizados. Por último, as ondas de rádio têm a capacidade de atravessar barreiras, como paredes, o que torna as redes sem fio convencionais vulneráveis a potenciais invasores. Em contrapartida, nos sistemas VLC, o que é visível é o que está sendo transmitido. Em outras palavras, devido às propriedades intrínsecas da luz, sistemas VLC em ambientes fechados se tornam notavelmente mais seguros [107].

No cenário das tecnologias de comunicações ópticas sem fio para aplicação nas redes 5G e 6G, VLC destaca-se como uma alternativa promissora para atender as possíveis demandas. A VLC faz uso de dispositivos emissores de luz, tais como diodos emissores de luz (LEDs, *light emitting diodes*) ou diodos laser (LDs, *laser diodes*), para a transmissão de dados, possibilitando o alcance de taxas de transmissão na ordem

de Gbit/s [125].

No que diz respeito ao modelo do sistema, tanto a comunicação por VLC quanto por RF possuem a mesma estrutura. Em outras palavras, os blocos comumente utilizados para caracterizar ambos os sistemas são os mesmos. A Fig 2.20 apresenta os principais subsistemas da comunicação por VLC. Note a semelhança entre o sistema VLC e o sistema RF. O VLC é um sistema de comunicação sem fio e, como a nomenclatura sugere, não há conexão física entre o transmissor e o receptor no sistema VLC. Consequentemente, a informação se propaga principalmente pelo ar na forma de luz visível. O transmissor tem a responsabilidade de modular de maneira adequada os dados em pulsos elétricos, que alimentam o LED. Os pulsos elétricos convertidos em ondas eletromagnéticas na frequência da luz visível pelo LED são recebidos pelo fotodetector.

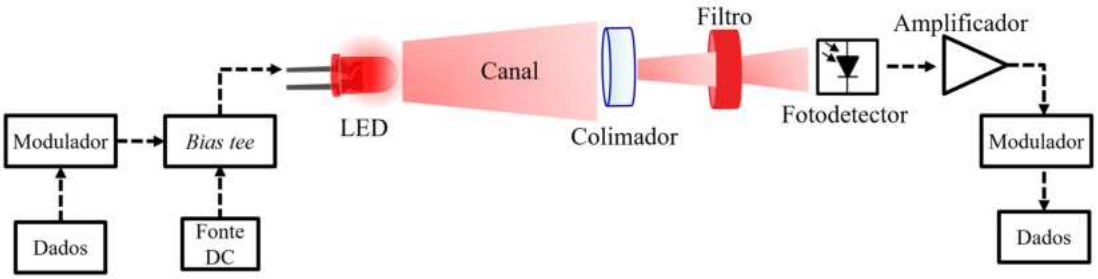

Figura 2.20: *Diagrama simplificado de um sistema de comunicação por luz visível.*

O Fotodetector converte os feixes de luz em sinais elétricos, que são então filtrados e demodulados no receptor. Outros componentes mostrados na Fig 2.20 incluem a fonte de alimentação DC e o colimador. Embora não sejam fundamentais para um sistema VLC, eles são frequentemente implementados em aplicações práticas. Se o projeto para implementar o sistema VLC envolve o compartilhamento da iluminação ambiente, a fonte de alimentação contínua é necessária. Um colimador é um dispositivo que estreita um feixe de partículas ou ondas. Geralmente, é quase sempre necessário ter uma linha de visada direta (LoS) em sistemas VLC, ou seja, uma trajetória direta entre transmissor e receptor. A comunicação sem LoS é possível apenas em casos extremamente raros e específicos.

O transmissor é responsável por adaptar o sinal de informação aos requisitos impostos pelo meio de propagação. No contexto dos sistemas VLC, o transmissor deve mo-

dular a informação em um feixe de luz da maneira mais eficiente possível. A principal proposta para o uso de VLC é a provisão simultânea de dados e iluminação. Portanto, é essencial que o tremor causado pela modulação do feixe de luz seja imperceptível ao olho humano e, ao mesmo tempo, não prejudique a saúde humana. Também é esperado que o sistema VLC não altere a intensidade média da luz ambiente. Em outras palavras, o sistema VLC não deve mudar o padrão de iluminação do ambiente. Esta é outra característica imposta ao transmissor de um sistema VLC. Consequentemente, a intensidade padrão da luz no ambiente define um parâmetro crucial do projeto do sistema VLC, a proteção do transmissor.

Como já mencionado, o transmissor deve modular os dados em um sinal luminoso, combinando os dados com o componente DC antes de alimentar o LED. De maneira geral, sistemas VLC permitem desde modulações mais simples, como OOK, até esquemas de modulação mais sofisticados, como modulação por divisão de frequência ortogonal com modulação em OFDM. A modulação utilizada no sistema deve ser cuidadosamente avaliada pelo projetista. Modulações mais sofisticadas podem exigir componentes eletrônicos, como (FPGA, *Field Programmable Gate Array*), e, portanto, impactar diretamente no custo do transmissor VLC.

Capítulo 3

Descrição dos Artigos Relacionados à Tese:

Esta tese é baseada em um conjunto de artigos submetidos para publicação em revistas científicas com revisão por pares, anais de conferências e trabalhos já publicados. Esses artigos apresentam os principais resultados obtidos durante o curso dos meus estudos de Doutorado em sistemas ópticos para aplicações em RAN. Além disso, esses artigos exploram tópicos como geração de micro-ondas baseada em fotônica, óptica de espaço livre, comunicação baseado em luz visível, rádio sobre fibra e sistemas FiWi para às redes 5G e 6G.

Artigo 1: Implementation of HetNet Architectures Based on FSO, VLC, RoF and Photonics RF Generation Towards 6G Applications

Celso Henrique de Souza Lopes, Tomas Powell Villena Andrade, Luiz Augusto Melo Pereira, Evandro Conforti and Arismar Cerqueira. S. Jr. ”Implementation of HetNet Architectures Based on FSO, VLC, RoF and Photonics RF Generation Towards 6G Applications”, *Journal of Optical Communications and Networking* (JOCN) -Submetido em 2024.

Implementation of HetNet Architectures Based on FSO, VLC, RoF and Photonics RF Generation Towards 6G Applications

CELSO HENRIQUE DE SOUZA LOPES[1], TOMAS POWELL VILLENA ANDRADE[1], LUIZ AUGUSTO MELO PEREIRA[1], EVANDRO CONFORTI[2], AND ARISMAR CERQUEIRA SODRÉ JUNIOR[1,*]

[1] National Institute of Telecommunications (Inatel), Santa Rita do Sapucaí, MG 37400-000 Brazil
[2] DECOM—University of Campinas, Campinas 13083-970, Brazil
[*] Corresponding author: arismar@inatel.br

Compiled March 13, 2024

The increasing need for ubiquitous broadband connectivity in the fifth and sixth generations of mobile communications (5G/6G) radio access networks (RANs) has made the centralized radio access (C-RAN) network topology the mainstream architecture for meeting the demands of growing traffic capacities and connection densities. In this context, we conducted experimental evaluations of two distinct hybrid architectures applied to 5G New Radio (5G NR) fiber-wireless (FiWi) systems, employing different optical fronthaul (FH) approaches. The first evaluated architecture proposes the integration of an analog radio over fiber (A-RoF)-based optical FH operating in mm-wave into a wavelength-division multiplexing passive optical network (WDM-PON). The specific FH employs photonics techniques for signal generation in the V-band. The employed technique, also known as carrier suppressed double side-band (CS-DSB), is composed of two cascaded stages of external modulation using Mach-Zehnder modulator (MZM). By optimizing the bias operating parameters of the modulator, 2-fold frequency multiplication in the electrical domain is achieved. The proposed solution enables the generation and transport of a 5G NR signal at 60 GHz with a bandwidth of 400 MHz and a quadrature phase shift keying (QPSK) modulation scheme. Based on the obtained results, the proposed solution demonstrated its feasibility for meeting the demands of cell densification of 5G/6G, achieving a data throughput of approximately 11.8 Gbit/s. The second experimental configuration converges into a unified network architecture that combines solutions based on FiWi, free space optics (FSO), and visible light communication (VLC) to meet the requirements of 6G solutions. To achieve this, the implemented architecture is based on the concept of an X-HAUL, using 20 km of optical fiber followed by an FSO link as the FH of the network, considering last-mile applications. In the access section, a 5G NR mm-wave link at 39 GHz was implemented at a distance of 2 m, and simultaneously, a VLC transmission using a quadrature amplitude modulation (M-QAM) signal at 550 MHz was evaluated for indoor 6G applications. Experimental results demonstrated satisfactory coexistence among the employed technologies, achieving a total data throughput of 1.5 Gbit/s. The two proposed architectures were evaluated according to the root mean square error vector magnitude (EVM_{RMS}) requirements set forth by the 3rd Generation Partnership Project (3GPP) Release 18.

http://dx.doi.org/10.1364/ao.XX.XXXXXX

1. INTRODUCTION

Motivated by the growing need for high data rates, increased cell densification, and low latency for human and/or machine communications, the next generation of wireless networks received considerable attention from academy and industry [1]. The deployment of fifth-generation of mobile networks (5G) technology allows for the implementation of a variety of new value-added applications, with enhanced mobile broadband being the primary focus, while other scenarios continue to mature [2]. Technical solutions such as the 5G new radio (5G NR) standard, employment of millimeter-wave (mm-wave) spectrum, heterogeneous networks, centralized radio access network (C-RAN), optical wireless communication (OWC), and optical-wireless convergence are proposed to meet the imminent demands of 5G [2, 3]. In the meantime, the sixth-generation of mobile networks (6G) has emerged as a solution to address the potential unfulfilled promises of 5G and meet future demands from 2030 and beyond with better efficiency [4]. In the 6G network, novel use case scenarios are anticipated to emerge, encompassing telepresence, zero-energy devices, the use of robots in different areas of daily life, biosensors, and potential applications that currently remain unidentified [5]. Potential technical solutions for 6G include the use of terahertz communications (THz) waves, artificial intelligence/machine learning to support autonomous networks, and innovative air-interface design [5, 6].

The primary goal of advancing towards 6G networks is to provide ultra-fast data speeds, high-capacity, and reliable services for mobile users. Small cells remain a promising solution for increasing speed and density by dividing a macrocell into smaller zones and spatially reusing radio resources [7]. However, the dense deployment of small cells presents challenges in terms of installation costs and energy consumption, which typically represent main concern of mobile network operators (MNOs) [7, 8]. The C-RAN architecture has been proposed to economically support radio acces network (RAN) densification by centralizing advanced signal processing functionalities in a centralized unit (CU) that serves multiple remote radio units (RRUs) [8]. The proposal involves installing a CU with multiple processing units at a single network location and dynamically interconnecting it with various RRUs deployed in the field through X-haul architectures [9]. The main objective of using this centralized architecture is to leverage the benefits of statistical multiplexing of hardware resources, resulting in higher energy efficiency and cost reduction [10, 11].

The 5G networks must operate across multiple frequency ranges to support a wide range of application scenarios. Among them, the industry focuses on bands including 15 GHz, 18 GHz, 28 GHz, 38 GHz, 45 GHz, 60 GHz, and 72 GHz [12]. To meet this requirement, the 3rd Generation Partnership Project (3GPP) has defined three frequency ranges in the 5G NR standard [13]. The first frequency range (FR1) spans from 0.410 to 7.125 GHz supporting bandwidth (BW) up to 100 MHz. The second frequency range (FR2-1) covers millimeter waves (mm-waves) in the range of 24.5 to 52.6 GHz with BW up to 400 MHz. Finally, the third frequency range (FR2-2) encompasses frequencies from 52.6 to 71 GHz, providing BW up to 2 GHz. The mm-wave band will enable multi-gigabit data transmission due to the large available BW and it is a promising solution for the spectrum scarcity below 6 GHz in future generations of mobile networks [14]. However, considering one of the main challenges of operating at higher frequencies is transmission loss and the requirement of a high-capacity fronthaul interface, analog RoF (A-RoF) and free space optics (FSO) technologies provide an effective solution [15]. These technologies enable transmitting signals with high bandwidth, immunity to electromagnetic interference, and low attenuation.

The traditional method of mm-wave frequency generation in the electrical domain may not be cost-effective due to the requirement of high-speed electrical components, which ultimately limits the overall achievable speed of the generated mm-wave signals [16, 17]. Optical mm-wave generation approaches are attractive for radio-over-fiber (RoF) fronthaul links as they overcome the limitation of electrical components and provide the necessary high-throughput RoF fronthaul for the next generation of RANs [17]. Various photonics mm-wave generation methods have been reported in the past decades and can be categorized into five groups: nonlinear effects based on stimulated Brillouin scattering [18], four-wave mixing [19], optical remote heterodyning [20], dual lasers based on phase locking techniques [21], external modulation techniques [22], and optical frequency combs (OFC) generated by a photonic integrated circuit (PIC) [23]. Among these approaches, the external modulation technique is emerging as a preferred scheme due to its ease of operation, relatively low phase noise, and high spectral purity of mm-wave signals. Traditionally, three modulation techniques that use external modulation have been explored to generate mm-wave frequency signals in the optical domain: optical single sideband (OSSB), double sideband (DSB), and optical carrier suppressed double sideband (CS-DSB) techniques [24]. These methods have been studied in various research works to evaluate their effectiveness in generating high-quality mm-wave signals over RoF links.

Several approaches based on the utilization of photonics techniques for mm-wave generation have being proposed to meet the requirements of 5G and future 6G networks. For instance, in [25] the authors present the integration and experimental performance evaluation of a 5G transceiver based on generalized frequency division multiplexing (GFDM) in a gigabit passive optical network (GPON) utilizing RoF for 5G applications. It has been demonstrated that utilizing techniques such as self-oscillating frequency comb generation (SOFCG) for mm-wave generation in RoF systems is an attractive solution in terms of low phase noise of the signal [26]. Two experimental setups of a hybrid K-band (25 GHz) microwave photonic link (MPL) are examined for seamless broadband wireless access networks [27]. The experimental setups involve optical fiber, FSO, and radiofrequency (RF) wireless channels. Solutions describe the implementation and experimental performance evaluation of a digital signal processing (DSP)-based flexible waveform fiber-wireless (FiWi) system for 5G enhanced mobile broadband (eMBB) and new vertical applications. The proposed RoF fronthaul solution employs a wavelength-division multiplexing passive optical network (WDM-PON) infrastructure, to enable 5G operation across multiple frequency bands [28]. In [29], the authors proposed a solution based on the DSB technique for transmitting 4- and 16-quadrature amplitude modulation (QAM) signals with a bandwidth of 400 MHz at 60 GHz. However, the distance of the optical fronthaul was limited to 1 km, which is relatively short for optical fronthauls applied in 5G networks.

Local and remote mm-wave photonics signal generation schemes are theoretically and experimentally evaluated to compare both approaches for practical deployment in a C-RAN fronthaul network. Practical experiments considering the transmission of quadrature phase shift keying (QPSK) signals with

Table 1. State-of-the-art in network architectures for 5G and 6G Systems.

[Ref] Year	Applied Technology	Application or Architecture	RF Signals	Techniques	Throughput
[24] 2017	A-RoF	Fronthaul	60.25 GHz	CS-DSB and OSSB	5 Gbit/s
[25] 2018	A-RoF	GPON	735 MHz and 26 GHz	DSB	1.1 Gbit/s
[26] 2018	A-RoF	Fronthaul	94.8 GHz	SOFCG	120 Mbit/s
[27] 2019	RoF and FSO	WDM	25 GHz	CS-DSB	300 Mbit/s
[28] 2020	FiWi	WDM-PON	788 MHz, 3.5 and 26 GHz	DSB	4.41 Gbit/s
[29] 2020	A-RoF	GPON	60 GHz	DSB	1.4 Gbit/s
[30] 2021	A-RoF	Fronthaul	40 GHz	CS-DSB	500 Mbit/s
[31] 2021	FiWi and FSO	Fronthaul	788 MHz, 3.5 and 26 GHz	DSB	3 Gbit/s
[32] 2021	A-RoF and FSO	Fronthaul	3.5, 27 and 39 GHz	DSB and CS-DSB	1.4 Gbit/s
[33] 2022	A-RoF	Fronthaul	40 GHz	CS-DSB	100 Mbit/s
[34] 2022	A-RoF	Fronthaul	3.5 and 28 GHz	DSB and OSSB	240 Mbit/s
[35] 2022	D-RoF and A-RoF	WDM-PON	10 and 60 GHz	DSB	40 Gbit/s
[36] 2022	D-RoF and FSO	GPON	Baseband	DSB	600 Mbit/s
[37] 2022	FiWi and FSO	X-HAUL	26 GHz	E/O OFC	4 Gbit/s
[38] 2023	A-RoF and VLC	Fronthaul	25 MHz	DSB	60 Mbit/s
[39] 2023	FiWi	X-HAUL	1.5 and 60 GHz	DSB	408 Mbit/s
This Work	A-RoF FiWi FSO VLC	WDM-PON X-Haul	Baseband 550 MHz 39 GHz 60 GHz	CS-DSB and DSB	1.5 and 11.8 Gbit/s

a 250 MHz BW centered at 0.5 GHz over 10 and 25 km fiber links, also validate the superior performance of the remote setup [30]. Lopes *et. al* [31] reports the implementation and experimental investigation of two different non-standalone 5G NR network architectures, aiming to fulfill the 5G demands. The first implementation applies direct modulation and detection for transmitting fourth-generation of mobile networks (4G) and 5G signals over a 25-km fiber optics fronthaul, followed by 105-m

wireless link. The second proposed architecture relies on a novel and efficient 5G heterogeneous optical-wireless network using RoF, FSO and wireless technologies toward enhanced remote area communications (eRAC) and eMBB applications. In [32], the transmission of 5G NR signals at 39 GHz was investigated for DSB and CS-DSB schemes in a combined A-RoF and FSO link in the 3.5 GHz, 27 GHz, and 39 GHz bands. The authors evaluated the impact of harmonic and intermodulation distortion in data transmission over local and remote photonically generated 40 GHz signal over an optical fronthaul based on a direct modulated laser (DML) and CS-DSB external modulation for frequency up-conversion [33]. Shi*et. al* proposed a dual-band RoF link is proposed where flexible switching between high-frequency RF channels (28 GHz) and low-frequency (3.5 GHz) is achieved through polarization control. The OSSB technique is employed for transmitting signals at 28 GHz, while the DSB technique is used for transmitting the signal at 3.5 GHz [34].

In order to enable bandwidth-intensive 5G applications, an experimental FiWi mobile fronthaul architecture is presented [35], supporting the coexistence of spectrally efficient analog transport formats with digital RoF (D-RoF) transport schemes, combined with high-capacity mm-wave wireless channels. The authors in [36] presented an experimental implementation of a gigabit Ethernet multiple input single output FSO communications link. Adaptive switching techniques, implemented using the GNU Radio open-source software-defined platform, were employed, and the performance of the system was analyzed. The work reported in [38] describes the implementation of a proof-of-concept of a 12.5-km A-RoF fronthaul link followed by an red-green-blue (RGB)-based visible light communication (VLC) link of 1.2 m for 6G applications. The initial proof-of-concept achieved a data throughput of 60 Mbit/s. An experimental demonstration of an OFC for generating 5G NR millimeter-wave signals, was presented in [37]. The proposed approach employs an electrical band-pass filter to isolate the low-phase noise 26 GHz carrier from the 2.6 GHz spaced electrical frequency comb, thus enhancing system spectral efficiency. The performance of the proposed integrated OFC-based 5G system is evaluated according to the 3GPP. In [39], a 4K video transmission at 60 GHz was demonstrated using FiWi technology in an X-Haul transport network infrastructure. Table 1 provides a summary of experimentally implemented works addressing the emerging demands of 5G and 6G.

The present work describes the implementation and experimental analysis of two distinct network architectures for 5G NR, with the goal of meeting the requirements posed by the evolution towards 6G. The first implementation applies the CS-DSB optical technique using two cascaded Mach-Zehnder modulator (MZM) to generate signals at 60 GHz in an RoF-based optical fronthaul. The architecture consists of integrating WDM-PON and RoF technologies within the same network infrastructure, aiming to leverage existing optical networks for the implementation of FiWi systems beyond 5G. In Fig. 1 we propose the simultaneous transmission of three data signals, namely: a 5G NR signal with a 400 MHz bandwidth at 60 GHz; a non-return-to-zero (NRZ) signal with a data rate of 10 Gbit/s; and a base-band signal from an active passive optical network (PON) for fiber to the home (FTTH) applications. The goal is to provide multiple services such as broadband Internet access and indoor mobile communications, while increasing system throughput. The proposed solution allows for a significant reduction in capital expenditures (CAPEX) and enhanced network coverage. For instance, in small cities, MNOs can lease available optical infrastructure from fiber-to-home Internet service providers (ISPs) as fronthaul for their 5G systems, instead of deploying a new optical network [25].

The second proposed architecture is based on a novel and efficient heterogeneous 6G wireless optical network using RoF, FSO, VLC, and wireless technologies for the transport and access layers of the network. It employs a hybrid fronthaul, comprising a 20-km RoF link followed by a 1.5-m FSO link, along with a 2-m indoor wireless access network and a 3-m indoor VLC access network. The additional multi-standard and multi-band optical-wireless network is based on a 20 MHz to 550 MHz bandwidth M-QAM signal and a 400 MHz to 39 GHz bandwidth 5G NR signal. The impact of atmospheric attenuation and turbulence on the FSO fronthaul performance in the RoF/FSO/Wireless heterogeneous networks (HetNet) is unprecedentedly evaluated in terms of the root mean square error vector magnitude (EVM_{RMS}) and in accordance with the 3GPP Release 18 requirements.

The manuscript is structured in four sections. Section 2 describes and presents the investigation of the Integrating WDM-PON and a 60-GHz RoF system towards 6G access networks, whereas Section 3 reports the proposed optical-wireless HetNet using RoF, OWC, and wireless technologies. Finally, the conclusions and future works are drawn in Section 4.

2. HETNET BASED ON ROF AND CS-DSB INTEGRATED INTO A WDM-PON INFRASTRUCTURE

The operational principle of the proposed WDM-PON system architecture relies on applying A-RoF technology to assist 5G/6G communications. The architecture primarily concentrates hardware components at the baseband unit (BBU) pool and facilitates the collective transport of all RF signals to the densely distributed and simplified remote radio head (RRH) by using wavelength-division multiplexing (WDM) couplers and optical fibers. As the optical fiber has a wide available bandwidth, the maximum link capacity is limited by the response of the optical components, such as the electro-optical response of the optical modulators and photodetectors.

Fig. 1 depicts the block diagram of the proposed system (a) and photograph (b). The system employs a photonically frequency doubling technique utilizing one MZM (MZM_1, Fujitsu FTM7939EK) biased at the null point (V_π = 6.6 V) to suppress the optical carrier and a second MZM (MZM_2, Fujitsu FTM7920FB) biased at quadrature point ($V_{\pi/2}$ = 2.6 V) for data modulation. We have employed a distributed-feedback (DFB) laser diode (LD_1) that operates at 1530 nm and has an output power of 15 dBm. A polarization controller (PC) is used to adjust the light polarization state at the MZM inputs. The MZM_1 is fed by an RF_1 = 24.5 GHz single-tone signal from an analog signal generator (ASG) (Keysight N5173B) and generates a CS-DSB signal with a frequency spacing between the sidebands of 49 GHz. An arbitrary waveform generator (AWG) (Keysight M8190A) generates the baseband 5G NR signal and a vector signal generator (VSG) (Keysight PSGE8267D) performs the frequency up-conversion, providing a 5G NR signal at 11 GHz, which is injected into MZM_2. The RF_1 carrier and RF_2 data power levels are 15 and 10 dBm, respectively. Furthermore, a second laser DFB (LD_2) emits an optical carrier with a power level of 5 dBm at 1560 nm. The optical carrier is modulated by the NRZ signal using a MZM (MZM_3, Fujitsu FTM7920FBA). The NRZ signal, operating at a data rate of 10 Gbit/s, is generated by a bit error rate test (BERT, MP2100B) and applied to the MZM_3. Additionally, within the central office (CO), a pair of media converters

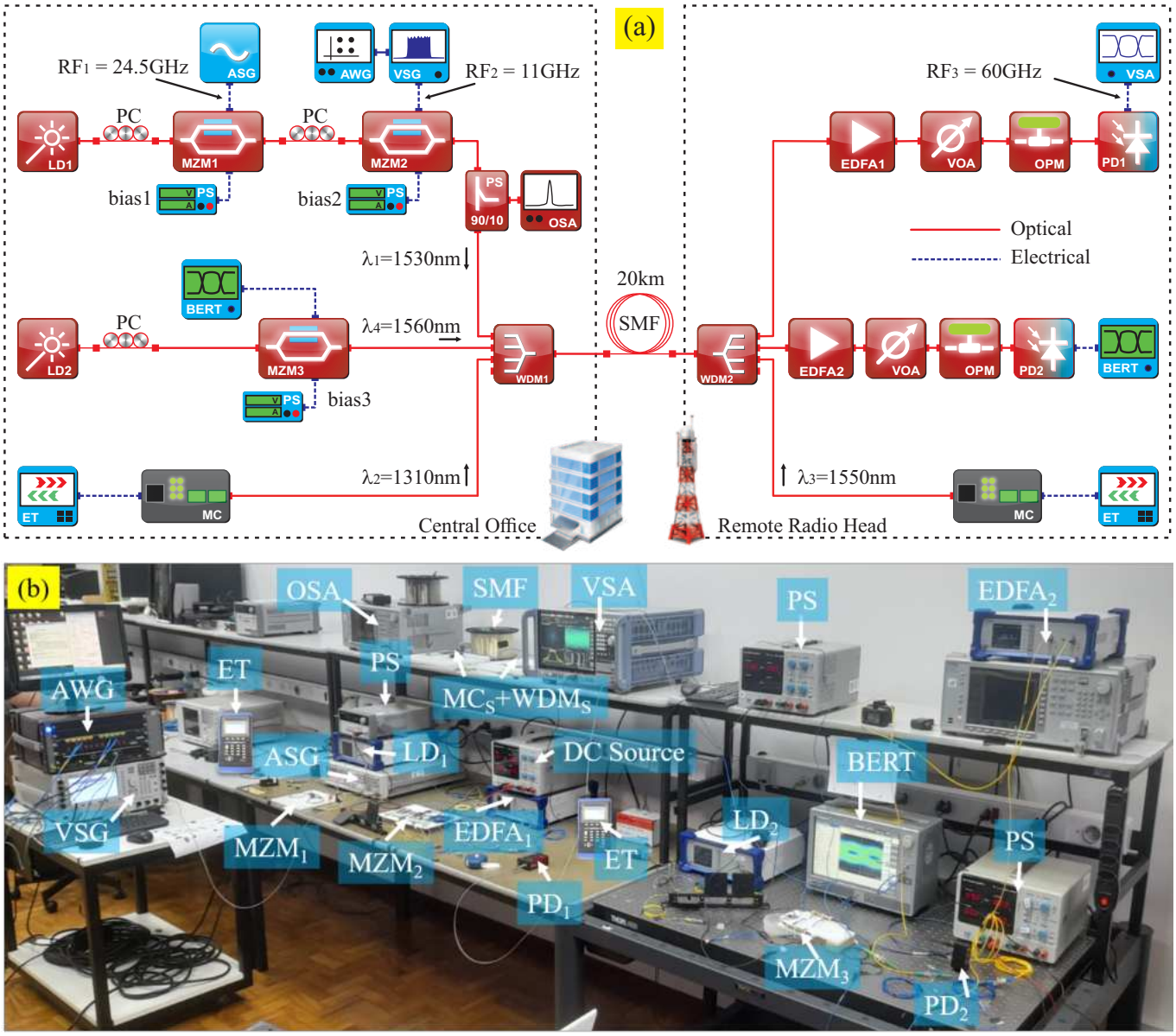

Fig. 1. Block diagram (a) and photograph (b) of the proposed WDM-PON system.

(MCs, GT-806A60) are employed, operating at wavelengths of 1310 nm for downlink and 1550 nm for uplink, respectively. These media converters enable bidirectional transmission of Transmission Control Protocol/Internet Protocol (TCP/IP) over an Ethernet Tester ET (TSW900ETH) in full-duplex mode.

Additionally, a WDM coupler (WDM_1) from Haphit, with an insertion loss of 2 dB, has been used to couple the modulated optical signal from MZMs and the one from MC_1. The resultant signal is launched into an optical fiber composed of 20 km. At the RRH, the WDM_2 component decouples the base-band signals and the RF-modulated optical signal. Two low-noise Erbium-doped fiber amplifiers (EDFAs) can be employed before the photodetectors (PDs) to compensate for the insertion losses of the MZMs, WDM couplers, and other link components. Two variable optical attenuators (VOAs) from Thorlabs (VOA50PM-FC) are employed to adjust the received optical power. The PD_1 (Thorlabs, DXM50AF) and PD_2 (EOT, 5000F) photodetectors receive the optical power of up the 8 dBm at 1530 nm and 0 dBm at 1560 nm, respectively. The received 5G NR signal is evaluated by a vector signal analyzer (VSA, R&S FSW67). A bit error rate tester (BERT) is used to receive and analyze the transmitted NRZ signal at 10 Gbit/s. In parallel, MC_2 receives the -10 dBm optical power at 1310 nm and converts it into Ethernet for feeding ET_2. The returning data traffic is inserted into the network using the MC_2 uplink wavelength at 1550 nm, and the performance analysis is realized by ET_1, which measures the throughput and latency. Thus, it was possible to experimentally assess the integration of various technologies coexisting within a single optical network. Table 2 presents a concise overview of the proposed system pertaining parameters.

The experimental measurement campaign was divided into three parts. The first part presents a performance evaluation of the A-RoF link using the CS-DSB technique for mm-wave generation, specifically at 60 GHz. The second part evaluates the transmission of a 10 Gbit/s NRZ signal, and finally, the third part assesses full-duplex transmission of 1 Gbit/s Ethernet pack-

Table 2. Key parameters of the experimental setup I.

	Parameter	Value
LD_1	Wavelength	1551 nm
	Output Power	15 dBm
LD_2	Wavelength	1560 nm
	Output Power	5 dBm
LD_3	Wavelength	1310 nm
	Output Power	0 dBm
LD_4	Wavelength	1550 nm
	Output Power	-8 dBm
	Power of RF_1 @ 24.5 GHz	15 dBm
	Power of RF_2 @ 11 GHz	10 dBm
MZM_1	Insertion Loss	8 dB
MZM_2	Insertion Loss	6 dB
MZM_3	Insertion Loss	4 dB
	SMF Lenght (loss)	20 km (4.4 dB)
$EDFA_1$	Output Power	9 dBm
	Noise Figure	5 dB
$EDFA_2$	Output Power	0 dBm
	Noise Figure	5 dB
PD_1	Responsivity	0.8 A/W @ 1550 nm
	Bandwidth	50 GHz
PD_2	Responsivity	0.6 A/W @ 1550 nm
	Bandwidth	12.5 GHz

ets. The testing model used was TM3-1, as specified by 3GPP, which outlines 5G NR signal configuration, i.e., subcarrier spacing, duplexing mode, modulation order, frequency range and bandwidth. For instance, in FR2, the testing model employs bandwidths of 50, 100, 200, and 400 MHz, with modulation orders of QPSK, 16-QAM, and 64-QAM. The subcarrier spacing used was 60 kHz for 50 and 100 MHz, and 120 kHz for 200 and 400 MHz. With the aforementioned characteristics of the 5G NR signal generation, a 400 MHz bandwidth signal can achieve a data throughput of up to 1386 Mbit/s when employing 64-QAM.

In the initial experimental analysis, we evaluate the A-RoF link performance in terms of EVM_{RMS} regarding the received optical power level. The 3GPP has specified maximum EVM_{RMS} values of 17.5%, 12.5%, and 8% for QPSK, 16-QAM, and 64-QAM switching, respectively [13]. A variable optical attenuator (VOA) and an optical power monitor (OPM) were employed to vary and visualize the optical power level at the input of the PD, respectively. The power level was varied from 1 to 8 dBm, and at the output of the PD, the electrical signal was demodulated and analyzed using a vector signal analyzer (VSA).

As shown in Fig. 2, four analyses were performed employing different characteristics of the 5G NR signal transmitted at 60 GHz. For a bandwidth of 50 MHz, a 64-QAM modulation scheme was employed, and an optical power level of 8 dBm was required to achieve EVM_{RMS} values below 8%. To increase the data system throughput, a signal with a bandwidth of 100 MHz was transmitted, using a 16-QAM modulation scheme. It was required optical power level of 6 dBm for attaining approximately 12% of EVM_{RMS}. Finally, when QPSK signal is employed with bandwidths of 200 and 400 MHz, the required optical power levels were 4 dBm and 5 dBm, respectively. EVM_{RMS} values of 16.5% and 16.9% were obtained for the 200 MHz and 400 MHz signals, respectively.

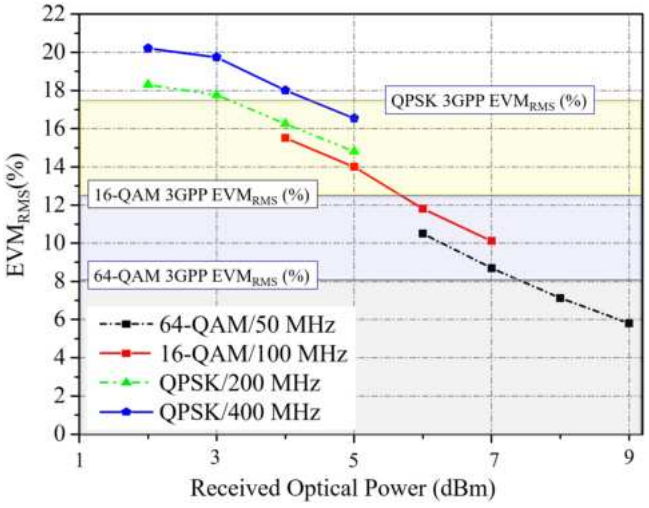

Fig. 2. RoF system digital performance as a function of the received optical power for QPSK, 16-QAM and 64-QAM signals.

The proposed A-RoF system achieved improved performance by optimizing and specifying fixed values of the optical power level at the receiver. For the 50 MHz signal, an EVM_{RMS} of 5.9% was achieved with an equivalent optical power at the receiver of 9 dBm. For the 100 MHz and 200 MHz signals, EVM_{RMS} values of 10.2% and 14.8% were observed with received optical power levels of 6 dBm and 4 dBm, respectively. Finally, the 400 MHz bandwidth signal exhibited the best performance with a received optical power level of 4 dBm. Fig. 3 shows the electrical spectra and constellation diagrams for the four transmitted signals. Specifically, Figs 3. (a) and 3. (b) correspond to the signals with a bandwidth of 50 MHz and 100 MHz, respectively, while Figs. 3. (c) and 3. (d) correspond to the signals with a bandwidth of 200 MHz and 400 MHz, respectively. Based on the measured EVM_{RMS}, it was observed that the system A-RoF proposed in this study adequately meets the specifications of 3GPP Release 18 [13], as the constellation points were clearly defined.

The second part of the measurement campaign is presented in Fig. 4. The experimental evaluation aims to assess the quality of NRZ signal reception as a function of the bit error rate (BER) per received optical power at PD_2. For this analysis, two measurement campaigns were considered. The first campaign, known as optical back-to-back (OB2B), evaluated the performance by connecting the output of MZM_3 to the input of $EDFA_2$. The second campaign involved interconnecting the WDM modules through a 20 km optical fronthaul. In addition to the WDM modules and the optical fronthaul, the second measurement campaign was conducted with all three systems operating simultaneously in the same network architecture. The received optical power was varied from -6 to 0 dBm for evaluating the performance of both

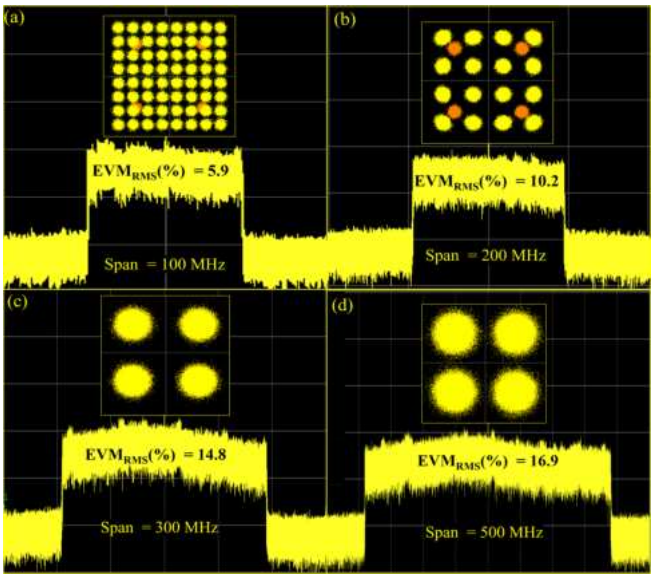

Fig. 3. The 5G NR constellation diagrams and spectra were obtained for four distinct symbol rate signals: (a) 64-QAM with a bandwidth of 50 MHz; (b) 16-QAM with a bandwidth of 100 MHz; (c) QPSK with a bandwidth of 200 MHz; and (d) QPSK with a bandwidth of 400 MHz.

methods.

A BERT was employed at the receiver side to evaluate the quality of the 10 Gbit/s NRZ signal transmission. In the OB2B configuration, the system achieved a BER value of 10^{-10} for a received optical power equivalent to 0 dBm. For the same level of received optical power, the WDM system operating simultaneously with other technologies achieved a BER margin of 10^{-9}. This degradation of the received signal can be attributed to attenuation due to the insertion of WDM modules and the effects of attenuation and dispersion in the optical fiber when the WDM system is operating at its full capacity. For a received optical power of 0 dBm, it is observed that a well-open eye pattern can be obtained with a relatively large dynamic range during a 40-minute measurement time. On the other hand, the measured eye diagram for a received optical power of -5 dBm exhibits distinct characteristics.

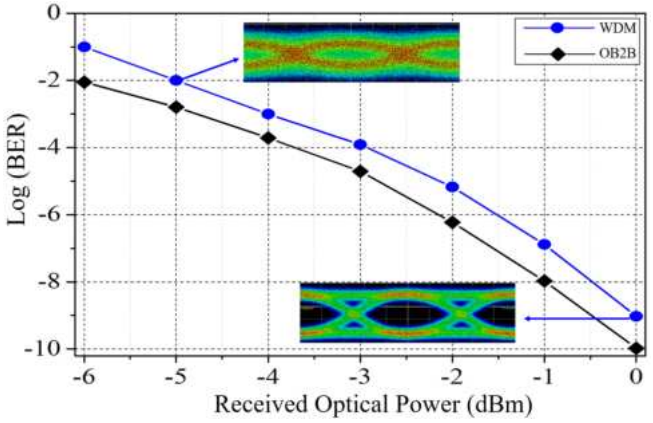

Fig. 4. Bit error rate as a function of the photodetector input power.

Finally, Fig. 5 illustrates the throughput and latency measurements for the transmitted base-band signal over GPON, as a function of frame size and various scenarios proposed in this study. The results indicate that the larger the frame size, the higher the throughput achieved, which remains almost constant across all evaluated scenarios for the corresponding frame sizes. The maximum throughput of over 947 Mbit/s was achieved using frames with 1518 Bytes, as observed in Fig. 5 (a). Additionally, the coexistence of WDM-PON and RF signals did not significantly affect the latency, as it remained almost constant for all scenarios and corresponding frame sizes. The maximum latency of only 5 μs was observed for the 1518 Bytes package, as presented in Fig. 5 (b). It is noteworthy that the WDM-PON was not able to achieve 1 Gbit/s, as provided by the Ethernet tester, even for the back-to-back (B2B) scenario, due to the transmission protocol and frame encapsulation limitations imposed by the media converter when using its electrical interface. Furthermore, the throughput and latency measurements for point-to-multipoint distribution were also successful, as they were in agreement with the expected behavior of a WDM-PON.

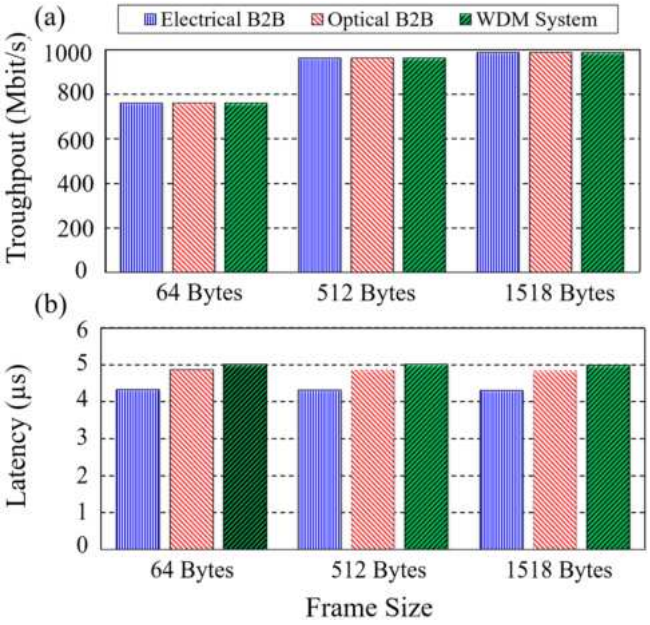

Fig. 5. GPON performance as a function of frame sizes: (a) Throughput; (b) Latency.

3. IMPLEMENTATION OF A HYBRID FIWI SYSTEM USING FSO, VLC AND MM-WAVES TOWARDS 6G APPLICATIONS

The schematic diagram of the experimental setup is depicted in Fig. 6 (a) and (b) respectively. All technologies are converged into a unified architecture, which employs a hybrid RoF/FSO link to integrate the midhaul and fronthaul of the network, while access is provided by a wireless link operating at 39 GHz, along with a VLC link operating at 550 MHz. The base-band 5G NR signal is designed using Keysight Signal Studio software and generated by a Keysight arbitrary waveform generator (AWG) M8190A. The test model 3.1 (TM 3.1) generated by the software was specified by 3GPP Release 15, which specifies that the 5G NR signal in frequency range 2 (FR2) operates with band-

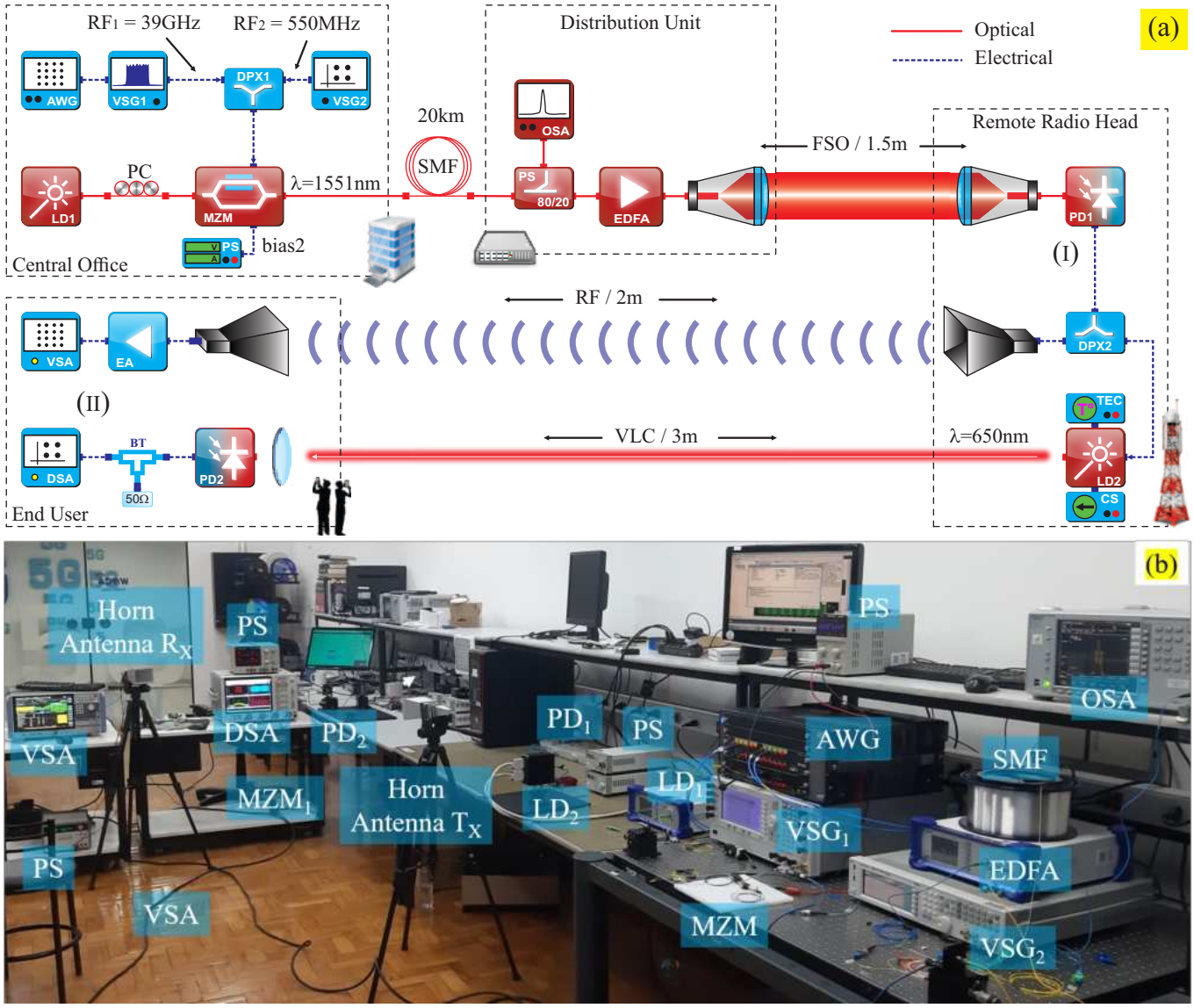

Fig. 6. Block diagram (a) and photograph (b) of the proposed system.

widths of up to 400 MHz and QPSK, 16-QAM, and 64-QAM modulation schemes. The base-band signal is applied to a VSG_1 (PSG-E8267D), which is used to convert the signal to RF_1 = 39 GHz and transmit it at a power of 4 dBm. In parallel, the M-QAM signal is generated by a VSG_2 (EXGN5172B) at RF_2 = 550 MHz with a transmission power equal to -10 dBm. The two RF signals are combined by a diplexer DPX_1 (DPX1721) before being applied to a single MZM (FTM7939EK). The MZM modulates an optical carrier from a laser centered at 1551 nm (LD_1) using the combined RF signals. The LD_1 transmission power is equal to 15 dBm, and the modulated optical signal is then launched into a 20 km single-mode fiber (SMF), giving rise to the optical midhaul.

We split the signal using an 80/20 optical splitter, in which 20% is applied to an optical spectrum analyzer (OSA) for real-time frequency domain measurements, and the remaining optical signal is amplified by an EDFA. The EDFA is located in the distribution unit (DU) that is connected to a RRH via a fronthaul link, which can be either optical or wireless. Afterward, the modulated optical signal reaches a collimator CFS18 for transmission and reception. A 1.5-m FSO fronthaul has been implemented as a proof-of-concept, integrating the hybrid RoF/FSO application. It is worth mentioning that FSO systems have a maximum allowed optical power to keep an eye-safe environment. Infrared communication around 1.5 μm does not reach the retina, however, optical beams with a diameter lower than 1 cm and power higher than 10 dBm imply risks to the human eyes. After being irradiated, the optical signal is photodetected by a 50 GHz bandwidth PD (DMX50AF) and separated by a DPX_2 (DPX1721) for analysis in the VSA.

Two distinct access networks were considered in this study. The first one is a wireless transmission using a pair of horn antennas with gains of 30 dBi each. In this case, the received signal is amplified by a 35 dB gain electrical amplifier (EA)(QLW-36464835) before being received and analyzed by the VSA (R&S FSW67). The other access network is based on a 3-m range VLC link for point-to-point applications. A red LD_2 at 650 nm is used to transmit the signal. On the receiver side, an optical lens is employed to focus the signal, which will be photodetected by another PD_2. Finally, the signal quality is evaluated using a digital signal analyzer (DSA) (V084A) from Keysight. Table 3 presents a concise overview of the primary parameters pertaining to the

proposed system.

Table 3. Key parameters of the experimental setup II.

	Parameter	Value
LD_1	Wavelength	1551 nm
	Output Power	15 dBm
LD_2	Wavelength	650 nm
	Output Power	4 dBm
	Power of RF_1 @ 39 GHz	4 dBm
	Power of RF_2 @ 550 MHz	-10 dBm
MZM_1	Insertion Loss	8 dB
	SMF Lenght (loss)	20 km (4.4 dB)
	FSO Lenght (loss)	1.5m (3 dB)
$EDFA_1$	Output Power	5 dBm
	Noise Figure	5 dB
PD_1	Responsivity	0.8 A/W @ 1550 nm
	Bandwidth	50 GHz
EA	Wireless Lenght	2m
	Gain and (NF)	35 dB and (4.8 dB)
	VLC Lenght	3m
PD_2	Responsivity	0.4 A/W @ 650 nm
	Bandwidth	1.2 GHz

The system performance investigation consisted of evaluating the hybrid architecture at the marks labeled (I) and (II) from Fig. 6 (a). The first investigated scenario (I), consisted of evaluating the system fronthaul performance at the PD output. In other words, evaluating the performance of the RoF followed by an FSO link. The second case (II) is regarding the analysis of the 6G FiWi/VLC systems implementation employing RoF and FSO as a midhaul and fronthaul. In both scenarios, the system performance has been realized in terms of EVM_{RMS} in accordance with the 3GPP Release 18 recommendations, namely: maximum EVM_{RMS} value of 8%, 12.5%, and 17.5% for 64-QAM, 16-QAM and QPSK, respectively.

Fig. 7 depicts the performance of the received signal as a function of the measured EVM_{RMS} regarding the optical power at the photodetector input. For the presented analysis, the 5G NR signal at 60 GHz was used with bandwidths of 50, 100, 200, and 400 MHz, employing a single modulation scheme of 64-QAM. The received optical power was controlled at the photodetector input by using a VOA and an OPM, leading to an optical power ranging from -5 to 5 dBm. The attenuation of optical power can be utilized to emulate atmospheric turbulence such as rain, fog, and visibility, enabling the analysis of their impact on FSO links. Particularly for a bandwidth of 50 MHz, the proposed RoF/FSO system easily met the 3GPP specifications for optical power levels higher than -6 dBm. To increase the data throughput of the system, the bandwidth was increased to 100 MHz, requiring an additional 1 dB of optical power level at the reception. For signals with bandwidths of 200 and 400 MHz, a reception optical power level of -3 dBm and -2 dBm, respectively, was necessary. The best performance point was around 5 dBm optical power and the EVM_{RMS} values were 3%, 3.9%, 4.8%, and 5.9% for 50, 100, 200, and 400 MHz bandwidth, respectively, attaining up the 1.38 Gbit/s throughput.

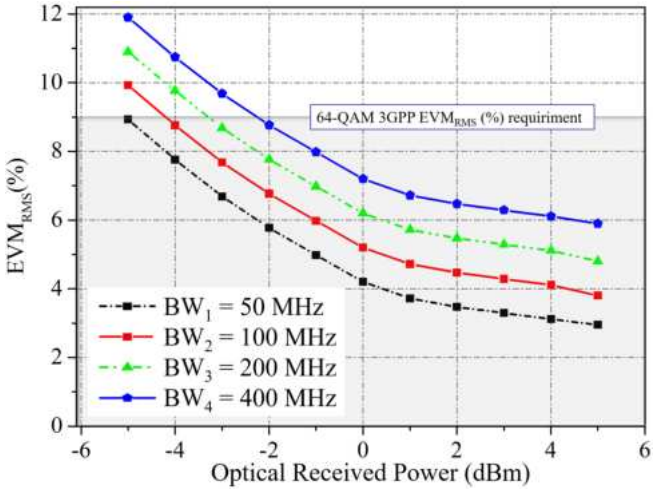

Fig. 7. RoF/FSO system digital performance as a function of the received optical power for 64-QAM signals.

The electric spectrum illustrated in Fig 8 presents the reception power levels for the 5G NR signal transmitted at 39 GHz and different bandwidths, which determine the frequency range FR2-1: 50, 100, 200, and 400 MHz represented by BW_1, BW_2, BW_3, and BW_4, respectively. The TM 3.1 test model was employed for generating this signal, and some characteristics related to the generation will be described as follows: the signal was transmitted using 50 and 100 MHz bandwidth and subcarrier spacing of 60 kHz, which results in data throughput of 178 and 360 Mbit/s, respectively. Considering signals with a bandwidth of 200 and 400 MHz, a spacing of 120 kHz was utilized between the subcarriers, resulting in a data throughput of approximately 692 and 1386 Mbit/s, respectively [32].

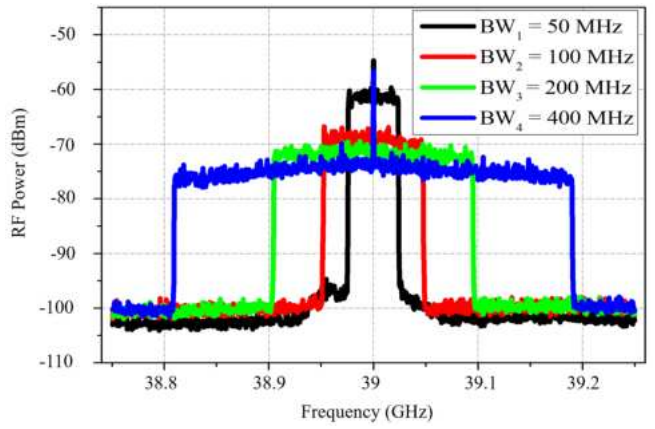

Fig. 8. Electrical spectrum measured at the output of the photodetector for bandwidths 50, 100, 200 and 400 MHz.

The second and most significant characterization of the proposed architecture involved the performance analysis of the system operating simultaneously with a wireless link at 39 GHz and a VLC link at 550 MHz, marked as (II) in Fig. 6(a). We

selected the optimal performance point of around 5 dBm of optical power at the reception of PD_1 to implement the hybrid 6G system. Fig. 9 presents the digital performance of the 16-QAM link operating at 550 MHz for the B2B, RoF/FSO/VLC, and RoF/FSO/VLC/Wireless configurations, including the measured constellations. The B2B condition involves directly connecting the vector signal generator and the vector signal analyzer using an RF cable, allowing us to quantify the impact of implementing the RoF/FSO and FiWi/VLC systems in terms of EVM_{RMS}.

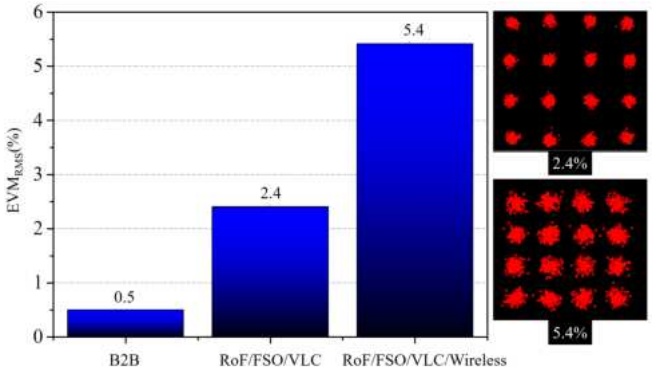

Fig. 9. *M*-QAM FiWi digital performance analysis at 550 MHz employing the hybrid RoF/FSO/VLC and Wireless System.

As expected, the EVM_{RMS} value for B2B was below 0.5%, resulting in an extremely well-defined constellation. The implementation of RoF/FSO/VLC did not degrade the overall system performance, and consequently, the EVM_{RMS} value was not significantly increased, around 2.4%. The VLC channel degrades the signal both in phase and magnitude, which is reflected in the symbol dispersion in the RoF/FSO/VLC/Wireless constellation. However, the *M*-QAM VLC system met the 3GPP requirements for modulation orders up to 64-QAM. Therefore, the hybrid 5G NR approach showed potential for integrating 6G networks, bringing the notable benefit of FSO flexibility.

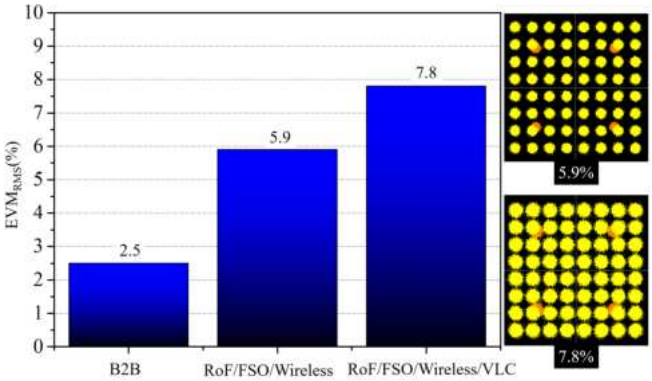

Fig. 10. 5G NR FiWi digital performance analysis at 39 GHz employing the hybrid RoF/FSO/Wireless and VLC System.

Similarly, the 400 MHz bandwidth 5G NR signal was experimentally evaluated for the B2B, RoF/FSO/Wireless, and RoF/FSO/Wireless/VLC systems, as presented in Fig. 10. Excellent digital performance is observed for the B2B and RoF/FSO cases, achieving EVM_{RMS} levels of 2.5% and 5.9%, respectively. After propagating the 39 GHz 5G NR signal over a distance of 2 meters, the measured EVM_{RMS} level was around 7.8%, close to the maximum acceptable value of 8%. The degradation in digital performance can be observed in the constellation, highlighting the challenging conditions of the wireless channel when operating at mm-wave frequencies. However, the hybrid RoF/FSO/VLC/Wireless system achieved a data throughput of approximately 1.46 Gbit/s, in accordance with the recommendations of 3GPP Release 18, demonstrating the feasibility of the FiWi 5G NR system employing different technologies to compose a hybrid network architecture.

Fig. 11 depicts the measured electrical spectrum at the output of the electrical amplifier. As illustrated, the 39 GHz transmitted 5G NR signal does not exhibit severe degradation along a wireless channel. A 67 GHz span was captured to demonstrate the feasibility of the proposed system. The most distinct spectrum is observed within the box represented in the figure, spanning 500 MHz, and with the use of an EA with a gain of 35 dB at the reception, the loss due to the wireless channel was compensated, and the observed EVM_{RMS} level was 7.8%, thus achieving a transmission rate of 1.5 Gbit/s considering the two access networks.

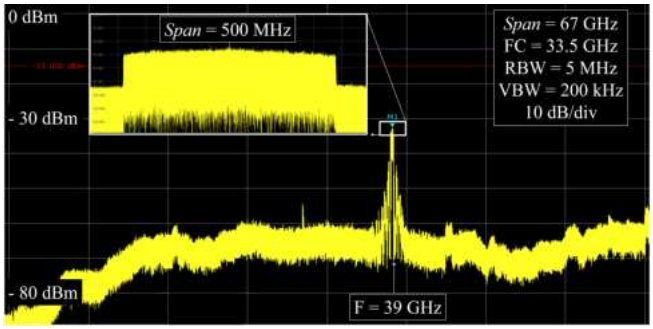

Fig. 11. Electrical spectrum measured after FiWi 5G NR transmission at 39 GHz.

4. CONCLUSIONS

We have successfully proposed and implemented an efficient FiWi system for 5G/6G optical-wireless scenarios, encompassing both indoor and outdoor applications. Two architectures were proposed, and their performance was evaluated based on the specifications outlined in 3GPP Release 18. The first evaluated architecture involves the integration of an A-RoF based optical fronthaul operating in mm-wave frequencies within a WDM-PON network. This approach utilized the CS-DSB technique to generate signals in the 60 GHz band. This solution enabled the generation and transport of a 5G NR signal at 60 GHz, with a bandwidth of 400 MHz and a QPSK modulation scheme. The obtained results demonstrated the feasibility of this approach in meeting the demands of cell densification for 5G/6G networks, achieving a total system data throughput of up to 11.8 Gbit/s.

The second experimental configuration converges into a unified network architecture that combines solutions based on FiWi, FSO, and VLC to fulfill the requirements of 6G solutions. This architecture, based on the concept of a C-RAN, utilized 20 km of optical fiber followed by an FSO link as the fronthaul of the network. In the access network, a 5G NR millimeter-wave link at 39 GHz is implemented, while enabling simultaneous VLC transmission using an M-QAM signal at 550 MHz for indoor 6G applications. Experimental results demonstrated satisfactory

coexistence among the employed technologies, achieving a total data throughput of 1.5 Gbit/s. The hybrid FiWi/OWC fronthaul solution has shown potential in increasing the flexibility of RANs by providing coverage in hard-to-reach areas. Future work includes implementing the proposed architecture for both downlink and uplink, as well as extending the range of FSO to hundreds of meters in outdoor scenarios.

FUNDING

This work was partially supported by RNP, with resources from MCTIC, Grant No. 01245.020548/2021-07, under the Brazil 6G project of the Radiocommunication Reference Center (Centro de Referência em Radiocomunicações - CRR) of the National Institute of Telecommunications (Instituto Nacional de Telecomunicações - Inatel), Brazil, and by Huawei, under the project Advanced Academic Education in Telecommunications Networks and Systems, contract No PPA6001BRA23032110257684. The authors also thank the financial support from CNPq, CAPES, FINEP, FAPEMIG and FAPESP (Contracts # 2021/06569-1 e # 2022/09319-9).

REFERENCES

1. Y. L. Lee, D. Qin, L.-C. Wang, and G. H. Sim, "6G Massive Radio Access Networks: Key Applications, Requirements and Challenges," IEEE Open J. Veh. Technol. **2**, 54–66 (2021).
2. A. Dogra, R. K. Jha, and S. Jain, "A Survey on Beyond 5G Network With the Advent of 6G: Architecture and Emerging Technologies," IEEE Access **9**, 67512–67547 (2021).
3. R. M. Borges, C. H. de Souza Lopes, E. S. Lima, M. A. de Oliveira, M. S. B. Cunha, L. C. Alexandre, L. G. da Silva, L. A. M. Pereira, D. H. Spadoti, M. A. Romero, and A. C. Sodré Junior, "Integrating Optical and Wireless Techniques towards Novel Fronthaul and Access Architectures in a 5G NR Framework," Appl. Sci. **11** (2021).
4. S. Dang, O. Amin, B. Shihada, and M.-S. Alouini, "What should 6g be?" Nat. Electron. **3**, 20–29 (2020).
5. N. Chen and M. Okada, "Toward 6g internet of things and the convergence with rof system," IEEE Internet Things J. **8**, 8719–8733 (2021).
6. L. Augusto Melo Pereira, L. L. Mendes, C. J. A. Bastos Filho, and A. Cerqueira Sodre, "Amplified radio-over-fiber system linearization using recurrent neural networks," J. Opt. Commun. Netw. **15**, 144–154 (2023).
7. Y. Yoshida, "Mobile Xhaul Evolution: Enabling Tools for a Flexible 5G Xhaul Network," in *2018 Optical Fiber Communications Conference and Exposition (OFC),* (2018), pp. 1–85.
8. C.-L. I, H. Li, J. Korhonen, J. Huang, and L. Han, "RAN Revolution With NGFI (xhaul) for 5G," J. Light. Technol. **36**, 541–550 (2018).
9. P. Zhu, Y. Yoshida, and K.-i. Kitayama, "Ultra-Low-Latency, High-Fidelity Analog-to-Digital-Compression Radio-Over-Fiber (ADX-RoF) for MIMO Fronthaul in 5G and Beyond," J. Light. Technol. **39**, 511–519 (2021).
10. X. Ge, S. Tu, G. Mao, C.-X. Wang, and T. Han, "5G Ultra-Dense Cellular Networks," IEEE Wirel. Commun. **23**, 72–79 (2016).
11. J. Navarro-Ortiz, P. Romero-Diaz, S. Sendra, P. Ameigeiras, J. J. Ramos-Munoz, and J. M. Lopez-Soler, "A survey on 5G usage scenarios and traffic models," IEEE Commun. Surv. & Tutorials **22**, 905–929 (2020).
12. K. Zeb, X. Zhang, and Z. Lu, "High Capacity Mode Division Multiplexing Based MIMO Enabled All-Optical Analog Millimeter-Wave Over Fiber Fronthaul Architecture for 5G and Beyond," IEEE Access **7**, 89522–89533 (2019).
13. 3GPP, "Technical Specification Group Radio Access Network; NR; Base Station (BS) radio transmission and reception; Part-1," Technical Specification (TS) 38.104, 3rd Generation Partnership Project (3GPP) (2023). TS 38.104 version 18.1.0 Release 18.
14. J. Lee, E. Tejedor, K. Ranta-aho, H. Wang, K.-T. Lee, E. Semaan, E. Mohyeldin, J. Song, C. Bergljung, and S. Jung, "Spectrum for 5G: Global Status, Challenges, and Enabling Technologies," IEEE Commun. Mag. **56**, 12–18 (2018).
15. A. Ghosh, A. Maeder, M. Baker, and D. Chandramouli, "5G Evolution: A View on 5G Cellular Technology Beyond 3GPP Release 15," IEEE Access **7**, 127639–127651 (2019).
16. J. Yu, G.-K. Chang, Z. Jia, A. Chowdhury, M.-F. Huang, H.-C. Chien, Y.-T. Hsueh, W. Jian, C. Liu, and Z. Dong, "Cost-Effective Optical Millimeter Technologies and Field Demonstrations for Very High Throughput Wireless-Over-Fiber Access Systems," J. Light. Technol. **28**, 2376–2397 (2010).
17. Y. Wang, L. Pei, J. Li, and Y. Li, "Millimeter-Wave Signal Generation With Tunable Frequency Multiplication Factor by Employing UFBG-Based Acousto-Optic Tunable Filter," IEEE Photonics J. **9**, 1–10 (2017).
18. J. Li, H. Lee, and K. J. Vahala, "Microwave synthesizer using an on-chip Brillouin oscillator," Nat. communications **4**, 2097 (2013).
19. P.-T. Shih, J. Chen, C.-T. Lin, W.-J. Jiang, H.-S. Huang, P.-C. Peng, and S. Chi, "Optical Millimeter-Wave Signal Generation Via Frequency 12-Tupling," J. Light. Technol. **28**, 71–78 (2010).
20. J. Li, T. Ning, L. Pei, C. Qi, Q. Zhou, X. Hu, and S. Gao, "60 GHz millimeter-wave generator based on a frequency-quadrupling feed-forward modulation technique," Opt. letters **35**, 3619–3621 (2010).
21. C. Lim, M. Attygalle, A. Nirmalathas, D. Novak, and R. Waterhouse, "Analysis of optical carrier-to-sideband ratio for improving transmission performance in fiber-radio links," IEEE Transactions on Microw. Theory Tech. **54**, 2181–2187 (2006).
22. G. H. Smith, D. Novak, and Z. Ahmed, "Overcoming chromatic-dispersion effects in fiber-wireless systems incorporating external modulators," IEEE Transactions on microwave theory techniques **45**, 1410–1415 (1997).
23. J. Liu, E. Lucas, A. S. Raja, J. He, J. Riemensberger, R. N. Wang, M. Karpov, H. Guo, R. Bouchand, and T. J. Kippenberg, "Photonic microwave generation in the X-and K-band using integrated soliton microcombs," Nat. Photonics **14**, 486–491 (2020).
24. Y. Tian, K.-L. Lee, C. Lim, and A. Nirmalathas, "60 GHz Analog Radio-Over-Fiber Fronthaul Investigations," J. Light. Technol. **35**, 4304–4310 (2017).
25. R. M. Borges, T. R. R. Marins, M. S. B. Cunha, H. R. D. Filgueiras, I. F. da Costa, R. N. da Silva, D. H. Spadoti, L. L. Mendes, and A. C. Sodré, "Integration of a GFDM-Based 5G Transceiver in a GPON Using Radio Over Fiber Technology," J. Light. Technol. **36**, 4468–4477 (2018).
26. G. K. M. Hasanuzzaman, A. Kanno, P. T. Dat, and S. Iezekiel, "Self-Oscillating Optical Frequency Comb: Application to Low Phase Noise Millimeter Wave Generation and Radio-Over-Fiber Link," J. Light. Technol. **36**, 4535–4542 (2018).
27. D.-N. Nguyen, J. Bohata, J. Spacil, D. Dousek, M. Komanec, S. Zvanovec, Z. Ghassemlooy, and B. Ortega, "M-QAM transmission over hybrid microwave photonic links at the K-band," Opt. express **27**, 33745–33756 (2019).
28. R. M. Borges, L. A. Melo Pereira, H. Rodrigues Dias Filgueiras, A. Carvalho Ferreira, M. Seda Borsato Cunha, E. Raimundo Neto, D. H. Spadoti, L. Leonel Mendes, and A. Cerqueira S., "DSP-Based Flexible-Waveform and Multi-Application 5G Fiber-Wireless System," J. Light. Technol. **38**, 642–653 (2020).
29. K. Kanta, A. Pagano, E. Ruggeri, M. Agus, I. Stratakos, R. Mercinelli, C. Vagionas, P. Toumasis, G. Kalfas, G. Giannoulis, A. Miliou, G. Lentaris, D. Apostolopoulos, N. Pleros, D. Soudris, and H. Avramopoulos, "Analog fiber-wireless downlink transmission of IFoF/mmWave over in-field deployed legacy PON infrastructure for 5G fronthauling," J. Opt. Commun. Netw. **12**, D57–D65 (2020).
30. L. Vallejo, J. Mora, D.-N. Nguyen, J. Bohata, V. Almenar, S. Zvanovec, and B. Ortega, "On the 40 GHz Remote Versus Local Photonic Generation for DML-Based C-RAN Optical Fronthaul," J. Light. Technol. **39**, 6712–6723 (2021).
31. C. H. d. S. Lopes, E. S. Lima, L. A. M. Pereira, R. M. Borges, A. C. Ferreira, M. Abreu, W. D. Dias, D. H. Spadoti, L. L. Mendes, and A. C. S. Junior, "Non-Standalone 5G NR Fiber-Wireless System Using FSO and Fiber-Optics Fronthauls," J. Light. Technol. **39**, 406–417 (2021).
32. J. Bohata, D. Nguyen, J. Spáčil, M. Komanec, B. Ortega, L. Vallejo,

Z. Ghassemlooy, and S. Zvánovec, "Experimental comparison of DSB and CS-DSB mmW formats over a hybrid fiber and FSO fronthaul network for 5G," Opt. Express **29**, 27768–27782 (2021).
33. L. Vallejo, J. Mora, and B. Ortega, "Harmonic and Intermodulation Distortion Analysis in Directly Modulated Lasers Over Local and Remote Photonically Generated Millimeter-Wave Signals," J. Light. Technol. **40**, 5128–5140 (2022).
34. F. Shi, Y. Fan, X. Wang, W. Zhang, and Y. Gao, "High-performance dual-band radio-over-fiber link for future 5G radio access applications," J. Opt. Commun. Netw. **14**, 267–277 (2022).
35. E. Ruggeri, C. Vagionas, R. Maximidis, G. Kalfas, D. Spasopoulos, N. Terzenidis, R. M. Oldenbeuving, P. W. L. van Dijk, C. G. H. Roeloffzen, N. Pleros, and A. Miliou, "Reconfigurable Fiber Wireless Fronthaul With A-RoF and D-RoF Co-Existence Through a Si3N4 ROADM for Heterogeneous Mmwave 5G C-RANs," J. Light. Technol. **40**, 5514–5521 (2022).
36. Z. Htay, C. Guerra-Yanez, Z. Ghassemlooy, S. Zvanovec, M. M. Abadi, and A. Burton, "Experimental real-time GbE MIMO FSO under fog conditions with software defined GNU Radio platform-based adaptive switching," J. Opt. Commun. Netw. **14**, 629–639 (2022).
37. E. S. Lima, R. M. Borges, N. Andriolli, E. Conforti, G. Contestabile, and A. C. Sodré Jr, "Integrated optical frequency comb for 5G NR Xhauls," Sci. Reports **12**, 16421 (2022).
38. T. P. Andrade, L. C. de Souza, E. S. Lima, and A. C. Sodré, "Demonstration of a hybrid A-RoF/VLC system for beyond 5G applications," Appl. Opt. **62**, C115–C121 (2023).
39. C. Vagionas, R. Maximidis, I. Stratakos, A. Margaris, A. Mesodiakaki, M. Gatzianas, K. Kanta, P. Toumasis, G. Giannoulis, D. Apostolopoulos *et al.*, "End-to-End Real-Time Service Provisioning over a SDN-controllable analog mmWave Fiber-Wireless 5G X-haul Network," J. Light. Technol. (2023).

Artigo 2: Implementation of a Hybrid FiWi System Using FSO, VLC and mm-Waves Toward 6G Applications

Celso Henrique de Souza Lopes, Luiz Augusto Melo Pereira, Tomas Powell Villena Andrade, Antonella Bogoni, Evandro Conforti and Arismar Cerqueira. S. Jr. ”Implementation of a Hybrid FiWi System Using FSO, VLC and mm-Waves Toward 6G Applications”, *IEEE Photonics Technology Letters (PTL)* VOL. 35, 2023.

Implementation of a Hybrid FiWi System Using FSO, VLC and mm-Waves Toward 6G Applications

Celso Henrique de Souza Lopes, Tomas Powell Villena Andrade, Luiz Augusto Melo Pereira, Antonella Bogoni, *Senior Member, IEEE*, Evandro Conforti, *Life Senior Member, IEEE*, and Arismar Cerqueira Sodré Jr.

***Abstract*— This letter presents an experimental investigation that integrates various technologies, such as fiber-wireless (FiWi), free-space optics (FSO), and visible light communication (VLC), as a network physical layer solution to meet the requirements for 5G and beyond scenarios. The implemented architecture is centered on the concept of a centralized radio access network (C-RAN), utilizing 20 km of optical fiber followed by an FSO link as the fronthaul of the network, with a focus on last-mile applications. In the access network, a 2-meters reach 5G New Radio (NR) mm-wave link operating at 39 GHz was simultaneously deployed with a VLC transmission utilizing quadrature amplitude modulation (M-QAM) at 550 MHz. The experimental results demonstrate a satisfactory coexistence among these technologies, achieving a total data throughput of 4.92 Gbit/s. The proposed architecture underwent evaluation based on the root mean square error vector magnitude (EVM_{RMS}) requirements specified in the 3rd Generation Partnership Project (3GPP) Release 18.**

***Index Terms*— 5G NR, 6G, microwave photonics, millimeter wave, OWC, radio over fiber.**

I. Introduction

MOTIVATED by the growing need for high data rates, increased cell densification, and low latency for human and/or machine communication, next-generation wireless systems, including radio access network (RAN), have received considerable attention from academia and industry [1]. The deployment of fifth-generation of mobile network (5G) technology allows for the implementation of a variety of new value-added applications, with enhanced mobile broadband being the primary focus, while other scenarios continue to mature [2]. Technical solutions such as the 5G New Radio (5G NR) standard, employment of millimeter-wave (mm-wave) spectrum, heterogeneous networks, centralized radio access network (C-RAN), optical-wireless communications (OWC), and optical-wireless convergence are proposed to meet the imminent demands of 5G [3].

X-Haul networks are a vital category of telecommunications infrastructure designed to meet the increasing demand for high-speed, low-latency connectivity, especially in the context of beyond 5G (B5G) networks [4]. They play a crucial role in deploying advanced technologies like 5G and future communication networks, carrying various services including data, voice, and video. X-Hauls feature a flexible architecture covering access, aggregation, and transport networks, facilitating seamless interconnection of devices, base stations, and data processing centers. The ability to dynamically adapt and optimize X-Haul infrastructure in real-time is essential for meeting the performance demands of next-generation applications and ensuring reliable, high-quality connectivity [5].

OWC has emerged as a promising solution to address the challenges of radiofrequency (RF) spectrum congestion and wireless throughput limitations. In OWC systems, the electrical signal is modulated onto an optical carrier, which is then transmitted through free space using wavelengths spanning from ultraviolet to infrared, encompassing the visible spectrum [6]. This technology offers significant advantages over traditional RF access points, including cost-effectiveness due to the absence of electromagnetic spectrum licensing requirements, immunity to electromagnetic interference enabling deployment in restricted areas, low power consumption (energy efficiency), and a broad spectrum allocation for data transmission, achieving throughput comparable to optical fiber. However, it is susceptible to atmospheric conditions and requires an unobstructed line of sight. In contrast, visible-light communication (VLC) is limited by its range and vulnerability to ambient light. The choice between free-space optics (FSO) and VLC depends on specific application requirements, considering factors such as range, security, and environmental conditions for an optimal wireless optical solution [7].

Technical and innovative solutions are being proposed to meet the demands required by 5G/sixth-generation of mobile network (6G). In article [8], two non-standalone 5G NR solutions were proposed to meet the initial demands of 5G. Different technologies were employed for the fronthaul application, including optical fiber and FSO for last-mile

Manuscript received 20 July 2023; revised 20 September 2023; accepted 15 October 2023. Date of publication 24 October 2023; date of current version 10 November 2023. This work was supported in part by RNP, with resources from MCTIC, under the Brazil 6G Project of the Radiocommunication Reference Center (CRR) of the National Institute of Telecommunications (Inatel), Brazil, under Grant 01245.020548/2021-07; in part by Huawei under the Project Advanced Academic Education in Telecommunications Networks and Systems under Contract PPA6001BRA23032110257684; and in part by CNPq, CAPES, FINEP, FAPEMIG, and FAPESP under Contract 2021/06569-1 and Contract 2022/09319-9. *(Corresponding author: Celso Henrique de Souza Lopes.)*

Celso Henrique de Souza Lopes, Tomas Powell Villena Andrade, Luiz Augusto Melo Pereira, and Arismar Cerqueira Sodré Jr. are with the Laboratory WOCA, Inatel, Santa Rita do Sapucaí 37540-000, Brazil (e-mail: celso.henrique@dtel.inatel.br; tomasvillena@dtel.inatel.br; luiz.melo@inatel.br; arismar@inatel.br).

Antonella Bogoni is with Scuola Superiore Sant'Anna, 56124 Pisa, Italy.

Evandro Conforti is with DECOM, University of Campinas, Campinas 13083-970, Brazil.

Color versions of one or more figures in this letter are available at https://doi.org/10.1109/LPT.2023.3327210.

Digital Object Identifier 10.1109/LPT.2023.3327210

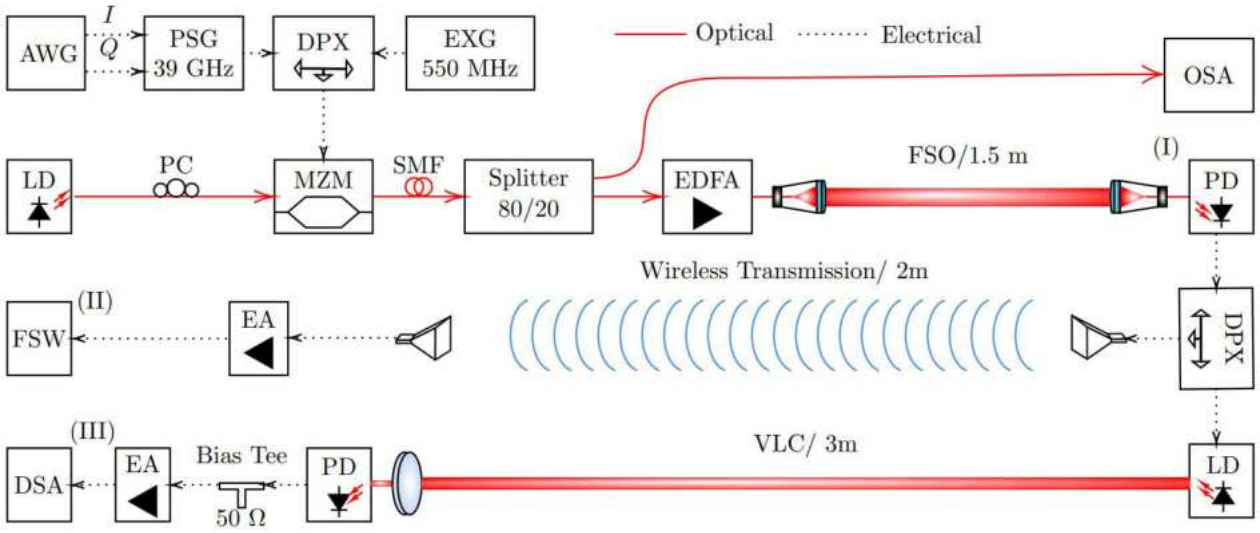

Fig. 1. Block diagram of the proposed system. AWG – arbitrary waveform generator; VSG – vector signal generator; OSA - optical spectrum analyzer; EDFA - amplifier erbium-doped fiber; LD – laser diode; DPX - diplexer; MZM – mach-zehnder modulator; SMF – single mode fiber; PD – photodetector; VSA - vector signal analyzer; DSA - digital signal analyser; SSA - signal and spectrum analyzer; EA - electrical amplifier.

applications. The experimental results demonstrated a secure and effective convergence between these technologies, achieving a data throughput of up to 3 Gbit/s. In [9], the authors presented an experimental measurement campaign involving a hybrid architecture proposal based on analog radio-over-fiber (A-RoF) and FSO to compose the 5G fronthaul link. For this purpose, they utilized 10 km of optical fiber followed by a 50 m FSO link. For the access network, they transmitted a 5G NR signal at 39 GHz over a distance equivalent to 1 m, achieving a total throughput of 2.4 Gbit/s. In [10], it was experimentally demonstrated the use of integrated optics to transmit 5G NR signals in the 26 GHz range. The architecture explored the X-Haul concept, applying solutions based on optical fiber, FSO, and wireless transmission to compose the physical layer of the network. A transmission rate of 900 Mbit/s was observed. The work reported in [11] describes the implementation of a proof of concept for a 12.5 km A-RoF fronthaul followed by a VLC based access link with a length of 1.2 m for 6G solutions. The initial proof of concept achieved a data throughput of 60 Mbit/s, considering the convergence between the technologies. Based on this bibliographic review, it was possible to pinpoint key areas of study pertaining to the implementation of novel solutions to meet post-5G demands. The experimental implementation and investigation of an X-Haul based on A-RoF, FSO, millimeter waves, and VLC, operating at 39 GHz and 550 MHz for 5G and 6G applications. We propose a simultaneous dual-access approach for high-capacity communications in dense urban environments, utilizing the 39 GHz frequency outdoors and a 550 MHz VLC connection indoors. The experimental findings substantiate a harmonious coexistence of these technologies, attaining an aggregate data throughput of 4.92 Gbit/s.

The utilization of heterogeneous networks in X-Haul architectures emerges as a response to the need to address a diversified range of connectivity requirements in the era of advanced communications. These architectures integrate a variety of access technologies, such as optical fiber, and millimeter waves, to optimize network efficiency and capacity. By combining different technologies types, it is possible to strike a balance between the high bandwidth demanded by high-density data applications like 5G, and the extensive coverage required in less densely populated areas. Furthermore, heterogeneous networks facilitate the deployment of diverse services, ranging from short-range communications to long-distance transmissions, promoting comprehensive and high-performance connectivity in both urban and rural environments. This flexible and adaptive approach becomes crucial in meeting the escalating demands for connectivity in an ever-evolving technological landscape.

Fig. 2. Photography of the proposed system.

Section II describes the experimental setup of the proposed system. Section III presents the results of the digital performance investigation in terms of the root mean square error vector magnitude (EVM_{RMS}). Finally, the conclusions and final remarks are presented in Section IV.

II. Experimental Setup

Fig. 1 and Fig. 2 depicts the block diagram and photography of the proposed 5G NR OWC system, respectively. The base-band 5G NR signal is designed using Keysight Signal Studio software and generated by an arbitrary waveform generator (AWG) M8190A, also from Keysight. The base-band signal is applied to an analog signal generator (PSG-E8267D), which is used for upconverting the signal to 39 GHz. In parallel, the

quadrature amplitude modulation (QAM) signal is generated by vector signal generator (EXG-N5172B) at 550 MHz. The two RF signals are combined by a diplexer (DPX) before being applied to a single drive Mach-Zehnder modulator (MZM) (FTM7937EZ). The MZM modulates an optical carrier from a laser diode (LD) using the combined RF signals. Afterward, the modulated optical signal is launched into a 20-km single-mode fiber (SMF), giving rise to the optical midhaul. We have split the signal using an 80/20 splitter in which 20% was applied to an optical spectrum analyzer (OSA) for frequency-domain real-time measurements, and the remainder of the optical signal was amplified by an Erbium-doped fiber amplifier (EDFA). The EDFA is located at distribution unit (DU) which is connected to a remote radio head (RRH) by using a fronthaul link, which might be optical or wireless. In this work, the fronthaul link is based on a 1.5 m FSO link. After radiated, the optical signal is photodetected by a 50-GHz bandwidth photodetector (PD) (DMX50AF) and separated by a DPX.

Two distinct access networks were considered in this work: the first one is a wireless transmission using a pair of horn antennas. In this case, the received signal is amplified by a 35-dB gain electrical amplifier (EA) before being received by a vector signal analyzer (VSA) (FSW) from Rohde & Schwarz. The other access network is based on 3 m reach VLC link. A red LD at 650 nm is used for transmitting the signal. At the receiver side, a condenser lens is employed to concentrate the signal that will be photodetected by another PD. Again, the photodetected RF signal is amplified before being evaluated. In this case, we have used a 50-dB gain EA and a bias tee to eliminate the direct current (DC) component introduced by PD. Finally, the signal quality is evaluated by employing a dynamic spectrum access (DSA) (DSA V084A) from Keysight. The utilization of red-wavelength laser diodes (LDs) for data communication, albeit less common, finds applicability in specific contexts [12]. Red LDs are employed in scenarios necessitating short-range, high-speed data transmission, such as intra-room communication or inter-sensor data exchange in laboratories. They also prove valuable in controlled environments where electromagnetic interference must be minimized, and where the presence of red light does not impede visibility [13]. Applications involving navigation, sensing, and industries such as medical devices and industrial automation may opt for red LDs due to tailored security and performance requirements. Nonetheless, it is essential to note that the usage of red LDs for data communication is more confined in comparison to other LD colors, necessitating careful consideration of application-specific needs and environmental conditions [14].

III. Results

The performance analysis of the proposed architecture was carried out in three stages. The first stage involved evaluating the quality of the received signals after the midhaul based on optical fiber and the fronthaul based on FSO, i.e., after electro/optical conversion at the photodetector, (Marker (I) from Fig. 1). Fig. 3 depicts the EVM_{RMS} measurements for quadrature phase shift keying (QPSK), 16- and

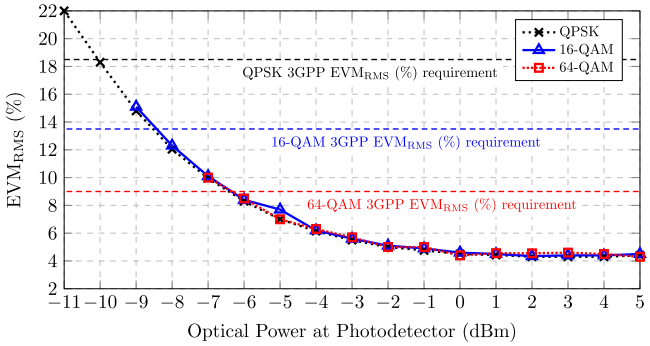

Fig. 3. EVM_{RMS} as a function of optical power at photodetector input.

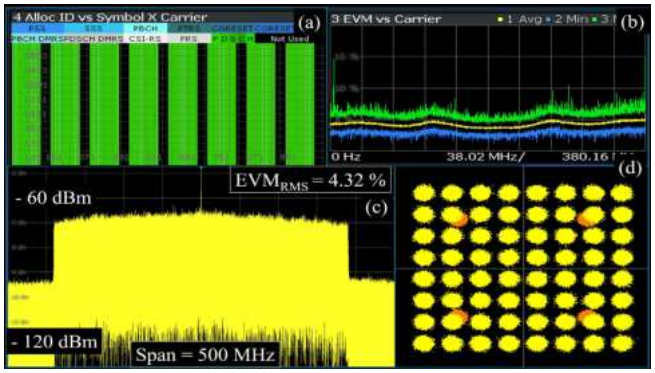

Fig. 4. Received 5G NR signal from the FSO/wireless link: (a) resource blocks of specific symbols; (b) EVM_{RMS} per subcarrier; (c) electrical spectrum and (d) constellation of the signal.

64-QAM signals. We have also included the EVM_{RMS} limit, defined by 3rd Generation Partnership Project (3GPP), for each modulation scheme. We can notice that ≈ -10, -8.5 and -7 dBm is required for fulfilling the 3GPP requirements for QPSK, 16-and 64-QAM, respectively. Therefore, we have fixed an optical power of ≈ 5 dBm at PD input for the next analysis.

We have transmitted a 400-MHz bandwidth signal using the time division duplexing (TDD) scheme. The signal generation employed the TM 3.1 test model, and certain characteristics related to signal generation are described below: for bandwidths of 50 and 100 MHz with a subcarrier spacing of 60 kHz, data throughputs of 178 and 360 Mbit/s were achieved, respectively. For signals with BWs of 200 and 400 MHz and subcarrier spacing of 120 kHz, the system achieved data throughputs in the order of 692 and 1386 Mbit/s, respectively. The FSO/wireless has achieved throughput of $\approx$ 1.38 Gbit/s with EVM_{RMS} of 4.32%, which is below than 3GPP specification for 64-QAM (9%). The duplexing scheme can be seen in the left-top part of Fig 4 (a), in which all resource blocks of specific symbols are left unoccupied for uplink transmissions. We can also notice that EVM_{RMS} was kept almost the same for all subcarriers, as demonstrated in the EVM_{RMS} per subcarrier result (b). The electrical spectrum shown displays the reception power levels for the 5G NR signal transmitted at 39 GHz with a bandwidth of 400 MHz (c). Finally, the constellation of the signal does not demonstrate any considerably apparent distortion (d).

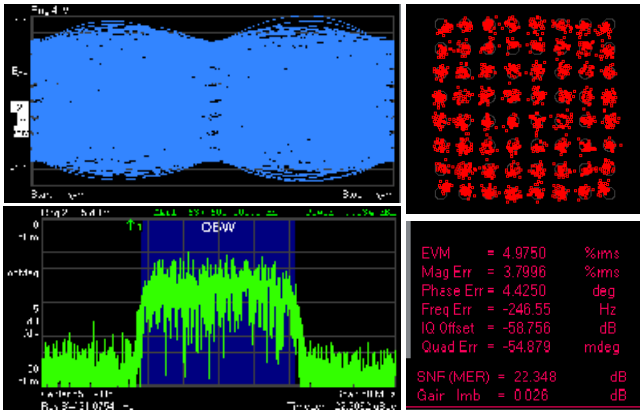

Fig. 5. EVM_{RMS} as a function of the optical power at the photodetector input for the VLC signal.

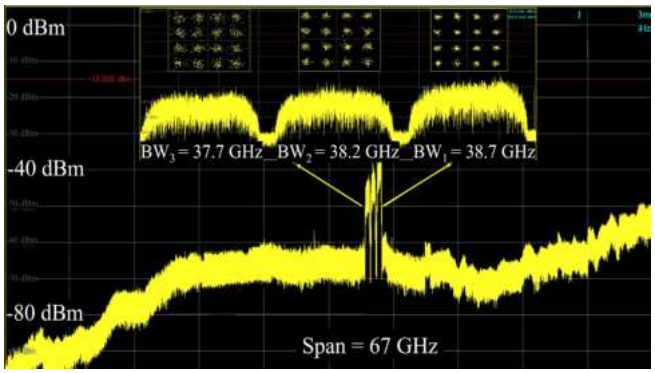

Fig. 6. Electric spectrum of 16-QAM 3 bands at 39 GHz measured at the FSW.

The proposed VLC system, considered a point-to-point network access option, was evaluated alongside a simultaneous and parallel transmission with the 5G NR link at 39 GHz. The performance of the FSO/VLC access network, measured using the EVM_{RMS} metric, was assessed at Marker (III) in Fig 2. We configured a 64-QAM signal at 550 MHz, achieving a data transfer rate of 120 Mbit/s. This signal was transmitted over a 3-meter link to a collimation lens. The collimation lens was positioned to focus the light onto the appropriate receiving region of the photodetector. The FSO/VLC system attained an EVM_{RMS} of 4.97%. Notably, no significant distortions were observed in the eye or constellation diagrams.

According to the specifications outlined in Release 18 from 3GPP, a bandwidth of up to 2000 MHz will be utilized in the frequency range FR2-2 [15]. However, in this study, the experiments were conducted within the FR2-1 band, where carrier aggregation is not an option, and the maximum bandwidth allowed is 400 MHz. To address this limitation, the goal was to implement an access network with carrier aggregation capabilities, similar to what is done in LTE. In this context, three signal bands were generated, each utilizing 16-QAM modulation and having a bandwidth of 400 MHz. Fig. 6 illustrates the electrical spectrum after fiber/wireless (FiWi) transmission. BW_1 centered at 38.7 GHz showed an EVM_{RMS} measurement of 6.5%, while $BW_2 = 38.2$ GHz and $BW_3 = 37.7$ GHz exhibited EVM_{RMS} measurements of 7% and 9%, respectively. With these results, the FiWi 5G NR system operating at 39 GHz achieved a data transfer rate of 4.8 Gbit/s.

IV. Conclusion

In this letter, we evaluated the 5G NR OWC system performance. An analog radio over fiber (RoF) midhaul link was used for transporting the signal up to a DU, in which the signal is transmitted to the RRH via FSO transmission. For the access network, we employed two distinct transmission techniques using wireless and VLC systems. The FSO/wireless link was used for transmitting a 5G NR signal at 39 GHz aiming high-throughput indoor femtocells. On the other hand, the FSO/VLC structure was employed to transmit a 550 MHz QAM signal, also for indoor applications. The FSO/wireless link has achieved throughput of $\approx$ 4.8 Gbit/s, whereas the FSO/VLC link attained 120 Mbit/s. Therefore, the hybrid OWC system total throughput was 4.92 Gbit/s. This proposed architecture takes advantage of fiber-optics transmission benefits whilst VLC, FSO, and wireless link increase network flexibility.

References

[1] Y. L. Lee, D. Qin, L.-C. Wang, and G. H. Sim, "6G massive radio access networks: Key applications, requirements and challenges," *IEEE Open J. Veh. Technol.*, vol. 2, pp. 54–66, 2021.

[2] A. Dogra, R. K. Jha, and S. Jain, "A survey on beyond 5G network with the advent of 6G: Architecture and emerging technologies," *IEEE Access*, vol. 9, pp. 67512–67547, 2021.

[3] H. R. D. Filgueiras et al., "Wireless and optical convergent access technologies toward 6G," *IEEE Access*, vol. 11, pp. 9232–9259, 2023.

[4] I. Chih-Lin, H. Li, J. Korhonen, J. Huang, and L. Han, "RAN revolution with NGFI (xhaul) for 5G," *J. Lightw. Technol.*, vol. 36, no. 2, pp. 541–550, Jan. 15, 2018.

[5] Y. Yoshida, "Mobile xhaul evolution: Enabling tools for a flexible 5G xhaul network," in *Proc. Opt. Fiber Commun. Conf. Exposit. (OFC)*, Mar. 2018, pp. 1–85.

[6] Z. Ghassemlooy, S. Arnon, M. Uysal, Z. Xu, and J. Cheng, "Emerging optical wireless communications-advances and challenges," *IEEE J. Sel. Areas Commun.*, vol. 33, no. 9, pp. 1738–1749, Sep. 2015.

[7] R. M. Borges et al., "Integrating optical and wireless techniques towards novel fronthaul and access architectures in a 5G NR framework," *Appl. Sci.*, vol. 11, no. 11, p. 5048, May 2021.

[8] C. H. de Souza Lopes et al., "Non-standalone 5G NR fiber-wireless system using FSO and fiber-optics fronthauls," *J. Lightw. Technol.*, vol. 39, no. 2, pp. 406–417, Jan. 15, 2021, doi: 10.1109/JLT.2020.3029500.

[9] J. Bohata et al., "Performance evaluation of seamless 5G outdoor RoFSO transmission at 39 GHz," *IEEE Photon. Technol. Lett.*, vol. 34, no. 1, pp. 7–10, Jan. 1, 2022, doi: 10.1109/LPT.2021.3134559.

[10] E. S. Lima, R. M. Borges, N. Andriolli, E. Conforti, G. Contestabile, and A. C. Sodré, "Integrated optical frequency comb for 5G NR xhauls," *Sci. Rep.*, vol. 12, no. 1, p. 16421, Sep. 2022.

[11] T. P. V. Andrade, L. C. de Souza, E. S. Lima, and A. C. Sodré, "Demonstration of a hybrid A-RoF/VLC system for beyond 5G applications," *Appl. Opt.*, vol. 62, no. 8, pp. C115–C121, 2023.

[12] B. Janjua et al., "Going beyond 4 Gbps data rate by employing RGB laser diodes for visible light communication," *Opt. Exp.*, vol. 23, no. 14, pp. 18746–18753, 2015.

[13] F. Zafar, M. Bakaul, and R. Parthiban, "Laser-diode-based visible light communication: Toward gigabit class communication," *IEEE Commun. Mag.*, vol. 55, no. 2, pp. 144–151, Feb. 2017.

[14] Y. G. Y. Guo et al., "A tutorial on laser-based lighting and visible light communications: Device and technology," *Chin. Opt. Lett.*, vol. 17, no. 4, 2019, Art. no. 040601.

[15] 3GPP, "Technical specification group radio access network; NR; base station (BS) radio transmission and reception; Part-1," 3rd Generation Partnership Project (3GPP), Tech. Rep. TS 38.104, Version 18.1.0, Release 18, 2023.

Artigo 3: 60-GHz 5G-NR Optical Fronthauls Based on CS-DSB Technique

Celso Henrique de Souza Lopes, Leticia Carneiro de Souza, Tomas Powell Villena Andrade, Evandro Conforti and Arismar Cerqueira. S. Jr. ”60-GHz 5G-NR Optical Fronthauls Based on CS-DSB Technique”, *SBFoton*, 2023.

60-GHz 5G-NR Optical Fronthauls Based on CS-DSB Technique

Celso H. S. Lopes[(1)], Letícia C. Souza[(1)], Tomás P. V. Andrade[(1)], E. Conforti[(2)], Arismar Cerqueira S. Jr[(1)].
[(1)]*Laboratory WOCA, National Institute of Telecommunications (Inatel)*
510 João de Camargo Av., Santa Rita do Sapucaí - MG,
Brazil, 37540-000.
[(2)] DECOM-University of Campinas, Campinas 13083-970, Brazil.
celso.henrique@dtel.inatel.br, arismar@inatel.br

***Abstract*—This paper reports the implementation of 5G New Radio (5G-NR) optical fronthauls based on radio-over-fiber (RoF) technology and optical carrier-suppressed double sideband (CS-DSB) technique, operating at 60 GHz. Experimental results over 20-km fiber-optics links demonstrate the successful transmission of QPSK, 16-QAM and 64-QAM modulated signals with up to 400-MHz bandwidth. The proposed 5G-NR RoF system performance meets the 3rd Generation Partnership Project (3GPP) requirements, achieving a total throughput of 800 Mbps.**

***Index Terms*—5G, 5G-NR, CS-DSB, mm-waves and radio-over-fiber.**

I. Introduction

In parallel with the deployment of fifth-generation (5G) mobile networks, researchers and industry experts are exploring the possibilities for the next generation of wireless communication systems, known as Beyond 5G (B5G) networks. The millimeter-wave (mm-wave) frequency band is expected to play a crucial role in enabling higher data rates in B5G systems, as it offers wider bandwidths compared to lower frequency bands used in current wireless networks [1]. In particular, the 3rd Generation Partnership Project (3GPP) has defined the frequency range from 52.6 GHz to 71 GHz as FR2-2 in the 5G new radio (NR) standard [2]. Although the 60-GHz frequency band is more susceptible to high attenuation and blockage, it has recently been considered for short-range applications due to the wide bandwidth and availability of unlicensed spectrum [3].

Photonic generation of mm-wave signals could be easily integrated with radio-over-fiber (RoF)-based fronthauls by providing wide bandwidth, high purity, low phase noise, and high stability. In particular, the authors in [4] demonstrated the use of optical frequency combs generated by a photonic integrated circuit (PIC) at 26 GHz. Vallejo *et. al* presented a solution based on directly modulated laser and carrier-suppressed (CS) external modulation for generating a 40-GHz signal [5]. The carrier-suppressed double sideband (CS-DSB) technique has also been reported in literature. Bohata *et. al* demonstrated that the CS-DSB technique employing two external modulators provides better performance compared to using a directly modulated laser in addition to an external modulator [6]. In this context, this paper presents the use of the CS-DSB technique for generating 5G-NR signals at 60 GHz followed by an RoF-based 20-km fronthaul transmission. The 5G NR standard transmission and analysis is performed in accordance with the 3GPP requirements [2].

979-8-3503-0402-2/23/$31,00 ©2023 IEEE

II. Experimental Setup

Fig. 1 depicts a block diagram of the proposed architecture. This setup is based on one Mach-Zehnder intensity modulator (MZM) (MZM_1, Fujitsu FTM7939EK) biased at the null point (V_π = 6.6 V), to suppress the optical carrier, and a second MZM (MZM_2, Fujitsu FTM7920FB) biased at quadrature point ($V_{\pi/2}$ = 2.6 V), to enable data modulation. We have employed a distributed feedback (DFB) laser diode (LD) that operates at 1530 nm and has an output power of 15 dBm. A polarization controller (PC) is used to adjust the light polarization state at the MZMs inputs. A 24.5-GHz single-tone signal (RF_1) generated by a signal generator (Keysight N5173B) is injected into the MZM_1. An arbitrary waveform generator (AWG) (Keysight M8190A) generates the baseband 5G-NR signal and a vector signal generator (VSG) (Keysight PSGE8267D) performs the frequency up-conversion, providing a 5G-NR signal at 11 GHz, which is injected into MZM_2. The RF_1 and RF_2 signals power levels are 15 and 10 dBm, respectively. The RF_1 signal creates two sidebands in the optical domain with a frequency spacing of 49 GHz. The optical distribution network consists of a 20-km single-mode fiber (SMF) link. Subsequently to the optical transmission, an optical erbium-doped fiber amplifier (EDFA) is used to compensate for the system loss. The EDFA was placed at the remote node in the laboratory setup to provide a maximum optical output power of 8 dBm. The optical-to-electrical conversion is performed by a high-frequency photodetector (PD) (Thorlabs DXM50AF). The two sidebands generated at the MZM2 output beat each other in the PD, which results in a frequency doubling. The recovered signal is evaluated in a spectral and signal analyzer (R&S FSW67).

III. Experimental Results

Fig. 2 presents the measured EVM_{RMS} results as a function of the received optical power at the PD input. By varying the EDFA gain, we were able to evaluate the EVM_{RMS} over an optical power range from 0 to 8 dBm. We have employed 5G NR quadrature phase shift keying (QPSK), 16-quadrature

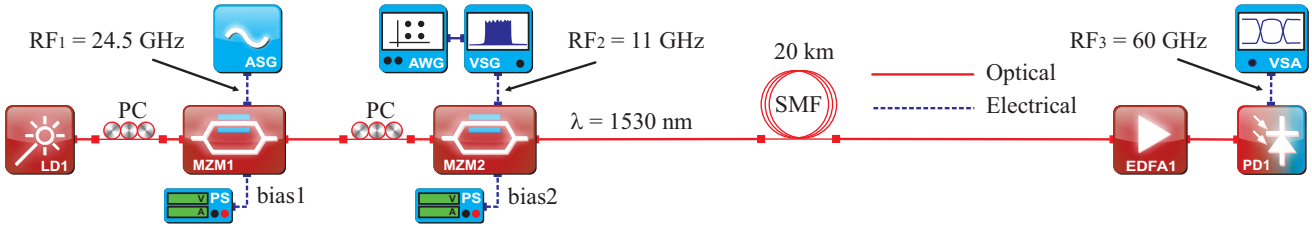

Fig. 1. Block diagram of the 5G-NR Fronthaul based on RoF technology and CS-DSB technique.

amplitude modulation (QAM), and 64-QAM signals with bandwidths of 50 MHz, 100 MHz, 200 MHz and 400 MHz, respectively. The 3GPP has specified maximum EVM_{RMS} values of 17.5%, 12.5%, and 8% for QPSK, 16-QAM, and 64-QAM, respectively [2]. The proposed RoF system meets the 3GPP requirements for optical powers ranging from 6 to 8 dBm for the 50-MHz 64-QAM signal, from 5 to 6 dBm for the 100-MHz 16-QAM signal, from 1 to 4 dBm for the 200-MHz QPSK signal, and from 3 to 4 dBm for the 400-MHz QPSK signal. The best performance measurements were obtained at 8 dBm, 6 dBm, and 4 dBm for the 64-QAM, 16-QAM, and QPSK modulation schemes, with EVM_{RMS} of 6%, 10%, 15%, 16.8%, respectively. From these points on, the EVM_{RMS} rises due to the increase in the EDFA amplified spontaneous emission (ASE), which degrades the overall signal-to-noise ratio (SNR). Fig. 3 depicts the 400-MHz QPSK signal received constellation and measured spectrum at 4-dBm optical power at the PD output. Overall, a maximum throughput of 800 Mbps was obtained with this bandwidth and modulation scheme.

IV. Conclusions

We have successfully implemented 20-km 5G-NR optical fronthauls based on RoF technology and CS-DSB technique operating in the 60 GHz frequency band. The overall system performance has been shown in accordance with the 3GPP requirements. For instance, EVM_{RMS} as low as 6% was obtained for a 50-MHz 64-QAM signal. Moreover, 800-Mbps throughput could be achieved with a 400-MHz bandwidth QPSK 60-GHz 5G NR signal, demonstrating the applicability of the proposed technique for the current 5G-NR deployments.

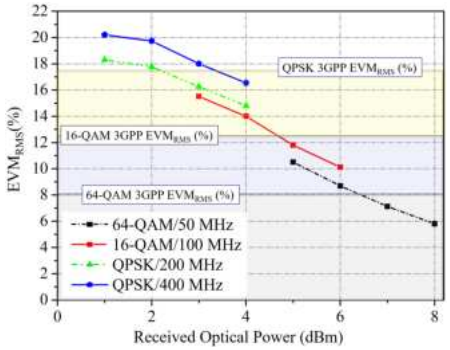

Fig. 2. RoF system digital performance as a function of the received optical power at the PD input for QPSK, 16-QAM and 64-QAM signals.

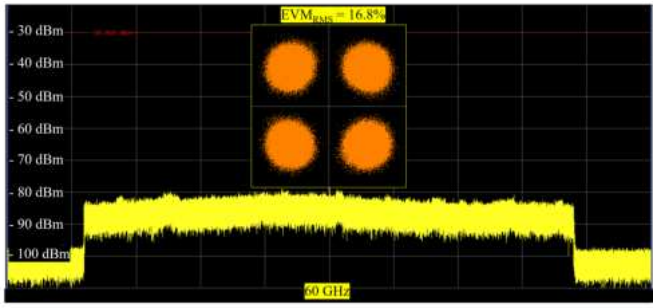

Fig. 3. 400-MHz QPSK signal received constellation and measured spectrum at 4-dBm optical power.

Acknowledgments

This work was partially supported by RNP, with resources from MCTIC, Grant No 01245.020548/2021-07, under the 6G Mobile Communications Systems project of the Radiocommunication Reference Center (Centro de Referência em Radiocomunicações - CRR) of the National Institute of Telecommunications (Instituto Nacional de Telecomunicações - Inatel), Brazil. The authors also thank the financial support from CNPq, CAPES, FINEP, RNP, FAPEMIG, and FAPESP Grant No. 2021/11380- 5 and Grant No. 2021/06569-1.

References

[1] C. H. d. S. Lopes, E. S. Lima, L. A. M. Pereira, R. M. Borges, A. C. Ferreira, M. Abreu, W. D. Dias, D. H. Spadoti, L. L. Mendes, and A. C. S. Junior, "Non-Standalone 5G NR Fiber-Wireless System Using FSO and Fiber-Optics Fronthauls," *Journal of Lightwave Technology*, vol. 39, no. 2, pp. 406–417, 2021.

[2] 3GPP, "Technical Specification Group Radio Access Network; NR; Base Station (BS) radio transmission and reception; Part-1," 3rd Generation Partnership Project (3GPP), Technical Specification (TS) 38.104, 2023, tS 38.104 version 18.1.0 Release 18.

[3] L. Carneiro de Souza, C. H. de Souza Lopes, R. de Cassia Carlleti dos Santos, A. Cerqueira Sodré Junior, and L. L. Mendes, "A study on propagation models for 60 GHz signals in indoor environments," *Frontiers in Communications and Networks*, vol. 2, p. 757842, 2022.

[4] E. S. Lima, R. M. Borges, N. Andriolli, E. Conforti, G. Contestabile, and A. C. Sodré Jr, "Integrated optical frequency comb for 5G NR Xhauls," *Scientific Reports*, vol. 12, no. 1, p. 16421, 2022.

[5] L. Vallejo, J. Mora, and B. Ortega, "Harmonic and Intermodulation Distortion Analysis in Directly Modulated Lasers Over Local and Remote Photonically Generated Millimeter-Wave Signals," *Journal of Lightwave Technology*, vol. 40, no. 15, pp. 5128–5140, 2022.

[6] J. Bohata, L. Vallejo, B. Ortega, and S. Zvánovec, "Optical CS-DSB Schemes for 5G mmW Fronthaul Seamless Transmission," *IEEE Photonics Journal*, vol. 14, no. 2, pp. 1–7, 2022.

Artigo 4 : Implementação de um Sistema Híbrido FiWi utilizando FSO, VLC e Ondas Milimétricas para Aplicações 6G

Celso Henrique de Souza Lopes, Luis Augusto Melo Pereira, Tomas Powell Villena Andrade, Evandro Conforti and Arismar Cerqueira. S. Jr. ”60-GHz 5G-NR Optical Fronthauls Based on CS-DSB Technique”, *SBrT*, 2023.

Implementação de um Sistema Híbrido FiWi utilizando FSO, VLC e Ondas Milimétricas para Aplicações 6G

C. H. S. Lopes, L. A. M. Pereira, T. P. V. Andrade, E. Conforti e Arismar Cerqueira S. Jr

***Resumo*— Neste trabalho, avaliamos experimentalmente uma arquitetura híbrida FiWi (*fiber/wireless*) que combina fibra óptica, (FSO, *free space optical*), ondas milimétricas e (VLC, *visible light communication*) em uma mesma topologia de rede. Para o *fronthaul*, um enlace de 20 km de fibra óptica seguido por um enlace FSO de 1,5 m foi implementado. Para o acesso, um enlace 5G NR sem fio de 2 m operando em 39 GHz e um enlace VLC ponto-a-ponto de 3 m em 550 MHz garantiram uma vazão de dados total do sistema na ordem de 1,5 Gbit/s, atendendo aos requisitos do 3GPP Release 18.**

***Palavras-Chave*— 5G, 5G-NR, 6G, FiWi, FSO, mm-waves, VLC e X-Haul.**

***Abstract*— In this work, we experimentally evaluated a hybrid FiWi (fiber/wireless) architecture that combines optical fiber, free space optical (FSO), millimeter waves, and visible light communication (VLC) in the same network topology. For the fronthaul, a 20 km optical fiber link followed by a 1.5 m FSO link was implemented. For the access, a 2 m 5G NR wireless link operating at 39 GHz and a 3 m point-to-point VLC link at 550 MHz ensured a total system data throughput in the order of 1.5 Gbit/s, meeting the requirements of 3GPP Release 18.**

***Keywords*— 5G, 5G-NR, 6G, FiWi, FSO, mm-waves, VLC e X-Haul.**

I. Introdução

Motivados pela crescente necessidade de altas taxas de dados, aumento na densificação de células e baixa latência para comunicação humana e/ou entre máquinas, os sistemas sem fio de quinta geração, incluindo as redes de acesso de rádio (RAN, *radio acces network*), têm sido objeto de considerável atenção perante a academia e indústria [1]. A implantação da tecnologia de redes móveis de quinta geração (5G, *fifth-generation of mobile network*) permite a implementação de uma variedade de novas aplicações, tendo como foco principal o acesso móvel operando em banda larga [1], [2]. Soluções técnicas como o novo padrão de rádio 5G (5G NR, *new radio*) utilização de espectro na faixa de ondas milimétricas (mm-wave, *millimeter waves*), RANs heterogêneas e centralizada (C-RAN, *centralized*-RAN), comunicação óptica sem fio (OWC, *optical wireless communication*) são propostas para atender as demandas iminentes [2], [3]. Ao mesmo tempo, a sexta geração de redes móveis (6G, *sixth-generation of mobile networks*) surge como um tópico popular para abordar as promessas não cumpridas do 5G e atender às demandas futuras a partir de 2030 com maior eficiência [4]. Na rede 6G, espera-se que surjam novos cenários de utilização, abrangendo telepresença, comunicação onipresente, utilização de robôs em diferentes áreas do cotidiano, biossensores e potenciais aplicações ainda não identificadas [5]. Soluções técnicas potenciais para o 6G incluem o uso de comunicações na faixa de terahertz (THz), inteligência artificial/aprendizado de máquina para atender redes autônomas e superfícies refletoras inteligentes [4], [5].

O objetivo fundamental de avançar em direção às redes 6G é fornecer velocidades de dados ultrarrápidas, alta capacidade e serviços confiáveis para usuários móveis. As células pequenas continuam sendo uma solução promissora para aumentar a velocidade e a densidade, pois aumentam a capacidade dividindo uma macrocélula em zonas menores e reutilizando os recursos de rádio de forma espacial [6]. No entanto, a implantação densa de células pequenas representa um desafio em termos de custos e consumo de energia dos locais de instalação, que normalmente representam os maiores custos e consumo de energia para um provedor de serviços móvel [6], [7]. A arquitetura C-RAN foi proposta para dar suporte de forma econômica à densificação da RAN, concentrando as funcionalidades avançadas de processamento de sinal em uma unidade centralizada (CU, *centralized unit*) que atende a múltiplas unidades remotas de rádio (RRUs, *remote radio units* [8]. A proposta consiste em instalar uma CU com múltiplas unidades de processamento em uma única localização da rede e portanto interconectá-la dinamicamente a várias RRUs implantadas no campo por meio de arquiteturas X-haul [9]. O objetivo principal de utilizar esta arquitetura centralizada é a possibilidade de explorar os benefícios da multiplexação estatística de recursos de hardware, resultando em maior eficiência energética e redução de custos [9], [10].

As redes 5G/6G devem operar em múltiplas faixas de frequências para suportar uma ampla gama de cenários e aplicações. Para atender a esse requisito, o 3GPP definiu três cenários de operação para o padrão 5G NR [11]. A primeira faixa de frequência (FR1) abrange de 0,410 GHz a 7,125 GHz, suportando larguras de banda (BW, *bandwidth*) de até 100 MHz. A segunda faixa de frequência (FR2-1) abrange as ondas milimétricas na faixa de 24,5 GHz a 52,6 GHz, com BW de até 400 MHz. E por fim, a terceira faixa de frequências (FR2-2) que vai de 52,6 GHz a 71 GHz com BW de até 2 GHz. No entanto, considerando um dos principais desafios de operar

C. H. S. Lopes, L. A. M. Pereira, T. P. V. Andrade e Arismar Cerqueira S. Jr. Instituto Nacional de Telecomunicações, Santa Rita do Sapucaí, MG 37400-000 Brasil (e-mails: celso.henrique@dtel.inatel.br luiz.melo@inatel.br; tomasvillena@dtel.inatel.br; arismar@inatel.br). E. Conforti. DECOM-Universidade Estadual de Campinas, Campinas 13083-970, Brazil (e-mail:conforti@unicamp.br).

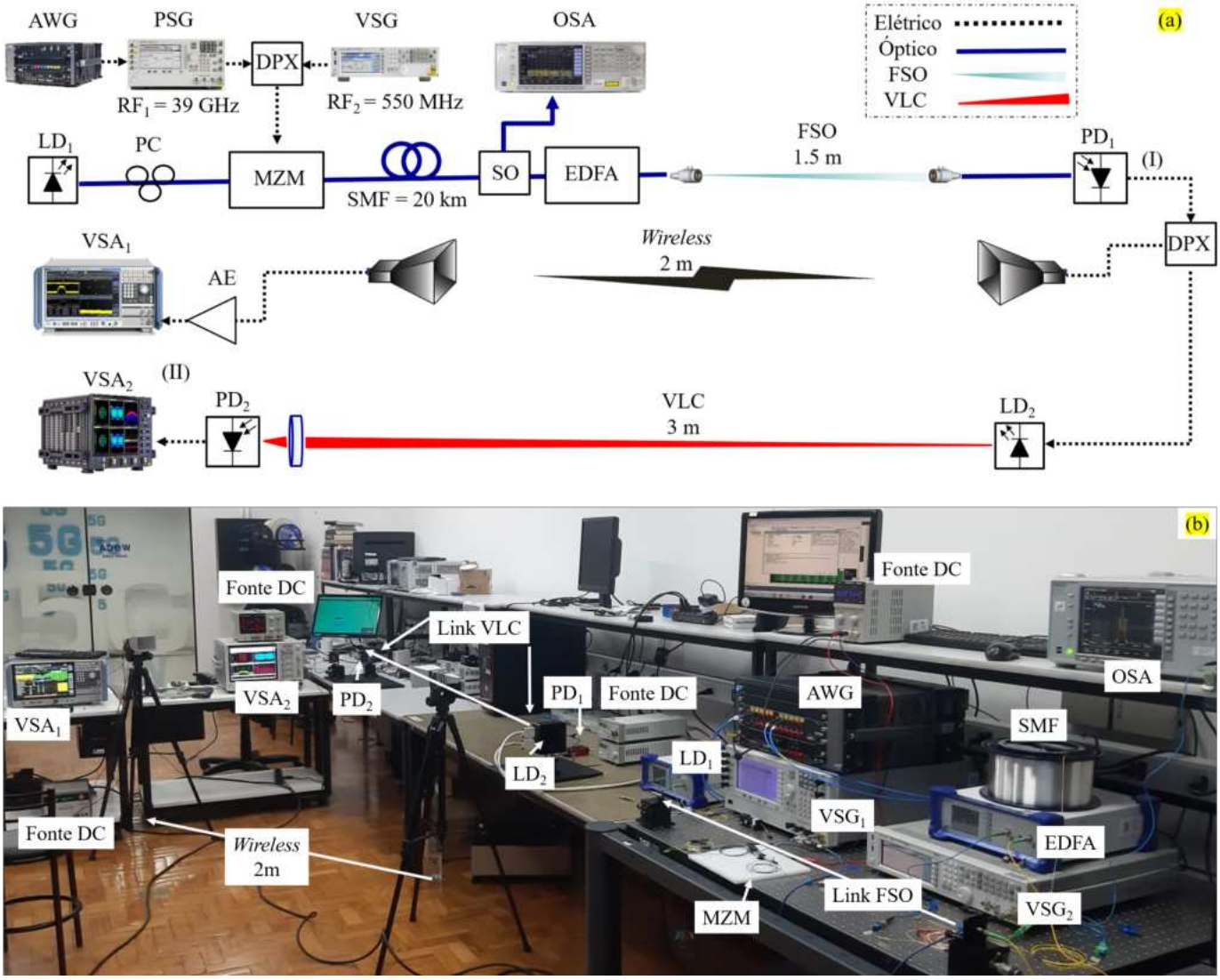

Fig. 1. Diagrama em blocos (a) e fotografia (b) do sistema FiWi proposto: AWG – *arbitrary waveform generator*; VSG – *vector signal generator*; OSA - *optical spectrum analyzer*; SO - *spliter optical*; EDFA - *amplifier erbium-doped fiber*; LD – *laser diode*; MZM – mach-zehnder modulator; SMF – *single mode fiber*; PD – *photodetector*; VSA - *vector signal analyzer*.

em frequências mais altas, que é a perda de transmissão e a necessidade de uma interface de *fronthaul* de alta capacidade, as tecnologias rádio analógico sobre fibra (A-RoF, *analog radio over fiber*) e óptica no espaço livre (FSO, *free space optical*) tornam-se extremamente interessantes [12]. Essas tecnologias possibilitam a transmissão de sinais com elevada bandwidth (BW), imunidade a interferências eletromagnéticas e baixa atenuação.

Soluções técnicas e inovadoras estão sendo propostas para atender as demandas requeridas pelo 5G/6G. A utilização de A-RoF para aplicações 5G foram descritas em [13], [14], [15]. No artigo [16], foram propostas duas soluções non-standalone 5G NR para atender às demandas iniciais do 5G. Foram empregadas diferentes tecnologias para a aplicação no fronthaul da rede, incluindo fibra óptica e FSO para aplicações de última milha. Os resultados experimentais demonstraram uma convergência segura e efetiva entre essas tecnologias, alcançando uma vazão de dados de até 3 Gbit/s e de acordo com as especificações do 3GPP Release 15. Em [17] os autores apresentaram uma campanha de medição experimental envolvendo uma proposta de arquitetura híbrida baseada em A-RoF e FSO para compor o fronthaul da rede 5G. Para isso, eles utilizaram 10 km de fibra óptica seguidos por um enlace FSO de 50 m. Para a rede de acesso eles transmitiram um sinal 5G NR em 39 GHz a uma distância equivalente a 1 m, atingindo uma taxa de transferência total de 2,4 Gbit/s. Foi demonstrado em [19] por meio de uma investigação experimental, o uso de óptica integrada para gerar sinais 5G NR na faixa de 26 GHz. A arquitetura explorou o conceito X-Haul, aplicando soluções baseadas em fibra óptica, FSO e transmissão sem fio para compor a camada física da rede. Foi observado uma taxa de transmissão de 900 Mbit/s demonstrando a viabilidade da técnica para gerar sinais de ondas milimétricas sintonizáveis de baixo ruído de fase. O trabalho relatado em [20] descreve a implementação de uma prova de conceito para um fronthaul A-RoF de 12,5 km seguido por um enlace de acesso baseado em VLC com comprimento de 1,2 m para soluções 6G. A prova de conceito inicial alcançou uma vazão de dados de

60 Mbit/s, considerando a convergência entre as tecnologias.

Neste trabalho, propõe-se a investigação experimental de uma arquitetura de rede proposta baseada no conceito X-Haul. No *fronthaul* da rede, a fibra óptica e FSO são utilizados para o transporte simultâneo de sinais operando em diferentes faixas de frequências. No acesso da arquitetura de rede proposta, um enlace 5G NR operando em 39 GHz é implementado e avaliado, enquanto que um segundo enlace de acesso baseado em luz visível opera em 550 MHz para aplicações 6G. A Seção II descreve o arranjo experimental do sistema proposto. A Seção III apresenta os resultados da investigação de desempenho digital em termos de magnitude de erro vetorial médio (EVM_{RMS}). Por fim, as conclusões e comentários finais são apresentadas na Seção IV.

II. Arquitetura Proposta

A configuração experimental é representada na Fig.1 em forma de diagramas em blocos (a) e fotografia do *setup* (b). Todas as tecnologias utilizadas no experimento são convergidas em uma arquitetura unificada, que emprega um enlace híbrido RoF e FSO para integrar o *fronthaul* da rede. Para o acesso é implementado um enlace *wireless* de 2 m operando em 39 GHz e paralelamente um enlace VLC operando em 550 MHz. O sinal 5G NR em banda base é projetado usando o *software* Keysight Signal Studio e gerado por um gerador de forma de onda arbitrária (AWG, *arbitrary waveform generator*) M8190A da Keysight. O modelo de teste escolhido foi o 3.1 (TM 3.1) especificado pelo 3GPP. Este modelo especifica que o sinal 5G NR operando na faixa de frequência 2.1 (FR2-1) tenha larguras de banda de até 400 MHz utilizando ordens de modulação QPSK, 16- e 64-QAM. O sinal de banda base é aplicado a um VSG_1 (PSG-E8267D), que é usado para converter o sinal para RF_1 = 39 GHz e transmitir a uma potência de 4 dBm. Em paralelo, o sinal *M*-QAM é gerado por um VSG_2 (EXGN5172B) a RF_2 = 550 MHz com potência de transmissão igual a -10 dBm. Os dois sinais de RF são combinados por um diplexer (DPX, 1721) antes de serem injetados em um MZM (FTM7937EZ). O MZM modula a portadora óptica do laser (LD) centrado em 1551 nm usando os sinais de RF combinados. A potência de transmissão do LD é igual a 15 dBm, e o sinal óptico modulado é então lançado em uma fibra monomodo (SMF) de 20 km, dando origem ao *fronthaul* óptico.

Antes da transmissão, o sinal óptico foi dividido utilizando um divisor óptico (SO, *spliter optical*) 80/20, no qual 20% do sinal é aplicado a um analisador de espectro óptico (OSA, *optical spectrum analyzer*) para medições no domínio da frequência em tempo real, e o equivalente a 80% é amplificado por um amplificador de fibra dopada com erbium (EDFA, *amplifier erbium-doped fiber*). O EDFA está localizado na unidade de distribuição (DU, *distribution unit*) que está conectado a um RRH por meio de um enlace *fronthaul* óptico. Posteriormente, o sinal óptico modulado é transportado por um enlace FSO de 1,5 m de comprimento. Dois colimadores (CFS18) são utilizados na transmissão e na recepção do enlace FSO, implementando como prova de conceito a rede híbrida RoF/FSO. Na recepção, o sinal óptico é fotodetectado por um (PD_1, *photodetector*) com largura de banda de 50 GHz (DMX50AF) e após o PD_1 o sinais são separados por um DPX (1721) para serem transmitidos em dois enlaces distintos e paralelos.

TABELA I
Parametros do sistema.

Parâmetro	Valor
Comprimento de onda do LD_1	1551 nm
Potência de transmissão do LD_1	15 dBm
Potência de RF_1 em 39 GHz	4 dBm
Potência de RF_2 em 550 MHz	−10 dBm
Comprimento da Fibra	20 km
Potência de Saída do EDFA	8 dBm
Comprimento do FSO	1.5 m
Potência óptica recebida no PD_1	5 dBm
Largura de banda do PD_1	50 GHz
Responsividade do PD_1	0,75 A/W @ 1550 nm
Comprimento do enlace sem fio	2 m
Comprimento de onda do LD_2	650 nm
Potência de transmissão do LD_2	4 dBm
Comprimento do enlace VLC	3 m
Potência óptica recebida no PD_2	4 dBm
Largura de banda do PD_2	1,2 GHz
Responsividade do PD_2	0,4 A/W @ 650 nm

Duas redes de acesso distintas foram consideradas neste estudo. A primeira é uma transmissão sem fio usando um par de antenas tipo corneta com ganhos de 30 dBi cada. Nesse caso, o sinal recebido é amplificado por um amplificador elétrico (EA, *electrical amplifier*) com ganho de 35 dB antes de ser recebido e analisado por um VSA_1 (R&S FSW67). A outra rede de acesso é baseada em um enlace VLC de alcance de 3 m para aplicações ponto-a-ponto. Um LD_2 com comprimento de onda de 650 nm é usado para transmitir o sinal. Do lado do receptor, uma lente óptica é empregada para focalizar o sinal, que será fotodetectado por outro PD_2 (EOT, 3020). Finalmente, a qualidade do sinal é avaliada usando um VSA_2 (V084A) da Keysight. A Tabela I resume os principais parametros do sistema proposto.

III. Resultados Experimentais

A análise de desempenho da arquitetura proposta foi realizada em duas etapas. A primeira etapa foi avaliar a qualidade dos sinais recebidos após o enlace de *fronthaul* óptico e FSO, ou seja, após a conversão eletro/óptica no fotodetector, demarcado na Fig. 1 (a) no ponto (I). O espectro elétrico ilustrado na Fig. 2 apresenta os níveis de potência de recepção para o sinal 5G NR transmitido em 39 GHz e para diferentes BWs, como determina a faixa de frequências FR2-1, 50, 100, 200 e 400 MHz representados por BW_1, BW_2, BW_3 e BW_4, respectivamente. Como o modelo de testes empregado na geração deste sinal foi o TM 3.1, algumas características relacionadas à geração dos sinais serão descritas a seguir: para larguras de banda de 50 e 100 MHz com espaçamento entre as subportadoras de 60 kHz, alcançou-se vazões de dados de 178 e 360 Mbit/s, respectivamente. Considerando os sinais com BW de 200 e 400 MHz e espaçamento entre as subportadoras de 120 kHz, o sistema atingiu vazão de dados na ordem de 692 e 1386 Mbit/s, respectivamente [21].

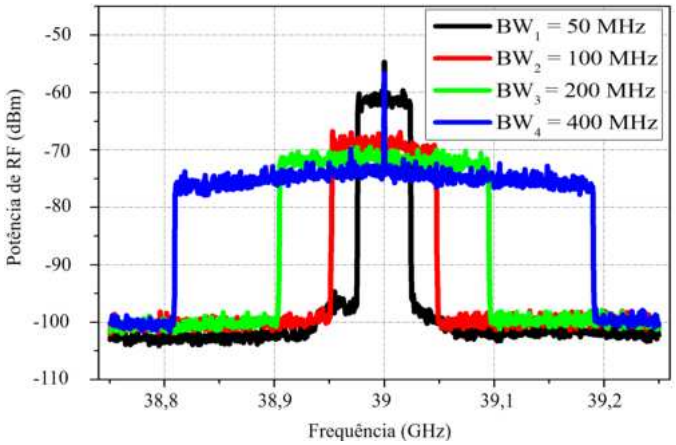

Fig. 2. Espectro elétrico medido na saída do fotodetector para larguras de banda 50, 100, 200 e 400 MHz.

A Fig. 3 reporta os diagramas de constelação para os sinais 5G NR recebidos no ponto (I) da arquitetura proposta. Para o sinal com BW_1 de 50 MHz, atingiu-se 3,3% de EVM_{RMS}, medido para uma potência óptica de recepção de 5 dBm. Enquanto que o BW_2 e BW_3 operando em 100 e 200 MHz atingiram 3,8 e 4,7%, respectivamente para o mesmo nível de potência óptica. Finalmente, o nível de EVM_{RMS} de 5,9% foi observado para a BW_4 = 400 MHz, considerando as mesmas condições de níveis de potência avaliadas anteriormente.

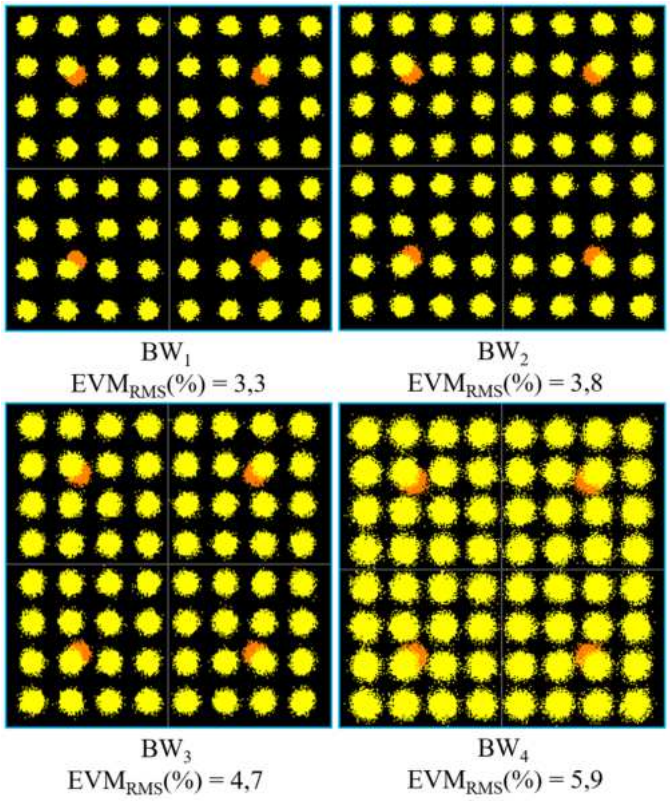

Fig. 3. Constelações 5G NR medidas para larguras de banda de 50, 100, 200 e 400 MHz e ordem de modulação 64-QAM.

Os valores de EVM_{RMS} observados estão abaixo do valor limite estipulado pelo 3GPP Release 18 para a ordem de modulação 64-QAM empregada, que é de 8%. Com isto, a transmissão explorando a faixa de frequências FR2-1, demonstrou ser viável do ponto de vista do *fronthaul* híbrido RoF/FSO da rede.

O sistema VLC proposto como uma opção de acesso ponto-a-ponto da rede, foi avaliado considerando uma transmissão simultânea e paralela ao enlace 5G NR em 39 GHz. Três campanhas de medição distintas foram realizadas, empregando a mesma BW de 20 MHz para o sinal *M*-QAM, valor limitado pelo equipamento de geração. Com o objetivo de aumentar a taxa de dados do enlace VLC, foram utilizadas três ordens de modulação diferentes: QPSK, 16-QAM e 64-QAM. É importante ressaltar que ordens de modulação mais altas requerem uma relação sinal-ruído (SNR) aprimorada para manter o mesmo nível de desempenho do sistema.

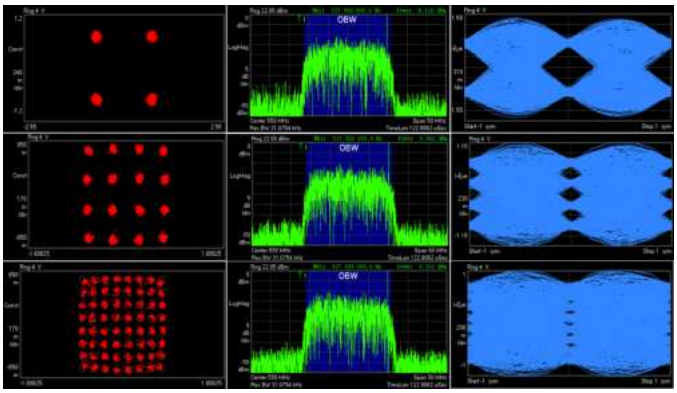

Fig. 4. Análise de desempenho VLC: Luz vermelha com modulação QPSK, 16- e 64-QAM com largura de banda de 20 MHz.

Para avaliar o desempenho do enlace VLC, variou-se o nível de potência do sinal de RF transmitido de -22 a 0 dBm. Para o sinal QPSK, observamos um valor de EVM_{RMS} de 16,4% para uma potência de RF de transmissão de -20 dBm, alcançando uma taxa de dados de 40 Mbit/s. Para aumentar a taxa de dados do sistema, as ordens de modulação 16-QAM e 64-QAM foram empregadas, exigindo um aumento na potência de RF para -18 e -15 dBm, respectivamente, para atingir níveis de EVM_{RMS} de 11,8% e 8,5%. A Fig. 4 ilustra o diagrama de constelação, o espectro elétrico e o diagrama de olho para as respectivas ordens de modulação transmitidas (a) QPSK, (b) 16-QAM e (c) 64-QAM, alcançando uma vazão total de 120 Mbit/s. Vale ressaltar que a Fig. 4 apresenta os diagramas medidos para uma potência do sinal de RF transmitido de -10 dBm, enquanto que a potência óptica na recepção foi de aproximadamente 4 dBm. Observou-se que estes valores otimizam o desempenho do sistema.

Após caracterizar o sistema RoF/FSO com relação a valores otimizados de potência transmitida de RF para o enlace VLC e de potência óptica recebida para o sinal em 39 GHz, foi implementado um enlace sem fio com distancia de 2 m. A Fig. 5 retrata o espectro elétrico medido na saída do amplificador elétrico. Conforme ilustrado, o sinal 5G NR transmitido a 39 GHz não aparenta degradações severas devido a fenômenos físicos de propagação tais como: reflexão, difração e bloqueio encontrados ao longo de um canal sem fio. Um *span* de 67 GHz foi capturado com objetivo de demonstrar

a viabilidade do sistema proposto. O espectro mais definido é observado na caixa representada na figura por um *span* de 500 MHz, e com o emprego de um EA com ganho de 35 dB na recepção, a perda devido ao canal sem fio foi compensada e o nível de EVM_{RMS} observado foi de 7,5%, atingindo assim uma taxa de transmissão de 1,5 Gbit/s considerando as duas redes de acesso.

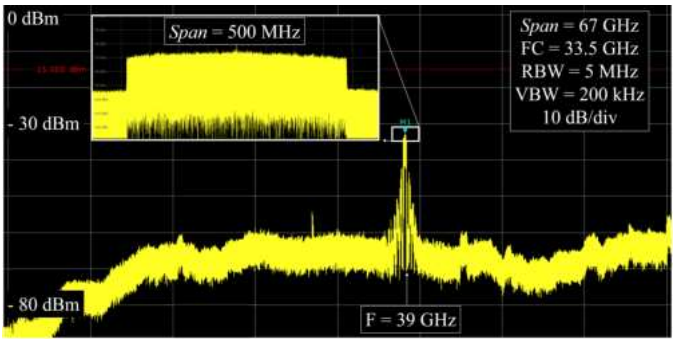

Fig. 5. Espectro elétrico medido após transmissão FiWi 5G NR a 39 GHz.

IV. Conclusões

Este trabalho descreveu a investigação experimental de uma proposta de arquitetura de rede híbrida baseada em A-RoF, FSO e VLC para atender às demandas das redes 5G e 6G. A arquitetura de rede demonstrada utiliza uma conexão de fronthaul baseada em A-RoF e FSO, enquanto o acesso é realizado por meio de ondas milimétricas operando a 39 GHz e VLC na faixa de 550 MHz. Os resultados experimentais comprovaram que as diversas tecnologias empregadas podem oferecer uma solução para a demanda crescente de largura de banda necessária para atender às diferentes aplicações. Foi obtida uma vazão máxima de dados de aproximadamente 1,5 Gbit/s utilizando uma modulação 64-QAM no sistema FiWi proposto. O desempenho do sistema foi avaliado de acordo com os parâmetros de EVM_{RMS} estabelecidos pela especificação 3GPP Release 18. Como trabalhos futuros, propõe-se a implementação da arquitetura avaliada em um sistema WDM, permitindo a transmissão simultânea de diferentes tecnologias para atender a um número maior de usuários

Agradecimentos

Os autores agradecem o apoio parcialmente financiado pela RNP, com recursos do MCTIC, processo No 01245.020548/2021-07, sob o projeto Brasil 6G do Centro de Referência em Radiocomunicações (CRR) do Instituto Nacional de Telecomunicações – Inatel, Brasil, e pela Huawei, sob o projeto Formação Avançada em Redes e Sistemas de Telecomunicações, contract No PPA6001BRA23032110257684. Adicionalmente, os autores também agradecem o apoio financeiro do CNPq, da CAPES, da FINEP, da FAPEMIG e da FAPESP.

Referências

[1] A. Dogra, R. K. Jha and S. Jain, "A Survey on Beyond 5G Network With the Advent of 6G: Architecture and Emerging Technologies,"in IEEE Access, vol. 9, pp. 67512-67547, 2021, doi: 10.1109/ACCESS.2020.3031234.

[2] A. Ghosh, A. Maeder, M. Baker and D. Chandramouli, "5G Evolution: A View on 5G Cellular Technology Beyond 3GPP Release 15,"in IEEE Access, vol. 7, pp. 127639-127651, 2019, doi: 10.1109/ACCESS.2019.2939938.

[3] Borges, R.M.; de Souza Lopes, C.H.; Lima, E.S.; de Oliveira, M.A.; Cunha, M.S.B.; Alexandre, L.C.; da Silva, L.G.; Pereira, L.A.M.; Spadoti, D.H.; Romero, M.A.; Sodré Junior, A.C. Integrating Optical and Wireless Techniques towards Novel Fronthaul and Access Architectures in a 5G NR Framework. Appl. Sci. 2021, 11, 5048. https://doi.org/10.3390/app11115048

[4] E. -K. Hong et al., "6G R&D vision: Requirements and candidate technologies,"in Journal of Communications and Networks, vol. 24, no. 2, pp. 232-245, April 2022, doi: 10.23919/JCN.2022.000015.

[5] L. Augusto Melo Pereira, L. L. Mendes, C. J. A. Bastos Filho and A. Cerqueira Sodre, "Amplified radio-over-fiber system linearization using recurrent neural networks,"in Journal of Optical Communications and Networking, vol. 15, no. 3, pp. 144-154, March 2023, doi: 10.1364/JOCN.474290.

[6] R. Maximidis and others, "A 51 Gb/s Reconfigurable mmWave Fiber-Wireless C-RAN supporting 5G/6G MNO Network Sharing,"in Journal of Lightwave Technology, doi: 10.1109/JLT.2023.3246597.

[7] E. Ruggeri et al., "A 5G Fiber Wireless 4Gb/s WDM Fronthaul for Flexible 360° Coverage in V-Band massive MIMO Small Cells,"in Journal of Lightwave Technology, vol. 39, no. 4, pp. 1081-1088, 15 Feb.15, 2021, doi: 10.1109/JLT.2020.3029608.

[8] C. Lim, Y. Tian, C. Ranaweera, T. A. Nirmalathas, E. Wong and K. -L. Lee, "Evolution of Radio-Over-Fiber Technology,"in Journal of Lightwave Technology, vol. 37, no. 6, pp. 1647-1656, 15 March15, 2019, doi: 10.1109/JLT.2018.2876722.

[9] C. Vagionas et al., "End-to-End Real-Time Service Provisioning Over a SDN-Controllable Analog mmWave Fiber -Wireless 5G X-Haul Network,"in Journal of Lightwave Technology, vol. 41, no. 4, pp. 1104-1113, 15 Feb.15, 2023, doi: 10.1109/JLT.2023.3234365.

[10] R. M. Borges et al., "Integration of a GFDM-Based 5G Transceiver in a GPON Using Radio Over Fiber Technology,"in Journal of Lightwave Technology, vol. 36, no. 19, pp. 4468-4477, Oct.1, 2018, doi: 10.1109/JLT.2018.2826483.

[11] 3GPP, "Technical Specification Group Radio Access Network; NR; Base Station (BS) radio transmission and reception; Part-1," Technical Specification (TS) 38.104, 3rd Generation Partnership Project (3GPP) (2023). TS 38.104 version 18.1.0 Release 18.

[12] H. Rodrigues Dias Filgueiras et al., "Wireless and Optical Convergent Access Technologies Toward 6G,"in IEEE Access, vol. 11, pp. 9232-9259, 2023, doi: 10.1109/ACCESS.2023.3239807.

[13] R. M. Borges et al., "DSP-Based Flexible-Waveform and Multi-Application 5G Fiber-Wireless System,"in Journal of Lightwave Technology, vol. 38, no. 3, pp. 642-653, 1 Feb.1, 2020, doi: 10.1109/JLT.2019.2947916.

[14] G. K. M. Hasanuzzaman and others, "Self-Oscillating Optical Frequency Comb: Application to Low Phase Noise Millimeter Wave Generation and Radio-Over-Fiber Link,"in Journal of Lightwave Technology, vol. 36, no. 19, pp. 4535-4542, Oct.1, 2018, doi: 10.1109/JLT.2018.2844344.

[15] F. Shi, Y. Fan, X. Wang, W. Zhang and Y. Gao, "High-performance dual-band radio-over-fiber link for future 5G radio access applications,"in Journal of Optical Communications and Networking, vol. 14, no. 4, pp. 267-277, April 2022, doi: 10.1364/JOCN.440530.

[16] C. H. d. S. Lopes et al., "Non-Standalone 5G NR Fiber-Wireless System Using FSO and Fiber-Optics Fronthauls,"in Journal of Lightwave Technology, vol. 39, no. 2, pp. 406-417, 15 Jan.15, 2021, doi: 10.1109/JLT.2020.3029500.

[17] J. Bohata et al., "Performance Evaluation of Seamless 5G Outdoor RoFSO Transmission at 39 GHz,"in IEEE Photonics Technology Letters, vol. 34, no. 1, pp. 7-10, 1 Jan.1, 2022, doi: 10.1109/LPT.2021.3134559.

[18] J. Bohata, D. N. Nguyen, J. Spáčil, M. Komanec, B. Ortega, L. Vallejo, Z. Ghassemlooy, and S. Zvánovec, "Experimental comparison of DSB and CS-DSB mmW formats over a hybrid fiber and FSO fronthaul network for 5G,"Opt. Express 29, 27768-27782 (2021).

[19] Lima, E.S., Borges, R.M., Andriolli, N. et al. Integrated optical frequency comb for 5G NR Xhauls. Sci Rep 12, 16421 (2022). https://doi.org/10.1038/s41598-022-20553-5

[20] Tomás P. V. Andrade, Letícia Carneiro de Souza, Eduardo Saia Lima, and Arismar Cerqueira Sodré, "Demonstration of a hybrid A-RoF/VLC system for beyond 5G applications,"Appl. Opt. 62, C115-C121 (2023)

[21] Dong-Nhat Nguyen, Jan Bohata, Jan Spacil, Daniel Dousek, Matej Komanec, Stanislav Zvanovec, Zabih Ghassemlooy, and Beatriz Ortega, "M-QAM transmission over hybrid microwave photonic links at the K-band,"Opt. Express 27, 33745-33756 (2019)

Artigo 5 : Non-Standalone 5G NR Fiber-Wireless System Using FSO and Fiber-Optics Fronthauls

Celso Henrique de Souza Lopes, Eduardo Saia Lima, Luiz Augusto Melo Pereira, Ramon Maia Borges, Alexandre Carvalho Ferreira, Marcelo Abreu, Whebert Damascena Dias, Danilo Henrique Spadoti, Luciano Leonel Mendes and Arismar Cerqueira. S. Jr. ”Non-Standalone 5G NR Fiber-Wireless System Using FSO and Fiber-Optics Fronthauls”, *JOURNAL OF LIGHTWAVE TECHNOLOGY*, VOL. 39, NO.2, 2021.

Non-Standalone 5G NR Fiber-Wireless System Using FSO and Fiber-Optics Fronthauls

Celso Henrique de Souza Lopes, Eduardo Saia Lima, Luiz Augusto Melo Pereira, Ramon Maia Borges, Alexandre Carvalho Ferreira, Marcelo Abreu, Whebert Damascena Dias, Danilo Henrique Spadoti, Luciano Leonel Mendes, and Arismar Cerqueira Sodre Junior

***Abstract*—The fifth-generation of mobile networks (5G) claims for a radio access network (RAN) update in order to support the enormous incoming wireless data traffic. In this context, we experimentally evaluate two distinct hybrid architectures applied to 5G New Radio (NR) FiWi systems based on different optical fronthaul approaches. The first architecture operates in non-standalone (NSA) mode, defined by the 3rd generation partnership project (3GPP), for simultaneously transmitting 4G and 5G technologies through an unique FiWi system. The three considered waveforms are as follows: a filtered orthogonal frequency division multiplexing (F-OFDM) signal at 778 MHz with 10 MHz bandwidth from our 5G flexible-waveform transceiver; a long-term evolution-advanced (LTE-A) signal with five 20 MHz sub-bands centralized at 2.24 GHz; a 5G NR signal at 2.35 GHz with 100 MHz bandwidth. On the other side, the second architecture employs radio over fiber (RoF), free space optics (FSO), and wireless technologies converged into a heterogeneous network (HetNet). The additional multi-standard and multiband optical-wireless network is based on a 10-MHz bandwidth F-OFDM signal at 788 MHz, a 100-MHz bandwidth 5G NR signal at 3.5 GHz, and a 400-MHz bandwidth *M*-QAM signal at 26 GHz. Throughput up to 3 and 1.4 Gbps are demonstrated for RoF/FSO and RoF/FSO/Wireless transmission, respectively.**

***Index Terms*—4G, 5G NR, FSO, fiwi, hetnet, NSA.**

I. Introduction

THE fifth-generation of mobile network fifth-generation of mobile networks (5G) has already started to be commercially implemented worldwide. The main application scenarios that 5G aims to serve are basically defined as: enhanced mobile broadband (eMBB); massive machine type communication (mMTC) and ultra-reliable low-latency communication (URLLC) [1]. In addition, the enhanced remote area communications (eRAC) scenario, aimed for long-range communications up to 50 km, has also be considered potential to be included in the next 3GPP release versions. [1]. Due to the 5G plurality of applications, it becomes necessary to use innovative technical solutions, including: 5G new radio (5G NR) standard; additional spectral bands; software-defined network (SDN); massive multiple-input multiple-output (mMIMO). The 3GPP Release 15 establishes the phase 1 for the 5G standardization, called the New Radio Phase 1. At this initial stage of implementation, 5G networks operate in NSA, hence leveraging the fourth-generation of mobile networks (4G) architecture for deploying the 5G NR [2], [3].

In parallel, microwave photonics (MWP) has been recognized as a key technology for generating, processing and transmitting radiofrequency (RF) signals in the optical domain [4]. Notably, Radio over Fiber (RoF) technology empowers to transport and distribute digital and/or analog signals among central office (CO) and remote radio unit (RRU) via fiber optic links. Sequentially, the signal is photodetected at base station (BS) before being radiated, giving rise to a fiber-wireless (FiWi) system, which has been proposed to meet the 5G scenarios [5]. The radio access network (RAN) architectures must complementarily evolve the evolution of transport networks. One of the most quoted architecture for 5G networks is the centralized RAN (C-RAN) [6]. In C-RAN architecture, the backhaul link connects CO to the core network, typically carrying digital user data, whereas the fronthaul link connects CO to RRUs. Currently, most fronthaul links are based on digital RoF (D-RoF) technology, using Common Public Radio Interface (CPRI). Nonetheless, this technique suffers from scalability issues, which suggests the use of alternatives fronthaul solutions [7]. Analog RoF (A-RoF) represents a promising solution to simplify the system and enhance its scalability, since there is no need for analog-to-digital converter (ADC) and digital-to-analog converter (DAC), either at RRUs and CO [8]. Another potential fronthaul approach is employing free space optics (FSO) links, which provide high capacity with

Manuscript received June 22, 2020; revised August 10, 2020, September 4, 2020, and September 29, 2020; accepted September 30, 2020. Date of publication October 7, 2020; date of current version January 15, 2021. This work was supported in part by RNP, with resources from MCTIC, under Grant 01250.075413/2018-04, under the Radiocommunication Reference Center (Centro de Referência em Radiocomunicações-CRR) Project of the National Institute of Telecommunications (Instituto Nacional de Telecomunicações-Inatel), Brazil, in part by CAPES, in part by FINEP, and in part by CNPq. *(Corresponding author: Arismar Cerqueira.)*

Celso Henrique de Souza Lopes, Eduardo Saia Lima, Luiz Augusto Melo Pereira, Alexandre Carvalho Ferreira, Whebert Damascena Dias, Luciano Leonel Mendes, and Arismar Cerqueira Sodré Junior are with Inatel, Santa Rita do Sapucaí, MG 37400-000, Brazil (e-mail: celso.lopes@mtel.inatel.br; elima@get.inatel.br; luiz_augusto@get.inatel.br; alexandrecf@inatel.br; wheberth@inatel.br; lucianol@inatel.br; arismar@inatel.br).

Ramon Maia Borges is with Inatel, Santa Rita do Sapucaí, MG 37540-000, Brazil, and also with the Federal University of Itajubá (UNIFEI), Itajubá, MG 37500-903, Brazil (e-mail: ramonmb@inatel.br).

Marcelo Abreu is with Venturus Innovation and Technology, 13086-530 Campinas, Brazil (e-mail: Marcelo.Abreu@venturus.org.br).

Danilo Henrique Spadoti is with UNIFEI, Itajubá, MG 37500-903, Brazil (e-mail: spadoti@unifei.edu.br).

Color versions of one or more of the figures in this article are available online at https://ieeexplore.ieee.org.

Digital Object Identifier 10.1109/JLT.2020.3029500

electromagnetic immunity and using the unlicensed Terahertz bands [9]. The use of FSO links requires to deal with atmospheric phenomena, that could degrade the transmission quality, e.g rain, fog, temperature variations and dust [10].

Diverse works have claimed the terahertz communications (THz) use to fulfill the future wireless network demands. Shakir *et al.* demonstrated a simultaneous transmission employing an FSO at 1.5 μm and a 60 GHz RF system [11]. Moreover, RoF/FSO/Wireless links enable to extend the fronthaul reach to regions, where the optical fiber is difficult to be deployed, maintaining the attractive features from the optical communications and wireless access to the end user. In [12], Chong Han *et al.* have reported a comparison among microwave, mm-waves, THz band and FSO approaches based on the following aspects: technical challenges, channel modelling and propagation characteristics, such as atmospheric and spreading losses, diffraction and weather influences.

Table I summarizes the state-of-the-art solutions based on RoF, FiWi and FSO for high transmission capacity links [13]–[21]. Delmade *et al.* [13] demonstrated the transmission of different 4G and 5G services coexisting on the same RoF link in the 700 MHz to 3.6 GHz band. The integration and experimental performance analysis of a 5G transceiver based on generalized frequency division multiplexing (GFDM) in a RoF-based gigabit passive optical network (GPON) has been reported by our research group in [14]. Bohata *et al.* [15] combined the FSO and FiWi techniques for transmitting a 100-MHz bandwidth signal using 64-QAM modulation. In [16], authors have experimentally analyzed the effects of dust storms on the performance of an FSO link, carrying a RF signal at 28 GHz; their results demonstrate the FSO all-optical link is significantly affected by low visibility. Furthermore, we have recently reported the implementation of a DSP-based flexible-waveform and multiband FiWi system, applied to 5G scenarios and PROFINET-based vertical applications [17]. A heterogeneous RoF/FSO/Wireless non-standalone (NSA) transmission of LTE-A and 5G NR signals in the 2.2 and 3.5 GHz bands, respectively, was demonstrated in [18]. According to the literature, the state-of-the-art proposes internal FSO links as proof of concept for lengths ranging from 0.9 to 2 m [15], [16]. For external environments, links with 500-m reach were demonstrated attaining 100 Gbps [19]. In [20], we have implemented a multiband and photonically amplified FiWi system, which allows to simultaneously transport and amplify multiple RF signals for providing a variety of 5G services, including Gbps throughput at 28 GHz. Finally, the reference [21] proposes a self-steering array beamformer (SSA-BF) receiving system, which is composed of a home-designed integrated circuits (IC) package with zero DC power consumption and a 4-element antenna array.

Fig. 1 illustrates the diversity of services that can be offered by using mobile networks operating in a hybrid mode. CO is physically connected to the network core, using a fiber optics-based backhaul (BH). Fronthaul links might be based on different photonics technologies, including fiber optics and FSO. The latter is commonly applied to bypass environments, where the use of optical fibers is impractical, such as mountainous regions, river and lake crossings. Wireless access networks could serve

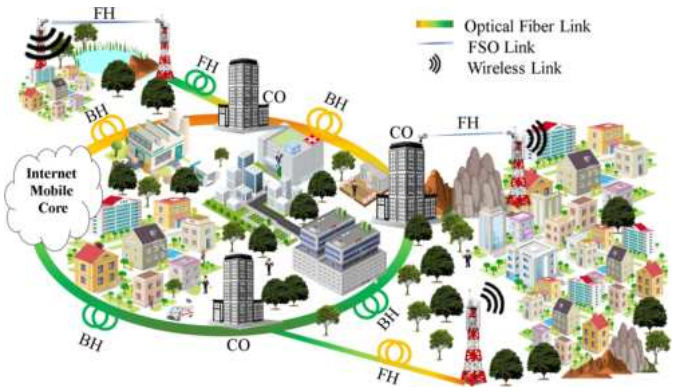

Fig. 1. FiWi system based on RoF/FSO/Wireless fronthaul implementation. BH-Backhaul; FH-Fronthaul; CO-Central Office; FSO-Free Space Optics.

remote and rural areas, as well as indoor and outdoor eMBB applications.

The current work reports the implementation and experimental investigation of two different non-standalone 5G NR networks architectures, aiming to fulfill the 5G demands. The first implementation applies direct modulation and detection for transmitting 4G and 5G signals over a 25-km fiber-optics fronthaul, followed by 105-m wireless link, namely: our digital signal processing (DSP)-based and flexible waveform 5G transceiver [17] using F-OFDM; a 100-MHz 5G NR standard signal at 2.35 GHz; a 100-MHz LTE-A signal at 2.24 GHz. Its main contribution over the state-of-the-art is the deployment of a non-standalone 4G/5G FiWi system based on A-RoF technology using adjacent channels, being one of them our DSP-based flexible waveform 5G transceiver. To the best of our knowledge, for the first time in literature the coexistence between LTE-A and 5G NR commercial standards in a NSA FiWi system is performed considering both optical and wireless media impairments. A peaceful coexistence is demonstrated, by properly managing the frequency offset between the LTE-A and 5G NR signals, providing an efficient spectrum sharing with interference mitigation. Completely, the F-OFDM waveform use plays an important role on the coexistence, due to its intrinsic lower out-of-band emission compared to the conventional CP-OFDM waveform.

The second proposed architecture relies on a novel and efficient 5G heterogeneous optical-wireless network using RoF, FSO and wireless technologies toward eRAC and eMBB applications. It employs a hybrid fronthaul, which embrases a 12.5-km RoF link followed by a 1-m FSO link, besides an 8-m indoor wireless access network. The additional multi-standard and multiband optical-wireless network is based on a 10-MHz bandwidth F-OFDM signal at 788 MHz, a 100-MHz bandwidth 5G NR signal at 3.5 GHz and a 400-MHz bandwidth M-QAM signal at 26 GHz. The impact of attenuation and atmospheric turbulence from the FSO fronthaul on the RoF/FSO/Wireless HetNet performance is unprecedentedly evaluated, as a function of the magnitude of the root mean square error vector ($\mathrm{EVM_{RMS}}$) and in according to the 3GPP Release 15 requirements.

The manuscript is structured in five sections. Section II describes our DSP-based and flexible waveform 5G transceiver, developed for remote areas coverage. Section III presents the

TABLE I
STATE-OF-THE-ART FOR PHOTONICS SOLUTIONS FOR 5G NETWORKS

Reference	Architecture	Waveform Standard	Frequency Range	Fronthaul	Wireless Access Network	Throughput
[13]	RoF	OFDM GFDM UF-OFDM	From 700 MHz to 3.6 GHz	Fiber-optics	No	8.1 Gbps
[14]	RoF	GFDM 16-QAM	735 MHz 26 GHz	Fiber-optics	No	100 Mbps 1 Gbps
[15]	FSO/FiWi	64-QAM	From 24 to 26 GHz	Fiber-optics	Yes	10 Gbps
[16]	FSO/Wireless	16-QAM	28 GHz	FSO	Yes	4 Gbps
[17]	FiWi	F-OFDM GFDM OFDM 16- and 64-QAM Standard 5G NR	Baseband 788 MHz 3.5 GHz 26 GHz	Fiber-optics	Yes	4.41 Gbps
[18]	RoF/FSO/Wireless	Standard LTE-A Standard 5G NR	2.12 and 1.72 GHz 2.68 and 2.56 GHz 3.5 GHz	Fiber-optics	No	—
[19]	FSO-UWOC	PAM4	1.7 GHz 1.8 GHz	FSO	Yes	100 Gbps
[20]	FiWi	16- and 64-QAM	7.5 GHz 28 GHz	Fiber-optics	Yes	10 Gbps
[21]	FiWi	OFDM	28 GHz	Fiber-optics	Yes	10 Gbps
This work	FiWi RoF/FSO/Wireless	F-OFDM Standard LTE-A Standard 5G NR 16-QAM	778 and 788 MHz From 2.2 to 2.28 GHz 2.35 and 3.5 GHz 26 GHz	Fiber-optics FSO	Yes	1.1 Gbps 3 Gbps 1.4 Gbps

investigation of the NSA 4G/5G FiWi system, using an fiber optics-based fronthaul, whereas Section IV reports the proposed 5G optical-wireless HetNet using RoF, FSO and wireless technologies. Finally, the conclusions and future works are drawn in Section V.

II. 5G FOR REMOTE AREAS TRANSCEIVER

The effort to develop a revolutionary mobile network is pushing 5G to cover a wide range of conflicting requirements. An important scenario for large size countries has received only partial attention. Internet wireless connectivity in remote and rural areas is a key future for 5G networks to support several new verticals, such as smart farms, road coverage, disaster monitoring and smart mines. Moreover, a mobile network for remote areas might bring a large parcel of the unconnected population to the Information era. However, Long-term Evolution (LTE) was developed to fulfil the requirements of urban environments. Therefore, the limited cyclic prefix of 4.7 μs, for normal mode, and 16.67 μs for the extended mode, does not avoid inter block interference among the orthogonal frequency division multiplexing (OFDM) symbols when the coverage increases. The cell radius of this network might achieve up to 50 km, while delivering up to 100 Mbps at the edge, allowing for an affordable mobile network deployment in remote areas. This section presents our digital signal processing (DSP)-based 5G transceiver, which has been developed in the context of the remote area access network for the 5th generation (5G-RANGE) project [22] to provide connectivity in remote and rural areas for different applications and satisfying the technical and economic requirements for remote area operation.

A. Requirements

The remote and rural areas applications demand different requirements, from low latency for rural machinery control to broadband connectivity for video monitoring of crops and cattle. Table II shows the main requirements addressed by the physical layer (PHY) and medium access control (MAC) layer described in this section [23].

High throughput is needed for providing broadband Internet access for those living in uncovered or underserved areas. Long-range coverage is important to increase the number of subscribers per cell, reducing the number of BSs necessary to provide the service. Additionally, long-range cell is important

TABLE II
REQUIREMENTS FOR REMOTE AND RURAL AREAS NETWORKS

Requirement	Value
Throughput	100 Mbps
Coverage	50 km
Latency	20 ms
Frequency band	unlicensed
Spectrum allocation	Fragmented, secondary
Out-of-band emissions	-50 dBc without RF filters

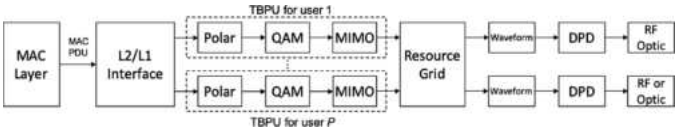

Fig. 2. Block diagram of our 5G transmitter.

for road coverage. Low latency is needed for controlling autonomous machinery, such as harvesters or drones for agribusiness. The cost for licensed spectrum is prohibitive in remote and rural areas, thus the network must exploit idle frequency bands as secondary user. TV white space (TVWS) exploitation [24] is an interesting solution, since the TV occupancy is rural and remote areas is low. Nevertheless, the primary users (PUs) must be protected and the waveform used by the secondary network must present very low out-of-band emission (OOBE) [25], while being able to employ discontinuous spectrum chunks without causing interference in legacy technologies.

B. Physical Layer

The transceiver proposed for remote and rural areas applications uses the most recent digital communication techniques to overcome the challenging doubly-dispersive channels [26]. Fig. 2 displays the basic block diagram of the proposed transmitter.

The data from the MAC layer is delivered to the PHY using an L2/L1 interface. The MAC Protocol Data Unit (PDU) contains all control information for the resource allocation and Modulation Coding Scheme (MCS) configuration [27], as well as the data to be transmitted in the frame. Data are processed individually for each user, by the Transport Block Processing Unit (TBPU), which is responsible for the channel encoding, quadrature amplitude modulation (QAM) modulation, multiple-input multiple-output (MIMO) encoder, and auxiliary signalling insertion. The transceiver employs the Polar code as forward error correction (FEC) because of its low complexity and high error correction capability. The code rate is flexible and it can assume different values. Puncturing is used to further improve the flexibility. The QAM mapper can use modulation order $J = 2^p$, for $p \in \{2, 4, 6, 8\}$. The combination of a code rate and a modulation order consists on a specific MCS.

In this transceiver, two MIMO schemes have been implemented for different goals. For the users close to the BS, where the signal-to-noise ratio (SNR) is high enough, the MIMO system is used to increase the network throughput, hence, space multiplex [28] is employed. For user located far away from BS, the MIMO scheme is used to increase the robustness, by providing diversity. In this case, an Space-Time Block Code (STBC) [29] is used. The decision on which MCS or MIMO scheme will be used for each user is based on a feedback quality parameter sent by the user equipment (UE) to the BS, called Channel Quality Indicator (CQI). Such parameter is evaluated by UE based on the received SNR or on the perceived bit error rate (BER). Low CQI trigger the BS to use more robust MCS and STBC for the specific user, while high CQI triggers BS to use spectrum efficient CQI and space multiplexing.

After the MIMO encoding, data samples are organized in a time-frequency grid, in which the pilot signalling as inserted. A waveform modulator is applied to produce the base-band signal to be transmitted. Transceiver can employ three different waveforms: OFDM [30], F-OFDM [31] and GFDM [32]. OFDM is the most common waveform in wireless system nowadays due to its simplicity and robustness against multipath channel. OFDM uses K orthogonal subcarriers to transmit K data samples, using a square pulse shape. Therefore, OFDM has very high OOBE. F-OFDM is a derivation from OFDM, but with base-band filter applied to the entire bandwidth. This filter reduces OOBE, while keeping the orthogonality within in the total bandwidth. GFDM is a new waveform that uses K subcarriers and M subsymbols to transmit $N = KM$ data symbols. A prototype Filter Impulse Response (FIR) is K times cyclically shifted in frequency and M times cyclically shifted in time to produce a set of N FIRs, one for each data symbol. The modulated FIRs are added together and a cyclic prefix (CP) is added to protect the signal from multipath channels. The subcarrier filtering reduces OOBE, which can be further reduced by using a time window applied over the modulated signal. The time window smooths the transition from one block to the other, improving the frequency localization of the signal. The time windowed GFDM can achieve OOBE below -50 dBc.

Finally, the signal provide by the GFDM modulators are applied to the Digital Pre-Distortion (DPD). This block is responsible for compensating the non-linearities introduces by the power amplifier. The pre-distorted signal is shifted to the band-pass operating frequency and amplified before being applied to the transmit antenna for wireless communication or applied to the optical system. On the receiver side. all the processes described for the transmitter are reversed, and the recovered PDU are delivered to the MAC layer by the L1/L2 interface.

C. MAC Layer

The MAC layer implemented in our transceiver is responsible for controlling PHY, defining the MCS and MIMO scheme to be used by each user, according with the corresponding CQI. The MAC layer is also responsible for the resource allocation in the time-frequency grid and for the spectrum allocation. This is one of the main innovation in this MAC layer, since secondary use of the idle channels is a demand for remote and rural areas operation, the MAC layer must be able to define which channels are available in the region where the network is being deployed.

As depicted in Fig. 3, the MAC layer uses a cognitive engine to decide about the channel allocation based on the spectrum

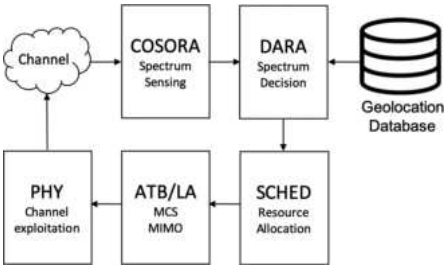

Fig. 3. MAC layer block diagram.

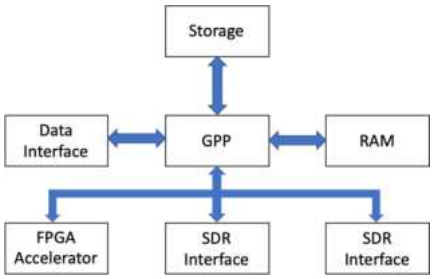

Fig. 4. Block diagram of the SDR platform.

sensing performed by selected UEs. The BS commands the UEs to measure the potentially available channels using the Collaborative Spectrum Sensing Optimized for Remote Areas (COSORA) block [33].

After performing the spectrum sensing, UEs reports their individual results to BS that fuses all measurements to obtain a final decision about the availability of the channels using the Dynamic Spectrum and Resource Allocation for Remote Areas (DARA) block [33]. This block also consults a geolocation database listing the available channels according with the spectrum regulator. The Scheduler is responsible for allocating the user data on the selected channels. Notice that Fragmented Spectrum Allocation (FSA) [34] might be used to exploit chunks of spectrum among TV signals. Finally, the Adaptive Transmission Bandwidth (ATB) and Link Adaptation (LA) blocks defines which MCS and MIMO scheme to be used for transmitting and receiving the data from a given user.

D. Implementation and Performance Analysis

Our 5G-RANGE transceiver has been implemented using software-defined radio (SDR) approach. Figure 4 describes the basic block diagram of the 5G-RANGE transceiver platform. A general purpose processor (GPP)-based platform has been used to process all base-band signals, while a radio front-end, named SDR interface and connected with the GPP through a peripheral component interconnect (PCI) express bus, provides an interface with the transmit and received antennas or the optical system. An field programmable gate array (FPGA) board is used as hardware accelerator for blocks that needs high parallelism, such as the Polar decoder.

The proposed 5G transceiver represents a low cost and highly flexible solution, since off-the-shelves computers can be used to implement state-of-the-art communication systems. Figure 5

Fig. 5. The our 5G-RANGE transceiver.

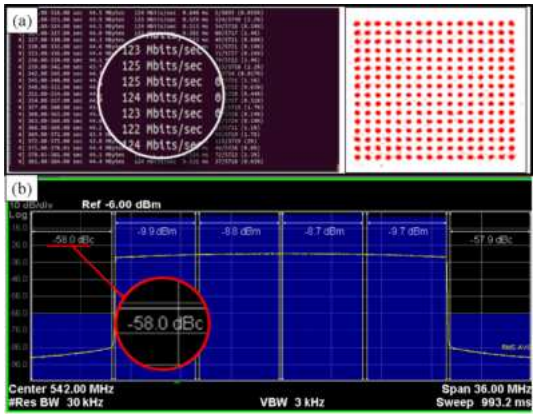

Fig. 6. (a) SDR transceiver maximum data rate (b) SDR OOBE performance.

shows a picture of the transceiver, where a mini personal computer (PC) is used as GPP and a National Instruments universal software radio peripheral (USRP) model 2954R is used as FPGA accelerator and SDR interface.

The 5G-RANGE transceiver achieves high performance in terms of throughput and OOBE. Figure 6 (a) reports that the transceiver is able to deliver up to 125 Mbps, whereas 6 (b) depicts an OOBE below −58 dBc without any RF filtering.

III. Implementation of the NSA 4G/5G FiWi System Using a Fiber-Optics Fronthaul

The implementation of the 4G/5G FiWi system using a fiber-optics fronthaul was based on the simultaneous transmission and distribution of different RF signals, using adjacent channels. Since the optical fiber has a broad available bandwidth, the maximum link capacity is going to be mainly limited by the response of the optical components. For instance, the electro-optical response of the optical modulator and photodetectors, as well as the antennas bandwidth. Fig. 7 depicts a block diagram of the proposed architecture based on ARoF. In accordance to the C-RAN concept, the scheme is divided into three main parts: CO, RRU and end user as indicated by the (i), (ii) and (iii) figure markers, respectively. The transport network regards the 25-km single-mode fiber (SMF)-based fronthaul, connecting CO with RRU, besides the 10-m wireless link, connecting remote radio

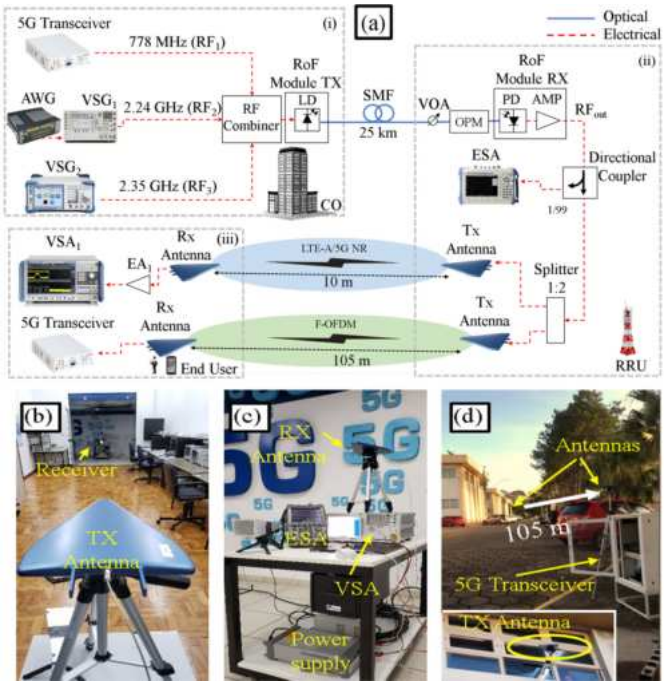

Fig. 7. The proposed 4G/5G FiWi architecture using radio over fiber: (a) block diagram; (b) 10-m wireless indoor link; (c) indoor receiver side; (d) the 105-m wireless outdoor link view. AWG - arbitrary waveform generator; VSG - vector signal generator; LD - laser diode; SMF - single mode fiber; VOA - variable optical attenuator; OPM - optical power monitor; PD - photodetector; AMP - amplifier; EA - electrical amplifier; VSA - vector signal analyzer.

head (RRH) with the end user unit. Our current implementation exploits the downlink path. The uplink path represents an important challenge owing power restriction, which might impact the system performance, e.g. increasing $\mathrm{EVM_{RMS}}$. Downlink and uplink are expected to be asymmetric in terms of throughput, despite the bandwidth symmetry. It means the transmission in the uplink direction might use more robust code and modulation, besides employing the MIMO scheme only to obtain robustness and diversity, instead of increasing throughput. Therefore, even with power restriction, the mobile terminal is expected to be able to establish a communication link with the base station. The uplink is going to be exploited in a future work.

At CO, the proposal 5G transceiver generates the first RF signal ($\mathrm{RF_1}$), corresponding to a 64-QAM and 10 MHz bandwidth F-OFDM signal at 778 MHz, toward eRAC applications. A M8190 A arbitrary waveform generator (AWG) from Keysight running the Signal Studio software generates five 256-QAM LTE-A subbands using carrier aggregation. These subbands are sequentially up converted by a PSGE8267D vector signal generator ($\mathrm{VSG_1}$), also from Keysight, giving rise to the second RF signal ($\mathrm{RF_2}$). The latter one has 100 MHz total bandwidth, central frequency of 2.24 GHz and is aimed for eMBB applications. Moreover, a SMBV100B vector signal generator ($\mathrm{VSG_2}$) from Rohde & Schwarz provides the third RF signal ($\mathrm{RF_3}$) to be transmitted, corresponding to the 5G NR standard in accordance with the 3GPP Release 15 [3]. Similarly to the LTE-A signal, $\mathrm{RF_3}$ has 256-QAM symbols and 100 MHz bandwidth to address the eMBB scenario. However, it is centered at 2.35 GHz. At CO, a RF combiner couples all generated RF signals for driven the electrical-to-optical (E/O) conversion stage based on a commercial RoF module from Oz Optics (OZ101mini TX). Basically, the RoF transmitter is composed of a 4 dBm distributed-feedback (DFB) laser centered at 1551 nm, a RF input and an optical output. The 1551 nm optical carrier is simultaneously modulated by the three mentioned RF signals and then launched into the 25-km G652D optical fiber-based fronthaul link. Analog radio over fiber (ARoF) systems might suffer from fading effect due to the fiber chromatic dispersion, since the beating of side-bands leads to periodic destructive interference depending on the operating frequency and fiber length. Specifically for 25 km of a G652D fiber with chromatic dispersion $\mathrm{D} = 17$ ps/nm.km, one could expect fading nodes for frequencies higher than 12 GHz. Since the maximum frequency of our 5G FiWi system implementation was 2.35 GHz ($\mathrm{RF_3}$), there was no degradation due to the fading effect. Moreover, it is important to highlight that the maximum fronthaul reach is limited by latency and not by optical power at RRU [35]. Therefore, it is not necessary to employ an Erbium-doped fiber amplifier (EDFA) for compensating de link losses, since the total attenuation is only 5 dB. At RRU, a variable optical attenuator (VOA) and an optical power monitor (OPM) are used to manage and measure the optical power at the photodetector input, respectively. VOA and OPM support our experimental characterization and are not required in a commercial deployment, which can apply the optical-to-electrical (O/E) conversion as the RRU first stage. In the implemented setup, a second commercial RoF module from Oz Optics (OZ101mini RX) performs the O/E conversion using direct detection. It is worth mentioning such device takes benefit of 22-dB integrated electrical amplification. The recovered and amplified RF signals are then submitted to a directional coupler, which provides a sample of the electrical field with 1% of the total energy to a BTS MT8222 A electrical spectrum analyzer (ESA) from Anritsu measuring/monitoring $\mathrm{RF_1}$, $\mathrm{RF_2}$ and $\mathrm{RF_3}$. In parallel, the directional coupler delivers 99% of total energy to a 1:2 power splitter, used for creating two versions of the RF signals. The latter ones feed commercial antennas (AARONIA HyperLOG 7040, with 5-dBi gain) for wireless transmission and are received by identical HyperLOG antennas. Finally, the 5G transceiver receiver block demodulates the 778 MHz F-OFDM signal at the end user, whereas $\mathrm{RF_2}$ and $\mathrm{RF_3}$ are 40-dB amplified by an electrical amplification stage and demodulated by the FSW-8351 vector signal analyzer ($\mathrm{VSA_1}$) from Rohde & Schwarz. Fig. 8 shows photographs of the experimental setup. We have divided the experimental investigation into two phases, namely: RoF system analysis; FiWi system analysis.

A. *Rof System Analysis*

First, the electrical spectrum at the RoF receiver module output is reported in Fig. 8, assuming -6 dBm RF power for each electrical signal at CO, as well as -7 dBm receiving optical power at RRU. One can note the presence of the three RF signals at 778.0 MHz, 2.24 GHz and 2.35 GHz, besides the absence of undesired spectral components. From the zoom-in-views

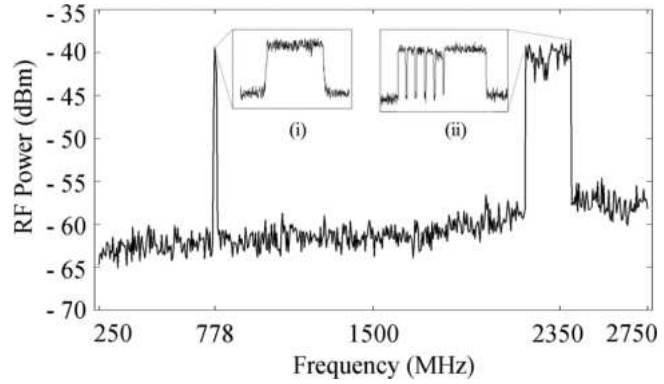

Fig. 8. Measured electrical spectrum at the RoF module output.

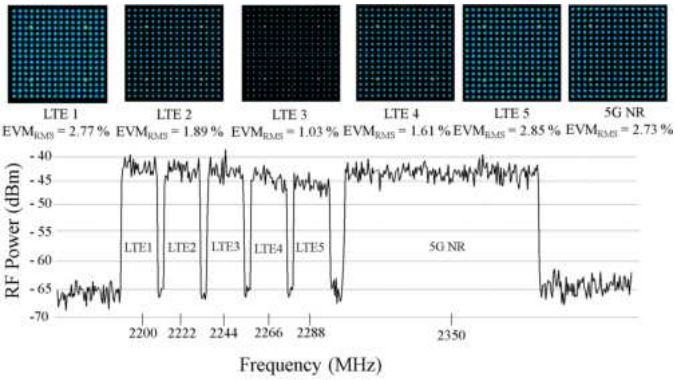

Fig. 9. Electrical spectrum, constellations and $\mathrm{EVM_{RMS}}$ measurements for the LTE-A and 5G NR signals with 106 MHz frequency offset.

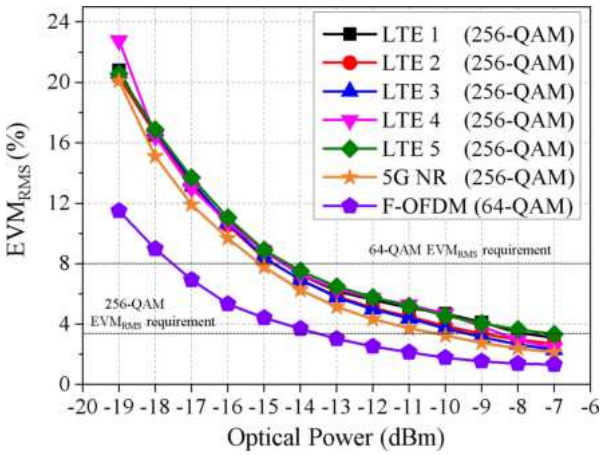

Fig. 10. $\mathrm{EVM_{RMS}}$ as a function of the optical power at the photodetector.

presented in the insets (i) and (ii), one can also observe there is no apparent distortion after the simultaneous modulation in the optical domain. Especially in the inset (ii), it is visible the five 20 MHz bandwidth LTE-A subbands, occupying a 100 MHz portion of the spectrum and coexisting with the 5G NR signal. The power level decay of the two upper LTE-A subbands is due to the fact these ones are closer to the $\mathrm{RF_2}$ generator bandwidth limit, which is 110 MHz for $\mathrm{FR_1}$.

The next step of our investigation was the 5G NR and 4G coexistence investigation, since many research groups and companies have claimed the 5G deployment on top of the existing LTE-A. In such analysis, $\mathrm{RF_2}$ was kept centered at 2.24 GHz, whereas the $\mathrm{RF_3}$ frequency carrier was varied, with the purpose of changing the frequency offset between the RF signals and evaluating a peaceful coexistence, i.e. the minimum frequency offset that does not impose interference between the LTE-A and 5G NR standards. The evaluated figure of merit was the error vector magnitude, in such way the obtained $\mathrm{EVM_{RMS}}$ values were compared to the 3GPP requirements in accordance with the Releases 14 and 15. The latter ones specify 8% and 3.5% as $\mathrm{EVM_{RMS}}$ limits for 64 and 256-QAM modulation orders, respectively [3].

By taking the aforementioned $\mathrm{EVM_{RMS}}$ values as reference, we found the minimum frequency offset of 106 MHz that allows efficiently meeting the 3GPP requirements, as reported in Fig. 9. This frequency offset corresponds to a guard band of 2 MHz. In case of setting 106 MHz offset, we achieved 490 Mbps throughput for LTE-A with $\mathrm{EVM_{RMS}}$ of 2.8%, assuming the extreme subbands, and lower than 1.9% for the central subbands. The extreme subbands present worst digital performance owing the generator bandwidth, which affects mainly the signals close to the cutoff frequency of the radio equipment. Moreover, the 5G NR signal has enabled 578 Mbps throughput with 2.7% $\mathrm{EVM_{RMS}}$. The measured constellations of each LTE-A subband and 5G NR signal are presented in the Fig. 9 insets, from which one can observe well defined symbols. It is worth mentioning two points: the F-OFDM signal at 778 MHz was kept on all the time, ensuring a 60 Mbps throughput with 2.8% $\mathrm{EVM_{RMS}}$; by reducing frequency offset to 105 MHz, $\mathrm{EVM_{RMS}}$ from both 4G and 5G signals exceeded 17% as a result of interference. From the reported results, one can conclude the 4G and 5G standards can have a peaceful coexistence in the proposed architecture, addressing eRAC and eMBB applications, as long as the minimum 106 MHz frequency offset is respected.

Before radiating the RF signals, we measured the $\mathrm{EVM_{RMS}}$ at the RoF system output, as a function of the photodetector input power, which was varied from -19 to -7 dBm. Our goal was identifying the optical power levels that allow meeting the 3GPP $\mathrm{EVM_{RMS}}$ requirements for the F-OFDM, LTE-A and 5G NR signals. For the analysis, the frequency offset between the 4G and 5G NR signals was kept as 106 MHz, and the electrical power at the RF combiner output was -5 dBm. As reported in Fig. 10, $\mathrm{EVM_{RMS}}$ of the 64-QAM F-OFDM signal at 778 MHz met the 3GPP $\mathrm{EVM_{RMS}}$ requirement of 8% for receiving optical power levels higher than -17.5 dBm.

The central subbands of the LTE-A signal presented $\mathrm{EVM_{RMS}}$ below 3.5% for an optical power higher or equal to -9 dBm, whereas the extreme LTE-A subbands demanded 2 dB more optical power to meet such $\mathrm{EVM_{RMS}}$ requirement. The 256-QAM 5G NR signal at 2.35 GHz met the 3GPP $\mathrm{EVM_{RMS}}$ requirement of 3.5% for receiving optical power levels higher or equal to -9 dBm. The F-OFDM enhanced digital performance at lower optical powers in relation to the other signals is justified by the use of the developed 5G transceiver as generator, which takes advantage of a lower bandwidth hardware over the

commercial VSGs, favoring performance improvements. Therefore, simultaneously addressing eRAC and eMBB applications in the presented conditions requires a minimum optical power level of −7 dBm at RRU, besides a minimum offset of 106 MHz between the LTE-A and 5G NR signals.

Regarding the interference mitigation for more general transmission cases, the 5G NR standard provides the flexibility of choosing the subcarrier spacing, unlike LTE-A that only permits 15-kHz subcarrier spacings. Particularly, 5G NR specifies 15, 30 and 60 kHz subcarrier spacing options in the frequency range 1 (FR1) range. As a consequence, the coexistence between LTE-A with a 5G NR signal, or even another multicarrier waveform scheme, might be enhanced by using the 15-kHz subcarrier spacing option. This solution aims to keep the orthogonality between the LTE-A and 5G NR subcarriers, enabling interference mitigation between the signals.

B. *Fiwi System Analysis*

We have implemented a 10-m reach indoor femtocell, embracing both LTE-A and 5G NR wireless transmission, after the RF distribution over 25-km optical fronthaul. The minimum frequency offset between the LTE-A and 5G NR of 106 MHz was kept toward a peaceful coexistence with the lower guard band as possible. The optical power at the photodetector input was set to −7 dBm. The effective isotropic radiated power (EIRP) was −17 and −16 dBm at 2.24 and 2.35 GHz, respectively. Fig. 11 reports the measured spectrum using VSA_1. The magnitude difference among the signals comes from the wireless channel response, and the additional spectrum components come from other active telecommunication services. The LTE-A signal presented well defined symbols in the constellation and a maximum EVM_{RMS} of 3.3% as reported in the insets, meeting the 3GPP EVM_{RMS} requirement of 3.5% for 256-QAM. A 3.3% EVM_{RMS} refers to the extreme subband on the right side, i.e. the worst case as previously demonstrated. In a similar way, the 5G NR signal presented well defined symbols in the constellation and 3.1% EVM_{RMS}, meeting the 3GPP requirement for this parameter. As a conclusion, the LTE-A and 5G NR signal proved to be able to coexist in the proposed FiWi system.

A digital performance comparison has been performed among back-to-back (B2B), RoF and FiWi configurations, as presented in Fig. 12. The B2B implementation considers the RF transmitter directly connected to the receiver, enabling to measure the minimum allowable EVM_{RMS} for evaluating the impact of the RoF and FiWi system implementations. It is worth mentioning that the F-OFDM signal has been transmitted over a 105-m wireless link, instead of 10-m as in the previous case. An EVM_{RMS} as low as 1.5% has been obtained for the B2B configuration. One can note the RoF implementation implied in increasing the EVM_{RMS} parameter, as a result of the propagation throughput 25 km of SMF, losses in the electrical-optical and optical-electrical conversion, as well as the photodetector noise sources, including thermal noise, shot noise and dark current. Particularly the LTE-A central sub-band suffers higher interference, due to the neighbor sub-bands at both sides. Nevertheless, all evaluated signals attained the 3GPP

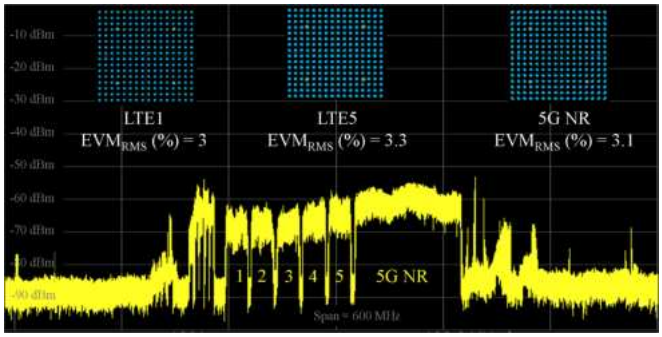

Fig. 11. The received electrical spectrum at the end user after 10-m wireless transmission and 25-km fiber-optic distribution.

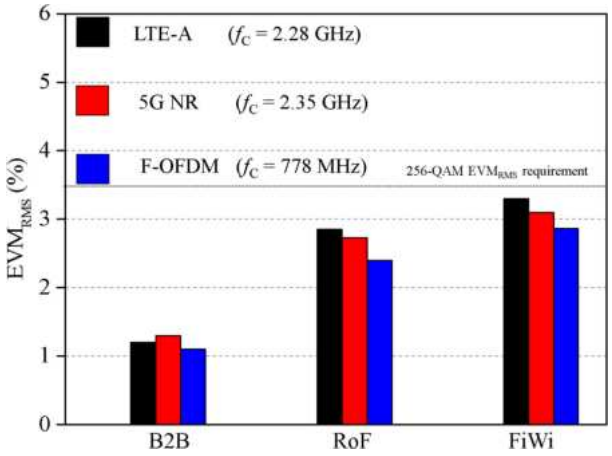

Fig. 12. EVM_{RMS} measurements for the LTE-A, 5G NR and F-OFDM signals in the back-to-back; RoF and FiWi configurations.

EVM_{RMS} requirements, providing 1.1 Gbps of total throughput. The multipaths imposed by the wireless channel impair the transmitted signals in either phase and magnitude. Despite the performance reduction, EVM_{RMS} has increased by only 0.5%, satisfying the 3GPP limit for 256-QAM (3.5%) for all assessed signals. Furthermore, the 5G transceiver for remote areas operating with F-OFDM presented enhanced digital performance in all evaluated scenarios, mainly due to its lower operating frequency. A maximum EVM_{RMS} of 3.3% demonstrates the proposed NSA 5G FiWi system feasibility and applicability.

The next step was the implementation of a 105-m reach outdoor link for investigating the coexistence between the 5G transceiver signal at 712 MHz and a 10-MHz bandwidth LTE signal. The carrier frequency of the later one has been varied from 722 MHz to 720.5 MHz, reducing then the co-channels guardband. The referred analysis considered 64-QAM modulation. For the LTE carrier frequencies of 722 and 721 MHz, the F-OFDM signal presented MER equals to 34.4 and 31.2 dB, respectively. By setting the LTE carrier to 720.5 MHz, the F-OFDM MER reduced to 30.4 dB, as indicates the LabVIEW print from Fig. 13, which also presents BER $= 7.7\times10^{-7}$,as well as the received constellation. When applying no guardband, i.e. LTE carrier at 720 MHz, the F-OFDM MER was only 25.1 dB, leading to 11.9×10^{-3} BER. The obtained results indicated that

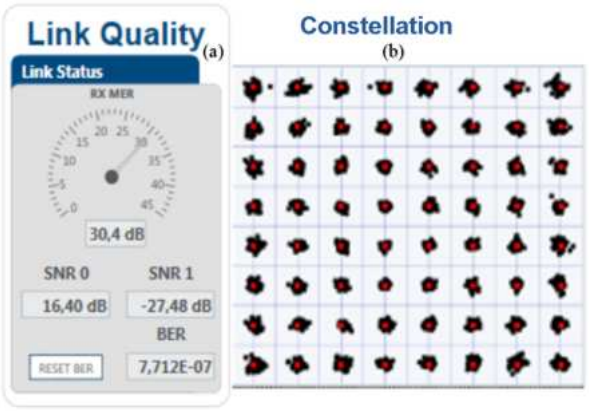

Fig. 13. Analysis of the 4G/5G signals over the RoF/FiWi system after 105 m wireless transmission: (a) LabVIEW meter; (b) Received constellation.

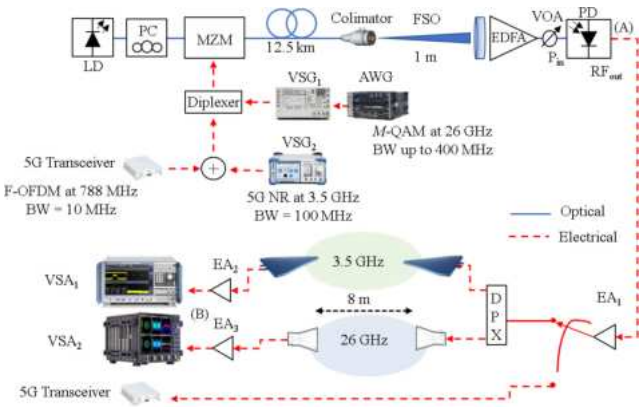

Fig. 14. Our hybrid 5G FiWi architecture using RoF and FSO. PC - polarization controller; AWG - arbitrary waveform generator; VSG - vector signal generator; LD - laserdiode; EDFA - Erbium-doped fiber amplifier; VOA - variable optical attenuator; PD - photodetector; EA - electrical amplifier; DPX - diplexer; VSA - vector signal analyzer.

a guardband of at least 500 kHz is required to avoid significant degradation and maintaining the received MER above 30 dB in the explored FiWi system.

IV. 5G Optical-Wireless HetNet Using RoF, FSO and Wireless Technologies

The 5G RoF/FSO/Wireless HetNet is described in terms of block diagram in Fig. 14. All technologies are converged into an unique architecture, which employs a hybrid RoF/FSO link for integrating the fronthaul, enabling a dual-band 5G wireless link. We proposed to simultaneously transmit three RF signals in the hybrid architecture, using the 5G frequency bands standardized by 3GPP Release 15, namely: F-OFDM signal centered at 788 MHz with 10-MHz bandwidth, generated by our 5G transceiver for remote areas [22]; 100-MHz bandwidth 5G NR standard at 3.5 GHz in accordance with 3GPP Release 15 specifications [3], aiming outdoor eMBB applications; *M*-QAM signal at 26 GHz and bandwidth up to 400 MHz for indoor eMBB scenarios.

A 3-dB insertion loss combiner has been used to combine the 788 MHz and 3.5 GHz signals and the resulting electrical signal has been combined with the *M*-QAM by using a diplexer. The RF signals power level has been properly set to 0 dBm, except for the *M*-QAM at 26 GHz, which has been employed 5 dBm due to the Mach-Zehnder modulator (MZM), photodetector (PD) and RF cable response over the frequency. The combined signals have been coupled to the MZM input, which modulates a 13-dBm optical carrier at 1549.70 nm, provided by a Golight OS-TL-D-C−50-200-1-S-FA DFB laser. Afterward, the modulated optical signal has been launched into 12.5-km SMF-based optical fronthaul, reaching a collimator. An 1-m FSO fronthaul has been implemented as a proof-of-concept, integrating the hybrid RoF/FSO application. It is worth mentioning that FSO systems have a maximum allowed optical power to keep an eye-safe environment. Infrared communication around 1.5 μm does not reach the retina, however, optical beams with diameter lower than 1 cm and power higher than 10 dBm imply in risks to the human eyes [36]. For this reason, we have placed the EDFA after the 12.5-km fiber optics and 1-m FSO hybrid fronthaul, ensuring a safe FSO environment. Additionally, using an optical low-noise amplifier at the receiver side is more attractive than employing a booster at the transmission side, which typically imposes more noise. Considering the total losses from MZM and optical fiber, the transmitting power in the FSO link was around 5 dBm, i.e. at the same level of other related works, such as [15].

At the reception, an optical lens with a five-fold magnification factor (5x) has been used for collimating the optical beam and coupling it to an optical cord. The sensitivity of the FSO link in terms of alignment of the optical beam must be taken into account, for this reason, a 3-axis micropositioner was used to reduce the attenuation due to misalignments and vibrations. The fiber-coupled optical signal has been amplified by an EDFA for compensating the system losses. Sequentially, a VOA and an OPM coupled to the EDFA output have been used for attenuating and monitoring the optical power level at the photodetector input, respectively. The RF signals have been converted to the electrical domain, amplified by EA_1 with 24-dB gain and divided by using an identical diplexer, which separates the 3.5 GHz and 26 GHz signals. The 5G signal has been transmitted and received by identical commercial 5-dBi gain log-periodic antennas, whereas, the *M*-QAM signal has been transmitted and received employing identical 25-dBi gain horn antennas, giving rise to 8-m reach wireless link. The received 5G signal has been individually amplified by using EA_2 (20-dB gain) and analyzed by a FSW-8351VSA, whereas, the mm-wave signal has been 35-dB amplified (EA_3) and demodulated by a DSAZ632 A oscilloscope.

The system performance investigation consisted of evaluating the hybrid architecture at the marks labeled as (A) and (B) from Fig. 14. The first investigated scenario (A), consisted of evaluating the system fronthaul performance at the photodetector output. In other words, evaluating the performance of the RoF followed by an FSO link. The second case (B) is regarding the analysis of the 5G FiWi system implementation employing RoF and FSO as a fronthaul. In both scenarios, the system performance has been realized in terms of EVM_{RMS} in accordance with the 3GPP Release 15 recommendations, namely: maximum EVM_{RMS} value of 3.5%, 8% and 12.5% for 256-QAM, 64-QAM and 16-QAM, respectively. Fig. 15 reports the EVM_{RMS} as a

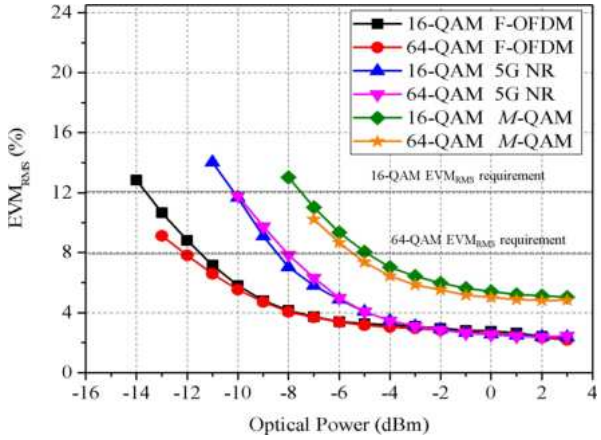

Fig. 15. RoF/FSO system digital performance as a function of the optical power, for F-OFDM, 5G NR and *M*-QAM signals.

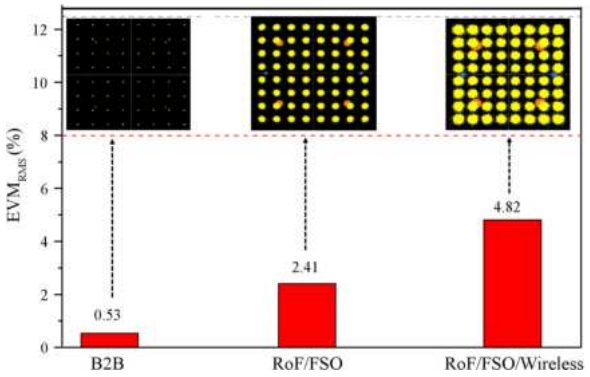

Fig. 16. 5G NR FiWi digital performance analysis at 3.5 GHz employing the hybrid RoF/FSO fronthaul.

function of the optical power at the photodetector input for the tree RF signals, employing 16-QAM and 64-QAM modulation orders (Marker (A) from Fig. 14).

The experimental results have been obtained employing a VOA and an OPM, resulting in a range from −14 to 3 dBm optical power at the photodetector input. The optical power attenuation can be used to emulate atmospheric turbulences such as rain, fog and visibility, enabling to analyze its impact in FSO links. Particularly for F-OFDM, the proposed RoF/FSO system easily accomplished the 3GPP specifications, for optical power levels higher than −14 dBm and −12 dBm, for 16-QAM and 64-QAM, respectively. The best performance point was around 3 dBm optical power and the $\mathrm{EVM_{RMS}}$ values were 2.33% and 2.11% for 16-QAM and 64-QAM, respectively, attaining 60 Mbps throughput. The 100-MHz bandwidth 5G NR signal provided 578 Mbps throughput and $\mathrm{EVM_{RMS}}$ as low as 2.37% and 2.45% for 16-QAM and 64-QAM, respectively. One can observe the 64-QAM reaches the 3GPP limit at approximately −8 dBm optical power, whereas for 16-QAM the recommendation is satisfied for optical powers higher than −10 dBm.

We have properly confronted the F-OFDM and 5G signal as a function of $\mathrm{EVM_{RMS}}$. One can note the curves are similar for optical power levels higher than −4 dBm. However, the 5G transceiver for remote areas presents enhanced digital performance at lower optical powers, due to its remarkable advantage when operating at lower RF power levels, reducing in 4 dB the required optical power for fulfilling the 3GPP specifications. For the *M*-QAM signal at 26 GHz, we have properly set 400-MHz bandwidth, which implies in 2.4 Gbps throughput for 64-QAM modulation order. This throughput has been achieved for optical power levels higher than −5 dBm, whereas 16-QAM provided 1.6 Gbps with 3-dB less optical power. One can note at 26 GHz, the acceptable $\mathrm{EVM_{RMS}}$ values occur for higher optical power levels due to RF cables, PD, and MZM responses over the frequency. The proposed hybrid RoF/FSO system provided 3 Gbps total throughput in accordance with 3GPP Release 15 specifications.

The second and most important characterization was the 5G FiWi system performance analysis using RoF and FSO. We have chosen the best RoF/FSO performance point (3 dBm) for implementing the hybrid 5G FiWi system. An 8-m reach wireless link has been established for demonstrating the system applicability. We have transmitted a standardized 5G NR signal at 3.5 GHz and an *M*-QAM signal at 26-GHz. Fig. 16 presents the 5G NR digital performance for B2B, RoF/FSO and FiWi using the hybrid RoF/FSO fronthaul, including the measured constellations. The B2B condition consists of directly connecting the transmitter and receiver by using an RF cable, enabling to quantify the impact of the RoF/FSO and 5G FiWi systems implementation in terms of $\mathrm{EVM_{RMS}}$.

As expected, the $\mathrm{EVM_{RMS}}$ value for B2B remained below 1%, giving rise to extremely well-defined constellation. The RoF/FSO implementation does not degrade the overall system performance and consequently, the $\mathrm{EVM_{RMS}}$ value has not been significantly increased. The wireless channel degrades the signal in both phase and magnitude, which is noticed by the symbols dispersion in the RoF/FSO/Wireless constellation. However, the 5G NR FiWi system met the 3GPP requirements with margins up to 3.2%, which might be used to extend the wireless link, since we use the maximum standardized bandwidth for FR1. Therefore, the hybrid 5G NR FiWi approach has shown potential for integrating the 5G networks, bringing the remarkable benefit of FSO-flexibility.

Similarly, the 400-MHz bandwidth *M*-QAM signal has been experimentally evaluated for B2B, RoF/FSO and FiWi systems, as presented in Fig. 17. One can note excellent digital performance for B2B and RoF/FSO cases, fulfilling the Release 15 with plenty of margin. In any case, the propagation at 26 GHz severely degrades the $\mathrm{EVM_{RMS}}$ digital performance and the FiWi system with 400-MHz bandwidth has exceeded the 3GPP specifications. For this reason, we have employed only 16-QAM modulation order and 200-MHz bandwidth to overcome this issue. Despite the bandwidth reduction, the hybrid FiWi system provided $\mathrm{EVM_{RMS}}$ around 12%, near to the maximum acceptable (12.5%). The digital performance degradation can be observed in both constellation and eye diagram, emphasizing the severe wireless channel conditions when operating at millimeter-wave (mm-wave) frequencies. Nevertheless, the hybrid RoF/FSO/Wireless system attaining 1.4 Gbps total throughput in accordance with the 3GPP Release 15 recommendations,

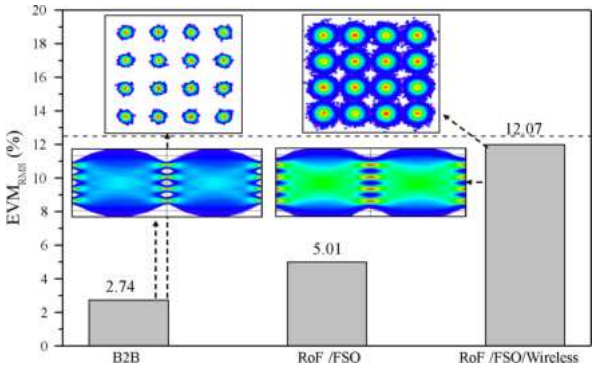

Fig. 17. *M*-QAM FiWi performance investigation at 26 GHz using the hybrid RoF/FSO fronthaul.

demonstrating the feasibility of the FiWi system employing FSO as a fronthaul.

By using MIMO for diversity and the state-of-the-art FEC schemes, 5G networks are robust against the wireless channel impairments, as has been demonstrated by the 5G-RANGE project [22]. In the current work, the performance of the proposed 4G/5G system over the optical link has been evaluated, showing that the co-existence is feasible. Nevertheless, the root mean square error vector magnitude ($\mathrm{EVM_{RMS}}$) performance of these networks can be improved by using an equalizer on the receiver side, which takes the influence of the optical link into consideration. Since the combined wireless-optical channel has a complex model, the use of artificial intelligence (AI) algorithms based on neural networks might improve the $\mathrm{EVM_{RMS}}$ performance. The AI algorithm can exploit the interference introduced among the systems, sharing the same optical channel and reduce the impact of the fiber link on the $\mathrm{EVM_{RMS}}$ performance. This innovation might be introduced in two different points of the communication chain: i) after the optical-electrical converter prior to the wireless transmission or; ii) on the mobile devices after the wireless channel. The advantage of the first approach relies on the fact that a single AI-based equalizer can improve the signal quality for a large set of users, reducing the implementation costs. The second approach, on the other hand, enables to deal with the combined effect of the optical and wireless channels, providing additional performance gain at the cost of higher complexity for the overall system. Both approaches are topics for future research efforts.

V. Conclusion

We have successfully proposed and implemented an efficient RoF/FSO/Wireless FiWi system applied to 5G optical-wireless scenarios, including indoor and outdoor eMBB and eRAC applications. Firstly, multiple signals were transmitted using a 25-km SMF-based fronthaul for evaluating the coexistence between 5G NR and LTE-A signals towards the implementation of an NSA-based network. The multiple signals referred to an F-OFDM signal at 778 MHz from our 5G transceiver, a standardized 5G NR and LTE-A signals at 3.5 GHz and 2.24 GHz, respectively. We have also implemented a 5G optical-wireless HetNet using RoF, FSO and wireless technologies toward eRAC and eMBB applications. It was based on a 12.5-km RoF link followed by a 1-m reach FSO fronthaul, aiming the transmission of a 5G NR signal at 3.5 GHz, an F-OFDM signal at 788 MHz and a 400-MHz bandwidth *M*-QAM signal at 26 GHz for exploiting high data rates. In the first analysis, the total attained throughput was 1.12 Gbps with $\mathrm{EVM_{RMS}}$ in accordance with 3GPP requirements. In this way, we could demonstrate a peaceful coexistence between 4G and 5G signals, both with 100 MHz bandwidth, in a 10-m reach FiWi system. The minimum offset for avoiding overlapping between the signals was 106 MHz, which corresponds to a 2-MHz guard band. In the second analysis, the maximum attained throughput was about 3 Gbps in a RoF system and 1.4 Gbps in a FiWi system. The hybrid RoF/FSO/Wireless fronthaul solution has being shown potential for increasing the flexibility of radio access networks, enabling coverage in difficult access areas. Future works regard the implementation of the proposed architecture for either downlink an uplink, as well as the increase in the FSO reach up to hundreds of meters in an outdoor scenario.

Acknowledgment

The authors would like to thank the technical support of José Reis from Rohde & Schwarz and Renato Guadagnini from Venturus.

References

[1] J. M. C. Brito, L. L. Mendes, and J. G. S. Gontijo, "Brazil 6G project-an approach to build a national-wise framework for 6G networks," in *Proc. 2nd 6G Wireless Summit (6G SUMMIT)*, 2020, pp. 1–5.

[2] D. Zhang, M. Matthe, L. L. Mendes, and G. Fettweis, "A study on the link level performance of advanced multicarrier waveforms under MIMO wireless communication channels," *IEEE Trans. Wireless Commun.*, vol. 16, no. 4, pp. 2350–2365, Apr. 2017.

[3] 3GPP, "5G; NR; Overall description; Stage-2," *TS 38.300 Version 15.3.1 Release 15*, 2018.

[4] J. Yao, "Microwave photonics," *J. Lightw. Technol.*, vol. 27, no. 3, pp. 314–335, 2009.

[5] G.-K. Chang and Y.-W. Chen, "Key fiber wireless integrated radio access technologies for 5G and beyond," in *Proc. 24th OptoElectron. Commun. Conf. Int. Conf. Photon. Switching Comput.*, 2019, pp. 1–3.

[6] I. Chih-Lin, H. Li, J. Korhonen, J. Huang, and L. Han, "Ran revolution with NGFI (xhaul) for 5G," *J. Lightw. Technol.*, vol. 36, no. 2, pp. 541–550, 2017.

[7] D. Chitimalla, K. Kondepu, L. Valcarenghi, M. Tornatore, and B. Mukherjee, "5G fronthaul-latency and jitter studies of CPRI over Ethernet," *IEEE J. Opt. Commun. Netw*, vol. 9, no. 2, pp. 172–182, Feb. 2017.

[8] D. Wake, A. Nkansah, and N. J. Gomes, "Radio over fiber link design for next generation wireless systems," *J. Lightw. Technol.*, vol. 28, no. 16, pp. 2456–2464, 2010.

[9] M. A. Khalighi and M. Uysal, "Survey on free space optical communication: A communication theory perspective," *IEEE Commun. Surveys Tuts.*, vol. 16, no. 4, pp. 2231–2258, Oct.–Dec. 2014.

[10] P. Singhal, P. Gupta, and P. Rana, "Basic concept of free space optics communication (FSO): An overview," in *Proc. Int. Conf. Commun. Signal Process.*, 2015, pp. 0439–0442.

[11] W. M. R. Shakir, "Performance evaluation of a selection combining scheme for the hybrid FSO/RF system," *IEEE Photon. J.*, vol. 10, no. 1, pp. 1–10, 2017.

[12] C. Han, Y. Wu, Z. Chen, and X. Wang, "Terahertz communications (teracom): Challenges and impact on 6G wireless systems," 2019, *arXiv:1912.06040*.

[13] A. Delmade *et al.*, "Performance analysis of analog if over fiber fronthaul link with 4G and 5G coexistence," *J. Opt. Commun. Netw.*, vol. 10, no. 3, pp. 174–182, 2018.

[14] R. M. Borges *et al.*, "Integration of a GFDM-based 5G transceiver in a GPON using radio over fiber technology," *J. Lightw. Technol.*, vol. 36, no. 19, pp. 4468–4477, 2018.

[15] J. Bohata, M. Komanec, J. Spáčil, Z. Ghassemlooy, S. Zvánovec, and R. Slavík, "24–26 GHz radio-over-fiber and free-space optics for fifth-generation systems," *Opt. Lett.*, vol. 43, no. 5, pp. 1035–1038, 2018.
[16] M. A. Esmail, A. M. Ragheb, H. A. Fathallah, M. Altamimi, and S. A. Alshebeili, "5G-28 GHz signal transmission over hybrid all-optical FSO/RF link in dusty weather conditions," *IEEE Access*, vol. 7, pp. 24 404–24 410, 2019.
[17] R. M. Borges *et al.*, "DSP-based flexible-waveform and multi-application 5G fiber-wireless system," *J. Lightw. Technol.*, vol. 38, no. 3, pp. 642–653, 2020.
[18] A. O. Mufutau, F. P. Guiomar, M. A. Fernandes, A. Lorences-Riesgo, A. Oliveira, and P. P. Monteiro, "Demonstration of a hybrid optical fiber–wireless 5G fronthaul coexisting with end-to-end 4G networks," *IEEE J. Opt. Commun. Netw*, vol. 12, no. 3, pp. 72–78, Mar. 2020.
[19] C.-Y. Li, X.-H. Huang, H.-H. Lu, Y.-C. Huang, Q.-P. Huang, and S.-C. Tu, "A WDM PAM4 FSO-UWOC integrated system with a channel capacity of 100 gb/s," *J. Lightw. Technol.*, vol. 38, no. 7, pp. 1766–1776, 2020.
[20] E. S. Lima, R. M. Borges, L. A. M. Pereira, H. R. D. Filgueiras, A. M. Alberti, and A. C. Sodré, "Multiband and photonically amplified fiber-wireless xhaul," *IEEE Access*, vol. 8, pp. 44 381–44 390, 2020.
[21] M.-Y. Huang, Y.-W. Chen, P.-C. Peng, H. Wang, and G.-K. Chang, "A full field-of-view self-steering beamformer for 5G mm-wave fiber-wireless mobile fronthaul," *J. Lightw. Technol.*, vol. 38, no. 6, pp. 1221–1229, 2020.
[22] G.-R. Project. Remote area Access Network for the 5th Generation. (2017). [Online]. Available: http://5g-range.eu/
[23] A. Chassaigne *et al.*, "5G-RANGE: Remote area access network for the 5th generation," ICT-777137 5G-RANGE Project, Tech. Rep. D2.1, Apr. 2018.
[24] S. Ghosh, S. Karar, and A. D. Barman, "A pricing-based rate allocation game in TVWS backhaul and access link for rural broadband," *IEEE Syst. J.*, vol. 13, no. 1, pp. 511–518, Mar. 2019.
[25] Z. You, I. Lu, and W. Li, "High-performing orthogonal frequency division multiplexing precoding scheme for OOBE suppression," *IET Commun.*, vol. 10, no. 17, pp. 2276–2280, Nov. 2016.
[26] L. Zhang, P. Xiao, A. Zafar, A. U. Quddus, and R. Tafazolli, "FBMC system: An insight into doubly dispersive channel impact," *IEEE Trans. Veh. Technol.*, vol. 66, no. 5, pp. 3942–3956, May 2017.
[27] W. Chung, C. Chang, K. Feng, and Y. Chen, "An MIMO configuration mode and MCS level selection scheme by fuzzy Q-learning for HSPA systems," *IEEE Trans. Mobile Comput.*, vol. 11, no. 7, pp. 1151–1162, Jul. 2012.
[28] S. Noh, Y. Jung, S. Lee, and J. Kim, "Low-complexity symbol detector for MIMO-OFDM-based wireless LANs," *IEEE Trans. Circuits Syst. II: Exp. Briefs*, vol. 53, no. 12, pp. 1403–1407, Dec. 2006.
[29] M. Khosraviyani, H. Kalbkhani, and M. G. Shayesteh, "Higher order statistics for modulation and STBC recognition in MIMO systems," *IET Commun.*, vol. 13, no. 16, pp. 2436–2446, 2019.
[30] J. A. C. Bingham, "Multicarrier modulation for data transmission: An idea whose time has come," *IEEE Commun. Mag.*, vol. 28, no. 5, pp. 5–14, May 1990.
[31] H. Kim, Y. Park, J. Kim, and D. Hong, "A low-complex SVD-based F-OFDM," *IEEE Trans. Wireless Commun.*, vol. 19, no. 2, pp. 1373–1385, 2020.
[32] N. Michailow *et al.*, "Generalized frequency division multiplexing for 5th generation cellular networks," *IEEE Trans. Commun.*, vol. 62, no. 9, pp. 3045–3061, Sep. 2014.
[33] F. Cardoso *et al.*, "5G-RANGE: Remote Area Access Network for the 5th Generation," ICT-777137 5G-RANGE Project, Tech. Rep. D4.1, Apr. 2018.
[34] Z. Huang, Y. Ma, Y. Li, and G. Wen, "A low complexity sub-optimal approach to dynamic spectrum allocation for white space devices with heterogeneous bandwidth requirements," *IEEE Commun. Lett.*, vol. 21, no. 1, pp. 188–191, Jan. 2017.
[35] S. Ahmadi, *5G NR: Archit., Technol., Implementation, Operation 3GPP New Radio Standards*. Amsterdam, The Netherlands: Elsevier, 2019. [Online]. Available: https://linkinghub.elsevier.com/retrieve/pii/C20160049446
[36] Stratix and TU/e, "Optical wireless communication: Options for extended spectrum use," Dutch Radio Communications Agency (Agentschap Telecom) for Ministry of Economic Affairs and Climate policy, Netherlands, Tech. Rep., 2017. [Online]. Available: https://www.agentschaptelecom.nl/binaries/agentschaptelecom/documenten/rapporten/2018/02/07/onderzoeklifi/Stratix++TUe+report+%27Optical+Wireless+Communication-+options+for+extended+spectrum+use%27.pdf Line

Celso Henrique de Souza Lopes received the B.Sc. degree from FAINOR, Vitória da Conquista, Brazil, in 2016 and the M.Sc. degree in 2020 from Inatel, Santa Rita do Sapucaí, Brazil, where he is currently working toward the Ph.D. degree.

Eduardo Saia Lima received the B.Sc. and M.Sc. degrees in 2017 and 2019, respectively from Inatel, Santa Rita do Sapucaí, Brazil, where he is currently working toward the Ph.D. degree.

Luiz Augusto Melo Pereira received the B.Sc. and M.Sc. degrees in 2017 and 2020, respectively from Inatel, Santa Rita do Sapucaí, Brazil, where he is currently working toward the Ph.D. degree.

Ramon Maia Borges received the B.Sc. and M.Sc. degrees from Inatel, Santa Rita do Sapucaí, Brazil, in 2012 and 2015, respectively, and the Ph.D. degree from UNIFEI, Itajubá, Brazil, in 2020. He is currently a Researcher with Inatel.

Alexandre Carvalho Ferreira received the B.Sc. and M.Sc. degrees from Inatel, Santa Rita do Sapucaí, Brazil, in 2004 and 2008, respectively. He is currently working toward the Ph.D. degree with the University of São Paulo, São Paulo, Brazil. He is currently a Researcher with Inatel.

Marcelo Abreu received the B.Sc. degree from Unicamp, Campinas, Brazil, in 1997. He is an Executive Manager with Venturus. His main responsibilities are innovation and new business manager, developing a new culture of innovation.

Whebert Damascena Dias received the B.Sc. degree in electrical engineering with an emphasis on telecommunications from Inatel, Santa Rita do Sapucaí, Brazil, in 2005. Currently, he is a researcher with Inatel Radiocommunication Reference Center (CRR).

Danilo Henrique Spadoti received the graduate degree in electrical engineering from UNIFEI, Itajubá, Brazil, in 2002, and the master's and Ph.D. degrees in electrical engineering with a major in telecommunications from the University of São Paulo, São Paulo, Brazil, in 2004 and 2008, respectively.

Luciano Leonel Mendes received the B.Sc. and M.Sc. degrees in electrical engineer from Inatel, Santa Rita do Sapucaí, Brazil, in 2001 and 2003, respectively, and the doctorate in electrical engineering from Unicamp, Campinas, Brazil, in 2007.

Arismar Cerqueira Sodre Junior received the B.Sc. degree in electrical engineering from the Federal University of Bahia, Salvador, Brazil, in 2001, the M.Sc. degree from Unicamp, Campinas, Brazil, in 2002, and the Ph.D. degree from Scuola Superiore Sant'Anna, Pisa, Italy, in 2006.

Artigo 6 : Integrating Optical and Wireless Techniques towards Novel Fronthaul and Access Architectures in a 5G NR Framework

Ramon Maia Borges, Celso Henrique de Souza Lopes, Eduardo Saia Lima, Marco Aurélio de Oliveira, Matheus Sêda Borsato Cunha, Luciano Camilo Alexandre, Luis Gustavo da Silva, Luiz Augusto Melo Pereira, Danilo Henrique Spadoti, Murilo Araujo da Silva and Arismar Cerqueira. S. Jr. "Integrating Optical and Wireless Techniques towards Novel Fronthaul and Access Architectures in a 5G NR Framework", *Appl. Sci. VOL. 11* 2021.

applied sciences

MDPI

Article

Integrating Optical and Wireless Techniques towards Novel Fronthaul and Access Architectures in a 5G NR Framework

Ramon Maia Borges [1,2], Celso Henrique de Souza Lopes [1], Eduardo Saia Lima [1], Marco Aurélio de Oliveira [1], Matheus Sêda Borsato Cunha [1,2], Luciano Camilo Alexandre [1], Luis Gustavo da Silva [1], Luiz Augusto Melo Pereira [1], Danilo Henrique Spadoti [2], Murilo Araujo Romero [3] and Arismar Cerqueira Sodré Junior [1,*]

[1] Laboratory WOCA, National Institute of Telecommunications (Inatel), Santa Rita do Sapucaí 37540-000, MG, Brazil; ramonmb@inatel.br (R.M.B.); celso.lopes@mtel.inatel.br (C.H.d.S.L.); elima@get.inatel.br (E.S.L.); marcoaurelio@mtel.inatel.br (M.A.d.O.); matheusseda@gee.inatel.br (M.S.B.C.); luciano.camilo@mtel.inatel.br (L.C.A.); luis.gustavo@inatel.br (L.G.d.S.); luiz_augusto@get.inatel.br (L.A.M.P.)

[2] Department of Electrical Engineering, Federal University of Itajubá (UNIFEI), Itajubá 37500-903, MG, Brazil; spadoti@unifei.edu.br

[3] Department of Electrical and Computer Engineering, University of São Paulo (USP), EESC/USP, São Carlos 13566-590, SP, Brazil; murilo.romero@usp.br

* Correspondence: arismar@inatel.br; Tel.: +55-35-3471-9200

Abstract: The fifth-generation of mobile network (5G) and beyond requires a radio access network (RAN) update in order to cope with the incoming increase of wireless data traffic and new applications. In this context, we propose an efficient optical-wireless architecture applied to the non-standalone (NSA) 5G new radio (NR) framework. Several distinct electrical- and optical-based fronthaul configurations combining free-space optical (FSO), wireless links, and radio over fiber (RoF) techniques were implemented and properly analyzed for selection according to network operator deployment requirements. In addition, visible light communication (VLC) was investigated as a future access network technology when immunity to electromagnetic interference is paramount. Experimental results demonstrated fourth-generation of mobile network (4G) and 5G coexistence at Gbit/s throughput and error vector magnitude (EVM) in accordance with 5G NR Release 15.

Keywords: 4G/5G; fronthaul; optical-wireless systems; VLC

Citation: Borges, R.M.; de Souza Lopes, C.H.; Lima, E.S.; de Oliveira, M.A.; Cunha, M.S.B.; Alexandre, L.C.; da Silva, L.G.; Pereira, L.A.M.; Spadoti, D.H.; Romero, M.A.; et al. Integrating Optical and Wireless Techniques towards Novel Fronthaul and Access Architectures in a 5G NR Framework. *Appl. Sci.* **2021**, *11*, 5048. https://doi.org/10.3390/app11115048

Academic Editor: Fabio Cavaliere

Received: 1 May 2021
Accepted: 24 May 2021
Published: 29 May 2021

1. Introduction

The fifth-generation of mobile network (5G) has already started to be commercially implemented around the world. At this initial implementation stage, 5G typically operates in the non-standalone (NSA) mode, aiming to take advantage of the fourth-generation (4G) infrastructure to deploy 5G new radio (5G NR) systems. Therefore, 5G and 4G share the network infrastructure and must coexist seamlessly [1]. Phase 1 of 5G systems is based on the 3rd Generation Partnership Project (3GPP) Release 15, which defines the 5G NR standard by focusing on the enhanced mobile broadband (eMBB) scenario. Technical solutions explored at this stage include radio equipment design, use of additional spectral bands encompassing millimeter-waves (mm-waves), flexible resource allocation, and multiple input multiple output (MIMO) schemes [2,3]. In addition, 5G deployment requires a radio access network (RAN) update in order to cope with the planned increase in wireless data traffic. Trends in network planning point to optical-wireless convergence, mobile dense heterogeneous networks (HetNet), centralized RAN (C-RAN), and the so-called "Xhaul", which integrates backhaul (BH), midhaul (MH), and fronthaul (FH) transport networks [4–6].

Recently, 3GPP completed Release 16 for phase 2 of 5G systems, which considers ultra-reliable low latency communication (URLLC) and massive machine-type communication

(mMTC) applications. According to the release, the technical solutions to be explored include integrated access and backhaul (IAB), industrial Internet of Things (IoT), satellite access, and NR-based access to unlicensed spectrum [7]. Releases 17 and 18 for 5G are currently in production and scheduled to end in 2021, with the goal of further enhancing mobile systems [8]. By the same token, planning of sixth-generation (6G) communications has already begun, focused on providing performance superior to 5G and satisfying future demands as far as 2030. Among the potential technologies for 6G, optical-wireless convergence continues to play an important role for future RANs, whereas terahertz and visible light communications (VLC) have also emerged [9,10].

In this context, a key area of study is microwave photonics (MWP), which takes advantage of optical and mobile communications for signal distribution in a heterogeneous architecture [11,12]. MWP techniques have been strongly applied to radiofrequency (RF) generation, processing, detection, transport, and distribution. Notably, radio over fiber (RoF) technology enables transportation and distribution of digital and/or analog signals among central office (CO) and remote radio units (RRUs) via fiber-optic links, giving rise to the fiber-wireless (FiWi) systems [11,13]. From a C-RAN point of view, HetNet in conjunction with picocell and femtocell implementations allows system coverage and data rate to be enhanced. In C-RAN architecture, the backhaul and fronthaul links connect CO to the core network, typically carrying digital user data and CO to RRUs, respectively.

Fifth-generation systems are mostly based on digital radio over fiber (D-RoF) using the common radio public interface (CPRI) protocol, in which radio signals are sampled and directly digitalized into baseband data at the remote radio head (RRH) from the cell site. Millimeter-wave operation requires high-speed A/D (analog-to-digital) and D/A (digital-to-analog) converters, creating a bandwidth bottleneck in uncompressed CPRI. To address this issue, two main network alternatives have been actively investigated. One possibility is functional split (FS), widespread by 3GPP under e-CPRI. The FS establishes that some network functionalities be carried out at RRHs, thereby alleviating the transmission rate requirements for the 5G fronthaul. Specifically, 3GPP has defined a series of options for functional split between BBU and RRHs. In short, functional splits decentralize control functionalities in such way as to establish a trade-off between reducing fronthaul throughput and increasing latency. The other option is analog fronthaul (A-RoF), in which the RF wireless signal modulates an optical carrier that is optically distributed. Because there is no high-speed A/D conversion, the system is far less complex and the overall latency is much smaller, dictated essentially by the optical fiber length.

Our research group has been intensely investigating A-RoF solutions for multiband and Gbit/s 5G systems in recent years [14–17]. The solution presented in [14] takes advantage of an operating gigabit passive optical network (GPON) from a local Internet service provider to distribute 5G-like signals, thus making use of an existing network infrastructure for 5G fronthaul in accordance with C-RAN. The approaches presented in [15,16] explore optical link not only for data transmission but also as a medium to perform photonics-assisted RF amplification. In [17], a dual-band wireless fronthaul using an FSS-based focal point/Cassegrain antenna assisted by an optical midhaul was demonstrated.

Alternatively, free-space optical (FSO) technology has also shown potential for 5G transport network deployment using the unlicensed terahertz bands [18,19]. For instance, Mufutau et al. successfully reported a hybrid RoF/FSO fronthaul approach in which 5G coexists with 4G by means of coarse wavelength division multiplexing (CWDM) [19]. These previous works considered wireless links operating at a variety of radiofrequencies for providing mobile access, which might be either indoor or outdoor. Overall, RF links correspond to the main technical solution employed for access, although visible light communications (VLC) have also been recognized as an alternative for indoor environments, particularly when RF electromagnetic interference must be avoided [20,21].

Apart from a tiny segment of the worldwide market already using VLC, wireless access networks are almost entirely based on electrical solutions, with approximately 70%

of macrosites in the world being connected by microwave fronthauls. Although there are many published works investigating individual proposals regarding fronthaul solutions, only a few of them present comparisons between different optical-based fronthaul solutions [22,23]. To the best of our knowledge, work addressing and confronting diverse electrical- and optical-based fronthauls is still missing in the specialized literature.

In this context, the current study relies on integrating optical and wireless techniques towards novel fronthaul and access architectures in a NSA 5G NR framework, as proposed in Figure 1. In other words, we report implementations and comparison of diverse MWP techniques towards a non-standalone 5G NR optical-wireless communications (OWC) architecture in such a way that a variety of integrated services may be offered according to the network operator needs.

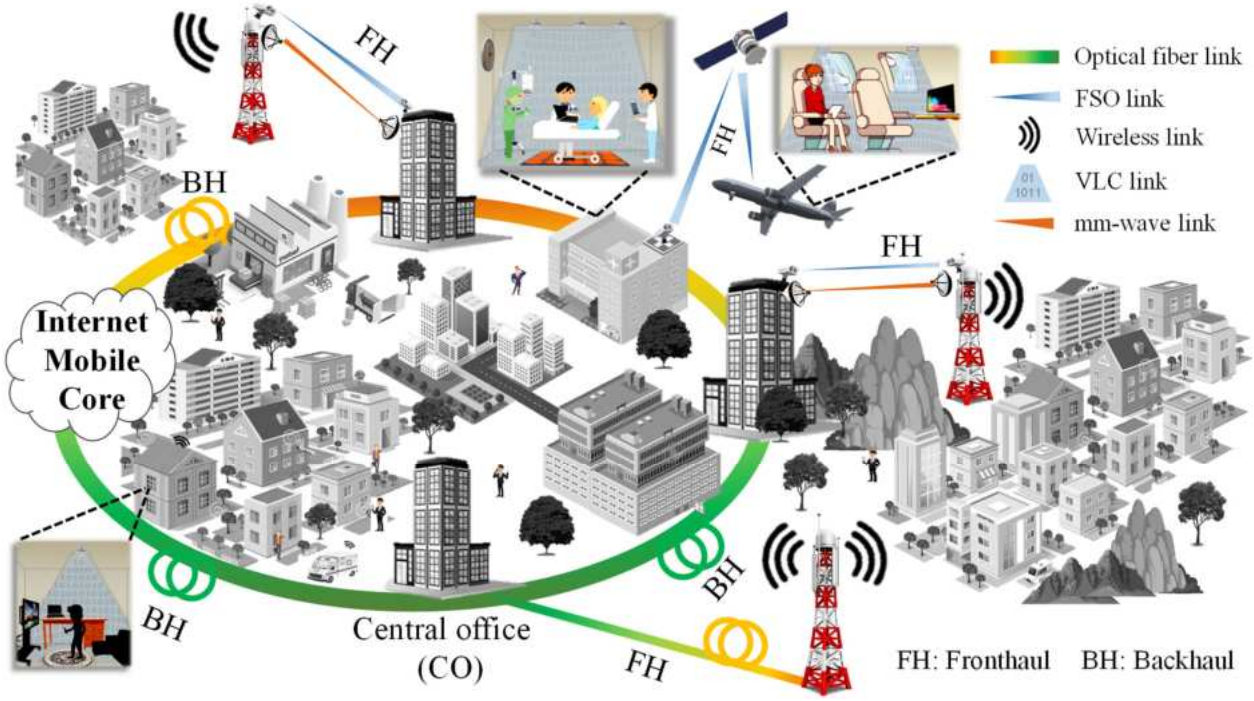

Figure 1. Optical-wireless communication system based on RoF/FSO/wireless fronthaul configurations combined to VLC/wireless access for 5G and beyond.

The main contributions of this study are as follows: proposal and implementation of optical-wireless architectures applied to the NSA 5G NR framework; evaluation of diverse transport and access network solutions, including 5G NR dual wireless and FSO-based fronthaul, 4G/5G NR fiber-wireless fronthaul, combined fiber-optic and FSO-based 5G fronthaul, and 4G/5G NR VLC-based access network; discussion of experimental results regarding 4G and 5G coexistence at Gbit/s throughput and error vector magnitude (EVM) in accordance with 3GPP Release 15.

The focus of our work is data transmission in the physical layer, although Figure 1 provides a unifying view of our applications in a single ecosystem. The rest of the paper is structured as follows. In Section 2, we address different fronthaul configurations. First, in Section 2.1, a dual wireless and FSO-based fronthaul that enables a backup link for high-reliability services is reported. In Section 2.2, a RoF-based fronthaul is demonstrated for simultaneous RF signal distribution at distinct spectral bands. Unlike previous works [7,8], a single wavelength is used to simultaneously cover 4G and 5G NR applications, including millimeter-wave bands. Next, in Section 2.3, we discuss a RoF/FSO-based fronthaul that enables high-capacity fronthaul extension for regions where optical fibers cannot be deployed all the way. A VLC-based access network for indoor applications is presented

in Section 3, targeting applications in which immunity to electromagnetic interference is crucial. Section 4 compares the obtained results to related works from the literature. Conclusions, final remarks, and future works are outlined in Section 5.

2. Fronthaul Solutions for 4G/5G

This section reports on the architectures and experimental results for the three fronthaul configurations illustrated in Figure 1, namely 5G NR dual wireless and FSO-based fronthaul, 4G/5G NR FiWi-based fronthaul, and combined fiber-optic and FSO-based 5G fronthaul.

2.1. The 5G NR Dual Wireless and FSO-Based Fronthaul

Figure 2a depicts a block diagram of the dual wireless and FSO-based fronthaul architecture, in which the two parallel data transmission paths enable link dynamic selection according to transmission performance at a given instant, while the other link serves as a backup. The FSO and RF links were implemented at 1550 nm and 38 GHz, respectively. The hybrid FSO/RF system was analyzed under the 5G NR standard operating with 400 MHz bandwidth and 120 kHz between orthogonal frequency division multiplexing (OFDM) subcarriers for quadrature phase shift keying (QPSK) and 16- and 64-quadrature amplitude modulation (QAM).

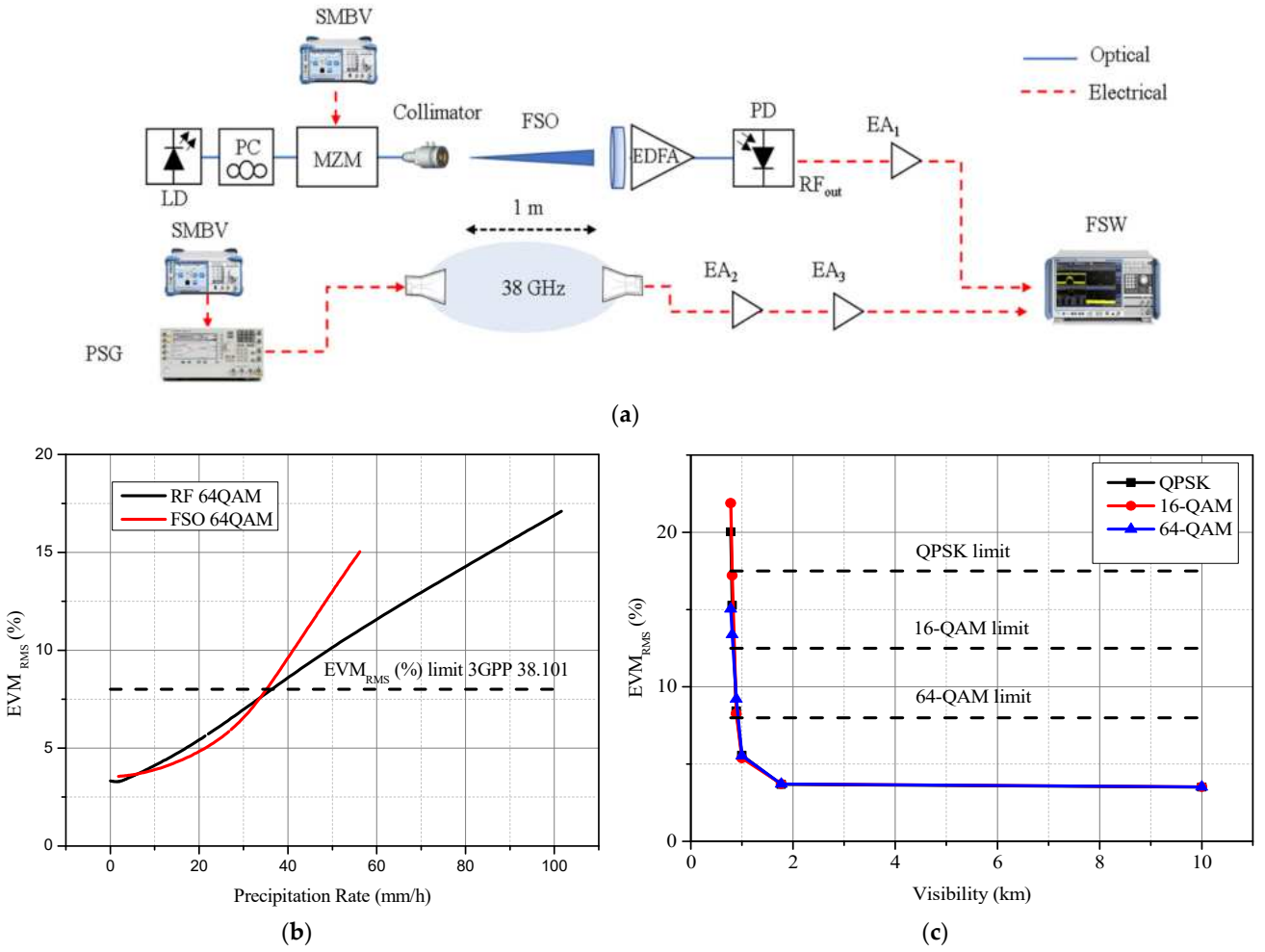

Figure 2. The 5G NR dual wireless and FSO-based fronthaul. (**a**) Block diagram of the proposed hybrid wireless-FSO system. From the left, the signal generated by the vector signal generator (VSG) SMVB100A reaches the FSW signal and spectrum analyzer via the two different links. (**b**) Dependence of hybrid FSO/RF EVM_{RMS} as a function of rain precipitation rate. (**c**) Dependence of hybrid FSO/RF EVM_{RMS} as a function of visibility.

In the experiments, a SMVB100A vector signal generator (VSG) was responsible for generating 5G NR signal at 1 GHz with 400 MHz bandwidth for the QPSK, 16-QAM, and 64-QAM schemes. In the FSO link, the modulated RF signal was inserted into a single-drive Mach–Zehnder modulator (MZM) based at the quadrature point. A distributed feedback (DFB) laser at 1550 nm provided the optical carrier, which fed the MZM after passing through a polarization controller (PC). The MZM output was coupled to a collimator to prepare the optical beam for transmission in free space. The transmitted optical beam was then captured by a M-5X objective lens and coupled to a single-mode fiber (SMF). The received signal was amplified by an Erbium-doped fiber amplifier (EDFA) and then photodetected by a *p*-intrinsic-*n* (PIN) broadband photodetector (u^2t XPDV2120RA). Before demodulation in the electrical spectrum analyzer (FSW), the RF signal was amplified by a low-noise amplifier (LNA, EA_1). As in references [24] and [25], an FSO link of a few meters was taken as a proof-of-concept for 5G networks to assure an eye-safe indoor environment. As shown below, real-life performance was emulated by varying the optical power reaching the optical receiver.

Meanwhile, for the RF link, the same 5G NR signal, once again generated by a SMVB100A VSG, was used to drive the PSG E8267D equipment, which upconverted the 5G NR frequency to 38 GHz. Posterior, its output was connected to a 25 dBi horn antenna, and an identical antenna was used at the receiver side with the same height and polarization. A two-stage amplification (EA_2 and EA_3) scheme was employed before demodulation.

The performance of the hybrid FSO/RF is presented in Figure 2b,c through EVM_{RMS} measurements at different power levels at the receiver, emulating equivalent attenuation levels according to visibility and rain conditions. These power levels at the receiver ranged from −41.9 to −7.4 dBm. Regarding the effect of rain attenuation, the attenuation levels used for the FSO link ranged from 0 to 56 mm/h, while the values ranged from 0 to 102 mm/h for the wireless link. For the specific case of 64-QAM, the 3GPP EVM_{RMS} limit was reached at about the same precipitation intensity for both FSO and 38 GHz wireless links (36 mm/h, Figure 2b). However, as shown in Figure 2b, while operating in a rainy environment, the wireless link suffered less significant performance degradation as the rain intensity increased.

Figure 2c depicts the dependance of EVM regarding visibility for the FSO link for three distinct modulation formats. In every case, successful transmission within the 3GPP standards required a visibility above 780 m. In contrast, the visibility issue was much less severe for the wireless link. In fact, our experimental results demonstrated a 1.61 Gbps 64-QAM throughput, which is within the 3GPP EVM requirements, as long as the rain intensity was less than 36.4 mm/h (see Figure 2a) and the visibility exceeded 40 m.

2.2. 4G/5G NR Fiber-Wireless (FiWi) Fronthaul

The long-term evolution-advanced (LTE-A) and 5G NR signals have similar physical channel configurations, including primary (P-SS) and secondary synchronization signal (S-SS), physical transmission channel (PBCH), demodulation reference (DMRS), and shared physical data channel (PDSCH). Different modulation formats are used for the data and control channels. For instance, data signals might be modulated in 64-QAM format, while binary phase shift keying (BPSK) modulation is applied for modulating the P-SS and S-SS channels. In addition, QPSK and 64-QAM are utilized for PBCH-DMRS and PDSCH signals, respectively [19].

The EVM_{RMS} performance of the FiWi system was investigated for the eRAC scenario operating in the 700 MHz frequency range. Figure 3a displays a block diagram of the experimental arrangement of the proposed FiWi system, which employs an A-RoF configuration based on external modulation and direct detection followed by a link access for increased reach.

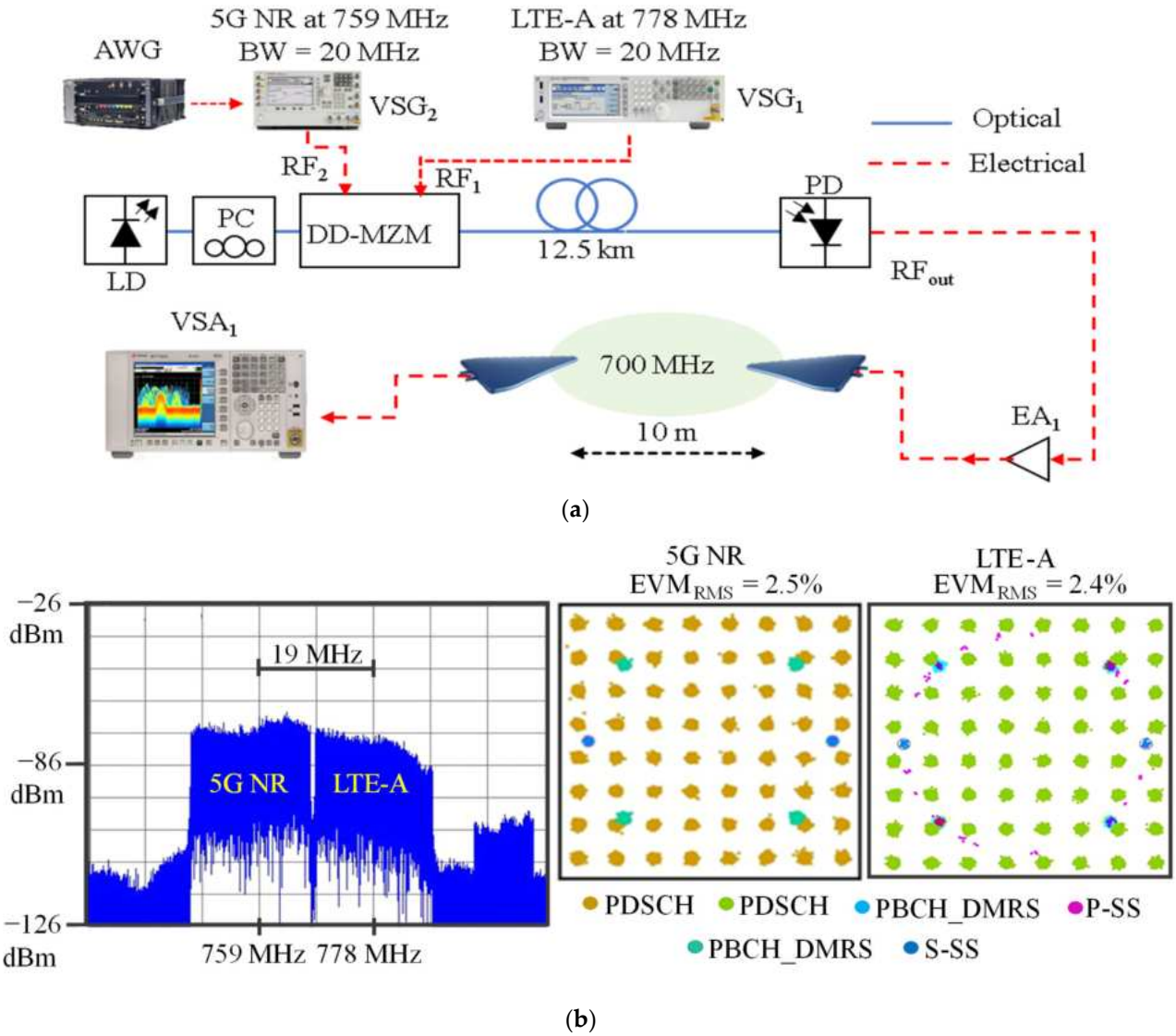

Figure 3. The 4G/5G NR fiber-optic-based fronthaul architecture. (**a**) Block diagram; (**b**) coexistence analysis between 4G and 5G technologies in the optical-wireless system.

An EXG generator (N5171B) from Keysight generated the LTE-A signal (VSG_2) at 778 MHz, which was configured offline using the Keysight Signal Studio software for generating signals with 20 MHz bandwidth and 64-QAM. The 20 MHz baseband 5G NR signal was also configured by means of the Signal Studio software in conjunction with an arbitrary waveform generator (AWG M9505A). Next, the PSG E8267D converted the baseband 5G NR signal to the 759 MHz band (VSG_1). This approach allowed the transmission of the LTE-A and 5G NR signals coexisting in adjacent channels, thereby making use of the non-standalone transmission mode proposed by 3GPP in Release 15 [3].

A dual-drive Mach–Zehnder modulator (DD-MZM) modulated an optical carrier provided by a laser at 1560 nm with two distinct RF signals. The optical beam was then launched into a single-mode fiber with 0 dBm of optical power. Nonlinearities were not observed in our approach as the optical power level in the SMF did not reach the power thresholds leading to nonlinear effects [26]. Regarding the electrical power levels, RF_1 and RF_2 signals were transmitted at −5 dBm, while the PIN photodetector (EOT ET-5000F) received a fixed optical power of −3 dBm. After photodetection, the signals in the electrical domain were amplified by about 44 dB (EA_1) to compensate for the overall system losses. Two log-periodic broadband antennas with 5 dBi gain were used to transmit and receive

both RF_1 and RF_2, and a 10 m wireless transmission was performed as a proof-of-concept. At the receiver side, a Keysight MXA N9020A vector signal analyzer (VSA_1) was used to demodulate the received signals and provide the EVM_{RMS} measurement results.

In the experiments, a 19 MHz frequency offset was employed between RF_1 and RF_2. This offset was determined as a preliminary step in order to find the minimum frequency offset allowing seamless coexistence between the RF_1 and RF_2 signals. Specifically, we measured the EVM_{RMS} as a function of the central frequency offset between the LTE-A and 5G NR signals. The LTE-A central frequency was kept at 778 MHz central frequency, whereas the 5G NR central frequency was varied from 760 to 758 MHz. For a 18 MHz frequency offset, there was a spectral overlap of 2 MHz between the signals, resulting in EVM_{RMS} higher than 19%. This exceeds the limits specified by 3GPP [27], making the system unsuitable for 64-QAM transmission. In contrast, the 19 MHz offset was enough to assure an EVM_{RMS} value below 3%. For this offset, there was still a spectral overlap of 1 MHz between the signals. However, this overlap occurred in the lateral lobes and did not significantly affect the quality of the received signal after the optical fronthaul.

Having established an offset of 19 MHz, the optical-wireless system based on non-standalone mode was implemented using a RF power level of -5 dBm for the RF_1 and RF_2 signals and an optical power of -3 dBm at the input of the photodetector. The RF signals were configured with 19 MHz frequency offset, 64-QAM, and 20 MHz bandwidth, thereby achieving a maximum throughput of 182.8 Mbit/s for the 5G NR and LTE-A signals. Figure 3b reports the measured spectrum and detected constellations for the LTE-A and 5G NR signals. One can clearly distinguish each synchronism, control, and data symbols transmitted as the obtained EVM_{RMS} were 2.5% and 2.4% for 5G NR and LTE-A, respectively. Furthermore, there were no noticeable phase rotation distortions in the detected constellations after the fiber-wireless transmission, thus demonstrating successful and seamless coexistence between 5G NR and LTE-A signals.

2.3. Combined Fiber-Optic and FSO-Based 5G Fronthaul

The combined fiber-optic and FSO-based 5G fronthaul followed by wireless access extension is described in a block diagram in Figure 4a. The system encompasses RoF, FSO, and wireless technologies in a single architecture that takes advantage of a hybrid RoF/FSO link for fronthaul integration followed by dual-band 5G NR wireless access. The FSO link enables last-mile applications when there are restrictions to the placement of a fiber-optic connection, thereby increasing system flexibility. After photodetection, further reach is achieved by wireless access.

For the experiments, we simultaneously transmitted two RF signals in the hybrid configuration in accordance with the frequency bands standardized by 3GPP Release 15. A 100 MHz bandwidth 5G NR signal at 3.5 GHz was generated using the VSG_1, whereas a 400 MHz bandwidth *M*-QAM signal was generated in baseband using an AWG and upconverted to 26 GHz by means of the VSG_2. Finally, a diplexer combined both signals, resulting in 3 dBm electrical power at the optical modulator. An OS-TL-D-C-50-200-1-S-FA DFB laser from Golight generated a 13 dBm optical carrier at 1550 nm, which was modulated by the RF-driven signals discussed above using a single-drive MZM. The modulated optical carrier was transmitted throughout a 12.5 km fiber-optic fronthaul to the collimator, and then, as a proof-of-concept, it followed a 1 m long FSO fronthaul in such a way as to assure an eye-safe FSO link.

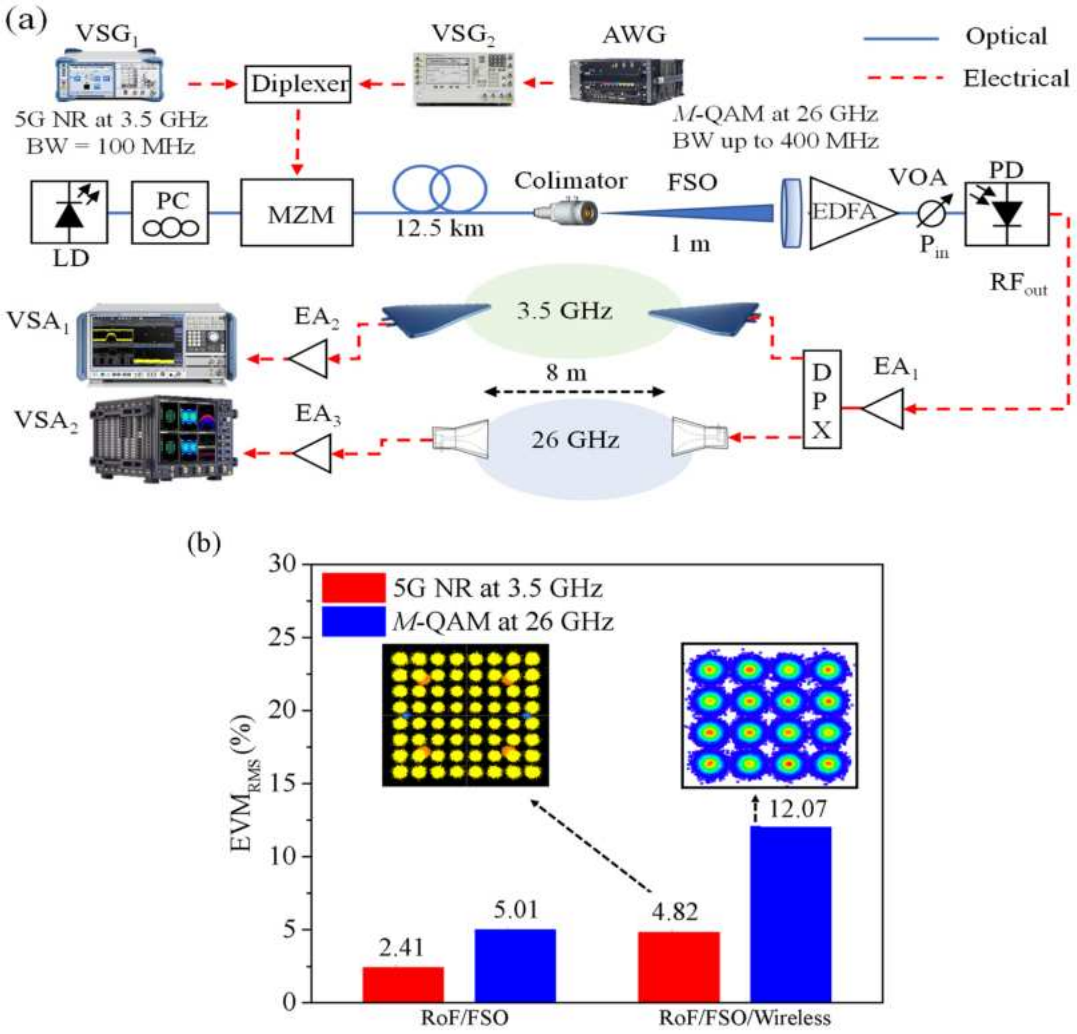

Figure 4. Combined fiber-optic and FSO-based 5G fronthaul architecture. (**a**) Block diagram; (**b**) performance analysis of 5G NR and *M*-QAM signals in the optical-wireless system. The constellations from the RoF/FSO/wireless approach show 16- and 64-QAM received symbols suitable for demodulation.

At the receiver side, an optical lens with a 5-fold collimation factor coupled the free-space optical beam into an optical patch cord. A 3-axis micropositioner was used to minimize vibration and misalignments losses. Next, the optical signal was amplified by an EDFA, whereas a variable optical attenuator (VOA) and an optical power monitor (OPM) were used for controlling and monitoring the optical power at the input of the PIN broadband photodetector from u^2t. It is worth highlighting that the EDFA noise was considered in the approach as there was no filter before the photodetector. If the EDFA amplified spontaneous emission (ASE) had been filtered out, an enhanced performance could have been achieved. After photodetection, the resulting RF signals were amplified by the electrical amplifier EA_1 by about 24 dB. A diplexer was used to separate the 3.5 and 26 GHz signals. Two 5 dBi gain log-periodic antennas were used for transmitting and receiving the 5G NR signal at 3.5 GHz. In parallel, two 25 dBi gain horn antennas enabled 8 m of mm-wave wireless link at 26 GHz aimed at indoor applications. At the receiver side, the 5G signal was amplified (EA_2) by 20 dB and evaluated employing an FSW-8351VSA (VSA_1). Meanwhile, the 400 MHz bandwidth *M*-QAM signal was amplified (EA_3) by 35 dB and evaluated using a DSAZ632A high-frequency oscilloscope (VSA_2).

The system performance was investigated by assessing the hybrid architecture in two distinct scenarios in terms of EVM_{RMS} and in accordance with 3GPP Release 15 specifications. The first step was to evaluate the hybrid RoF/FSO fronthaul at the photodetector

output, whereas the second step consisted of actually analyzing the dual-band 5G NR wireless system employing the hybrid RoF/FSO fronthaul, as depicted in Figure 4b. It is worth mentioning that the experimental results were achieved using 3 dBm optical power at the photodetector input for both scenarios. In particular, for the 5G NR signal at 3.5 GHz, we selected 64-QAM, which resulted in 578 Mbit/s and measured EVM_{RMS} of around 2.4%, thereby satisfying the 3GPP requirements (8%) by a wide margin. Likewise, the received 400 MHz bandwidth signal at 26 GHz was within the 3GPP recommendations, providing 2.4 Gbit/s throughput. The increased EVM_{RMS} value (5%) for mm-wave transmission was due to the RF cables, SD-MZM, and photodetector frequency responses at the mm-wave band. Overall, the proposed hybrid RoF/FSO fronthaul provided 3 Gbit/s of total throughput, which is within the 3GPP requirements for EVM_{RMS}, thereby enabling further network reach by wireless access.

The second analysis consisted of evaluating the combined fiber-optic and FSO-based 5G fronthaul followed by the 8 m wireless access, as reported in Figure 4b. As expected, the wireless channel impaired the transmitted signal in both phase and magnitude as could be observed by the received symbols in the RoF/FSO/wireless constellations. Nevertheless, the 5G NR signal attained the EVM_{RMS} requirements with 3.2% margin, which may be explored for either increasing the signal data rate or extending the wireless reach. In contrast, the propagation conditions at 26 GHz critically impaired the 400 MHz bandwidth signal, and hence the EVM_{RMS} did not meet the 3GPP recommendations. As an alternative, we employed a 200 MHz bandwidth under 16-QAM to overcome this performance shortcoming. With this bandwidth reduction, the hybrid dual-band 5G NR system achieved an EVM_{RMS} value of around 12%, which is still within the 3GPP limit for 16-QAM (12.5%), due to the severe propagation impairments at mm-waves. In spite of the bandwidth reduction at 26 GHz, the hybrid RoF/FSO/wireless 5G NR system was able to provide 1.4 Gbit/s total throughput, thus fulfilling the Release 15 recommendations and demonstrating feasibility of the system while giving the remarkable additional advantage of FSO fronthaul flexibility.

3. 4G/5G NR VLC-Based Access Network

VLC has emerged as an alternative for transmitting the 5G NR standard or other wireless signals in environments where electromagnetic interferences must be minimal, such as in hospitals, petrochemical industrial plants, and airplanes. Furthermore, LED-based VLC systems can take advantage of environment lighting to provide free-space data transmission using wavelengths in the visible part of the optical spectrum. The LED is directly modulated, and the optical link operates in IM-DD mode at the photodiode [28]. By using an LED, the wide light beam divergence allows the desired area to be fully eliminated, thereby enabling simultaneous access for multiple devices and/or patterns of data traffic [21]. In addition, carrier aggregation strategies can be employed to increase the effective user throughput.

Figure 5a depicts the experimental set-up diagram of the LED-based VLC access point for simultaneous transmission of the 5G NR standard signal and an LTE-A three-band signal. RGBA (red, green, blue, and amber) LEDs were considered as the light source because they provide larger modulation bandwidth in comparison to white commercial LEDs [29]. In particular, the final selection of red LED (623 nm optical carrier) was dictated by the manufacturer's datasheet, which indicates that this wavelength offers the best trade-off between output power and quantum efficiency. In the experiments, the 5G NR signal was generated using a SMBV100B vector signal generator (VSG_1), while a PSGE8267D vector signal generator (VSG_2) and a M9505A arbitrary waveform generator (AWG) were employed to generate the LTE-A three-band signal. The RF signals were electrically combined and directly modulated the red LED by means of a bias tee. The LED light beam directivity was enhanced by a reflector and launched in a free-space link of 0.75 m.

At the receiver side, a plane convex lens with the diameter and focal distance of 25.4 and 35.0 mm, respectively, was used to focus the incident beam at the input of the PIN

photodetector (EOT ET-2030). Next, an RLC equalizer similar to the one described in [29] was implemented to compensate for the LED frequency response. A DC blocker ensured that the DC component from the OE conversion did not reach the VSA. Finally, a cascade of four electrical amplifiers (EAs) assured a 50 dB gain in the received signal.

The system performance was evaluated by EVM_{RMS} measurements. The 5G NR signal was generated with a bandwidth of 10 MHz, 64-QAM, centered at 46 MHz. The configuration of the LTE-A signal represented the aggregation of three intra-band carriers in order to triplicate the effective throughput of a single user. Specifically, the LTE-A signal was generated with three sub-bands of 12 MHz, 64-QAM, at 57, 69, and 81 MHz, named as 64-QAM_1, 64-QAM_2, and 64-QAM_3, respectively.

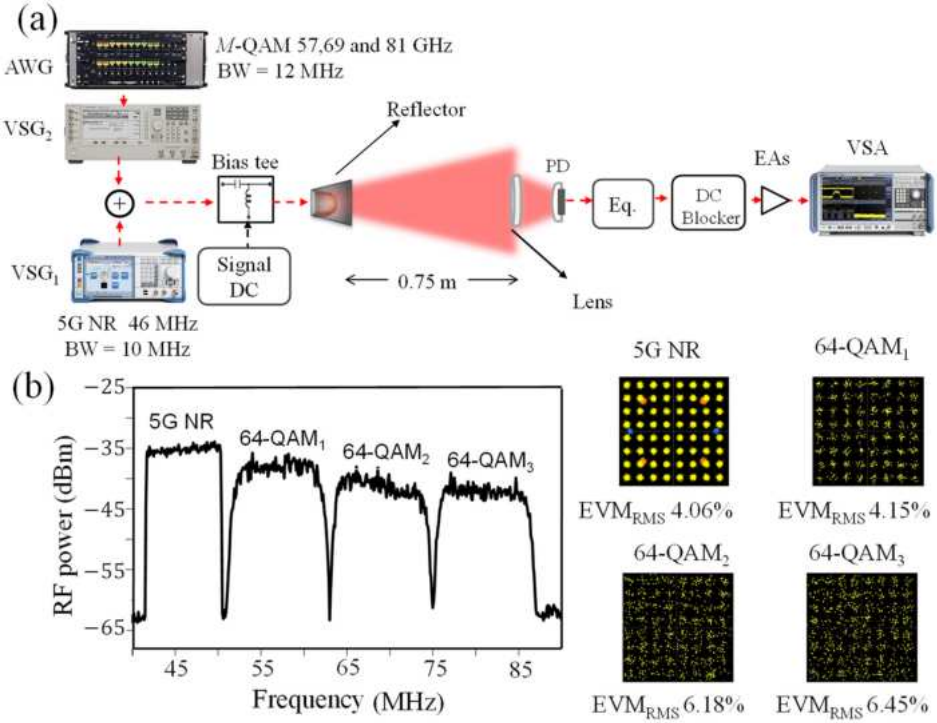

Figure 5. The 4G/5G NR VLC-based access network architecture. (**a**) Block diagram; (**b**) electrical spectrum and EVM_{RMS} at the receiver.

Figure 5b shows the received spectrum as well as the measured constellations and EVM_{RMS} values. The received signal power decreased as the operation frequency increased on account of the LED frequency response, degrading both the signal-noise ratio (SNR) and the EVM_{RMS} value. The constellations in Figure 5b illustrate these performance issues by considering the four transmitted bands. The measured EVM_{RMS} values were 4.06%, 4.15%, 6.18%, and 6.45% for 5G NR, 64-QAM_1, 64-QAM_2, and 64-QAM_3, respectively, which are all within the 3GPP limit of 8% for the 64-QAM format [27]. The effective throughputs measured for the 5G NR signal and the aggregation of the three 64-QAM signals were 38 and 180 Mbit/s, respectively, rates which are attractive for a VLC access point.

4. Related Works and Comparison to the State of the Art

This section reports on a review of the state of the art by comparing optical-wireless techniques for 5G radio access network reported in the literature to the results of our implementation. Five architectures were considered, namely FiWi mm-wave/IFoF links, multiuser FiWi links, parallel FiWi and FSO relay links, RoF links followed by a FSO-section, and VLC access. Table 1 summarizes the aforementioned literature and comparisons to our work with the aim of contributing to and advancing the body of knowledge in this field.

Table 1. State of the art on optical-wireless techniques for 5G radio access network.

Reference	Architecture	Application	RF Bands	Modulation/ Waveform	Transmitter	Throughput
[30]	- FiWi mm-wave/ IFoF link	- RF	- 57 GHz - 91 GHz	- OFDM	- External cavity laser + in-phase and quadrature (IQ)-MZM	- 24 Gbit/s
[31]	- FiWi mm-wave/ IFoF link	- 5G	- 57-64 GHz	- QPSK -16-QAM	- LD + SD-MZM	- 24 Gbit/s
[32]	- FiWi mm-wave/ IFoF link	- 5G - FTTH	- 60 GHz	- 16-QAM	- LD + SD-MZM	- Not specified
[14]	- Multi-user FiWi links	- 5G - FTTH - M2M	- Baseband - 700 MHz - 3.5 GHz - 26 GHz	- OFDM, GFDM, F-OFDM, *M*-QAM and Standard 5G NR	- LD + DD-MZM	- 4.41 Gbit/s
[33]	- Multi-user FiWi links	- 5G	- 60 GHz	- QPSK	- LD + SD-MZM	- 0.6 Gbit/s
[34]	- Multi-user FiWi links	- 5G	- 28 GHz	- 16- and 64-QAM	- RF combiner + LD	- 6 Gbit/s
[35]	- Multi-user FiWi links	- 5G	- 17.6 GHz - 26 GHz	- *M*-QAM	- LD + SD-MZM + optical ring resonators	- 21 Gbit/s
[36]	- mm-wave/FSO links	- Backhaul /fronthaul	- 60 GHz	- BPSK	- Bias tee + LD	- 1 Gbit/s
[37]	- mm-wave/FSO links	- 5G	- 60 GHz	- 16-QAM - OFDM	- DFB laser + MZM	- 4 Gbit/s
[25]	- mm-wave/FSO links	- 5G	- 28 GHz	- 16-QAM - 5G	- LD + MZM	- 1 Gbit/s
[18]	- RoF/FSO/Wireless links	- 5G	- 25 GHz	- Standard LTE	- LD + 2-MZMs	- 120 Mbit/s
[19]	- RoF/FSO/Wireless links	- 5G	- 2.12 GHz - 2.6 GHz - 3.5 GHz	- Standard LTE-A - 5G NR	- SFP module	- Not specified
[24]	- RoF/FSO/Wireless links	- Fronthaul - Access	- 24–26 GHz	- 64-QAM	- Bias tee + LD	- 600 Mbit/s
[38]	- VLC access	- Access point	-	- OOK	- Bias tee + GaN-based LED	- 2.3 Gbit/s
[39]	- VLC access	- 5G	-	- OFDM, GFDM and FBMC	- Bias tee + LED	- 10 Mbit/s
[40]	- VLC access	- Access point	-	- DCO-OFDM	- Bias tee + phosphor LD	- 6.9 Gbit/s
This work	- FiWi multi-user mm-Wave/RoF link - Parallel FiWi and FSO links - RoF/FSO-based link - VLC access	- 4G - 5G	- 700 MHz - 3.5 GHz - 26 GHz - 38 GHz	- *M*-QAM - LTE standard - 5G NR standard	- LD + SD-MZM - LD + DD-MZM - Bias tee + LED	- 182.8 Mbit/s - 1.61 Gbit/s - 1.4 Gbit/s - 218 Mbit/s

FiWi mm-wave/IFoF architectures, which include digital or analog RoF approaches followed by wireless transmission, have benefited from diverse technical solutions aimed at improving capacity and coverage [30–32]. For instance, Li et al. reported a 24 Gbit/s FiWi mm-wave link by exploiting 6 GHz bandwidth [30], whereas Argyris et al. demonstrated a similar bit rate in a mm-wave/IFoF link with electrical subcarrier multiplexing [31]. Mm-wave/IFoF links have even been deployed over legacy PON as an alternative for 5G fronthauling [32].

Advances in the multiuser FiWi links include simultaneous transmission of multiple RF signals at distinct frequency bands [14] as well as the use of phased array antennas for beamforming and beamsteering [33–35]. In [14], we presented a FiWi system over legacy PON based on DD-MZM that was able to cover the 5G eMBB scenario at FR1 and FR2, thereby enabling applications including long reach, fiber-to-the-home, and machine-to-machine communication. In [33], Ruggeri et al. reported a multiuser FiWi mm-wave/IFoF system taking advantage of a 32-element 60 GHz phased array antenna with beamsteering capability. In [34], Huang et al. demonstrated the possibility of integrating self-steering array beamforming to the FiWi architecture. Additionally, a photonic beamforming-based FiWi architecture was experimentally demonstrated in [35].

Multiple works have reported a hybrid mm-wave and FSO fronthaul aimed at increasing system reliability. The FSO and mm-waves links can operate in distinct architectures, namely simultaneous transmission for increased throughput in parallel with switchable transmission and a cascade system with FSO followed by a wireless link. Shakir et al. reported a hybrid system that simultaneously transmitted the same data over both links, namely an FSO at 1550 nm and mm-waves at 60 GHz [36]. The link selection was based on SNR for both approaches in accordance with decision thresholds aimed at evaluating BPSK transmission in a turbulent channel. Zhang et al. presented a hybrid FSO and mm-wave link for 5G backhauls operating at 1553.96 nm and 60 GHz, respectively. The link option was based on maximum-ratio combining (MRC) and was evaluated in terms of EVM_{RMS} for a 16-QAM signal in turbulent, fog, and rain conditions [37]. Additionally, the authors in [25] reported a hybrid 1550 nm FSO link cascaded with a 28 GHz RF link for 5G backhaul and fronthaul applications. The experiments consisted of evaluating the cascaded approach in terms of bit error rate (BER), EVM, and visibility range under the same dusty conditions. The experimental results demonstrated that the dust environment did not impair the RF link at 28 GHz, enabling the RF link to operate as a backup for FSO [25].

The FSO link has also been employed for extending the RoF fronthaul to sites where fiber optics do not reach, thus maintaining the optical communication advantages. In this way, Mufutau et al. demonstrated a hybrid 4G/5G optical fiber-wireless system, including a free-space optics fronthaul [19]. The results showed that a 100 MHz bandwidth 5G signal transmission using A-RoF throughout a 8 km fiber-optic fronthaul could coexist on the same LTE fronthaul infrastructure. Additionally, a hybrid fiber and FSO fronthaul demonstrated the 4G and 5G operability at 2.6 and 3.5 GHz, respectively. Nguyen et al. experimentally implemented a radio-over-fiber followed by an FSO fronthaul and mm-waves wireless transmission aimed at broadband wireless access [18]. The performance was evaluated by transmitting 4-, 16-, and 64-QAM LTE signals over the hybrid link and evaluating the EVM parameter as a function of weak-to-strong atmospheric turbulence regimes. Furthermore, Bohata et al. presented a radio-over-fiber combined with FSO and RF transmission for the 5G networks [24]. The authors used the 24–26 GHz frequency band and a particular direct intensity modulation solution for transmitting a 100 MHz bandwidth 64-QAM signal. The link performance was evaluated by exposing the FSO section to atmospheric turbulence and analyzing the SNR and EVM_{RMS}.

In parallel with the wireless techniques for access point, VLC systems have been emerging as a potential technology to accomplish the 5G requirements and beyond. They are mainly composed of light-emitting diodes, which can be used for simultaneously lighting the environment and transmitting data. In this way, Yeh et al. reported a GaN LED-based visible light communication using a 4×4 color polarization multiplexing and on–off keying (OOK) [38]. The system attained 2.3 Gbit/s over 1 m employing MIMO and pre-equalization under the illumination of 6.9–136.1 lux. Recent works have shown the use of VLC for 5G. For instance, Monteiro et al. reported a comparison among 5G waveform candidates, namely filter bank multicarrier (FBMC), generalized frequency division multiplexing (GFDM), and OFDM, with regard to a single-input single-output VLC system [39]. On the other hand, VLC systems may employ lasers as a light source to achieve higher throughput. Wei et al. reported a VLC system employing a white-light phosphor laser for illuminating and providing 6.9 Gbit/s over 1.5 m [40].

In this work, we examined an innovative proposal for optical-wireless architectures applied to the NSA 5G new radio framework. In contrast to previous works, we experimentally demonstrated 4G and 5G NR coexistence in the 700 MHz band taking into account a FiWi system.

Regarding the dual wireless and FSO-based fronthaul architecture, our implementation employed the 5G NR standard. The parallel FSO at 1550 nm and mm-wave link at 38 GHz enabled a dynamic selection according to its transmission performance, whereas the other link operated as a backup. Its performance was investigated by assessing the EVM_{RMS} for different power levels at the receiver to emulate the equivalent attenuation

levels for visibility and rain conditions. The attenuation levels used for the FSO link were from 0 to 56 mm/h, whereas the values ranged from 0 to 102 mm/h for the wireless link. Overall, our 5G NR experimental results demonstrated 1.61 Gbit/s total throughput, which is within the 3GPP EVM_{RMS} requirements, for rain intensity less than 36.4 mm/h and visibility above 40 m.

Moreover, we examined a fiber-optic and FSO-based 5G fronthaul followed by a dual-band 5G NR wireless access, including mm-waves. The FSO link enables last-mile applications, thereby increasing system flexibility and providing optical fiber-like throughput. The system performance was investigated by assessing the hybrid architecture in two distinct scenarios in terms of EVM_{RMS} and in accordance with 3GPP, namely the RoF/FSO fronthaul at the photodetector output and the dual-band 5G NR wireless system employing RoF/FSO as fronthaul. Overall, the proposed hybrid RoF/FSO fronthaul provided 3 Gbit/s total throughput with plenty of margin in terms of EVM_{RMS}, thereby enabling wireless access. The dual-band 5G NR wireless system assisted by a hybrid RoF/FSO fronthaul demonstrated the feasibility of the system by providing 1.4 Gbit/s total throughput, thus fulfilling the 3GPP Release 15 specifications.

Finally, the RGB-based VLC system for indoor applications was examined, in which immunity to electromagnetic interference is crucial. We transmitted a standard 5G NR signal and 3 LTE-A bands in order to attend to multiple users employing a single red LED, which offers the best trade-off between output power and quantum efficiency. The system performance was evaluated by assessing each transmitted signal in terms of SNR, constellation symbols dispersion, and consequently the EVM_{RMS}. The 5G NR VLC system provided 218 Mbit/s throughput and EVM_{RMS} as low as 6.45% considering all transmitted signals, thereby demonstrating the viability of VLC for 5G networks.

5. Conclusions

We have successfully proposed and reported on an efficient optical-wireless architecture applied to the non-standalone 5G new radio framework and compared the system to related works in the literature. Several distinct electrical- and optical-based fronthaul approaches combining free-space optical, wireless links, and RoF techniques were deployed for selection according to network operator requirements. First, a dual 38 GHz wireless and FSO-based fronthaul architecture enabled a backup link for high-reliability services. Next, a fiber-wireless configuration based on an analog RoF link followed by a wireless extension was studied for simultaneous RF signal distribution of both LTE-A and 5G NR signals. Finally, fiber optics and FSO techniques were integrated into a single fronthaul to extend the fronthaul reach where fiber optics cannot be deployed. After photodetection, further access extension was achieved by wireless signal transmission of the two 3GPP Release 15 spectral bands of 3.5 and 26 GHz. All three investigated approaches demonstrated performance within the 3GPP EVM_{RMS} requirements prescribed by 5G NR Release 15. In addition, a VLC access network with carrier aggregation was examined to increase user throughput when immunity to EM interference is paramount. The reported solutions may be integrated in a flexible optical-wireless platform for 5G and beyond, allowing their coexistence with 4G over a shared fronthaul infrastructure. Future works should consider implementation of the proposed architecture to either downlink an uplink or to increase the FSO reach up to hundreds of meters in an outdoor scenario.

Author Contributions: Conceptualization, A.C.S.J.; methodology, R.M.B.; validation, D.H.S. and M.A.R.; formal analysis, R.M.B., D.H.S., M.A.R. and A.C.S.J.; investigation, C.H.d.S.L., E.S.L., M.A.d.O., M.S.B.C., L.C.A., L.G.d.S. and L.A.M.P.; resources, A.C.S.J.; writing—original draft preparation, R.M.B., C.H.d.S.L., E.S.L., M.A.d.O., M.S.B.C., L.C.A., L.G.d.S. and L.A.M.P.; writing—review and editing, R.M.B. and M.A.R.; visualization, R.M.B.; supervision, D.H.S., M.A.R. and A.C.S.J.; project administration, A.C.S.J.; funding acquisition, M.A.R. and A.C.S.J. All authors have read and agreed to the published version of the manuscript.

Funding: This work was partially supported by RNP with resources from MCTIC, Grant No. 01245.010604/2020-14, under the 6G Mobile Communications Systems project of the Radiocommunication Reference Center (Centro de Referência em Radiocomunicações-CRR) of the National Institute of Telecommunications (Instituto Nacional de Telecomunicações-Inatel), Brazil. The authors would also like to thank CNPq, CAPES, FINEP, and FAPEMIG for the financial support.

Institutional Review Board Statement: Not applicable.

Informed Consent Statement: Not applicable.

Data Availability Statement: Not applicable.

Conflicts of Interest: The authors declare no conflict of interest.

References

1. Parkvall, S.; Dahlman, E.; Furuskär, A.; Frenne, M. NR: The new 5G radio access technology. *IEEE Commun. Stand. Mag.* **2017**, *1*, 24–30. [CrossRef]
2. 5GPP. View on 5G architecture. *White Paper*. 2017. Available online: https://5g-ppp.eu/wp-content/uploads/2018/01/5G-PPP-5G-Architecture-White-Paper-Jan-2018-v2.0.pdf (accessed on 26 May 2021).
3. 3GPP. 5G.; NR.; Overall description; Stage-2. TS 38.300 version 15.8.0 Release 15. 2020. Available online: https://www.etsi.org/deliver/etsi_ts/138300_138399/138300/15.08.00_60/ts_138300v150800p.pdf (accessed on 26 May 2021).
4. Tzanakaki, A.; Anastasopoulos, M.; Berberana, I.; Syrivelis, D.; Flegkas, P.; Korakis, T.; Mur, D.C.; Demirkol, I.; Gutierrez, J.; Grass, E.; et al. Wireless-optical network convergence: Enabling the 5G architecture to support operational and end-user services. *IEEE Commun. Mag.* **2017**, *55*, 184–192. [CrossRef]
5. Zhang, N.; Cheng, N.; Gamage, A.P.K.T.; Zhang, K.; Mark, J.W.; Shen, X. Cloud assisted HetNets toward 5G wireless networks. *IEEE Commun. Mag.* **2015**, *53*, 59–65. [CrossRef]
6. I, C.-L.; Li, H.; Korhonen, J.; Huang, J.; Han, L. RAN revolution with NGFI (xhaul) for 5G. *J. Lightw. Technol.* **2018**, *36*, 541–550. [CrossRef]
7. 3GPP. Release 16 description; Summary of Rel-16 work items. TR 21.916 v0.5.0. 2020. Available online: https://www.3gpp.org/release-16 (accessed on 26 May 2021).
8. 3GPP. Release17. Available online: 3gpp.org/release-17 (accessed on 26 May 2021).
9. Dang, S.; Amin, O.; Shihada, B.; Alouini, M. What should 6G be? *Nat. Electron.* **2020**, *3*, 20–29. [CrossRef]
10. Zhang, Z.; Xiao, Y.; Ma, Z.; Xiao, M.; Ding, Z.; Lei, X.; Karagiannidis, G.K.; Fan, P. 6G wireless networks: Vision, requirements, architecture and key technologies. *IEEE Veh. Technol. Mag.* **2019**, *14*, 28–41. [CrossRef]
11. Kalfas, G.; Vagionas, C.; Antonopoulos, A.; Kartsakli, E.; Mesodiakaki, A.; Papaioannou, S.; Maniotis, P.; Vardakas, J.S.; Verikoukis, C.; Pleros, N. Next generation fiber-wireless fronthaul for 5G mmWave networks. *IEEE Commun. Mag.* **2019**, *57*, 138–144. [CrossRef]
12. Liu, C.; Wang, J.; Cheng, L.; Zhu, M.; Chang, G.-K. Key microwave-photonics technologies for next generation cloud-based radio access networks. *J. Lightw. Technol.* **2014**, *32*, 3452–3460. [CrossRef]
13. Yao, S.; Chen, Y.-W.; Su, S.-J.; Alfadhli, Y.; Shen, S.; Zhang, R.; Zhou, Q.; Chang, G.-K. Non-orthogonal uplink services through co-transport of D-RoF/A-RoF in mobile fronthaul. *J. Lightw. Technol.* **2020**, *38*, 3637–3643. [CrossRef]
14. Borges, R.M.; Pereira, L.A.M.; Filgueiras, H.R.D.; Ferreira, A.C.; Cunha, M.S.B.; Neto, E.R.; Spadoti, D.H.; Mendes, L.L.; Sodré Jr., A.C. DSP-based flexible-waveform and multi-application 5G fiber-wireless system. *J. Lightw. Technol.* **2020**, *38*, 642–653. [CrossRef]
15. Borges, R.M.; Lima, E.S.; Ferreira, A.C.; Spadoti, D.H.; Abreu, M.; Mendes, L.L.; Sodré Jr., A.C.; Junior, A.C.S. Multiband 5G NR system with photonic-assisted RF amplification. *Opt. Lett.* **2020**, *45*, 1539–1542. [CrossRef]
16. Lima, E.S.; Borges, R.M.; Pereira, L.A.M.; Filgueiras, H.R.D.; Alberti, A.M.; Sodré Jr., A.C. Multiband and photonically amplified fiber-wireless Xhaul. *IEEE Access* **2020**, *8*, 44381–44390. [CrossRef]
17. Filgueiras, H.R.D.; Borges, R.M.; Melo, M.C.; Brandao, T.H.; Sodré Jr., A.C. Dual-band wireless fronthaul using a FSS-based focal-point/Cassegrain antenna assisted by an optical midhaul. *IEEE Access* **2019**, *7*, 112578–112587. [CrossRef]
18. Nguyen, D.-N.; Bohata, J.; Komanec, M.; Zvanovec, S.; Ortega, B.; Ghassemlooy, Z. Seamless 25 GHz transmission of LTE 4/16/64-QAM signals over hybrid SMF/FSO and wireless link. *J. Lightw. Technol.* **2019**, *37*, 6040–6047. [CrossRef]
19. Mufutau, A.O.; Guiomar, F.P.; Fernandes, M.A.; Lorences-Riesgo, A.; Oliveira, A.; Monteiro, P.P. Demonstration of a hybrid optical fiber-wireless 5G fronthaul coexisting with end-to-end 4G networks. *J. Opt. Commun. Netw.* **2020**, *12*, 72–78. [CrossRef]
20. Koonen, T. Indoor optical wireless systems: Technology, trends, and applications. *J. Lightw. Technol.* **2018**, *36*, 1459–1467. [CrossRef]
21. Feng, L.; Hu, R.Q.; Wang, J.; Xu, P.; Qian, Y. Applying VLC in 5G networks: Architectures and key technologies. *IEEE Netw.* **2016**, *30*, 77–83. [CrossRef]
22. Ranaweera, C.; Wong, E.; Nirmalathas, A.; Jayasundara, C.; Lim, C. 5G C-RAN With Optical Fronthaul: An Analysis From a Deployment Perspective. *J. Lightw. Technol.* **2018**, *36*, 2059–2068. [CrossRef]

23. ACG Research. An Economic Comparison of Fronthaul Architectures for 5G Networks. Available online: https://www.acgcc.com (accessed on 17 August 2020).
24. Bohata, J.; Komanec, M.; Spácil, J.; Ghassemlooy, Z.; Zvánovec, S.; Slavık, R. 24–26 GHz radio-over-fiber and free-space optics for fifth- generation systems. *Opt. Lett.* **2018**, *43*, 1035–1038. [CrossRef] [PubMed]
25. Esmail, M.A.; Ragheb, A.M.; Fathallah, H.A.; Altamimi, M.; Alshebeili, S.A. 5G-28 GHz signal transmission over hybrid all-optical FSO/RF link in dusty weather conditions. *IEEE Access* **2019**, *7*, 24404–24410. [CrossRef]
26. Agrawal, G.P. *Applications of Nonlinear Fiber Optics*, 1st ed.; Academic Press: Cambridge, MA, USA, 2001.
27. 3GPP. *Group radio access network; NR.; User equipment (UE) radio transmission and reception; Part 1: Range 1 Standalone. TS 38.101–1 version 15.5.0 Release 15*. 2019. Available online: https://www.etsi.org/deliver/etsi_ts/138100_138199/13810101/15.05.00_60/ts_13810101v150500p.pdf (accessed on 17 August 2020).
28. Haas, H.; Yin, L.; Wang, Y.; Chen, C. What is lifi? *J. Lightw. Technol.* **2016**, *34*, 1533–1544. [CrossRef]
29. Huang, X.; Shi, J.; Li, J.; Wang, Y.; Wang, Y.; Chi, N. 750Mbit/s visible light communications employing 64QAM-OFDM based on amplitude equalization circuit. In Proceedings of the Optical Fiber Communication Conference, Los Angeles, CA, USA, 22–26 March 2015.
30. Li, X.; Xiao, X.; Xu, Y.; Wang, K.; Zhao, L.; Xiao, J.; Yu, J. Real-time demonstration of over 20 Gbit/s V- and W-band wireless transmission capacity in one OFDM-RoF system. In Proceedings of the Optical Fiber Communications Conference (OFC), Los Angeles, CA, USA, 19–23 March 2017.
31. Argyris, N.; Giannoulis, G.; Kanta, K.; Iliadis, N.; Vagionas, C.; Papaioannou, S.; Kalfas, G.; Apostolopoulos, D.; Caillaud, C.; Debrégeas, H.; et al. A 5G mmWave fiber-wireless IFoF analog mobile fronthaul link with up to 24 Gb/s multi-band wireless capacity. *J. Lightw. Technol.* **2019**, *37*, 2883–2891. [CrossRef]
32. Kanta, K.; Pagano, A.; Ruggeri, E.; Agus, M.; Stratakos, I.; Mercinelli, R.; Vagionas, C.; Toumasis, P.; Kalfas, G.; Giannoulis, G.; et al. Analog fiber-wireless downlink transmission of IFoF/mmWave over in-field deployed legacy PON infrastructure for 5G fronthauling. *J. Opt. Commun. Netw.* **2020**, *12*, D57–D65. [CrossRef]
33. Ruggeri, E.; Tsakyridis, A.; Vagionas, C.; Leiba, Y.; Kalfas, G.; Pleros, N.; Miliou, A. Multi-user V-band uplink using a massive MIMO antenna and a fiber-wireless IFoF fronthaul for 5G mmWave small-cells. *J. Lightw. Technol.* **2020**, *38*, 5368–5374. [CrossRef]
34. Huang, M.-Y.; Chen, Y.-W.; Peng, P.-C.; Wang, H.; Chang, G.-K. A full field-of-view self-steering beamformer for 5G mm-wave fiber-wireless mobile fronthaul. *J. Lightw. Technol.* **2020**, *38*, 1221–1229. [CrossRef]
35. Morant, M.; Trinidad, A.; Tangdiongga, E.; Koonen, T.; Llorente, R. Experimental demonstration of mm-Wave 5G NR photonic beamforming based on ORRs and multicore fiber. *IEEE Trans. Microw. Theory Techn.* **2019**, *67*, 2928–2935. [CrossRef]
36. Shakir, W.M.R. Performance evaluation of a selection combining scheme for the hybrid FSO/RF system. *IEEE Photon. J.* **2017**, *10*, 1–10. [CrossRef]
37. Zhang, J.; Wang, J.; Xu, Y.; Xu, M.; Lu, F.; Cheng, L.; Yu, J.; Chang, G.-K. Fiber–wireless integrated mobile backhaul network based on a hybrid millimeter-wave and free-space-optics architecture with an adaptive diversity combining technique. *Opt. Lett.* **2016**, *41*, 1909–1912. [CrossRef]
38. Yeh, C.-H.; Weng, J.-H.; Chow, C.-W.; Luo, C.-M.; Xie, Y.-R.; Chen, C.-J.; Wu, M.-C. 1.7 to 2.3 Gbps OOK LED VLC transmission based on 4× 4 color-polarization-multiplexing at extremely low illumination. *IEEE Photon. J.* **2019**, *11*, 1–6. [CrossRef]
39. Monteiro, F.T.; Costa, W.S.; Neves, J.L.C.; Silva, D.M.I.; Rocha, H.R.O.; Salles, E.O.T.; Silva, J.A.L. Experimental evaluation of pulse shaping based 5G multicarrier modulation formats in visible light communication systems. *Opt. Commun.* **2020**, *457*. [CrossRef]
40. Wei, L.-Y.; Liu, Y.; Chow, C.-W.; Chen, G.-H.; Peng, C.-W.; Guo, P.-C.; Tsai, J.-F.; Yeh, C.-H. 6.915-Gbit/s white-light phosphor laser diode-based DCO-OFDM visible light communication (VLC) system with functional transmission distance. *Electron. Lett.* **2020**, *56*, 945–947. [CrossRef]

Artigo 7 : Peaceful Coexistence Between 5G NR and LTE-A Over a RoF-Based Fronthaul

Celso Henrique de Souza Lopes, Eduardo Saia Lima, Luiz Augusto Melo Pereira and Arismar Cerqueira. S. Jr. ”Peaceful Coexistence Between 5G NR and LTE-A Over a RoF-Based Fronthaul”, *SBFoton* 2021.

Peaceful Coexistence Between 5G NR and LTE-A Over a RoF-Based Fronthaul

Celso Henrique de Souza Lopes
Lab.WOCA
National Institute of Telecommunications (Inatel)
Santa Rita do Sapucaí, Brazil
celso.lopes@mtel.inatel.br

Eduardo Saia Lima
Lab.WOCA
Inatel
Santa Rita do Sapucaí, Brazil
elima@get.inatel.br

Luiz Augusto Melo Pereira
Lab.WOCA
Inatel
Santa Rita do Sapucaí, Brazil
luiz.augusto@dtel.inatel.br

Arismar Cerqueira Sodré Junior
Lab.WOCA
Inatel
Santa Rita do Sapucaí, Brazil
arismar@inatel.br

2021 SBFoton International Optics and Photonics Conference (SBFoton IOPC) | 978-1-6654-1948-2/21/$31.00 ©2021 IEEE | DOI: 10.1109/SBFOTONIOPC50774.2021.9461959

***Abstract*—This work presents the implementation and peaceful coexistence analysis between a 5G New Radio (5G NR) and Long Term Evolution-Advanced (LTE-A) signals over radio over fiber (RoF) based 25-km fronthaul, operating in the non-standalone (NSA) mode. Three signals are investigated, namely: 10-MHz bandwidth Filtered Orthogonal Frequency Division Multiplexing (F-OFDM) at 778 MHz; five 20-MHz LTE-A subbands at 2.24 GHz; 100-MHz bandwidth 5G NR signal at 2.35 GHz. The system performance is estimated measuring the root mean square error vector magnitude (EVM_{RMS}), as a function of the optical power and the 5G NR and LTE-A frequency offset, achieving 1.4 Gbps throughput.**

***Index Terms*—5G NR, Coexistence, Fronthaul and Non-standalone.**

I. Introduction

The fifth-generation of mobile networks (5G) comes up as a substantial improvement on the wireless systems in terms of capacity, throughput, flexibility, energy efficiency, and low end-to-end latency [1]. The 5G was specified with the initial focus on meeting requirements associated with the following 3rd Generation Partnership Project (3GPP) application scenarios: enhanced mobile broadband (eMBB); ultra-reliable low-latency communication (URLLC); massive machine type communication (mMTC) and the enhanced remote area communications (eRAC) [2]. The 3GPP initially establishes in the Release 15, the phase 1 for the 5G standardization, called the New Radio (NR) phase 1 [1]. At this initial stage, 5G networks might operate in non-standalone mode (NSA), i.e. employing the fourth-generation of mobile networks (4G) architecture and core for deploying the 5G networks to enable new services and applications [3].

The 5G systems employ several innovative technical solutions for covering the plurality of applications and new services. The main technologies exploited include new spectral bands, software-defined network (SDN), massive multiple-input multiple-output (mMIMO) and microwave photonics (MWP). The latter one, more specifically the radio over fiber (RoF) technique, have been widely employed to compose the cellular communication systems architecture, enabling to transport radiofrequency (RF) signals in the optical domain [4,5].

The centralized radio access network (C-RAN) is the one of proposed architectures for 5G networks [5]. In C-RAN, the backhaul link connects the central office (CO) to the core network, typically carrying digital user data, whereas the fronthaul link connects CO to remote remote radio units (RRUs) [6]. Currently, the C-RAN architectures fronthaul links are based on digital RoF (D-RoF) technology, using Common Public Radio Interface (CPRI). However, such technique suffers from scalability issues, which suggests the use of alternatives fronthaul solutions, for instance, analog RoF (A-RoF) [7]. This solution simplifies the system operation and enhances its scalability, since there is no need for an analog-to-digital converter (ADC) and digital-to-analog converter (DAC), as well as up-conversion requirement at the RRU [8].

Several A-RoF-based fronthaul solutions for 5G networks have been proposed along the years. Delmade et al. [9] demonstrated the transmission of 4G and 5G signals coexisting on the same A-RoF link in the 700 MHz to 3.6 GHz band. The integration and experimental performance analysis of a 5G transceiver based on generalized frequency division multiplexing (GFDM) in an RoF-based gigabit passive optical network (GPON), have been reported by our research group in [10]. In [11] the authors report the implementation and experimental investigation of two different non-standalone 5G NR networks architectures, aiming to fulfill the 5G demands. In [12], was demonstrated the use of a monolithically integrated multi-

wavelength transmitter for multi-band 5G NR RoF systems, simultaneously operating in the standalone (SA) and NSA modes.

The current work reports the implementation and experimental investigation of the 5G NR and Long-Term Evolution-Advanced (LTE-A) coexistence on a non-standalone based transmission, aiming to fulfill the eMBB and eRAC services. The implementation employs direct modulation and detection for transmitting 4G and 5G signals simultaneously over a 25-km fiber optics fronthaul. The signals encompass our digital signal processing (DSP)-based and flexible waveform 5G transceiver using filtered orthogonal frequency division multiplexing (F-OFDM); a 100-MHz 5G NR standard signal at 2.35 GHz; a 100-MHz LTE-A signal at 2.24 GHz. Its main contribution over the state-of-the-art is the deployment of a non-standalone 4G/5G based on A-RoF technology using adjacent channels in the aggregation carrier mode. Experimental results demonstrated a peaceful coexistence between the 4G/5G signals operating in adjacent channels.

The manuscript is structured in four sections. Section II presents the investigation of the NSA 4G/5G A-RoF system, using a fiber optics-based fronthaul. Section III reports the experimental results and finally, the conclusions and future works are drawn in Section IV.

II. RoF BASED FRONTHAUL IMPLEMENTATION

The experimental coexistence evaluation between 5G NR and LTE-A signals is described in terms of block diagram in Fig. 1. The architecture is based on the C-RAN concept, A-RoF technique and downlink transmission direction. At the CO, we have transmitted three distinct RF signals, namely: a 10-MHz bandwidth 64-QAM F-OFDM signal at 778 MHz (RF_1), generated by our 5G transceiver, developed for remote and rural areas communication, in the context of the remote area access network for the 5th generation (5G-RANGE) project [13]; five 20-MHz LTE-A sub-bands (RF_2) centralized at 2.24 GHz, generated by a A M8190A arbitrary waveform generator (AWG) and upconverted by a PSGE8267D vector signal generator (VSG_1), both from Keysight; a 100-MHz bandwidth 5G NR signal at 2.35 GHz (RF_3) in accordance with 3GPP Release 15 specifications, employing a SMBV100B vector signal generator (VSG_2) from Rohde & Schwarz. A RF combiner has been used for combining the three mentioned RF signals, resulting in 0 dBm electrical power. The combined electrical signal driven a commercial RoF Tx module from Oz Optics, composed by a 4-dBm direct modulated laser (DML) operating at 1551 nm. Afterwards, the modulated optical signal has been launched throughout 25-km G657 optical fiber fronthaul. Therefore, the chromatic dispersion does not severely impact the RoF system, since the dispersion accumulated was around 400 ps/nm.

At the reception side (RRU), the modulated optical carrier reaches a variable optical attenuator (VOA) and an optical power monitor (OPM), which enable to control and manage the optical power at the RoF Rx module input. The receiver comprises a photodetector (PD) and subsequently a 22-dB integrated electrical amplifier. After the optical-to-electrical conversion, a directional coupler has been used for providing 1% of the total power to a electrical spectrum analyzer (ESA). The remaining 99% power fed a 1:2 power splitter, which equally divided the signal in two parts. In this way, a 5G transceiver has been used for evaluating the 5G signal at 778 MHz, whereas a vector signal analyzer (VSA_1) has been used for assessing the 5G NR and the LTE-A signals in the 2.35 and 2.24 GHz bands, respectively. Fig. 2. depicts a experimental setup photography, which is in accordance with the description and block diagram.

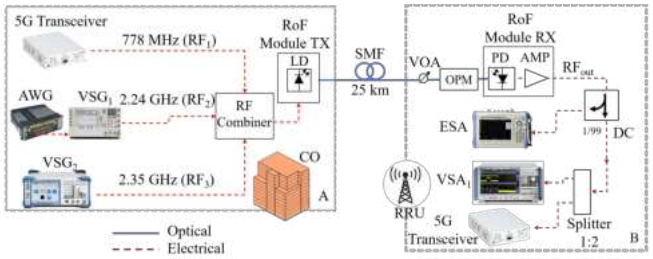

Fig. 1. RoF based fronthaul implementation. AWG - arbitrary waveform generator; VSG - vector signal generator; LD - laser diode; SMF - single mode fiber; VOA - variable optical attenuator; OPM - optical power monitor; PD - photodetector; AMP - amplifier; VSA - vector signal analyzer.

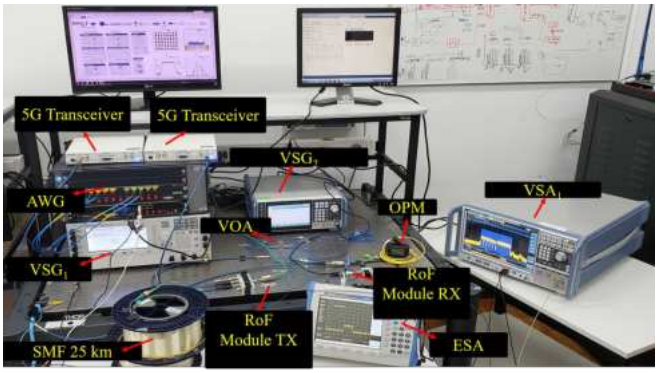

Fig. 2. Experimental setup.

The RF signals performance have been evaluated by analyzing the measured root mean square error vector magnitude (EVM_{RMS}) in accordance with the 3GPP Release 15 specifications. The first system characterization consisted on performing the coexistence between the 5G NR and the LTE-A for investigating the minimum frequency offset between then, aiming for a peaceful coexistence. It is worth mentioning that the optical power level for the first investigation remained around -7 dBm. The second characterization consisted on assessing all the transmitted signals as a function of the optical power at the Rx module input, in order to identify the best operating point.

III. Coexistence analisys between 5G NR and LTE-A

Fig. 3 reports the coexistence analyses for offset of 0, 20, 40, 60, 80 and 104 MHz, measured at the Rx module output. For 0 MHz, all the signal are overlapped, as a result, the EVM_{RMS} measured exceeded the limits stipulated by 3GPP for the 5G NR signal and all LTE-A sub-bands. Similarly, for 20-MHz offset, which is, the LTE-A 1 sub-band centered at 2288 MHz, the measured EVM_{RMS} was 2.3%, however, sub-bands from 2 to 5 are still overlapping with the 5G NR signal. One can note as the offset increases the overlapping between the LTE-A subbands and the 5G signal becomes less significant. As a result, each subband, which are not overlapped for the current offset, presents EVM_{RMS} lower than 3.5% and the LTE-A symbols, carried by the subbands, could be efficiently demodulated. The last measurement was carried out with 104-MHz frequency deviation between the central carriers, as shown in Fig. 4. One can observe there no more spectral overlapping between LTE-A and the NR signal, as a consequence, all the evaluated signals accomplished the 3GPP EVM_{RMS} requirements with margins, ensuring that the signals coexist peacefully in the proposed experimental setup. In addition, all the measured constellations presented well-defined symbols and no noticeable phase and magnitude variations, emphasising the obtained performance. The total attained throughput was 1.4 Gbps, considering all transmitted signals. Table I summarizes the EVM_{RMS} measurements for each signal and the investigated offset.

Posteriorly, we measured the EVM_{RMS} at the RoF system output, as a function of the photodetector input power, which was varied from -19 to -7 dBm, as reported in Fig 5. Our goal was to identify the optical power levels that allow meeting the 3GPP EVM_{RMS} requirements for the F-OFDM, LTE-A

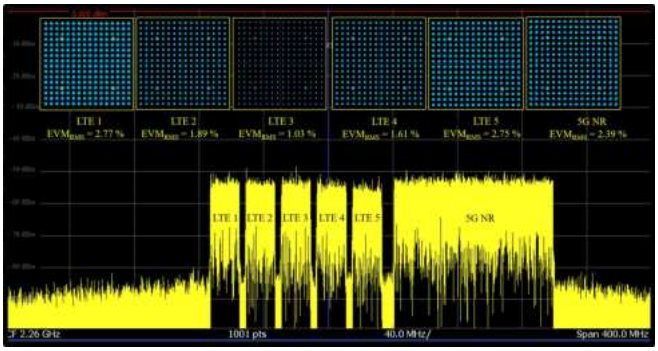

Fig. 4. The received electrical spectrum at the end user after 25-km fiber-optics transport.

TABLE I
EVM_{RMS}(%) as a function of frequency offset.

	Offset [MHz]	LTE-A Subband 1	LTE-A Subband 2	LTE-A Subband 3	LTE-A Subband 4	LTE-A Subband 5	5G NR
EVM_{RMS} (%)	0	—	—	—	—	—	—
	20	2.3	—	—	—	—	—
	40	2.44	2	—	—	—	—
	60	2.55	1.95	1.55	—	—	—
	80	2.60	1.75	1.28	1.7	—	—
	104	2.77	1.89	1.03	1.61	2.75	2.39

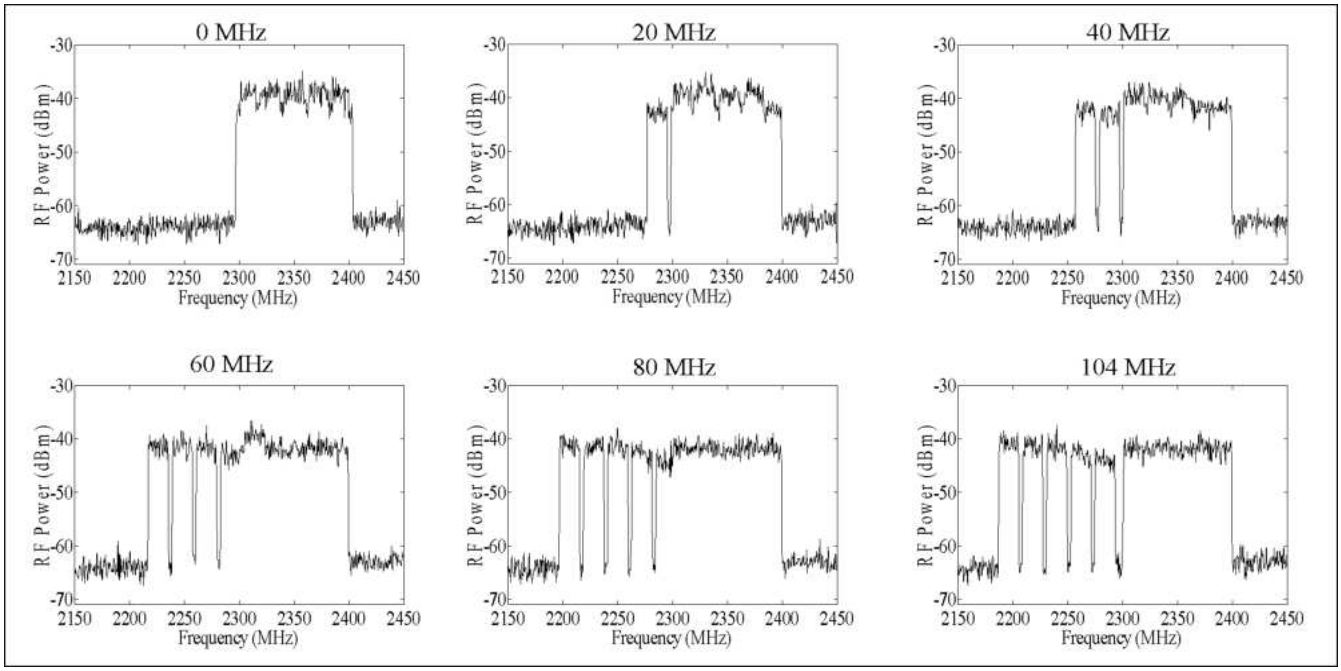

Fig. 3. Peaceful coexistence between LTE-A and 5G NR signals.

and 5G NR signals. In this case, the frequency offset between the 4G and 5G NR signals was kept as 104 MHz, and the electrical power at the RF combiner output was -5 dBm. The EVM_{RMS} value for the 64-QAM F-OFDM signal at 778 MHz met the 3GPP EVM_{RMS} requirement of 8% for receiving optical power levels higher than -17.5 dBm. Whereas, the central sub-bands of the LTE-A signal presented EVM_{RMS} below 3.5% for an optical power higher than -9 dBm and the extreme LTE-A subbands demanded 2-dB additional optical power to accomplish the specifications. The 256-QAM 5G NR signal at 2.35 GHz met the 3GPP EVM_{RMS} requirement of 3.5% for receiving optical power levels higher or equal to -9 dBm. Therefore, simultaneously addressing eRAC and eMBB applications in the presented conditions, requiring a minimum optical power level of -7 dBm at RRU, besides a minimum offset of 104 MHz between the LTE-A and 5G NR signals. Additionally, the 5G NR standard enables the flexibility of choosing the sub-carrier spacing, unlike LTE-A that only permits 15-kHz sub-carrier spacing. Particularly, 5G NR specifies 15, 30 and 60 kHz sub-carrier spacing options for frequencies below 8 GHz. As a consequence, the coexistence between LTE-A with a 5G NR signal, might be enhanced by using the 15-kHz sub-carrier spacing option aiming to keep the orthogonality between the subcarriers signals. Overall, the 5G NR/LTE-A system employing A-RoF in the NSA mode was able to reach 1.4 Gbit/s, demonstrating the system feasibility for integrating the 5G core and access.

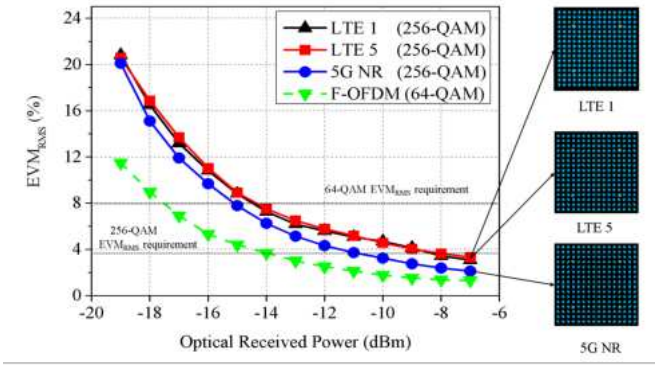

Fig. 5. EVM_{RMS} as a function of the optical power at the photodetector input.

IV. Conclusions

We have successfully implemented a multiband RoF fronthaul based on 5G NR and LTE-A applied to 5G radio access scenarios, including indoor and outdoor eMBB and eRAC applications. Multiple RF signals have been transmitted using a 25-km optical fiber fronthaul for evaluating the coexistence between 5G new radio (5G NR) and LTE-A signals towards the implementation of an NSA-based network. The aforementioned signals referred to an F-OFDM signal at 778 MHz from our 5G transceiver, a standardized 5G NR and LTE-A signals around 2.24 GHz. The total attained throughput was 1.4 Gbps with EVM_{RMS} in accordance to the 3GPP requirements. The minimum offset for avoiding overlapping between the signals was 104 MHz, which corresponds to a 2-MHz guard band, demonstrating a peaceful coexistence between 4G and 5G signals over an A-RoF system. Future works regard the implementation of the proposed architecture for either downlink and uplink, as well as to the exploiting the millimeter-wave frequency bands.

Acknowledgments

This work was partially supported by RNP, with resources from MCTIC, Grant No. No 01245.010604/2020-14, under the 6G Mobile Communications Systems project of the Radiocommunication Reference Center (Centro de Referência em Radiocomunicações - CRR) of the National Institute of Telecommunications (Instituto Nacional de Telecomunicações - Inatel), Brazil. The authors also thank the financial support from CNPq, CAPES, FINEP and FAPEMIG.

References

[1] M. Series, "IMT vision–framework and overall objectives of the future development of IMT for 2020 and beyond," *Recommendation ITU*, vol. 2083, 2015.

[2] A. Osseiran, F. Boccardi, V. Braun, K. Kusume, P. Marsch, M. Maternia, O. Queseth, M. Schellmann, H. Schotten, H. Taoka, H. Tullberg, M. A. Uusitalo, B. Timus, and M. Fallgren, "Scenarios for 5G mobile and wireless communications: The vision of the METIS project," *IEEE Communications Magazine*, vol. 52, no. 5, pp. 26–35, May. 2014.

[3] A. Hoglund, D. P. Van, T. Tirronen, O. Liberg, Y. Sui, and E. A. Yavuz, "3GPP release 15 early data transmission," *IEEE Communications Standards Magazine*, vol. 2, no. 2, pp. 90–96, 2018.

[4] M. Matthé, I. S. Gaspar, L. L. Mendes, D. Zhang, M. Danneberg, N. Michailow, and G. Fettweis, "Generalized frequency division multiplexing: a flexible multi-carrier waveform for 5G," in *5G Mobile Communications*. Springer, 2017, pp. 223–259.

[5] E. S. Lima, R. M. Borges, L. A. M. Pereira, H. R. D. Filgueiras, A. M. Alberti, and A. C. Sodré, "Multiband and photonically amplified fiber-wireless xhaul," *IEEE Access*, vol. 8, pp. 44 381–44 390, 2020.

[6] M. A. Habibi, M. Nasimi, B. Han, and H. D. Schotten, "A Comprehensive Survey of RAN Architectures Toward 5G Mobile Communication System," *IEEE Access*, vol. 7, pp. 70 371–70 421, May. 2019.

[7] D. Chitimalla, K. Kondepu, L. Valcarenghi, M. Tornatore, and B. Mukherjee, "5G fronthaul–latency and jitter studies of CPRI over ethernet," *Journal of Optical Communications and Networking*, vol. 9, no. 2, pp. 172–182, 2017.

[8] D. Wake, A. Nkansah, and N. J. Gomes, "Radio over fiber link design for next generation wireless systems," *Journal of lightwave Technology*, vol. 28, no. 16, pp. 2456–2464, 2010.

[9] A. Delmade, C. Browning, A. Farhang, N. Marchetti, L. E. Doyle, R. D. Koilpillai, L. P. Barry, and D. Venkitesh, "Performance analysis of analog IF over fiber fronthaul link with 4G and 5G coexistence," *Journal of Optical Communications and Networking*, vol. 10, no. 3, pp. 174–182, 2018.

[10] R. M. Borges, T. R. R. Marins, M. S. B. Cunha, H. R. D. Filgueiras, I. F. da Costa, R. N. da Silva, D. H. Spadoti, L. L. Mendes, and A. C. Sodré, "Integration of a GFDM-based 5G transceiver in a GPON using radio over fiber technology," *Journal of Lightwave Technology*, vol. 36, no. 19, pp. 4468–4477, 2018.

[11] C. H. de Souza Lopes, E. S. Lima, L. A. M. Pereira, R. M. Borges, A. C. Ferreira, M. Abreu, W. D. Dias, D. H. Spadoti, L. L. Mendes, and A. C. S. Junior, "Non-standalone 5G NR fiber-wireless system using FSO and fiber-optics fronthauls," *Journal of Lightwave Technology*, vol. 39, no. 2, pp. 406–417, 2020.

[12] M. S. B. Cunha, E. S. Lima, N. Andriolli, D. H. Spadoti, G. Contestabile, and A. Cerqueira, "5G NR RoF system based on a monolithically integrated multi-wavelength transmitter," *IEEE Journal of Selected Topics in Quantum Electronics*, vol. 27, no. 2, pp. 1–8, 2020.

[13] G.-R. Project. (2017) Remote area Access Network for the 5th GEneration. [Online]. Available: http://5g-range.eu/

Artigo 8 : Wireless and Optical Convergent Access Technologies Toward 6G

Hugo Rodrigues Dias Filgueiras, Eduardo Saia Lima, Matheus Sêda Borsato Cunha, Celso Henrique de Souza Lopes, Leticia Carneiro de Souza, Ramon Maia Borges, Luiz Augusto Melo Pereira, Tiago Henrique Brandão, Tomás Powell Villena Andrade, Luciano Camilo Alexandre, Geraldo Neto, Agostinho Linhares, Luciano Leonel Mendes, Murilo Araujo Romero and Arismar Cerqueira. S. Jr. ”Integrating Optical and Wireless Techniques towards Novel Fronthaul and Access Architectures in a 5G NR Framework”, *IEEE ACCES* VOL. 11, 2023.

IEEE Access
Multidisciplinary | Rapid Review | Open Access Journal

Received 22 December 2022, accepted 23 January 2023, date of publication 25 January 2023, date of current version 31 January 2023.

Digital Object Identifier 10.1109/ACCESS.2023.3239807

TOPICAL REVIEW

Wireless and Optical Convergent Access Technologies Toward 6G

HUGO RODRIGUES DIAS FILGUEIRAS[1,2], (Associate Member, IEEE), EDUARDO SAIA LIMA[2], MATHEUS SÊDA BORSATO CUNHA[2], CELSO HENRIQUE DE SOUZA LOPES[2], LETÍCIA CARNEIRO DE SOUZA[2], RAMON MAIA BORGES[3], LUIZ AUGUSTO MELO PEREIRA[2], TIAGO HENRIQUE BRANDÃO[2], TOMÁS POWELL VILLENA ANDRADE[2], LUCIANO CAMILO ALEXANDRE[2], GERALDO NETO[4], AGOSTINHO LINHARES[5], LUCIANO LEONEL MENDES[6], (Member, IEEE), MURILO ARAUJO ROMERO[7], (Senior Member, IEEE), AND ARISMAR CERQUEIRA S. JR.[2]

[1]VS Telecom, São Paulo 04213-001, Brazil
[2]Laboratory Wireless and Optical Convergent Access (WOCA), National Telecommunications Institute (Inatel), Santa Rita do Sapucaí, Minas Gerais 37540-000, Brazil
[3]Institute of Systems Engineering and Information Technology, Federal University of Itajubá, Itajubá, Minas Gerais 37500-903, Brazil
[4]TMG, Vancouver, WA 98662, USA
[5]Brazilian Ministry of Communications, Brasília, Distrito Federal 70044-900, Brazil
[6]Radiocommunications Reference Center (CRR), National Telecommunications Institute (Inatel), Santa Rita do Sapucaí 37540-000, Brazil
[7]Department of Electrical and Computer Engineering, University of São Paulo (USP), EESC/USP, São Carlos, São Paulo 13566-590, Brazil

Corresponding author: Arismar Cerqueira S. Jr. (arismar@inatel.br)

This work was supported in part by the National Education and Research Network (RNP) with resources from Ministry of Science, Technology, Innovation and Communication (MCTIC) under the 6G Mobile Communications Systems Project of the Radiocommunication Reference Center [Centro de Referência em Radiocomunicações (CRR)] of the National Institute of Telecommunications (Instituto Nacional de Telecomunicações—Inatel), Brazil, under Grant 01245.020548/2021-07; in part by the National Scientific and Technological Development Council (CNPq); in part by the Higher Education Personnel Improvement Coordination (CAPES); in part by the Financier of Studies and Projects (FINEP); and in part by the Research Support Foundation of the State of Minas Gerais (FAPEMIG).

ABSTRACT The sixth generation of mobile communication (6G) systems is recently rising a lot of interest, introducing new futuristic and challenging use cases that will demand much more than just communications to become a reality. Higher throughput, lower latencies, higher number of connections will push the requirement of the future mobile networks to a new level, but also sensing, positioning and imaging will play an important role in the new foreseen use cases. The integration of techniques developed for wireless communications with those conceived for optical links will be essential to provide the infrastructure for the 6G networks. In this context, this paper presents a review on wireless and optical convergent access solutions towards the 6G systems. The manuscript brings the use cases, requirements and enablers for 6G networks including a discussion about the state-of-the-art on THz and sub-THz communications, wireless and optical convergence, visible light communication, integrated and free-space optics, new antenna designs, power-over-fiber deployments and the use of machine learning in the physical layer of future networks. By reviewing the most relevant contributions available in the literature for wireless and optical communications and presenting their main contributions, this paper clearly shows that, more than a technological trend, the convergence of wireless and optical technologies is a fundamental step towards the development of the 6G network infrastructure.

INDEX TERMS 6G, antennas, FSO, optical-wireless convergence, physical layer, PIC, PoF, THz, VLC.

I. INTRODUCTION

The evolution from the first generation of mobile communications (1G) to the fourth generation of mobile communications (4G) has been mainly focused on increasing the system capacity in terms of data rate and number of users. The fifth generation of mobile network (5G), on the other hand, has been designed to support three main scenarios according with international mobile telecommunications (IMT)-2020 vision [1], [2], [3]: enhanced mobile broadband

The associate editor coordinating the review of this manuscript and approving it for publication was Leo Spiekman.

communication (eMBB); massive machine-type communication (mMTC); ultra-reliable low-latency communications (URLLC) [1], [2], [3], [4], [5]. Additionally, remote and rural access have been also triggering a lot of interest, mainly in continental-sized countries [6].

The 5G network has been recently standardized in its first release, 3rd generation partnership project (3GPP)-Release 15 [7], which focuses on eMBB. Release 16 [8] is focused on the URLLC scenario, whereas Release 17 [9], scheduled for early 2022, expects to address both mMTC and enhanced remote area communication (eRAC) scenarios. Beyond 5G, the sixth generation of mobile network (6G) is a vision for the 2030s, which will require a much wider and holistic approach to identify the system needs [10], [11], [12], [13]. Latva-aho et al. claim that the main idea for the future mobile system is to be a network based on the term "Ubiquitous Wireless Intelligence" [12], which means services following users everywhere and seamlessly, with wireless connectivity and context-aware smart services and applications for both human and non-human users.

The advent of 5G networks brought the possibility of new services that will increase the importance of mobile networks for the modern society. Although these new generation is still being deployed and evolving, it is clear that even more profunding changes will be needed to support the application scenarios foreseen for 2030. Several research projects around the world have shown that innovative solutions for spectrum allocation, network integration and coverage improvement are key to provide solutions for applications that cannot be supported by the restrictive frame and waveforms introduced by the 5G new radio (NR). The next generation of mobile communication needs to seamlessly connect the user by using the proper available network, being it a satellite, optical, wired or wireless network.

Particularly, our research group has contributed to 5G and 6G projects worldwide. The Radiocommunications Reference Center (CRR) has its goal of researching, evaluating, and developing technologies and solutions aimed to Brazilian society demands, considering specific demographics, geographical, and economic features [14]. It is focused on five subject areas including long-range, high-capacity radio links, wireless broadband access, 5G networks and satellite communication links [14]. Under the CRR scope, multiple projects have been also proposed including the development of a 5G transceiver using flexible and manageable waveform applied to long-range communications [15], [16]. The 5G Range project, for designing, developing, implementing and validating mechanisms to enable 5G networks to provide an economically effective solution for Internet access in remote areas [15], [16], [17]. The 5G Internet of things (IoT) project, which has aimed its research on developing IoT technical solutions embedded into a 5G network [18] and, finally, the "6G Brasil" [19], [20], which is the first Brazilian project focused on 6G and has established a formal partnership with 6G Flagship Project from University of Oulu in Finland, which is one of the main 6G research group worldwide coordinated by Latva-aho [21].

The requirements imposed by the future applications also bring challenges for the transport network, the proposed access network is nominated as centralized/cloud radio access network (C-RAN), which needs to support high data rates and low latency. The transport network also needs to support physical and virtual network functions, providing the infrastructure for all foreseen use cases [5]. In C-RAN architectures [22], the core network is connected directly on a central office (CO), containing the baseband unit (BBU) pool, through a backhaul (BH), typically using wavelength division multiplexing (WDM) systems. A BH can also connect multiple COs to each other. COs provide the baseband processed signals to a distributed unit (DU) or directly to remote radio unit (RRU). The connections between BBUs and DUs are named midhaul (MH) and between BBUs and RRUs are named fronthaul (FH). FHs are also used to connect DUs to RRUs and MHs are also used to provide high data traffic to femtocells [23]. Some wireless FH could be assisted by a photonic MH, resulting in a hybrid Xhaul [22], [23], [24]. The proposed architecture has to jointly use wireless [25] and photonic [26], [27], [28] techniques for increasing the spectral efficiency and, as a result, the data traffic in both optical MH and wireless FH. Furthermore, supercells operating with reasonable throughputs (up to 600 Mbit/s) can manage a massive number of micro and femtocells in its coverage area, creating extremely high throughput hotspots reaching up to 20 Gbit/s per user [29], [30], [31], leading to a heterogeneous networks (HetNet).

Wireless and optical convergent technologies might enable mobile network systems to meet the wireless systems needs, such as high throughput, latency, coverage and geographical positioning. For example, eMBB can benefit from the available wide bandwidth from optical communication followed by millimeter waves (mmWaves) and tera-hertz (THz) communications [24] in order to ensure very high throughput wireless access. Latency might be reduced in HetNet systems, by employing analog radio-over-fiber (A-RoF) systems for reducing processing time at remote radio head (RRH), jointly with edge computing [32], bringing core functions closer to the users to achieve dynamic orchestration, storage, and computing resources [32], [33]. Additionally, coverage can be enhanced by using new waveforms to increase power efficiency and lower frequency bands in the wireless domain, whereas fiber-based FH is potential to take RRHs even further [15], [16], [17]. Finally, accurate positioning becomes feasible by properly using visible light communication (VLC) communications as access technology [34], [35].

In this paper, we are focusing on identifying state-of-the-art research related to radiofrequency (RF) and optical communication systems, to be applied in 6G networks. The manuscript is structured in five sections, in which Section II presents the use cases, requirements and enablers for 6G networks. Section III describes the main wireless technologies trends

and features, including channel losses and capacity, THz communications, antenna design and high altitude platform as IMT base stations (HIBS). The optical and wireless convergent systems towards 6G are presented in Section IV, which includes fiber/wireless systems, free space optical (FSO), VLC, integrated optics, power-over-fiber (PoF) and also the use of machine-learning (ML) in optical fronthauls. Finally, Section V outlines the conclusions and future researches.

II. USE CASES, REQUIREMENTS AND ENABLERS FOR 6G NETWORKS

During the conception of the 5G networks, the IMT 2020 defined several audacious and futuristic use cases scenarios that posed very challenging requirements for the physical layer (PHY). Contrasting requirements, i.e. high throughput and low latency, were necessary to support applications such as remote surgery, autonomous driving, and many others. A very innovative PHY was necessary to provide the flexibility demanded by those applications. However, the standardization procedure that resulted in the 5G NR can be considered conservative and the frame structure and waveforms might be seen as an evolution based on the 4G PHY. As a result, several applications scenarios foreseen by IMT-2020 are not feasible with the 5G networks.

Besides the technical limitations from the 5G networks to cover all IMT-2020 visions, new applications have being proposed for future mobile networks [10], [11]. For example, during the COVID-19 pandemic, it was clear the bi-dimensional video and stereo sound were not enough to provide emotionally comforting communications. Multisensory holographic communication enhanced by haptic data is considered to be the next step for advanced remote communication [11], requiring high data rate and fast response from the network to achieve acceptable quality of experience (QoE). The International Telecommunication Union - Telecommunication Standardization Sector (ITU-T) vision for future remote communications agrees that holographic and multi-sense media will have an important role in future remote interactions [10]. ITU-T highlights four emerging scenarios, named as Holographic-Type Communications (HTC), multi-sense networks (MSN), time engineered applications (TEA) and critical infrastructure (CrI) [10], [11].

Clearly, personal communication is not the only class of applications that will benefit from the expected high data rate and low latency supported by 6G networks. The low latency achieved by the future infrastructure can be exploited to control remote devices, while instantaneous feedback allows for precision operation. These are the key enablers for the remote surgery, remote driving and many other applications.

Besides the enhanced communication capabilities, the 6G networks will need new features to support all upcoming services and applications. Imaging, sensing and mapping will be as important as communications for the next generation of mobile networks [36]. The use of frequencies in the sub-THz and THz bands have being seeing as a solution for increasing the data rate while also providing sensing, imaging and mapping capabilities for the network. The tiny wavelength at these high-frequency bands allows the signal to interact with the materials at the molecular level, opening the opportunity to exploit the RF front-end as a spectroscopic imaging system. On the other hand, the use of such high frequencies leads to several challenges where channel modeling and channel attenuation deserve special attention.

Since the 6G networks must support a multitude of scenarios, applications and services, it is clear that the future network will need a multi-radio access network (RAN) approach to deal with all demands. Fig. 1 depicts the main foreseen applications, enablers and requirements, organized according with the necessary cell size.

In this vision of the 6G networks, the small cells will provide connectivity and functionalities to support the applications that require very high data rates (up to 1 Tbit/s), very small latencies (below 0.1 ms) and very precise positioning and map resolutions (below 1 cm). Here, THz communications, VLC and ultra massive multiple-input multiple-output (umMIMO) are the key technologies to address these requirements. The challenges within the macro cells are still impressive. Because coverage now increases to up to 5 km from the base station (BS), THz communications becomes very difficult. Signals at millimeter wave are more likely to succeed in providing data rates of up 100 Gbit/s with latencies below 1 ms and precision up to 10 cm. However, intelligent reflecting surface (IRS) and smart beamforming aided by artificial intelligence (AI)-based antennas will be important to provide reliable communication over a doubly-dispersive channel, while light detection and raging (LiDAR) can help to increase the mapping and positioning capabilities of the 6G networks. In the future mobile systems, the super cell is expected to provide reliable connectivity in remote and rural areas, a task that, so far, has not been satisfactorily performed by any network. In this case, long-range links of up to 50 km are necessary to offer digital services for farms, mines, planes, ships, trains and cars. Even in remote areas, data rates up to 1 Gbit/s and latencies below 10 ms are necessary for remote controlling and video and data acquisition, while precision up to 0.1 m is necessary for autonomous machinery operation in mines and farms. In this case, radio over fiber (RoF) can be used to reduce deployment costs in remote areas and multiple-input multiple-output (MIMO) for diversity can improve the signal robustness to increase the coverage range and feasibility. TV white space (TVWS) can also play an important role in reducing the operational cost, since licences are not required to exploit the vacant ultra high frequency (UHF) channels. Finally, satellite networks can be jointly used with terrestrial networks to complement coverage or provide backhauling for terrestrial BS.

The 6G networks are being designed to fully fulfil the IMT visions but also to support new applications. The requirements, architecture and enabling technologies are still under discussion in several initiatives and research projects around the world, but it is clear that THz and sub-THz communications, wireless-optical integration, VLC and new antennas

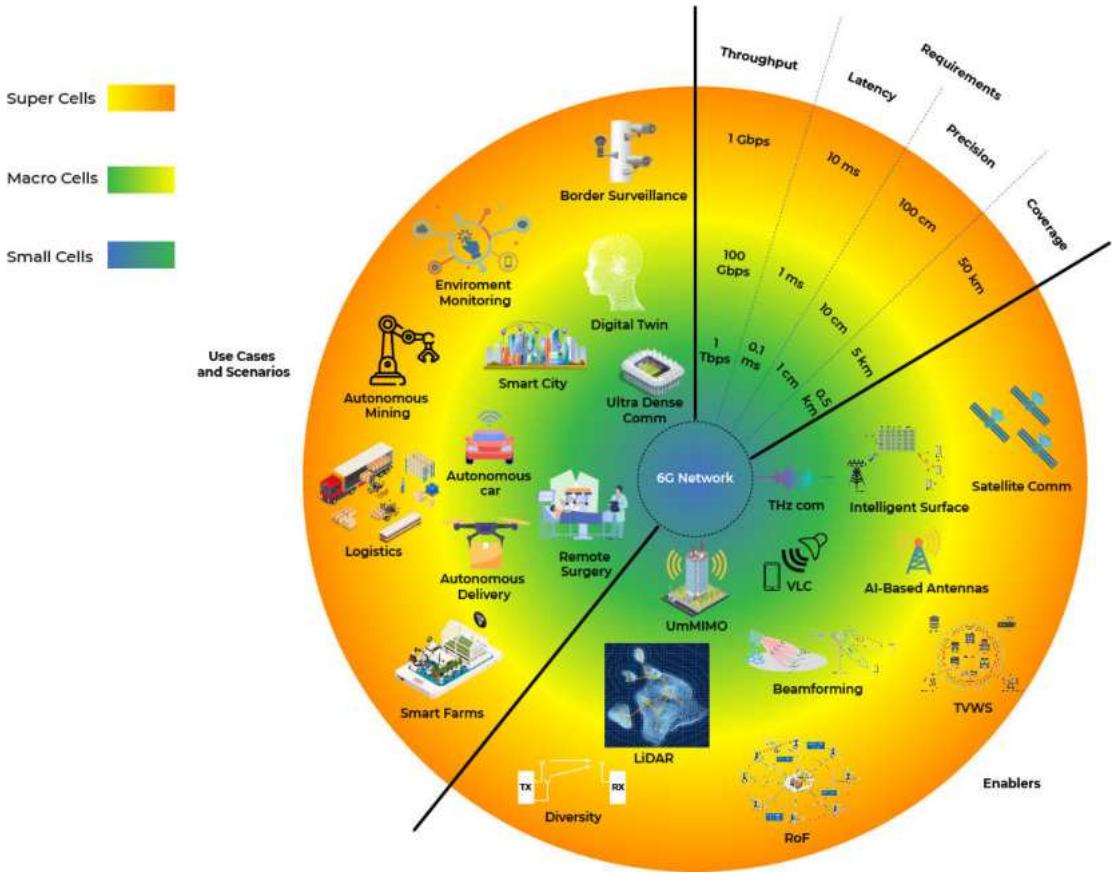

FIGURE 1. Main use cases, enablers and requirements for the 6G networks.

designs are important players in the definition of the next generation of mobile networks.

III. WIRELESS TECHNOLOGY TRENDS

Technologies for wireless communication will be the main enablers for several applications and services. As mentioned in Section II, new frequencies bands and new requirements will demand innovative solutions. This Section describes the main wireless technologies for the future mobile networks.

A. CHANNEL CHALLENGES AND CAPACITY FEATURES

As the data traffic increases throughout the mobile generation systems, exploitation of higher frequencies is necessary as illustrated in Fig. 2. For example, from 1G to 4G the mobile communication system has been allocated at different frequencies between 400 MHz and 2.9 GHz worldwide. Techniques of carrier aggregation has enabled throughput up to 1 Gbit/s in 4G by using multiple channels of 5-, 10-, 15- or even 20-MHz bandwidth simultaneously. By allocating theses multiple channels, it has been possible to increase the system capacity for enabling high-throughput applications [37], [38]. The 5G network was the first generation of mobile communication that uses two different frequency range (FR), i.e, FR 1 from 410 to 7,125 MHz and FR 2 from 24.25 to 52.6 GHz [7], [37]. 5G was the first network to use mmWaves as a solution for the RAN, also employing

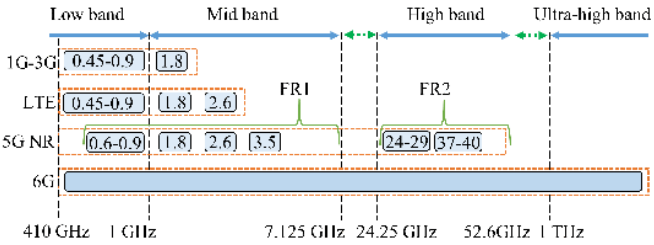

FIGURE 2. Evolution of wireless communication frequency range from 1G to 6G.

bandwidth up to 400 MHz. These new frequency allocation has increased the system complexity, requiring high cost RF components. The high propagation and penetration losses in in the FR 2 range is one of the biggest challenges related with the use of mmWaves in the RAN [38].

Many techniques have been proposed in the literature to overcome the high path loss from mmWaves. Classical methods of MIMO technique can be used to improve the reliability of the links, in which diversity can be achieved by multiple transmitting and receiving antennas, increasing the signal-to-noise ratio (SNR) at the reception and minimizing the outage probability. Spatial multiplexing, on the other hand, consists of using multiple transmitting and receiving antennas for improving the spectrum efficiency by sending multiple parallel data streams. Beamforming is another technique that can use the multiple transmit antennas to create a well-defined,

high-gain and manageable beam. The basic idea is to increase the system link budget by pointing the beam to a specific location, or, in other words, only to a specific user equipment (UE) [37], [39].

The high operating frequency introduced by the mmWaves allows for reducing the antenna sizes. A high number of small antennas elements can be packed into antennas array, resulting in massive MIMO (mMIMO). This large number of antennas can be used to provide precise beamforming using maximum ratio transmission (MRT), in which the data transmitted to a given user is weighted by the complex conjugate of the channel response among the transmit antennas and the user receive antenna. This procedure allows for spacing multiplexing, since the high number of transmit signals will be cancelled out in any other location other than the position of the desired user. Therefore, it is possible to take advantage from the massive number of paths on scattering environments for enabling also multiple access. If jointly used with time-division duplexing (TDD), mMIMO can acquire channel state information (CSI) from the uplink (UL) and use it in the downlink (DL) due to the channel reciprocity. No prior assumptions on the propagation environment and no predetermined beams are needed. Pilot subcarriers are transmitted by the UE, allowing for the BS to estimate the channel responses in the UL, which will be used to precode the data to be sent to the respective user. It is important to guarantee that the total TDD frame duration is smaller than the channel coherence time, which means that this technique might suffer performance loss in high mobility scenario [40], [41], [42].

The use of high frequencies bands in mobile communications brings several challenges for the RF front ends. Solutions based on new algorithms for the base band processing and integrated with new RF designs has shown to be promising. New antennas array design and precise channels estimation algorithms based on AI has proved to be a powerful tool for improving system capacity in mobile communication systems [43], [44].

The 6G system should be even more ambitious. Researchers are already expecting that 6G should be the first mobile network to allocate sub-THz and even THz bands for the RAN, as illustrated in Fig. 2. The idea is to provide Tbit/s per user in the next decade [13], [45]. Due to the importance of THz communications for future mobile networks, this subject will be further detailed following.

B. THz COMMUNICATIONS

In this sub-section, we briefly review the fundamentals of THz communications. In fact, following the use of the mmWaves and sub-mmWaves band (above 20 GHz) as carrier frequencies for 5G, the need for tens of Gbit/s data rates will require the use of THz (from 0.1 to 10 THz) carrier frequencies in 6G. However, for this to become a reality, there are several technological hurdles to be addressed. Considering the state-of-the-art in THz technologies, some of these hurdles can be understood with the help of Shannon theorem, which relates the channel capacity (C), with the available bandwidth (B) and the SNR, in the form:

$$C = B \log_2(1 + \text{SNR}). \tag{1}$$

Unlike current mobile systems operating below 6 GHz, in the THz range the main issue is not the available contiguous bandwidth, but rather the SNR, directly related to the output power at the THz transmitter. An interesting consequence is a shift in design paradigm, since the use of higher-order modulation formats, which require a more stringent SNR, is not necessarily advantageous in terms of system performance [46].

Apart from that remark, THz behave as any other wireless system: the link budget is mostly dictated by the very high free-space path loss, which reaches 140 dB for a 1-km link at 300 GHz [47]. In addition, atmospheric absorption and rain attenuation (in outdoor applications) also come into play. To circumvent this signal loss, an increase on the link budget can arise from a combination of high gain antenna systems, phased-array-based beamforming and ultra-mMIMO techniques. Another way to improve SNR consists on the increase of the transmitted power and/or the receiver sensitivity, focus of the following discussion.

Historically, the THz band has not been widely considered for communications applications, mostly due to the lack of efficient THz transceivers. In fact, this portion of the electromagnetic spectrum (0.1-10 THz) has suffered from the so-called THz technological gap. Specifically regarding the analog front-end, the two most usual pathways present hurdles to be overcome. On one hand, from the electronics side of the spectrum, the output power of frequency-multiplier circuits was too low at such high frequencies. On the other hand, in the corresponding wavelength range from the photonics side, apart from the quantum cascade laser [48], no efficient laser was available to generate far-infrared and THz low-energy photons required in those communications systems.

This is the reason why in most early demonstrations, the THz signal carrier is generated in high-speed photoconductors and photodiodes, by means of down-conversion in a photomixing processes [49]. In other words, a down-converted THz-wave carrier can be generated by heterodyning two distinct wavelengths, arising from laser sources. The output carrier frequency is widely tunable, being defined by the difference between wavelengths λ_1 and λ_2. However, since the two lasers are not synchronized, both frequency and phase should be stabilized and the spectral distance between the two laser lines has to be kept fixed, to assure low jitter and low phase-noise [50]. Some of the most popular alternative techniques to achieve this locked spectral behavior include the use of dual-mode lasers [51] or optical frequency comb generators [52], [53].

Before photomixing, the photonic modulation can be based on two configurations: double sub-carrier modulation, in which both sub-carriers are modulated, or single sub-carrier modulation. The double modulation scheme usually

provides higher SNR. However, the output power after photomixing is still low and most configurations require a electronic power amplifier operating in the THz range, before the signal carrier can reach the transmitter antenna. Finally, to establish a THz wireless link, the receiver can be based on direct detection (typically Schottky or uni-traveling-carrier photodiode (UTC-PD)) [54] or heterodyne detection, using sub-harmonic diode mixers to obtain an IF frequency in the mmWaves or microwave range [55].

There are other emerging photonic technologies capable of generating THz waves. Among those, we can mention quantum cascade laser (QCL) which operates emitting photons whose wavelength is dictated by electronic transitions between conduction band energy-levels in a sequence of quantum wells [48]. The operating principle results in photon emission the high-frequency range, above 2 THz, and current devices typically requires cryogenic operation in order to provide a useful output power, around a few hundred mW [56]. These drawbacks make very unlike that QCL-based THz transmitters will be used in communications systems, at least in the short and medium terms.

Another alternative would be to rely on the oscillation surface plasmon-polariton (SPP) waves, particularly in graphene or other two-dimensional (2D) materials such as molybdenum disulfide (MoS2) [57]. This plasmonics-based approach is very promising, particularly regarding the possibility of small footprint and high frequency operation. Unfortunately, this technology is still on its infancy, particularly concerning output power and it is not likely to be mature enough for 6G.

Indeed, output power is also a limitation for photonic systems based on photomixing. Even using state of the art UTC-PDs for down-conversion, these system can typically produce less than 10 mW at a few hundreds of GHz [58]. It is then inevitable that even these photonics-based transceivers will have to incorporate THz-electronics power amplifiers. As a consequence, if that is the case, it is probably convenient to approach the THz transceiver configuration from the other end of the THz gap, namely, to seek an all-electronic transceiver. As an additional advantage, such all-electronic implementation would be much more familiar to the wireless industry, thereby likely to facilitate future 6G deployments.

Although oscillators using two-terminal devices, such as resonant tunneling diode (RTD), have already pushed the 1-THz boundary [59], most work on THz carrier generation by electronic means is based on the concatenation of a chain of frequency multipliers, in such way to up-convert a mmWaves carrier to the THz band. Early demonstrations of such schemes have used radio-astronomy hardware on GaAs technology [60]. Today, although Si-based technologies are gaining ground, particularly on the basis of SiGe Heterojunction Bipolar Transistors [61], best results are achieved using InP high electron mobility transistors (HEMT), as transmission powers of hundreds of mW at hundreds of GHz have been already demonstrated [62], which are well above the current results for photonic down-conversion. As the technology evolves and the maximum oscillation frequency of high-speed transistors has already surpassed 1 THz [63], the short-term trends should favor all-electronic THz transceiver configurations, due to the increasing availability of several useful integrated circuits. For instance, an InP-based, higher power density amplifier has been already demonstrated, with a bandwidth as high as 235 GHz [64].

TABLE 1. State-of-the-art on antenna for 5G towards 6G.

Ref.	Antenna type	Number of elements	Bandwidth [GHz]	Application
[65]	Slot with S-PIN	1	27.75 to 27.35	Switched-beam
[66]	Dipoles integrated cavity	1	27 to 29.5	Ommidirectional coverage for broadcast
[67]	PCB-stacked Luneburg lens	1	26 to 37	Switched-beam
[68]	Patch	18	3.6 to 3.8	MIMO
[69]	Dipole with cavity	16	4.9 to 6	Analog Beamforming
[70]	Dipole with reflector	128	3.8 to 4.3	TDD-based digital mMIMO
[71]	Tapered slot	16	24.5 to 27.5	Digital Beamsteering
[72]	Patch	64	5.17 to 6.1	Multiple-beam
[73]	Patch based on suspended plate	18	4 to 4.7	TDD-based digital mMIMO
[74]	Patch	256	26.5 to 29.5	Beamforming
[75]	SWAA	4	27.6 to 30.8 36.8 to 38.4	Dual-band sectorial coverage at mmWaves
[22]	FSS-based Focal-point/ Cassegrain parabolic	2	6.9 to 8 25.85 to 30.15	Point-to-point link
[76]	SWAA	1	23.45 to 24.54	Omnidirectional indoor femtocell
[77]	SICL-based Slot	64	24.5 to 26.5	TDD-based digital mMIMO

C. ANTENNA TECHNOLOGIES FOR SUB-6 GHz AND mmWaves

This sub-Section presents the state-of-the-art on antennas and antenna arrays for sub-6 GHz and mmWaves, focusing on disruptive technologies and application-oriented antenna proposals for 5G that could also be applied to 6G systems. Manuscripts published from 2016 to 2021 have been preferred for this literature review, as complied in Table 1.

A 28 GHz switched-beam slot antenna based on surface PIN (S-PIN) diodes has been proposed for 5G systems in 2017 by Yashchyshyn et al. [65]. This research goal was to achieve multiple beams and enable switching among them. The designed reconfigurable structure was composed of 15 reconfigurable slots with embedded S-PIN diodes. In this

way, the slots could be reconfigured by appropriate biasing them, with the purpose of enabling or not radiation through them. The authors have been able to switch among five beams, pointed towards 0°, ±30° and ±45°. In the worst-case scenario, the proposed antenna has provided 600 MHz bandwidth centered at 28.05 GHz, reaching up to 7 dBi gain.

In [66], Mao et al. have proposed a planar sub-mmWaves array antenna with enhanced gain and reduced sidelobes for 5G broadcast applications at 26 GHz. The proposed prototype was based on two dipoles and a substrate integrated cavity as a power splitter. The dipoles were placed side-by-side to create an uniform pattern in the azimuth plane. The authors have been able to combine the dipole and cavity resonance to provide a wide bandwidth from 27 to 29.5 GHz. Finally, they have structured an eight-element array for enhancing its gain, reaching up to 12 dBi omnidirectional coverage for broadcast applications. A wideband printed-circuit board (PCB)-stacked Luneburg lens antenna with a flared open edge for multi-beam scanning application at 5G mmWaves band was proposed in 2021 by Wang et al. in [67]. They were aimed to fulfill the increased data traffic in mobile communications, by proposing a high-gain (15.4 dBi) and wideband antenna (from 26 to 37 GHz) for switched-beam applications. It consists of 11 resonant elements, shifted among each other by 15°, around a unique circular Luneburg lens. We can notice the possibility of applying distinct technologies for encompassing all 5G demands. For instance, multiple probes [67] or S-PIN-based SWAAs [65] could be employed for switched-beam applications, whereas waveguide-based slot antennas [65], Luneburg lenses [67] and cavities could be used for increasing the antenna gain [65].

There are also some important works from literature on MIMO and mMIMO systems, which define the antenna array requirements. In 2016, Gao et al. proposed a dual-polarized patch antenna array with low mutual coupling [68], which is a very important MIMO requirement [78]. The proposed system was composed of 144 ports operating at 3.7 GHz and 18 low-profile subarrays for allowing 360° coverage. Each subarray was based on four patch antenna elements with two ports, one for each polarization, which allowed to reach mutual coupling lower than −35 dB.

A dipole-based and dual-polarized 16-elements antenna array was proposed by Komandla et al. in 2017 [69]. They have proposed the usage of cross-polarized dipoles, one on each side of a substrate, with a back cavity acting as a reflector. The coupling among the array elements was kept lower than −20 dB through the entire operating bandwidth from 4.9 to 6 GHz. Finally, they have numerically demonstrated beam-steering feature over 50°, four beams for a multi-user environment and gain higher than 20 dBi for all evaluated scenarios.

The research conducted by Yang et al. [70] in 2017 was regarding the design and implementation of a TDD-based 128-element mMIMO system, including an analytical model and a link-level simulation. The prototype was divided into 8 sub-arrays of 16 printed-dipoles mounted above metallic reflectors and arranged as a planar antenna array spaced by 0.8λ (at 4.1 GHz). From the antenna point-of-view, 0.8λ spacing is acceptable for creating a unique directive beam, without prohibitive levels of grating lobes. However, such a spacing could degrade mMIMO performance due to lack of channel diversity. Nonetheless, since the array has been divided into 8 sub-arrays, the spacing among the array elements was approximately 3.2λ, which ensured channel diversity and, consequently, high mMIMO performance, as a result of a maximum −25 dB mutual coupling. As a final result, authors reached up to 69.12 bit/s/Hz spectral efficiency using quadrature phase-shift keying (QPSK) modulation, which provides only 1 bit/s/Hz in a conventional single antenna system.

Hu et al. have proposed a digital multi-beam array with 16 elements for the 26 GHz band in 2018 [71]. The manuscript has focused on the beamsteering feature instead of mMIMO application. The array element was a dual exponentially tapered slot antenna (DETSA), which is a variation of a conventional Vivaldi antenna. Each element was excited by transverse electric (TE) propagation mode using substrate integrated waveguide (SIW) in order to ensure mutual coupling lower than −20 dB for an element spacing of 6 mm. Moreover, a Jerusalem Cross planar lens enabled to increases the array gain from 20 to 25 dBi and beamsteering from −50° to 50°, by properly managing the element phase.

In 2020, Li et al. [72] proposed the use of a metasurface lens antenna in a 64-element dual-polarization patch antenna array, envisaging to cover both multibeam and mMIMO applications. The manuscript reported bandwidth form 5.17 to 6.1 GHz, a scanning angle of ±25°, gain up to 22.4 dBi with 3.3 dB variation and mutual coupling lower than −20 dB. The switched-beam feature comes from selecting a port or a combination of ports of the array feeding network. In this way, either multiple beams at the same frequency or frequency division multiplexing for each beam, aiming to increase the system throughput, might be implemented.

Two important researches on the array topology are presented in [73] and [74]. In [73], Temiz et al. investigated the impact of the antenna array geometry in the mutual coupling and channel correlation, by exploiting a directional wideband single antenna element for the antenna array and UE. Particularly, two planar antenna arrays were considered in the channel correlation analysis: a uniform antenna array and a shifted antenna array. The uniform one was composed of equally distributed elements, aligned in both horizontal and vertical directions, whereas the shifted array consisted of shifting lines of radiating elements in the matrix, increasing the spacing between adjacent elements without compromising the array area. The obtained results proved the shifted array outperforms the uniform conventional array in terms of network capacity, due to a lower level of mutual coupling and lower channel correlation (lower than −15 dB for the linear array and −20 dB for the shifted array), especially in lineline-of-sight (LOS) propagation. Additionally, an element spacing periodicity investigation on the array topology

was made by Aslan et al. [74] in 2021. They considered four different array topologies for evaluating the interference among multiple users and demonstrating aperiodic element distribution has the potential of increasing the system quality of service (QoS) in terms of inter-user interference reduction. Using element spacing of at least λ increases the inter-user interference due to side-lobe level (SLL) increment in a LOS environment. The advantages of using more spaced elements in this scenario are thermal dissipation and creating space for electronics in active antenna deployments at a limited impact on quality of service (QoS).

Most papers on beamforming and MIMO applications from literature are only regarding the array antenna element (mainly patch, dipole or slot antennas) or feeding network, as summarized by [68], [69], [70], [71], [72], [73], and [74]. Regardless the application, reducing mutual coupling is an important performance metric that was required to be lower than -20 dB in most papers, using element spacing from 0.5 to 1λ for beamforming and multiple beams applications. On the other side, MIMO systems make use of channel diversity, the array elements need to be further spaced.

Operating frequency and application are also important pieces of information from Table 1. Fig. 3 compiles the most common antenna types related to their application and frequency ranges. It is noticed that classical dipoles, patch and Vivaldi antennas are mostly used in the sub-6 GHz band, whereas in mmWaves more types of antennas and antenna arrays, waveguide-based antennas, have been proposed for encompassing different access scenarios. Undoubtedly higher frequencies enable high-order antenna arrays, due to smaller wavelengths. However, most papers on antenna arrays from literature are focused on the sub-6 GHz band, probably due to the complexity and high-cost of mmWaves components and pieces of equipment. Furthermore, it has been noticed there are more published solutions for beamforming, beam steering and multiple-beam than TDD-based digital mMIMO applications. Once again, this is related to implementation costs, since beamforming techniques can be applied with a smaller number of RF chains. However, it is important to emphasize that analog beamforming and steering techniques consider communication with few users (some manuscripts are applied to only one user). On the other hand, TDD-based digital beamforming guarantees multiple-access for multiple users, as a result of the channel diversity in a non line-of-sight (NLOS) scenario, which is more realistic in a dense urban environment.

Our research group from the Laboratory Wireless and Optical Convergent Access (WOCA) has been intensely contributing to the development of mmWaves antennas for 5G in the past few years, as complied in Table 1 [22], [75], [76], [77], [79], [80], [81], [82] and illustrated by prototypes shown in Figure 4. In 2017, da Costa et al. have reported the first optically controlled reconfigurable slotted-waveguide antenna array (SWAA) (Fig. 4(a)) for mmWaves from literature [75]. The physics behind its design was managing the

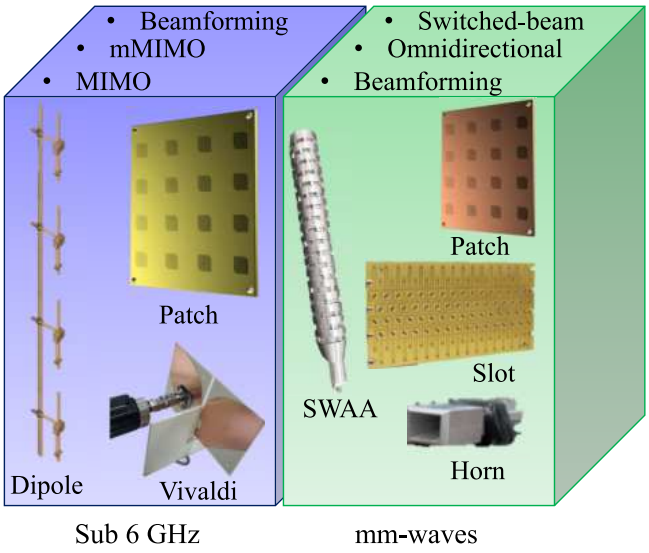

FIGURE 3. Most common antenna types related to their usual applications and frequency range.

slots electrical length by partially covering them with photoconductive switches in order to enable frequency tunability and radiation pattern reconfiguration over the 28 and 38 GHz bands.

Two novel mmWaves antenna designs were introduced in 2018 [79]. First, a 28-GHz omnidirectional SWAA based on metallic rings for disturbing a traveling wave inside a dielectric waveguide was manufactured, as displayed in Fig. 4(b). Furthermore, dual-band and dual coverage SWAA (Fig. 4(c)) for simultaneous operation in the 28 and 38 GHz band was proposed, using two groups of slots with different electrical lengths on the opposite faces of a retangular waveguide. Such dual-band SWAA has been applied to a switched-beam MIMO system by Vilas Boas et al. [80] in 2019, by arranging four SWAA elements as shown in Fig. 4(d). Experimental results demonstrated mutual coupling lower than -35 dB through the entire evaluated bandwidth (24 to 40 GHz).

Vilas Boas et al. have further investigated SWAA antennas at mmWaves in 2020 [81]. In this new research, a low-profile and high-gain SWAA (Fig. 4(e)) was developed for point-to-point links and self-backhaul applications. Six pairs of metal grooves have been integrated to the SWAA structure, which implied in aperture efficiency of 20% and 9 dB gain enhancement, reaching 27.7 dBi without using metallic parabolic reflectors. Finally, the grooved-assisted prototype provided a bandwidth of 900 MHz, which is compatible with the 5G-NR standard from 3GPP.

Another approach for point-to-point links was implemented in 2019 [22], by making use of a dual-band wireless fronthaul using a frequency selective surface (FSS)-based focal-point/Cassegrain antenna (Fig. 4(f)) [25], assisted by an optical midhaul. That innovative 5G-Xhaul fiber-wireless architecture takes advantage of digital pre-distortion in order to guarantee up to 18 Gbit/s throughput in accordance to the 3GPP requirements. Particularly, the antenna consisted of two

feeders individually operating at 7.5 and 28 GHz, a main reflector and a FSS based sub-reflector. The latter one acts as a conductor at 28 GHz and is electromagnetic transparent at 7.5 GHz, enabling the dual-band feature using a unique main reflector.

We have also developed an omnidirectional high-gain SWAA (Fig. 4(g)) operating at 24 GHz for femtocell applications [76]. It was based on a novel approach for designing wideband SWAA, which relies on using trapezoidal-shaped slots with two different electrical lengths, as well as a twisted distribution of slot groups along the array longitudinal axis. The trapezoidal slots are formed by gradually increasing the slot length between the waveguide interior and exterior surfaces. In this way, a smoother impedance transition between waveguide and air is obtained for increasing the array operating bandwidth. In addition, the twisting technique allows to improve the omnidirectional pattern, by reducing the gain ripple in the azimuth plane. Experimental results have demonstrated 1.09 GHz bandwidth centered at 24 GHz (4.54% fractional bandwidth), gain up to 14.71 dBi over the operating bandwidth and only 2.7 dB gain variation in the azimuth plane. Such novel SWAA is promising for mmWaves applications, including 5G eMBB communications in indoor scenarios, as demonstrated in in 2021, as a result of its implementation in a 91-m^2 indoor femtocell [82].

Recently, Filgueiras and Sodre Jr. [77] have conceived and fabricated a 64-element, slot-based, dual-polarized and substrate integrated coaxial line (SICL)-fed antenna array applied to TDD-based digital mMIMO applications. The prototype from Fig. 4(h) has 64 independent feeding points and each radiating element provides a 2-GHz bandwidth, from 25 to 27 GHz, beamwidth of approximately 85° in both main orthogonal planes and 7.5-dBi gain.

D. ANTENNAS FOR THz

The specialized literature also presents antennas for THz, as summarized in Table 2 [83], [84], [85], [86], [87], [88], [89], [90], [91], [92], [93], [94]. Many of them are conventional microwave and mmWaves antenna design, re-tuned for higher frequencies. For instance, horn antennas, planar antennas, dielectric lens-based antennas, reflectarrays and resonant cavities designed for THz were exploited not only in the Review Paper [91], which presented many manufacturing techniques and antenna types, but also in [94]. Particularly, 3D printing typically achieve up to 0.01 mm precision. If higher precision is required, micro-milling still represents a more appropriate choice, such as Computer numerical control (CNC)-based manufacturing, electric erosion and Low-temperature co-fired ceramic (LTCC). A conventional cavity-based radiating structure at 135-GHz fabricated by 3D printing and a SWAA antenna operating at 141 GHz were reported in [85] and [86], respectively. In the last one, authors have used gap-waveguide for overcoming the electric contact issue associated with mechanical mounting at high-frequencies, enabling to manufacture it using simple micro-milling techniques.

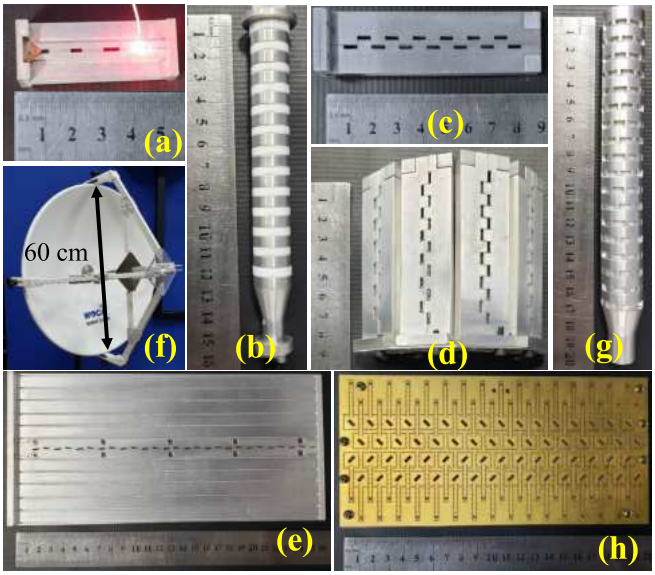

FIGURE 4. Laboratory WOCA antenna array prototypes for 5G and towards 6G. (a) Optically-controlled SWAA from [75]; (b) Omnidirectional SWAA from [79]; (c) Dual-band SWAA from [79]; (d) 4-element SWAA from [80]; (e) High-gain SWAA from [81]; (f) Dual-band Focal-point/Cassegrain from [22]; (g) Omnidirectional SWAA from [76], [82]; (h) mMIMO slot antenna array from [77].

TABLE 2. State-of-the-art on THz antennas.

Ref.	Technology	Bandwidth [THz]	Fabrication method
[83]	SIW	0.124 to 0.158	LTCC
[84]	SIW	0.54 to 0.56	PCB
[85]	Resonant Cavity	0.125 to 0.144	Metallic and dielectric 3D printing with post-metallization
[86]	Gap-waveguide (gapWG)-based SWAA	0.134 to 0.148	Micro milling
[87]	Cassegrain	0.22 to 0.31	CNC-based micro milling
[88]	Waveguide	0.22 to 0.30	Micro milling
[90]	Printed slots	0.39 to 0.41	CNC and PCB
[95]	Dipoles and plantennas	302 to 541	Numerical design only
[96]	Photoconductive antenna	9 to 47	Numerical design only

In [83], authors have proposed using a SIW feeding line for exciting wideband dipole-based radiators from 124 to 158 GHz. Similarly in [84], authors have achieved a 20 GHz bandwidth at 550 GHz, by properly manufacturing a PCB-based antenna with SIW. Additionally, A. Kosogor and Y. Tikhov manufactured a Cassegrain parabolic antenna with a polished gold-plated for reducing losses

associated with its paraboloid roughness and conductivity [87]. It provided bandwidth from 220 to 310 GHz and gain of 48 dBi at 265 GHz. Beam-steering capability from −75° to 30° at 260 GHz in conjunction with 28.5 dBi gain have been ensured by a waveguide-based antenna filled with dielectric material [88]. Its authors claim the achieved high performance and their silica micro-milling technique, aimed for mass production, make their antenna a low-cost and potential solution for many THz applications, including radars and 6G systems. The fabrication of a travelling-wave antenna with reduced SLL operating from 390 to 410 GHz was described in [90], using CNC and PCB techniques. Finally, plasmonics-based antennas [96], photoconductive antennas [94] and new materials, including graphene [97], have also been investigated for THz generation and detection. A photoconductive antenna is basically composed of a gap-based antenna, an electrode and a photoconductive substrate. On the other hand, the main advantage of using graphene is its resistivity, which is lower than that of copper and gold [97], [98].

E. HIBS - HIGH ALTITUDE PLATFORM AS IMT BASE STATIONS

Studies involving high-altitude plataform systems (HAPS) for communications started in the 1990s. The first spectrum for their use in the Fixed Services from Radio Regulations was made available in 1997. Industry initiatives have started from 1990 to 2000, but the technological aspects blocked the airborne platform evolution. Particularly, HIBS has the potential of providing connection to the use many cases, such as health emergencies, rural areas, natural disasters and drone operations, as properly elucidated in our previous publication [99]. As a consequence, the HIBS-based mobile network can complement terrestrial IMT services, by covering remote and unconnected areas. The COVID-19 pandemic has demonstrated the major Internet inequalities among countries, proving more then never the need for increasing connectivity and guarantee digital inclusion in poor regions [99], [100].

Non-terrestrial solutions are focused on global attendance. In this context, low Earth orbit (LEO) satellites and HIBS represent potential options for overcoming coverage flaws. Even though LEO satellites have been gaining attention for mobile communication services, due to the aerospace market growth, their user equipment has to be specific. On the other hand, HIBS shares the spectrum already in use by the terrestrial IMT networks worldwide, allowing UE connection using conventional handsets. The HIBS operational altitude in the stratosphere, around 20 km, ensures lower propagation delay compared with the LEO satellites, enabling low-latency applications, such as industrial remote security sensing and control [99], [101].

HIBS is versatile in terms of deployment and supporting the existing network infrastructure. An airborne platform is placed at a quasi-stationary position above the deployment area, typically using a cruise speed of 110km/h. Furthermore, they can be equipped with 4G, 5G, or even future 6G standard technologies, maintaining a reliable connection over a cell coverage from 180 to 200 km. In September of 2020, HAPSMobile has successfully tested a LEO-based HIBS, by means of making a video call between members in the United States of America and Japan. The flight at the stratosphere spent 5 hours and 38 minutes at an altitude of 19.81 km, in which the wind speed reached around 30 m/s and temperature was as low as −73° C [102]. Fig. 5 presents the ''Sunglider'' camera spot perspective of the long-term evolution (LTE) test flight with the Earth horizon view around 500 km of distance from HIBS Nadir. The LTE payload test has been conducted at Spaceport America, New Mexico (USA), where it was obtained the following experimental licenses from the Federal Communications Commission (FCC): service link at the Band 28 (700 MHz); feeder links at 5.8 GHz and from 70 to 80 GHz; payload control and data collection channel from 902 to 928 MHz and 1200 to 1700 MHz, respectively [103].

FIGURE 5. "Sunglider" HIBS Platform flying at the stratosphere during an LTE video call communication test between United States and Japan. [Courtesy of HAPSMobile/Loon].

The three-dimensional (3D) coverage expectation from the future 6G technologies is one of the remarkable and unique capabilities for HIBS. It is also important to highlight that HIBS is a sustainable solution, due to the carbon neutrality, the low impact on the environment and no use of any kind of fossil fuel. Such unmanned platform uses solar panels to generate energy during the day and uses batteries power during the night flight. The IMT-2030 technical requirements, aiming for future technologies as 6G, have been continuing discussed in International Telecommunication Union (ITU) Working Party 5D (WP 5D) in the document named as "*IMT-2030 to assess the trends of IMT for 2030 and beyond*" [99], [101], [102].

In 2014, Google and Facebook have launched HAPS initiatives trying to provide global connectivity. In 2019, HAPSMobile and Loon started an alliance and in February of 2020, a group of aerospace and telecommunications companies joined efforts to create HAPS Alliance, to promote HIBS connectivity around the globe. Since then, HAPS Alliance has been promoting the technology and some trials and flight tests have been conducted. Fig. 6 presents the Sunglider airborne platform in HAPSMobile facility [102], in which solar panels cover the top of the HIBS fuselage.

FIGURE 6. "Sunglider" HIBS Platform at HAPSMobile facility [Courtesy of HAPSMobile].

According to the ITU Radio Regulations from the Article No. 5.388A, HIBS may use the following frequency bands; from 1,885 to 1,980 MHz, from 2,010 to 2,025 MHz and 2,110 to 2,170 MHz in ITU Regions 1 and 3; the 1,885 to 1,980 MHz and 2,110 to 2,160 MHz bands in Region 2. The ITU Agenda Item 1.4, for the World Radiocommunications Conference 2023, addresses the discussions on the HIBS technical and operational features, including sharing and compatibility studies with other services in the frequency bands lower than 2.7 GHz, identified for IMT.

The IMT terrestrial evolves to new requirements and uses cases, due to the final user demand applications. HIBS is a part of the IMT system, as the non-terrestrial solution is categorized as unmanned aerial vehicles (UAV) equipped with Base Stations, which was standardized by the 3GPP Release 17 [99], [101], [102], [104], [105]. In this context, looking forward to the future 6G technologies, HIBS could be considered potential to provide the Global spectrum usability for attending remote areas and complementing future 6G terrestrial networks in order to reduce the digital divide.

Our research group has recently published a paper entitled "High- Altitude Platform Stations as IMT Base Stations: Connectivity from the Stratosphere" [99], in which we have explained into details the HIBS current scenario, use cases, regulatory aspects and sharing studies. Furthermore, we have presented a coexistence analysis between HIBS and Fixed Services at adjacent channels to support decisions to be made at the World Radiocommunication Conference 2023 (WRC-23). In [105], authors have presented the HIBS concept, spectrum aspects and initiatives in 3GPP. Furthermore, the challenges associated with super macro base station constellations using HAPS are discussed in [101]. Complementary, Dong Zhou *et.al.* presented an overview of the HIBS regulatory aspects and challenges from the International Telecommunication Union - Radiocommunication Sector (ITU-R) community and Study Groups [104]. Finally, Global System for Mobile Communications Association (GSMA) has released a report on HIBS in 2022 on its use cases, benefits, and opportunities, implementation scenarios, market analysis, regulation and spectrum standard, comprising aviation regulation and business model scenarios [106].

IV. OPTICAL AND WIRELESS TECHNOLOGY TRENDS

The RAN architecture has evolved over the years to support mobile communications networks demands, which include the recent 5G networks standardization efforts as well as early discussions regarding 6G and its requirements, as mentioned in Section II. The RAN evolution points out to the convergence between fiber and radio system interfaces, as depicted in Fig. 7, a configuration known as fiber-wireless (FiWi) systems [23]. Important trends also include heterogeneous networks (HetNets) [107] and C-RAN [108] architectures. In addition, optical wireless communications (OWC) systems, which are based on FSO [109], have emerged as a promising candidates for the next RAN generation, providing a bandwidth of the order of GHz, to work in combination with the other technologies mentioned above. Among the variations of OWC, VLC, and infrared communications, in particular, beam-steered infrared light communication (BS-ILC) stand out [109].

The C-RAN deployment is very important for optical/wireless convergence. In distributed radio access networks (D-RANs), BBU and RRU are physically located at BS, increasing the management effort and operational costs in a scenario with a large number of small cells. On the other hand, the C-RAN architecture allows the use of simplified RRU at the antenna location, by means of moving BBUs to a CO and, consequently, centralizing their baseband processing, which gives rise to the concept of BBU pool [108].

A centralized network brings notable benefits, including infrastructure reuse, operational and management simplification, multiple technologies coexistence and lower energy consumption, as well as lower capital expense (CAPEX) and operating expense (OPEX) [107], [108]. In addition, the C-RAN architectures also take benefits of innovative technologies such as software-defined networking (SDN) [110] and network function virtualization (NFV) [111]. SDN enables the physical/link layer functional splitting, such as the separation of control and data planes at higher layers, supporting advanced management techniques. The application plane is based on network monitoring and security, which is directly connected to the control plane. The latter consists of SDN controllers, e.g., Open Network Operating System [112] and OpenDayLight [113], responsible for managing network devices positioned in the data plane. The OpenFlow protocol has been widely adopted to achieve the interconnection between control and data planes [114].

In addition, the NFV approach provides flexibility and scalability, by sharing network resources in a dynamic way [115]. These functionalities allow the deployment of network functions as specialized devices or virtualized as virtual network functions (VNFs) [116]. The optimal split can be dynamically achieved by software-based orchestration

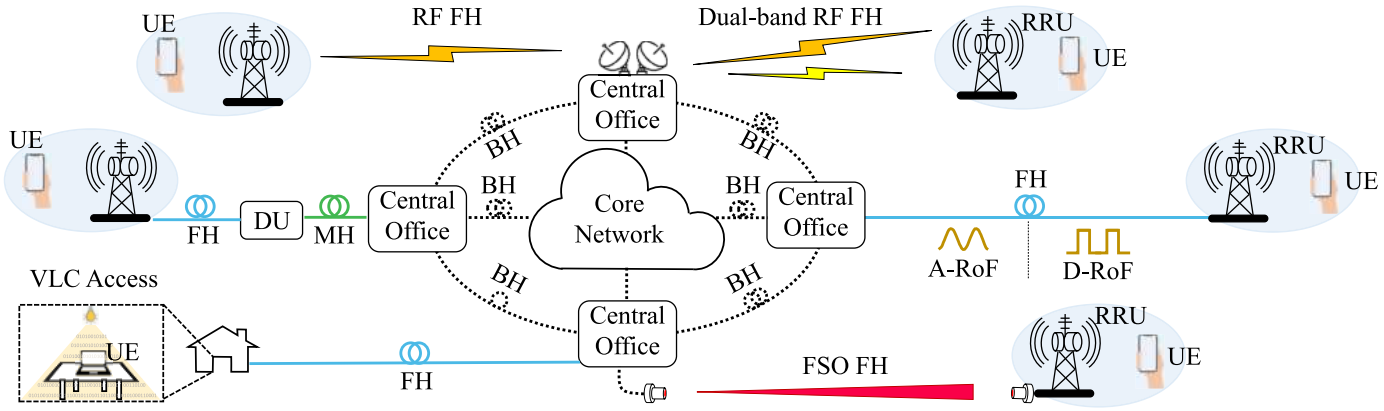

FIGURE 7. Diagram of a fiber-wireless system: RF- radio-frequency; MH- midhaul; BH- backhaul; FH- fronthaul; A-RoF- analog radio over fiber; D-RoF- digital radio over fiber; DU- distribution unit.

and control, based on the service requirements and failures. Therefore, the optimal physical/link layer functional splitting can be achieved depending on the vertical application, for instance, low latency, reliability, or high throughput [117]. Overall, an optimal combination of network function virtualization (NFV), SDN and C-RAN is fundamental for integrating optical and wireless systems in a flexible and reliable mobile network [118]. In this context, landmark C-RAN solutions have been developed over the years, such as: SoftRAN [119], SoftAir [120], FluidNet [121], FlexCRAN [122] and O-RAN [123].

The remaining of this Section encompasses the main optical-wireless technology trends based on the C-RAN concept. We describe challenges and potential solutions, discussing FiWi system implementations, incorporating technologies based on FSO and VLC. In addition, we also discuss PoF and integrated optics applications.

A. FiWi–Fiber/WIRELESS SYSTEMS

FiWi systems play an important role in the current and future mobile communication networks, since they can be used to support a wide range of applications and services. Indeed, a full integration of 5G enabling technologies with FiWi systems is expected [24], [28]. Fig. 7 illustrates a fiber/wireless system within the C-RAN framework, in which the FH link can be implemented using a series of distinct technologies: radio link, radio-over-fiber (RoF), free-space optics (FSO) or even a combination of those. The BH optical link connects multiple COs to the core network and can also connect multiple COs to each other. A DU can be implemented as an extension of the FH link. In this case, a MH link is used to connect CO to the DU.

Table 3 summarizes the state-of-the-art on FiWi systems, addressing diverse applications. All listed works are based on the C-RAN architecture and demonstrate implementations to enable 5G solutions integrated to FiWi systems. Remarkable advances include carrier aggregation for 5G communications; MIMO use for increasing capacity; 5G coexistence with legacy technologies; distribution of 5G signals over passive optical network (PON); and photonics-based signal amplification and FiWi systems fed by a PoF scheme.

An important challenge from FiWi systems is the fiber-radio integration, typically achieved by applying the RoF technology, which is classified in at least two types: digital radio over fiber (D-RoF) and A-RoF [24]. The D-RoF schemes digitize RF signals for launching them into the optical fronthaul using commercial interfaces, such as common public radio interface (CPRI), open base station architecture initiative (OBSAI) and open radio equipment interface (ORI). CPRI-based D-RoF links found commercial success with 4G networks, supporting multiple radio standards and the C-RAN functional split is expected for 5G. Such approaches also bring the advantages of interoperability with diffused small form-factor pluggable (SFP) modules and robustness against dispersion-induced power fading from microwaves and millimeter-waves over fiber [108]. However, the following drawbacks arise from the D-RoF solution when considering the requirements of 5G and 6G: the need of digitization equipment and RF conversion stages at the remote site, even more critical when introducing the mm-waves access that requires complex and expensive hardware remotely; the total data rate that D-RoF links require, which is significantly higher than peak rates achieved on the radio interface and demands a huge fixed bandwidth in the optical fronthaul; the increase on the number of optical transceivers for addressing the data rate [108], [124].

On the other hand, the A-RoF schemes concentrate the most complex radio functions at CO and distribute radio signals at the wireless carrier frequency through the optical fibers. Such methodology has been gradually becoming attractive as the envisaged throughput in the air increases and the industry begins to deploy mm-waves access. The A-RoF advantages include: the capability of transporting RF signals through optical fibers at low processing complexity, i.e. without the need for digitization and RF remote conversion; optical bandwidth and computational power saving, due to the digitization absence; remote site simplification.

TABLE 3. State-of-the-art on FiWi systems.

Ref.	Application	Frequency Range	Throughput
[28]	5G signal distribution over PON	FR1 and FR2	4.4 Gbit/s
[134]	Carrier aggregation for 5G communications	FR2	24 Gbit/s
[135]	5G communications	FR1	21 Gbit/s
[136]	5G communications	FR2	1 Gbit/s
[137]	Beam steered for 5G communications	FR2	8 Gbit/s
[138]	3 × 3 MIMO	Not Specified	132 Gbit/s
[139]	5G and 4G communications coexistence	FR1	Not Specified
[140]	5G signal distribution over PON	FR1 and FR2	1.4 Gbit/s
[141]	Photonically amplified FiWi for 5G	FR1 and FR2	16 Gbit/s
[142]	Optically-powered FiWi for 5G	FR1	500 Mbit/s

Despite these remarkable advantages, drawbacks might also be listed as follows: the non-direct compatibility with established passive optical networks, since requires A-RoF modules instead of SFPs; susceptibility to nonlinear effects from the electro-optic components; susceptibility to chromatic dispersion [24], [125].

To make D-RoF powerfull for 5G/6G, technical solutions toward a bandwidth-efficient digital fronthaul have been proposed, such as data compression, new functional splits and enhanced CPRI interface design. High capacity (hundreds of Gbit/s) optical transceivers have also been designed to deal with the expected throughput in the optical link [108], [126], [127], [128]. In parallel, techniques to compensate dispersion and combat power fading have been successfully demonstrated to maintain A-RoF attractive for 5G/6G [125], [129]. The possibility of using A-RoF in WDM overlay topologies has also been highlighted as an alternative for integration with PONs [26], [28].

Once there is no standardization for the 5G/6G transport schemes, combinations of D-RoF and A-RoF in a hybrid solution has been proposed as an optimum solution [130]. In this context, hybrid digital-analog transport approaches based on diverse techniques have been developed in the last years, including WDM overlay, polarization division multiplexing [131], subcarrier multiplexing [132], A-RoF signal allocation at the null point of the D-RoF spectrum [133] and non-orthogonal multiplexing [130].

B. FIBER-OPTICS-BASED FRONTHAUL ASSISTED BY MACHINE LEARNING

As indicated in Fig. 7, the FH link might be implemented using distinct technologies, including fiber-optics. In this case, both D-RoF and A-RoF have been considered and extensively discussed in the literature [143]. Although D-RoF presents some scalability issues, it has been widely employed in the FH link [108]. Scalability is an issue in D-RoF because the radio signals are sampled and directly digitalized into baseband data at the Remote Radio Head (RRH) from the cell site. 5G and 6G systems, operating at mm-wave and THz-wave ranges will demand ultra high-speed analog-to-digital conversion (ADC) and digital-to-analog conversion (DAC) components which are not available. To overcome this problem, A-RoF becomes attractive, since it enables higher spectral efficiency and remote radio unit simplification, when compared to D-RoF configurations [24]. In addition, the reduced signal processing in A-RoF results in diminished latency.

Considering an A-RoF-based FH architecture, a seamless signal distribution is achieved by using linearization techniques [28], [144], [145]. Fig. 8 illustrates an A-RoF assisted by linearization techniques. Such techniques are usually based on digital signal processing (DSP) solutions, including digital pre-distortion (DPD) and equalization. More recently, ML techniques have also been considered attractive to implement the DPD and equalizer processing blocks, since they are capable of performing complex computational tasks without excessive computational effort.

The remarkable generalization and representation capability of ML algorithms might be considered a powerful tool to further improve the development of convergent fiber-wireless systems. However, there are a couple of technical challenges to be overcome. Particularly for the fiber-optics based fronthaul assisted by machine learning, one important challenge is related to the need for representative data-set for training neural networks. Researches have pointed out reinforcement learning techniques, which do not demand a previously generated data set, since the reinforcement learning model is trained on the fly [146]. In parallel, recent mobile communication systems have embraced a plurality of new services and applications, which increase the demand for computing processing and storage capabilities. Moreover, quantum computing with machine learning has been recently proposed to increase efficiency, enhance and speed up the system computing capabilities [147]. When considering the ML-based linearization techniques, another important challenge must be considered. Once the response of the devices that compose the A-RoF-based FH varies with time, a non-re-calibrated linearization technique is desirable. Otherwise, it will be necessary re-training the linearization algorithm, which will generate considerable expenses, since the communication system must be turned off for re-training, leaving customers without coverage. To overcome this issue, a ML-based scheme able to generalize possible variations of the A-RoF response was proposed by our research group, enabling a non-recalibrated linearization technique [148].

In this context, Andres Najarro *et.al* have demonstrated a neural network-based approach to compensate the nonlinear distortions in RoF systems. The neural network is employed to compute the RoF system inverse response, which is

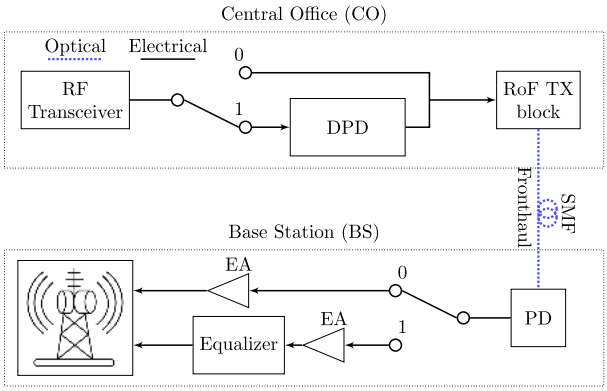

FIGURE 8. Block diagram of an A-RoF assisted by a linearization technique.

then used to compensate the inherent nonlinear degradation. Liu et al. and Liu et al. have employed a neural network as an equalizer [149], [150]. In this case, the neural network processing block is placed at the base station to eliminate the signal nonlinear distortions before the wireless transmission. Indeed, our research group have proposed and implemented DPD and equalizer schemes based on a multi layer perceptron (MLP) neural network [151]. The proposed implementation allows increasing the operating RF power, with no significant distortions, thereby providing more flexibility for telecommunication operators making use of dynamic RF power allocation to the several antenna sites.

C. FSO–FREE SPACE OPTICS

FSO wireless communication systems have attracted increasing interest and undergone strong development in the last decade [152].Some of the key advantages of FSO technology are large bandwidth, immunity to electromagnetic interference, no need for spectrum licensing, and high data rates. These features make FSO highly attractive to meet the increasing traffic demand [153]. However, a FSO transmission requires tight alignment tolerances and it is prone to impairments arising mainly from non-ideal propagation conditions. In other words, a FSO beam is highly vulnerable to weather conditions such as turbulence, rain, fog, haze, and dust, which will attenuate the light beam or even disrupt the entire propagation link [154]. Hence, the FSO system should be thoroughly characterized under severe weather conditions, to assure that the received optical power is higher than the receiver sensitivity, allowing the signal processing.

FSO systems operate in the wireless medium, consequently, alignment losses can be quite common [155], [156]. A precise alignment in an FSO system can be well-achieved when transceivers operate in LOS with no physical obstacles obstructing the optical beam propagation. In a practical FSO system, the primary reason for misalignment is the base motion (building sway) in buildings, especially for FSO systems installed on skyscrapers, which are heavily subjected to sway [155], [157]. To minimize the misalignment loss, an automatic pointing and tracking system can be integrated into the FSO apparatus, in such a way this tracking system consistently adjusts the transceivers for an optimal alignment.

To minimize losses due to adverse weather conditions one of the key methods for determining the FSO proper operation is the link budget. The latter is used to predict how much margin or extra power will be needed in a link under any particular set of operating conditions. The margin is then integrated with a model of atmospheric attenuation to calculate the expected losses from both, scattering and scintillation. Typically, a FSO link budget includes inputs for the transmitted optical power, receive sensitivity, link attenuation, geometric and alignment losses [158].

FSO systems can be used for high data rate communications between two fixed points over distances from hundreds of meters up to a few kilometers. They have initially been proposed as an efficient solution for the ‘‘last mile’’ problem, in order to bridge the gap between the end-user and the fiber optic infrastructure [159]. More recently, FSO systems are also appealing for a wide range of applications such as metropolitan networks, inter-building communication, backhaul for wireless systems, indoor links, fiber backup, service acceleration, security, military purposes and satellite communications [160].

Table 4 summarizes some of the state-of-the-art FSO-based configurations for high transmission capacity links [139], [161], [162], [163], [164], [165], [166]. In [161] the authors combined FSO and FiWi techniques to transmit a 100 MHz bandwidth signal using 64-QAM modulation. Performance is evaluated by exposing the RoF/FSO section to atmospheric turbulence. The authors demonstrated that a 100-meters free-space-optics link span, even under strong turbulence, can still deliver acceptable error vector magnitude (EVM) below 9% with SNR levels of 22 dB. Esmail et al. [162] have experimentally analyzed the effect of dust storms on the performance of an FSO link carrying a RF signal at 28 GHz. The results indicate that the FSO link operating at an optical carrier frequency of about 193 THz is significantly affected by low visibility. In addition, the analysis showed that dust storms condition introduces a flat fading over the frequency range under study, i.e., 21–29 GHz bandwidth. Also, a comparison between the FSO and RF channels under the same dusty conditions was performed. The results showed that the effects of the dust storm are negligible for the RF link which makes it a suitable backup for FSO link in case of severe dust conditions. Finally, a 8 Gbit/s transmission over the RoF/FSO link has been demonstrated for a 40 GHz signal. System penalties have been measured under distinct thermal-induced turbulence distributions along the FSO channel [163].

A heterogeneous RoF/FSO/Wireless non-standalone (NSA) transmission of LTE-A and 5G NR signals in the 2.2 and 3.5 GHz bands, respectively, has been carried out in [139]. The experimental results demonstrated the benefits of employing hybrid analog/digital heterogeneous transmission. The authors have achieved [164] the transmission of high-speed radio signals in the 90 GHz band over a seamless fiber–FSO system in both DL and UL directions, by using the

TABLE 4. State-of-the-art FSO solutions for mobile fronthauls.

Ref.	Architecture	RF frequency [GHz]	DL throughput [Gbit/s]
[161]	FSO/FiWi	24 to 26	10
[162]	FSO/Wireless	28	4
[163]	RoF/FSO	26 to 40	8
[139]	RoF/FSO/Wireless	2.2 to 3.5	Not Specified
[164]	RoF/FSO/Wireless	90	80
[165]	RoF/FSO/Wireless	39	3
[166]	RoF/FSO/Wireless	0.788 3.5 and 26	1.4

intermediate-frequency-over-fiber (IFoF) method. Specifically, a transmitted data rate of approximately 80 Gbit/s over a seamless RoF/FSO/Wireless system in the DL direction has been demonstrated. In addition, the authors established reliable full-duplex transmission of millimeter-wave signals over a hybrid single-mode fiber (SMF) and FSO link for the 5G radio access networks [165]. 3 Gbit/s data rates have been transmitted over a hybrid system, composed of 10 km SMF and 1.2 m FSO link. In particular, our research group has proposed an architecture which relies on a novel and efficient heterogeneous optical-wireless network using RoF, FSO and wireless technologies for 5G and beyond applications [166]. A hybrid fronthaul, which encompasses a 12.5-km RoF link followed by a 1-m FSO link and an 8-m indoor wireless access network, has been implemented. Specific combinations of multi-standard and multi-band optical-wireless network reached throughputs up to 3 Gbit/s and 1.4 Gbit/s based on hybrid RoF/FSO and RoF/FSO/Wireless configurations, respectively.

D. VLC–VISIBLE LIGHT COMMUNICATIONS

Visible light communications based on light emitting diodes (LEDs) have emerged as a cost-effective, energy-efficient and secure wireless access technology to address the demands brought about by the future 6G network [167], [168]. In this technique, the lightning infrastructure can be exploited for simultaneously providing multiple wireless services for offices, aircrafts, homes, and hospitals, as well as vehicular applications such as vehicle to vehicle (V2V) and vehicle to infrastructure (V2I) [109]. The VLC system offers important advantages when compared to the conventional RF systems, such as absence of licensing requirements and immunity to electromagnetic interference, enabling access to areas restricted to RF and frequency reuse. In addition, VLC systems offer a huge amount of available bandwidth (BW) for modulation, enhancing indoor security and privacy [169].

For these reasons, VLC technology represents an attractive alternative to RF wireless communications. A carrier in the visible light wavelength range (380-780 nm) enables a bandwidth of up to one thousand times greater than RF communications [168], allowing high data throughput, in the order of Gbit/s [170], [171]. Also, the use of the non-regulated visible light spectrum allows for a reduced cost for the deployment of the VLC technology.

The literature registers several investigations of LED-based VLC systems for indoor applications. Sifaou et al. [172] numerically demonstrated the benefits of using precoding techniques. They also established the improvement of the signal-to-interference-plus-noise ratio (SINR) in systems with multiple MIMO users, when the receivers are placed at different beam arrival angles. In [173], the authors experimentally demonstrated the joint implementation of WDM and MIMO techniques to transmit modulated data streams in discrete multitone (DTM). Mejia and Georghiades [174] presented an overview of color-shift-keying (CSK), based on red, green and blue (RGB) LEDs, by considering different coding methods, with emphasis on CSK trellis-coded modulation (TCM) and CSK finite-state-machines (FSM) codings, which provided higher SNR. In [175], an experimental work discussed DPD and pre-equalization techniques to mitigate the degrading non-linear effects of VLC systems.

In the context of VLC systems applied to 5G networks, many investigations are also available in the technical literature [176], [177], [178], [179], [180], [181], [182], [183]. In [176], the authors performed a numerical performance analysis of the asymmetrically clipped DC-biased optical OFDM (ADC-OFDM) waveform in a relay-assisted VLC system employing two radiant sources. The simulation results show that the proposed configuration improves the system performance [176]. In [177], the researchers numerically analyzed the discrete wavelet transform OFDM (DWT-OFDM) waveform performance for the combined use of power line communication (PLC) and VLC technologies. The theoretical and simulation results, as a function of bit error rate (BER), show that the DWT-OFDM outperforms a OFDM-based PLC-VLC system. In [178], a numerical study was carried out to optimize the number of optical attocells accordingly to the number of users and the required throughput. The simulated results showed that an attocell can guarantee the quality of service of up to four users with a large half-power half-angle [178].

Chou and Tsai [179] implemented and experimentally analyzed a micro-projection enabling short-range communication (SRC) system for a personal communication device in a 5G application using LEDs with a micro liquid crystal display. 4-PAM, 8-PSK and 16-QAM waveforms were transmitted and a maximum throughput of 892 Mbit/s was reached for a distance of 0,65 meters between transmitter and receiver [179]. Shi et al. [180] experimentally demonstrated the implementation of the 5G NR standard in a VLC system. The transmission of QPSK modulated signals was carried out, and a maximum throughput of 14.4 Mbit/s was achieved for a distance of 0.55 m [180]. Valluri et al. [181] experimentally demonstrated the reduction of the peak average power of the DC-biased optical OFDM (DCO-OFDM) waveform,

FIGURE 9. Photograph of the visible light communication setup for experiments.

by means of a channel estimation algorithm. The experimental results indicated a significant reduction in peak-to-average power ratio (PAPR) without affecting the real-time channel response [181]. Monteiro et al. [182] carried out a experimental performance analysis of the orthogonal frequency division multiplexing (OFDM), generalized frequency division multiplexing (GFDM) and filter bank multi-carrier (FBMC). The results suggested that the GFDM provides improved performance for the analyzed system, reaching a throughput of 9.94 Mbit/s for a distance of 2 m [182].

Our research group has also contributed to the advancement of the VLC technology. For instance, in [183], we developed an RGB-based VLC system using the 5G NR standard. In this proposition, a four LEDs array with the red, green, blue and amber (RGBA) colors was used in order to enable WDM transmission while still generating white light for environment illumination. During the experiments, we decided not to use the amber wavelength, due to its low optical output power. Yet, it was possible to transmit signals at 872 Mbit/s. Transmission is based on the VLC technique, operating simultaneously in three remaining RGB colors. Additionally, M-QAM signals were also transmitted, making use of the DPD in order to increase the data throughput, which reached 1.92 Gbit/s. Fig. 9 depicts a photograph of the experimental setup implemented in our laboratory [183].

Although VLC systems present remarkable advantages in comparison to traditional wireless links, there are several implementation hurdles that must be overcome to enable a commercial VLC system with all the required features. One of the challenges refers to throughput enhancement since there is a huge bandwidth available in the visible light spectrum and the commercial LEDs 3-dB bandwidth is limited, reaching only a few MHz [184], [185]. For this reason, several techniques have been proposed to overcome the LED bandwidth limitation. A simple and low-cost approach is to place a blue optical filter at the received for enhancing the 3-dB bandwidth, however, throughput remains low in contrast with the available bandwidth [186]. Laser diodes have also been employed as a VLC transmitter, enabling higher bandwidths. For instance, Wei et al. reported a 6.9 Gbit/s VLC system with functional transmission distance based on white-light phosphor laser [187]. In addition, as reported in some of the previously highlighted works, techniques to linearize and compensate the LED response over the frequency can be used, applying pre-distorter or equalizer, and also MIMO techniques, to enhance the total throughput [172], [173], [175], [183].

Other VLC systems challenges are concerning the uplink. VLC links in an indoor environment focus on the use of white LED broadcasting characteristics to enable lighting and communication, typically downlink. Accordingly, there is a need to establish an uplink, in order to create a bidirectional communication [188]. The deployment of an uplink connection using VLC is not an alternative, since the connected devices might have multiple LEDs pointing in random directions, which increases cost and can cause discomfort to the user eyes [189]. In this context, a hybrid solution must be used in bidirectional VLC links. Thus, the VLC provides a high throughput downlink, whereas RF [190], [191], [192], [193] or infrared [194], [195] communication enables the uplink, combining the advantages of each technology.

E. IMWP–INTEGRATED MICROWAVE PHOTONICS

Integrated microwave photonics (IMWP) [196] can support widespread applications in the fields of radar, broadband wireless access networks, optical processing, as well as in emerging areas such as FiWi convergence, Terahertz systems for medical imaging, personal area networks (wireless-body), among others [141], [197], [198], [199], [200]. Although part of this potential can be unleashed by conventional microwave photonics (MWP) [201], [202], several applications are limited by its high cost and complexity, which establishes typical ranges of size, weight and power (SWaP), of the order of $0.04 – 0.2\ m^2$, 1.5 – 10 kg, and 15 – 20 W, respectively [112]. Such values are detrimental for practical applications and unfeasible for large-scale production. Thus, approaches based on integrated optics have emerged, aiming to reduce research, development, and prototyping costs, as well as the photonic integrated circuits (PICs) processing time, by more than an order of magnitude [196], [203], [204], [205].

A major challenge in microwave photonics implies reducing SWaP characteristics of its devices, subsystems and systems. However, all-in-one platform integration is also challenging for this technology. Integrated photonics has the potential to change the scaling laws of high-bandwidth systems through proper architectural choices, which combine photonics with electronics to optimize performance, power, footprint, and cost. Drastic space and weight reductions are immediate gains from integration [206], [207]. This technology is transformative as it enables the integration of complete sets of microwave and optical components, such as light sources, analog and digital signal processing circuits, light detectors, optical control circuits, and others RF circuits, all-in-one platform to achieve high-performance and

low-cost mixed signal optical links. In addition, integrated photonics offers much more than a reduction in footprint and complexity. For example, confining light in the small mode volume enhances its interaction with matter, most of the time through nonlinear optical processes, which resulted in new technological tools for IMWP, such as Kerr microresonator combs, hybrid organic–plasmonic modulators and on–chip stimulated Brioullin scattering (SBS) [197].

Generally, such integration technologies are composed of highly standardized photonic integration processes which allow the implementation of a range of application-specific photonic integrated circuits (ASPICs) from a small set of basic building blocks (BBB) [203]. Then, it becomes possible to support a number of different applications, reducing the PICs development cost and achieving improved performance and reliability [208]. Also, several different designs can be combined on the same wafer, the so-called multi-project wafer (MPW), also reducing manufacturing costs, as they will be divided among different users [203], [208].

Technologies and integration platforms available for IMWP can be classified into monolithic, heterogeneous, and hybrid [196]. Monolithic approaches require either a single material system or a single-chip implementation. Heterogeneous integration can be accomplished by combining two or more materials technologies into a single PIC. Meanwhile, hybrid integration is a process which employs two or more PICs, generally from different materials technologies, into a single package [209], [210]. Typical components manufactured in integrated optics include lasers, modulators, photodetectors, optical amplifiers and filters, as well as passive components such as couplers, splitters, and delay lines. It is worth mentioning that the performance characteristics of each integrated component vary accordingly to the technological platform used. Among the various available integration platforms, the five most common are those based on indium phosphide (InP), Silicon Photonics (SiPh), Silicon Nitride (Si_3N_4), Lithium Niobate ($LiNbO_3$) and polymers [196], [209], [211]. Fig. 10 illustrates typical integrated components within the PIC platform.

InP platforms enable the high-bandwidth lasers, modulators, photodiodes, and optical amplifiers, offering a pathway to optoelectronic monolithic integration and good reliability [212], [213]. SiPh leverages existing complementary metal–oxide–semiconductor (CMOS) process technology, thereby offering a more cost-effective implementation and a more compact footprint [214], [215]. The Si_3N_4 platform provides very low propagation losses, low fiber coupling loss, enabling filtering and beam shaping applications, at a potentially low cost [216], [217]. $LiNbO_3$ technology provides a strong E/O effect and relatively low loss, making it suitable for wide-bandwidth modulators, by taking advantage of a well-established technology base [218], [219]. Regarding the electro-optic (EO) polymer technology, it offers intrinsic advantages such as a large EO coefficients, low dielectric constant and loss, as well as excellent compatibility with other material systems [220], [221]. In recent years, transmitter

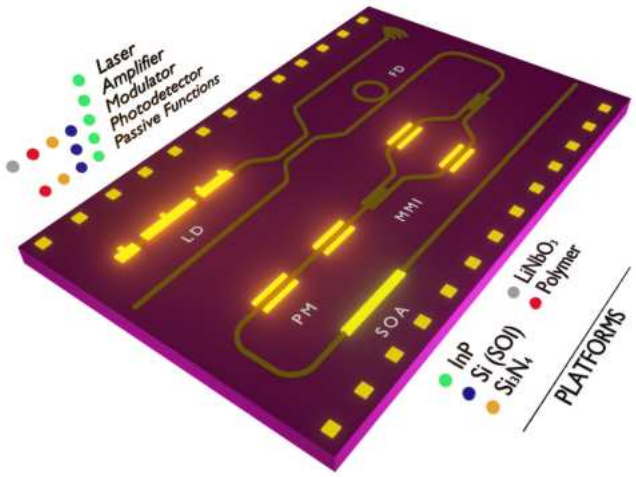

FIGURE 10. Integrated components within the photonic integrated circuits platform.

and receiver modules using IMWP are being presented in the literature as show in [222] and [223].

The development of photonic transmitters based on wavelength-tunable lasers arrays is an example of integrated optics research which has been addressed in the literature because it is a required building block for many microwave photonics applications. The multi-wavelength transmitter (MWT) are considered promising for short-distance links in data center networks, mobile backhaul, and access networks [201]. In addition, the MWTs can be employed to feed phased array antennas, allowing beamforming/beam steering capabilities [224].

The MWTs investigations reported in the literature are based either on the directly modulated lasers (DMLs) or externally modulated lasers (EMLs) configurations. Implementations based on EMLs are less compact, more complex and expensive, requiring a larger footprint, due to the use of external modulators. On the other hand, it offers the benefit of low chirp, which is a limiting impairment in systems employing DMLs. In [225], the authors reported a transmitter based on the integration of four widely tunable EMLs on a InP substrate. Each generated beam passes through a semiconductor optical amplifier (SOA) and an external electro-absorption modulator at 10 Gbit/s in baseband operation [225]. Yao et al. [226] demonstrated a six-channel array based on EML using Mach-Zehnder modulators integrated into a InP platform. The baseband non-return to zero (NRZ) optical signals were transmitted at 20 Gbit/s and 30 Gbit/s throughputs. The photodetected signals were analyzed using the eye diagram and BER [226].

In [227], the authors implemented an array of eight InP-based DMLs in the wavelengths around 1550 nm. A 2^{31}-1 NRZ pseudo random binary sequence (PRBS) was transmitted at 10 Gbit/s in the back-to-back (B2B) condition as well as for a baseband-over-fiber (BBoF) link of 2km over SMF [227]. In [228], the authors described an array of four DMLs with a 17 GHz electrical bandwidth, in the

wavelength range between 1295 and 1310 nm, for Local Area Network WDM (LAN-WDM) applications. Data transmission tests was performed with the standard 2^{31}-1 NRZ PRBS, at 25 Gbit/s per channel, analyzing the B2B condition and the impact of 30-km propagation in BBoF link from SMF [228]. Andriolli et al. [229] implemented an integrated MWT, manufactured with eight channels with a 12 GHz electrical bandwidth between 1541.4 and 1547.0 nm, in which each laser could be tuned around 4 nm. The experiments demonstrated baseband transmission of 15 Gbit/s over 2.1 km of SMF [229].

It is noticed that the investigations described so far concern the optical transmission of baseband signals. However, the use of multi-wavelength transmitters is also promising for WDM-based RoF and/or FiWi systems [24], [230]. Regarding the 5G networks, MWTs can be useful for fronthaul architectures using the WDM technnique.

In this regard, our research group described in [231], a 4G/5G shared optical fronthaul implementation on the basis of an integrated MWT [229]. The experiments were carried out in two conditions, the first scenario based on WDM, where each RF signal was transmitted on a different optical carrier, and the second scenario based on subcarrier multiplexing (SCM), where the RF signals were combined in the electrical domain and then transmitted by a single laser. Maximum throughput of 1.04 Gbit/s was demonstratd, by means of two signals in the 5G NR standard and one signal in the LTE standard, through a 12.5-km optical link [231]. Next, we reported a FiWi architecture using the integrated MWT [232]. Three RF signals were transmitted in WDM by a 12.5-km long RoF link and radiated through an indoor wireless link within a 10 m range or an outdoor wireless link of about 115 m. A maximum throughput of 1.36 Gbit/s and 230 Mbit/s were experimentally demonstrated, in the 10 m and 115 m scenarios, respectively [232]. Finally, in [233] we reported a RoF/FSO system employing the integrated MWT combined with the use of BS-ILC. In these experiments, an M-QAM signal was transmitted over a 12.5 km RoF link followed by a 1.5 m FSO link. The RoF/FSO combination achieved a maximum bit rate of 160 Mbit/s using a bandwidth of only 20 MHz [233].

F. PoF–POWER-OVER-FIBER

The PoF technology has become an attractive solution to transport electrical power to remote locations. In short, this technology consists of transmitting power by means of an optical fiber, which provides excellent electrical isolation and immunity to RF, magnetic fields, sparks, and interference. Other features include galvanic isolation, weight reduction, and resistance to corrosion, moisture, and extreme temperatures [234], [235], [236]. In this context, PoF may be considered as an attractive alternative to increase safety and reliability of a number of applications by replacing conventional power supplies, metallic cables, and batteries. PoF systems typically employ three main components: a high-power laser diode (HPLD), responsible for generating high optical power; an optical fiber as the light transmission medium; a photovoltaic power converter (PPC), which performs the optical-to-electrical (O/E) conversion [237]. One of the key performance metrics in a PoF system is power transmission efficiency (PTE), defined as the ratio between the HPLD output power and total electrical power delivered by the PPC [238]. As simultaneous data and power transmission has become feasible, delivered power levels have reached over 40 W [239], [240], PoF has been employed to power devices in a wide range of applications, including 5G and future mobile networks.

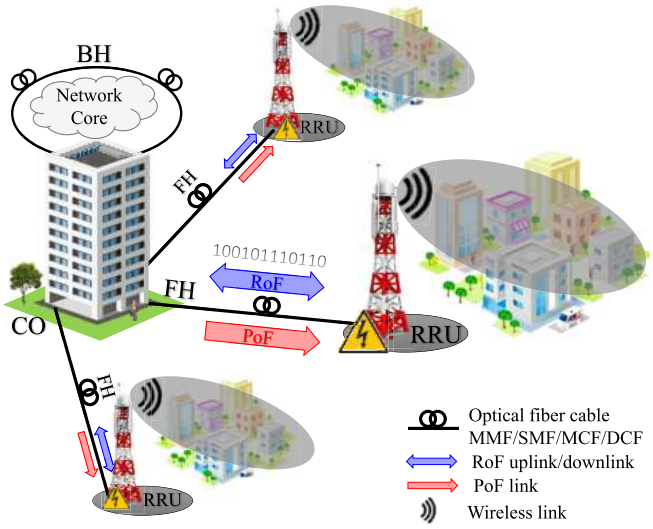

FIGURE 11. Optically-powered FiWi system towards 6G mobile networks (modified from [142]). CO - central office; BH - backhaul; FH - fronthaul; PoF - power-over-fiber; RoF - radio-over-fiber; RRU - remote radio unit.

Cell densification is a promising approach to meet the coverage and capacity requirements of future 6G networks. An effective way to achieve the required desinsification is to reduce the cell size and to increase the number of deployed BSs. However, the BS typically consumes around 60% of the total available power of mobile systems, leading to a substantial rise in power consumption [241]. Consequently, it is crucial to provide solutions to properly supply the required power to BSs, ensuring network operation stability, safety and robustness. In this context, PoF may be considered a potential approach to power BSs in future wireless networks. Fig. 11 depicts an optically powered FiWi system based on the C-RAN architecture and employing PoF and RoF technologies. This implementation consists of a CO from which power and data are simultaneously transmitted through an optical fiber cable, which can be composed of multimode fibers (MMFs), SMFs or multicore fibers (MCFs). Although the PoF technology typically provides lower PTE compared to the conventional power lines, it can still be extremely efficient, thereby contributing to the required significant increase in the number of BSs across 5G and 6G networks [240].

Several architectures employing the PoF technology have been reported in literature regarding mobile fronthaul

configurations. Table 5 reports the main performance parameters for the state-of-the-art PoF solutions for mobile fronthauls. In particular, an optically-powered RoF system employing a MCF link has been proposed [242]. A 12-Gbps OFDM signal with intermediate frequency (IF) of 92 GHz was simultaneously transmitted with a 0.8-W optical power beam to feed an UTC-PD and an RF amplifier, aiming at 5G applications. Regarding high-power delivery, Matsuura et al. [238] demonstrated a 150-W optical power transmission over a 300-m double-clad fiber (DCF) link. Four 808-nm HPLDs and 18 PPCs were used for providing 40 W of electrical power, resulting in PTE of approximately 30%. A PoF system capable of delivering roughly 2-W of electrical power over a 100-m MMF link was reported in [243]. A RRH control board was developed and different sleep mode configurations were implemented aiming at efficient 5G C-RAN fronthauls. Al-Zubaidi et al. [244] reported the use of a SMF link for optically powering remote antenna units (RAUs) of 5G systems. Approximately 870 mW was delivered to an optical power meter (OPM). Also, a 5G fronthaul configuration has been deployed in [245]. In this work, 10-W optical power and 1.5-Gbit/s 5G NR signal carrier centered at 3.5 GHz were simultaneously transmitted over a 1-km SMF link. Over 7 W electrical power was delivered to an OPM, resulting in PTE of 25.1%. Lopéz-Cardona et al. [246] reported a PoF-based 5G NR network employing RoF technology and a MCF link. More recently, the simultaneous transmission of a 5G NR signal and 60-W energy light has been reported in [247] employing 1-km of weakly-coupled seven-core fiber (WC-7CF). Over 11.5 W electrical power was delivered in this scheme.

Our research group, WOCA, from National Institute of Telecommunications (Inatel), has implemented an optically-powered 5G NR FiWi system employing PoF and RoF technologies, aiming at high-throughput short-range 5G NR cells [142]. Our approach enabled the simultaneous transmission of a 5G NR signal at 3.5 GHz with bandwidth up to 100 MHz as well as a 2.2-W optical power signal employing dedicated fiber-optics links. The proposed PoF system was able to deliver up to 516 mW electrical power, by means of a 100-m MMF link, in order to optically power a 5G NR RAU. An overall PTE of 23.5% was achieved with this configuration.

One may notice from Table 5 that the main challenge regarding PoF systems is the fiber link reach. In a shared scenario, in which a single optical fiber is used for simultaneous power and data transmission (see Fig. 11), long-distance fronthaul links are not feasible due to the higher attenuation at the shorter wavelengths employed in PoF systems, e.g. 808 nm and 980 nm, which limits the power transmission link to a few kilometers. On the other hand, in a dedicated configuration, data and high-power signals are individually transmitted through dedicated fibers. In this context, a centralized power supply station (CPSS) could be implemented for distributing power to each RRU by means of a dedicated PoF link, as reported in [142], and the PoF link distance limitation would not have any impact on the fronthaul link distance.

TABLE 5. State-of-the-art PoF solutions for mobile fronthauls.

Ref.	Optical Power [W]	Distance [m]	Electrical Power [W]	PTE [%]
[242]	0.8	-	0.05	6.25
[238]	150	300	43.7	30
[243]	5.4	100	2.343	43.4
[244]	2	100	-	-
[245]	10	1000	2.51	25.1
[246]	1.26	10000	0.133	10.5
[247]	60	1000	11.5	19.2
[142]	2.2	100	0.516	23.5

The PoF system capacity of delivering high power is also critical. As reported in Table 5, the maximum electrical power delivered by a PoF system reported in literature is 43.7 W. However, the typical maximum power consumption of a 5G site is currently higher than 11 kW [248]. Consequently, current PoF systems would not deliver enough power to feed an RRU in 5G sites. On the other hand, PoF systems could be employed to enable low-power small cells. For instance, a commercial femtocell typically consumes up to 24 W [249]. In addition, base stations operating in sleep mode have been proposed, saving up to 60% energy in networks and enabling PoF integration [238]. Nevertheless, PPCs conversion efficiencies are expected to improve as the technology matures, increasing the capacity of power delivery in PoF systems.

V. CONCLUSION

This paper presented a review on wireless and optical convergent access solutions towards 6G systems. The manuscript started with an brief overview on the mobile communication systems evolution trends, focusing on the challenges and the vision for the future 6G RAN. Next, the use cases, requirements and enablers for 6G networks were discussed. It was pointed out that they are still under discussion worldwide, suggesting that THz and sub-THz communications, wireless-optical integration, VLC and new antennas designs can be considered major building blocks for the future wireless systems. The manuscript also presented the main wireless technology trends, which encompassed the channel capacity opportunities and issues, considering the expected high frequencies, including mmWaves and THz communications and last mile solutions such as HIBS technologies. Also, the paper conducts a discussion on the state-of-the-art on antenna design for sub-6 GHz, mmWaves and THz frequency ranges. It was concluded that the literature on beamforming

and MIMO applications from literature are usually concerned with the array antenna element (mainly patch, dipole or slot antennas), feeding network or scanning range enhancement. In any case, regardless the application, reducing mutual coupling is an important performance metric. Furthermore, THz antenna design is divided in two main categories: conventional microwave and mmWaves antenna design, re-tuned for higher frequencies and photoconductive antenna design for THz signal generation, by using antennas, photonics and concepts and plasma physics concepts.

Next, the manuscript presented the RAN evolution towards optical and wireless convergence, to support current and future mobile communications networks requirements. In this context, FiWi systems within the C-RAN architecture and fiber-optics-based fronthaul assisted by ML were considered candidates to solve flexibility and scalability issues. In addition, OWC systems, specially FSO and VLC, have emerged as promising candidates for enabling optical-fiber like performance. Also, new approaches in photonic integration have emerged, aiming to reduce research, development, and prototyping costs of MWP devices. Finally, the PoF technology was proposed as a joint solution to transport data and electrical power to remote locations.

All discussed technologies are still ongoing research, which brings many opportunities as future works for researchers worldwide. For example, the manuscript has pointed out that antenna design is continuously evolving towards higher frequencies, up to THz frequency range. This leads to the conclusion that active and integrated circuits, jointly with new materials, should be investigated for covering these unprecedented frequency bands. FiWi systems are limited if employed as D-RoF due to the need for high-speed ADCs and RF conversion in remote sites, whereas A-RoF drawbacks are related to the compatibility issues with established passive optical networks. If a ML-based linearization technique is employed, FiWi systems challenges are related to the need for a representative data set for training a neural network. FSO systems can be unfeasible in case of low alignment precision and stability, whereas VLC systems provide an extremely wide bandwidth in the optical domain, but are limited by the electric bandwidth from the LED components, which is quite narrow. A major challenge in microwave photonics implies reducing the SWaP characteristics of its devices, subsystems and systems. Finally, on joint deployment of PoF and communication links, the main challenge is the fiber spam length. Long-distance fronthaul links are not feasible due to the high attenuation at the shorter wavelengths employed in PoF systems.

REFERENCES

[1] *Cisco 5G Vision Series: Laying the Foundation for New Technologies*, Cisco, San Jose, CA, USA, 2016.

[2] *5G Vision*, DMC R&D Center, Samsung Electronics, Suwon-Si, South Korea, 2015.

[3] *5G; Study on Scenarios and Requirements for Next Generation Access Technologies*, 3GPP, document TR 38.913, 2017.

[4] E. Westerberg, "4G/5G RAN architecture: How a split can make the difference," *Ericsson Technol. Rev.*, vol. 93, no. 6, pp. 1–15, 2016.

[5] A. De La Oliva, X. C. Pérez, A. Azcorra, A. Di Giglio, F. Cavaliere, D. Tiegelbekkers, J. Lessmann, T. Haustein, A. Mourad, and P. Iovanna, "Xhaul: Toward an integrated fronthaul/backhaul architecture in 5G networks," *IEEE Wireless Commun.*, vol. 22, no. 5, pp. 32–40, Oct. 2015.

[6] I. Philbeck, "Connecting the unconnected: Working together to achieve connect 2020 agenda targets," ITU, Geneva, Switzerland, White Paper, 2017.

[7] *Group Radio Access Network; NR; User Equipment (UE) Radio Transmission and Reception; Part 1: Range 1 Standalone*, 3GPP, document TS 38.101-1, 2019.

[8] *Technical Specification Group Services and System Aspects; Release 16 Description; Summary of Rel-16 Work Items*, 3GPP, document TR 21.916, 2022.

[9] *Technical Specification Group Services and System Aspects; Release 17 Description; Summary of Rel-17 Work Items*, 3GPP, document TR 21.917, 2022.

[10] C. Han, Y. Wu, and Z. Chen. (2018). *Network 2030 a Blueprint of Technology, Applications and Market Drivers Towards the Year 2030 and Beyond*. [Online]. Available: https://www.itu.int/en/ITU-T/focusgroups/net2030/Documents/White_Paper.pdf

[11] H. Tataria, M. Shafi, A. F. Molisch, M. Dohler, H. Sjoland, and F. Tufvesson, "6G wireless systems: Vision, requirements, challenges, insights, and opportunities," *Proc. IEEE*, vol. 109, no. 7, pp. 1166–1199, Jul. 2021.

[12] M. Latva-aho, K. Leppänen, F. Clazzer, and A. Munari, "Key drivers and research challenges for 6G ubiquitous wireless intelligence," 6G Flagship, Univ. Oulu, Oulu, Finland, White Paper, 2019.

[13] Z. Zhang, Y. Xiao, Z. Ma, M. Xiao, Z. Ding, X. Lei, G. K. Karagiannidis, and P. Fan, "6G wireless networks: Vision, requirements, architecture, and key technologies," *IEEE Veh. Technol. Mag.*, vol. 14, no. 3, pp. 28–41, Sep. 2019.

[14] CRR. (2021). *Radiocommunications Reference Center (CRR) From Inatel*. [Online]. Available: https://inatel.br/crr/

[15] W. Dias, D. Gaspar, L. Mendes, M. Chafii, M. Matthe, P. Neuhaus, and G. Fettweis, "Performance analysis of a 5G transceiver implementation for remote areas scenarios," in *Proc. Eur. Conf. Netw. Commun. (EuCNC)*, Jun. 2018, pp. 363–367.

[16] W. Dias, A. Ferreira, R. Kagami, J. S. Ferreira, D. Silva, and L. Mendes, "5G-RANGE: A transceiver for remote areas based on software-defined radio," in *Proc. Eur. Conf. Netw. Commun. (EuCNC)*, Jun. 2020, pp. 100–104.

[17] CRR. (2021). *5G Range*. [Online]. Available: http://5g-range.eu/

[18] I. B. F. de Almeida, L. L. Mendes, J. J. P. C. Rodrigues, and M. A. A. da Cruz, "5G waveforms for IoT applications," *IEEE Commun. Surveys Tuts.*, vol. 21, no. 3, pp. 2554–2567, 3rd Quart., 2019.

[19] Inatel. (2021). *Evolving With Telecommunications, Inatel Integrates a Pioneer Group in the World of 6G Research*. [Online]. Available: https://inatel.br/imprensa/noticias/pesquisa-e-inovacao/3426-inatel-integra-grupo-pioneiro-no-mundo-de-pesquisas-sobre-6g

[20] Instituto Nacional de Telecomunicações. (2021). *6G Brasil*. [Online]. Available: https://cursos.inatel.br/lp-workshop-de-6g

[21] University of Oulu. (2021). *6G Flagship*. [Online]. Available: https://www.oulu.fi/6gflagship/

[22] H. R. D. Filgueiras, R. M. Borges, M. C. T. H. Brandao, and A. C. Sodre, "Dual-band wireless fronthaul using a FSS-based focal-point/cassegrain antenna assisted by an optical midhaul," *IEEE Access*, vol. 7, pp. 112578–112587, 2019.

[23] A. Tzanakaki et al., "Wireless-optical network convergence: Enabling the 5G architecture to support operational and end-user services," *IEEE Commun. Mag.*, vol. 55, no. 10, pp. 184–192, Oct. 2017.

[24] G. Kalfas, C. Vagionas, A. Antonopoulos, E. Kartsakli, A. Mesodiakaki, S. Papaioannou, P. Maniotis, J. S. Vardakas, C. Verikoukis, and N. Pleros, "Next generation fiber-wireless fronthaul for 5G mmWave networks," *IEEE Commun. Mag.*, vol. 57, no. 3, pp. 138–144, Mar. 2019.

[25] T. H. Brandão, F. Scotti, H. R. D. Filgueiras, A. A. de Castro Alves, D. Onori, S. Melo, A. Bogoni, and A. C. Sodré, "Coherent dual-band radar system based on a unique antenna and a photonics-based transceiver," *IET Radar, Sonar Navigat.*, vol. 13, no. 4, pp. 505–511, Apr. 2019.

[26] R. M. Borges, T. R. R. Marins, M. S. B. Cunha, H. R. D. Filgueiras, I. F. da Costa, R. N. da Silva, D. H. Spadoti, L. L. Mendes, and A. C. Sodré, "Integration of a GFDM-based 5G transceiver in a GPON using radio over fiber technology," *J. Lightw. Technol.*, vol. 36, no. 19, pp. 4468–4477, Oct. 1, 2018.

[27] C. Lim, Y. Tian, C. Ranaweera, T. A. Nirmalathas, E. Wong, and K.-L. Lee, "Evolution of radio-over-fiber technology," *J. Lightw. Technol.*, vol. 37, no. 6, pp. 1647–1656, Mar. 15, 2019.

[28] R. M. Borges, L. A. M. Pereira, H. R. D. Filgueiras, A. C. Ferreira, M. S. B. Cunha, E. R. Neto, D. H. Spadoti, L. L. Mendes, and A. Cerqueira, "DSP-based flexible-waveform and multi-application 5G fiber-wireless system," *J. Lightw. Technol.*, vol. 38, no. 3, pp. 642–653, Feb. 1, 2020.

[29] G. Brown and H. Reading, "Exploring the potential of mmWave for 5G mobile access," Qualcomm, San Diego, CA, USA, White Paper, 2016.

[30] C. Wallace, "Bringing 5G networks indoors," Ericsson, Stockholm, Sweden, White Paper, 2019.

[31] G. Huawei, "Indoor 5G scenario oriented white paper," Huawei, Shenzhen, China, White Paper, 2019.

[32] J. Liu, G. Shou, Y. Liu, Y. Hu, and Z. Guo, "Performance evaluation of integrated multi-access edge computing and fiber-wireless access networks," *IEEE Access*, vol. 6, pp. 30269–30279, 2018.

[33] Q.-V. Pham, F. Fang, V. N. Ha, M. J. Piran, M. Le, L. B. Le, H. Won-Joo, and Z. Ding, "A survey of multi-access edge computing in 5G and beyond: Fundamentals, technology integration, and state-of-the-art," *IEEE Access*, vol. 8, pp. 116974–117017, 2020.

[34] Z. Jiao, B. Zhang, M. Liu, and C. Li, "Visible light communication based indoor positioning techniques," *IEEE Netw.*, vol. 31, no. 5, pp. 115–121, Jul. 2017.

[35] Y. Zhuang, L. Hua, L. Qi, J. Yang, P. Cao, Y. Cao, Y. Wu, J. Thompson, and H. Haas, "A survey of positioning systems using visible LED lights," *IEEE Commun. Surveys Tuts.*, vol. 20, no. 3, pp. 1963–1988, 3rd Quart., 2018.

[36] C. De Lima, D. Belot, R. Berkvens, A. Bourdoux, D. Dardari, M. Guillaud, and M. Isomursu, "Convergent communication, sensing and localization in 6G systems: An overview of technologies, opportunities and challenges," *IEEE Access*, vol. 9, pp. 26902–26925, 2021.

[37] S. Ahmadi. (2019). *5G NR: Architecture, Technology, Implementation, and Operation of 3GPP New Radio Standards*. Elsevier Science. [Online]. Available: https://books.google.com.br/books?id=N0hgtAEACAAJ

[38] A. Ghosh, A. Maeder, M. Baker, and D. Chandramouli, "5G evolution: A view on 5G cellular technology beyond 3GPP release 15," *IEEE Access*, vol. 7, pp. 127639–127651, 2019.

[39] A. Gupta and R. K. Jha, "A survey of 5G network: Architecture and emerging technologies," *IEEE Access*, vol. 3, pp. 1206–1232, 2015.

[40] A. Sheikhi, S. M. Razavizadeh, and I. Lee, "A comparison of TDD and FDD massive MIMO systems against smart jamming," *IEEE Access*, vol. 8, pp. 72068–72077, 2020.

[41] J. O. Nielsen, A. Karstensen, P. C. F. Eggers, E. De Carvalho, G. Steinbock, and M. Alm, "Precoding for TDD and FDD in measured massive MIMO channels," *IEEE Access*, vol. 8, pp. 193644–193654, 2020.

[42] J. Flordelis, F. Rusek, F. Tufvesson, E. G. Larsson, and O. Edfors, "Massive MIMO performance—TDD versus FDD: What do measurements say?" *IEEE Trans. Wireless Commun.*, vol. 17, no. 4, pp. 2247–2261, Apr. 2018.

[43] P. V. B. H. Asplund and D. Astely, *Advanced Antenna Systems for 5G Network Deployments*. Amsterdam, The Netherlands: Elsevier, 2020.

[44] J. Gao, C. Zhong, G. Y. Li, and Z. Zhang, "Deep learning-based channel estimation for massive MIMO with hybrid transceivers," *IEEE Trans. Wireless Commun.*, vol. 21, no. 7, pp. 5162–5174, Jul. 2022.

[45] C. D. Alwis, A. Kalla, Q.-V. Pham, P. Kumar, K. Dev, W.-J. Hwang, and M. Liyanage, "Survey on 6G frontiers: Trends, applications, requirements, technologies and future research," *IEEE Open J. Commun. Soc.*, vol. 2, pp. 836–886, 2021.

[46] H.-J. Song, "Terahertz wireless communications: Recent developments including a prototype system for short-range data downloading," *IEEE Microw. Mag.*, vol. 22, no. 5, pp. 88–99, May 2021.

[47] T. Nagatsuma, G. Ducournau, and C. C. Renaud, "Advances in terahertz communications accelerated by photonics," *Nature Photon.*, vol. 10, pp. 371–379, Jun. 2016.

[48] J. Faist, F. Capasso, D. L. Sivco, C. Sirtori, A. L. Hutchinson, and A. Y. Cho, "Quantum cascade laser," *Science*, vol. 264, no. 5158, pp. 553–556, 1994.

[49] H. J. Song, K. Ajito, Y. Muramoto, A. Wakatsuki, T. Nagatsuma, and N. Kukutsu, "Uni-travelling-carrier photodiode module generating 300 GHz power greater than 1 mW," *IEEE Microw. Wireless Compon. Lett.*, vol. 22, no. 7, pp. 363–365, Jul. 2012.

[50] E. S. Lima, N. Andriolli, E. Conforti, G. Contestabile, and A. C. Sodre, "Low-phase-noise tenfold frequency multiplication based on integrated optical frequency combs," *IEEE Photon. Technol. Lett.*, vol. 34, no. 16, pp. 878–881, Aug. 15, 2022.

[51] G. Danion, C. Hamel, L. Frein, F. Bondu, G. Loas, and M. Alouini, "Dual frequency laser with two continuously and widely tunable frequencies for optical referencing of GHz to THz beatnotes," *Opt. Exp.*, vol. 22, no. 15, pp. 17673–17678, 2014.

[52] Q. Lu, F. Wang, D. Wu, S. Slivken, and M. Razeghi, "Room temperature terahertz semiconductor frequency comb," *Nature Commun.*, vol. 10, no. 1, pp. 1–7, Jun. 2019.

[53] E. S. Lima, R. M. Borges, N. Andriolli, E. Conforti, G. Contestabile, and A. C. Sodré, "Integrated optical frequency comb for 5G NR Xhauls," *Sci. Rep.*, vol. 12, no. 1, p. 16421, Sep. 2022.

[54] L. Lei, J. L. Hesler, H. Xu, A. W. Lichtenberger, and R. M. Weikle, "A broadband quasi-optical terahertz detector utilizing a zero bias Schottky diode," *IEEE Microw. Wireless Compon. Lett.*, vol. 20, no. 9, pp. 504–506, Sep. 2010.

[55] G. Ducournau, Y. Yoshimizu, S. Hisatake, F. Pavanello, E. Peytavit, M. Zaknoune, T. Nagatsuma, and J.-F. Lampin, "Coherent THz communication at 200 GHz using a frequency comb, UTC-PD and electronic detection," *Electron. Lett.*, vol. 50, no. 5, pp. 386–388, 2014.

[56] B. S. Williams, "Terahertz quantum-cascade lasers," *Nature Photon.*, vol. 1, no. 9, pp. 517–525, 2007.

[57] J. M. Jornet and I. F. Akyildiz, "Graphene-based plasmonic nano-transceiver for terahertz band communication," in *Proc. 8th Eur. Conf. Antennas Propag. (EuCAP)*, Apr. 2014, pp. 492–496.

[58] L. Zhang, X. Pang, S. Jia, S. Wang, and X. Yu, "Beyond 100 Gb/s opto-electronic terahertz communications: Key technologies and directions," *IEEE Commun. Mag.*, vol. 58, no. 11, pp. 34–40, Nov. 2020.

[59] D. Cimbri, J. Wang, A. Al-Khalidi, and E. Wasige, "Resonant tunnelling diodes high-speed terahertz wireless communications—A review," *IEEE Trans. THz Sci. Technol.*, vol. 12, no. 3, pp. 226–244, May 2022.

[60] J. Federici and L. Moeller, "Review of terahertz and subterahertz wireless communications," *J. Appl. Phys.*, vol. 107, no. 11, Jun. 2010, Art. no. 111101.

[61] P. Rodríguez-Vázquez, J. Grzyb, B. Heinemann, and U. R. Pfeiffer, "A 16-QAM 100-Gb/s 1-M wireless link with an EVM of 17% at 230 GHz in an SiGe technology," *IEEE Microw. Wireless Compon. Lett.*, vol. 29, no. 4, pp. 297–299, Apr. 2019.

[62] K. M. Leong, X. Mei, W. H. Yoshida, A. Zamora, J. G. Padilla, B. S. Gorospe, K. Nguyen, and W. R. Deal, "850 GHz receiver and transmitter front-ends using InP HEMT," *IEEE Trans. THz Sci. Technol.*, vol. 7, no. 4, pp. 466–475, Jul. 2017.

[63] R. Lai, X. B. Mei, W. R. Deal, W. Yoshida, Y. M. Kim, P. H. Liu, J. Lee, J. Uyeda, V. Radisic, M. Lange, T. Gaier, L. Samoska, and A. Fung, "Sub 50 nm InP HEMT device with Fmax greater than 1 THz," in *IEDM Tech. Dig.*, Dec. 2007, pp. 609–611.

[64] V. Radisic, D. Scott, S. Wang, A. Cavus, A. Gutierrez-Aitken, and W. R. Deal, "235 GHz amplifier using 150 nm InP HBT high power density transistor," *IEEE Microw. Wireless Compon. Lett.*, vol. 21, no. 6, pp. 335–337, Jun. 2011.

[65] Y. Yashchyshyn, K. Derzakowski, G. Bogdan, K. Godziszewski, D. Nyzovets, C. H. Kim, and B. Park, "28 GHz switched-beam antenna based on S-PIN diodes for 5G mobile communications," *IEEE Antennas Wireless Propag. Lett.*, vol. 17, no. 2, pp. 225–228, Feb. 2018.

[66] C. Mao, M. Khalily, P. Xiao, T. W. C. Brown, and S. Gao, "Planar sub-millimeter-wave array antenna with enhanced gain and reduced sidelobes for 5G broadcast applications," *IEEE Trans. Antennas Propag.*, vol. 67, no. 1, pp. 160–168, Jan. 2019.

[67] X. Wang, Y. Cheng, and Y. Dong, "A wideband PCB-stacked air-filled Luneburg lens antenna for 5G millimeter-wave applications," *IEEE Antennas Wireless Propag. Lett.*, vol. 20, no. 3, pp. 327–331, Mar. 2021.

[68] Y. Gao, R. Ma, Y. Wang, Q. Zhang, and C. Parini, "Stacked patch antenna with dual-polarization and low mutual coupling for massive MIMO," *IEEE Trans. Antennas Propag.*, vol. 64, no. 10, pp. 4544–4549, Oct. 2016.

[69] M. V. Komandla, G. Mishra, and S. K. Sharma, "Investigations on dual slant polarized cavity-backed massive MIMO antenna panel with beamforming," *IEEE Trans. Antennas Propag.*, vol. 65, no. 12, pp. 6794–6799, Dec. 2017.

[70] X. Yang, W. Lu, N. Wang, K. Nieman, C.-K. Wen, C. Zhang, S. Jin, X. Mu, I. Wong, Y. Huang, and X. You, "Design and implementation of a TDD-based 128-antenna massive MIMO prototype system," *China Commun.*, vol. 14, no. 12, pp. 162–187, 2017.

[71] Y. Hu, W. Hong, C. Yu, Y. Yu, H. Zhang, Z. Yu, and N. Zhang, "A digital multibeam array with wide scanning angle and enhanced beam gain for millimeter-wave massive MIMO applications," *IEEE Trans. Antennas Propag.*, vol. 66, no. 11, pp. 5827–5837, Nov. 2018.

[72] S. Li, Z. N. Chen, T. Li, F. H. Lin, and X. Yin, "Characterization of metasurface lens antenna for sub-6 GHz dual-polarization full-dimension massive MIMO and multibeam systems," *IEEE Trans. Antennas Propag.*, vol. 68, no. 3, pp. 1366–1377, Mar. 2020.

[73] M. Temiz, E. Alsusa, L. Danoon, and Y. Zhang, "On the impact of antenna array geometry on indoor wideband massive MIMO networks," *IEEE Trans. Antennas Propag.*, vol. 69, no. 1, pp. 406–416, Jan. 2021.

[74] Y. Aslan, A. Roederer, and A. Yarovoy, "System advantages of using large-scale aperiodic array topologies in future mm-wave 5G/6G base stations: An interdisciplinary look," *IEEE Syst. J.*, vol.16, no. 1, pp. 1239–1248, Mar. 2022.

[75] I. F. da Costa, A. Cerqueira, D. H. Spadoti, L. G. da Silva, J. A. J. Ribeiro, and S. E. Barbin, "Optically controlled reconfigurable antenna array for mm-wave applications," *IEEE Antennas Wireless Propag. Lett.*, vol. 16, pp. 2142–2145, 2017.

[76] H. R. D. Filgueiras, J. R. Kelly, P. Xiao, I. F. da Costa, and A. C. Sodré, "Wideband omnidirectional slotted-waveguide antenna array based on trapezoidal slots," *Int. J. Antennas Propag.*, vol. 2019, pp. 1–8, Oct. 2019.

[77] H. R. D. Filgueiras and A. C. Sodre, "A 64-element and dual-polarized SICL-based slot antenna array development applied to TDD massive MIMO," *IEEE Antennas Wireless Propag. Lett.*, vol. 21, no. 4, pp. 750–754, Apr. 2022.

[78] H. Q. Ngo, E. G. Larsson, and T. L. Marzetta, "Aspects of favorable propagation in massive MIMO," in *Proc. 22nd Eur. Signal Process. Conf. (EUSIPCO)*, 2014, pp. 76–80.

[79] A. C. Sodré, I. F. da Costa, R. A. D. Santos, H. R. D. Filgueiras, and D. H. Spadoti, "Waveguide-based antenna arrays for 5G networks," *Int. J. Antennas Propag.*, vol. 2018, pp. 1–10, Jan. 2018.

[80] E. C. V. Boas, H. R. D. Filgueiras, I. F. da Costa, J. A. J. Ribeiro, and A. C. Sodre, "Dual-band switched-beam antenna array for MIMO systems," *IET Microw., Antennas Propag.*, vol. 14, no. 1, pp. 82–87, Jan. 2020.

[81] E. C. V. Boas, R. Mittra, and A. C. Sodre, "A low-profile high-gain slotted waveguide antenna array with grooved structures," *IEEE Antennas Wireless Propag. Lett.*, vol. 19, no. 12, pp. 2107–2111, Dec. 2020.

[82] H. R. D. Filgueiras, E. S. Lima, T. H. Brandao, and A. Cerqueira, "5G NR FR2 femtocell coverage map using an omnidirectional twisted SWAA," *IEEE Open J. Antennas Propag.*, vol. 2, pp. 72–78, 2021.

[83] Z.-W. Miao, Z.-C. Hao, G. Q. Luo, L. Gao, J. Wang, X. Wang, and W. Hong, "140 GHz high-gain LTCC-integrated transmit-array antenna using a wideband SIW aperture-coupling phase delay structure," *IEEE Trans. Antennas Propag.*, vol. 66, no. 1, pp. 182–190, Jan. 2018.

[84] K. Dhwaj, Y. Zhao, R. A. Hadi, X. Li, F. M.-C. Chang, and T. Itoh, "A 0.55 THz on-chip substrate integrated waveguide antenna," in *Proc. 43rd Int. Conf. Infr., Millim., THz Waves (IRMMW-THz)*, Sep. 2018, pp. 1–2.

[85] C. Gu, V. Fusco, G. Gibbons, B. Sanz-Izquierdo, A. Standaert, and P. Reynaert, "A D-band 3D-printed antenna," *IEEE Trans. THz Sci. Technol.*, vol. 10, no. 5, pp. 433–442, Sep. 2020.

[86] D. Zarifi, A. Farahbakhsh, and A. U. Zaman, "A D-band center-feed linear slot array antenna based on gap waveguide," in *Proc. 13th Eur. Conf. Antennas Propag. (EUCAP)*, Mar. 2019, pp. 1–3.

[87] A. Kosogor and Y. Tikhov, "A 220–300 GHz offset dual-reflector antenna for point-to-point radio," in *Proc. 14th Eur. Conf. Antennas Propag. (EuCAP)*, Mar. 2020, pp. 1–3.

[88] A. Gomez-Torrent, M. Garcia-Vigueras, L. Le Coq, A. Mahmoud, M. Ettorre, R. Sauleau, and J. Oberhammer, "A low-profile and high-gain frequency beam steering subterahertz antenna enabled by silicon micromachining," *IEEE Trans. Antennas Propag.*, vol. 68, no. 2, pp. 672–682, Feb. 2020.

[89] Z.-W. Miao, Z.-C. Hao, Y. Wang, B.-B. Jin, J.-B. Wu, and W. Hong, "A 400-GHz high-gain quartz-based single layered folded reflectarray antenna for terahertz applications," *IEEE Trans. THz Sci. Technol.*, vol. 9, no. 1, pp. 78–88, Jan. 2019.

[90] Y.-W. Wu, Z. Jiang, and Z.-C. Hao, "A 400-GHz low cost planar leaky-wave antenna with low sidelobe level and low cross-polarization level," *IEEE Trans. THz Sci. Technol.*, vol. 10, no. 4, pp. 427–430, Jul. 2020.

[91] R. Xu, S. Gao, B. S. Izquierdo, C. Gu, P. Reynaert, A. Standaert, G. J. Gibbons, W. Bösch, M. E. Gadringer, and D. Li, "A review of broadband low-cost and high-gain low-terahertz antennas for wireless communications applications," *IEEE Access*, vol. 8, pp. 57615–57629, 2020.

[92] X. Li, L. Lin, L.-S. Wu, W.-Y. Yin, and J.-F. Mao, "A bandpass graphene frequency selective surface with tunable polarization rotation for THz applications," *IEEE Trans. Antennas Propag.*, vol. 65, no. 2, pp. 662–672, Feb. 2016.

[93] K.-M. Luk, S.-F. Zhou, Y. J. Li, F. Wu, K.-B. Ng, C.-H. Chan, and S. W. Pang, "A microfabricated low-profile wideband antenna array for terahertz communications," *Sci. Rep.*, vol. 7, pp. 1–11, Apr. 2017.

[94] Y. He, Y. Chen, L. Zhang, S.-W. Wong, and Z. N. Chen, "An overview of terahertz antennas," *China Commun.*, vol. 17, no. 7, pp. 124–165, Jul. 2020.

[95] A. A. C. Alves, M. C. Melo, J. J. Siqueira, F. Zanella, J. R. Mejia-Salazar, and C. S. Arismar, "Plasmonic nanoantennas for 6G intra/inter-chip optical-wireless communications," in *Proc. 2nd 6G Wireless Summit (6G SUMMIT)*, Mar. 2020, pp. 1–4.

[96] F. Zanella, H. R. D. Filgueiras, G. Valerio, C. A. Dartora, A. A. Mariano, and S. A. Cerqueira, "Nano-antenna modelling based on plasmonic charge distribution for THz-based 6G applications," in *Proc. 2nd 6G Wireless Summit (6G SUMMIT)*, Mar. 2020, pp. 1–4.

[97] M. C. Lemme, T. J. Echtermeyer, M. Baus, and H. Kurz, "A graphene field-effect device," *IEEE Electron Device Lett.*, vol. 28, no. 4, pp. 282–284, Apr. 2007.

[98] E. W. Hill, A. Vijayaragahvan, and K. Novoselov, "Graphene sensors," *IEEE Sensors J.*, vol. 11, no. 12, pp. 3161–3170, Dec. 2011.

[99] L. C. Alexandre, A. Linhares, G. Neto, and A. C. Sodre, "High-altitude platform stations as IMT base stations: Connectivity from the stratosphere," *IEEE Commun. Mag.*, vol. 59, no. 12, pp. 30–35, Dec. 2021.

[100] *How Many Children and Young People Have Internet Access at Home?: Estimating Digital Connectivity During the COVID-19 Pandemic*, UNICEF, New York, NY, USA, 2020.

[101] M. S. Alam, G. K. Kurt, H. Yanikomeroglu, P. Zhu, and N. D. Dao, "High altitude platform station based super macro base station constellations," *IEEE Commun. Mag.*, vol. 59, no. 1, pp. 103–109, Jan. 2021.

[102] HAPSMobile. (2020). *HAPSMobile's Sunglider Succeeds in Stratospheric Test Flight*. [Online]. Available: https://www.hapsmobile.com/en/news/press/2020/20201008_01/

[103] H. Alliance, "HAPS flight test results show path to unlock stratospheric communications," Bridging Digit. Divide Aviation Stratosphere, HAPS Alliance, White Paper, 2021.

[104] D. Zhou, S. Gao, R. Liu, F. Gao, and M. Guizani, "Overview of development and regulatory aspects of high altitude platform system," *Intell. Converged Netw.*, vol. 1, no. 1, pp. 58–78, Jun. 2020.

[105] S. Euler, X. Lin, E. Tejedor, and E. Obregon, "A primer on HIBS—High altitude platform stations as IMT base stations," 2021, *arXiv:2101.03072*.

[106] *High Altitude Platform Systems: Towers in the Skies*, GSMA, London, U.K., 2022.

[107] N. Zhang, N. Cheng, A. T. Gamage, K. Zhang, J. W. Mark, and X. Shen, "Cloud assisted HetNets toward 5G wireless networks," *IEEE Commun. Mag.*, vol. 53, no. 6, pp. 59–65, Jun. 2015.

[108] I. Chih-Lin, H. Li, J. Korhonen, J. Huang, and L. Han, "RAN revolution with NGFI (xHaul) for 5G," *J. Lightw. Technol.*, vol. 36, no. 2, pp. 541–550, Jan. 15, 2018.

[109] T. Koonen, "Indoor optical wireless systems: Technology, trends, and applications," *J. Lightw. Technol.*, vol. 36, no. 8, pp. 1459–1467, Apr. 15, 2018.

[110] Q. Yan, F. R. Yu, Q. Gong, and J. Li, "Software-defined networking (SDN) and distributed denial of service (DDoS) attacks in cloud computing environments: A survey, some research issues, and challenges," *IEEE Commun. Surveys Tuts.*, vol. 18, no. 1, pp. 602–622, 1st Quart., 2015.

[111] J. G. Herrera and J. F. Botero, "Resource allocation in NFV: A comprehensive survey," *IEEE Trans. Netw. Service Manage.*, vol. 13, no. 3, pp. 518–532, Sep. 2016.
[112] S. Badotra and S. N. Panda, "Evaluation and comparison of OpenDayLight and open networking operating system in software-defined networking," *Cluster Comput.*, vol. 23, no. 2, pp. 1281–1291, Jun. 2020.
[113] Z. K. Khattak, M. Awais, and A. Iqbal, "Performance evaluation of OpenDaylight SDN controller," in *Proc. 20th IEEE Int. Conf. Parallel Distrib. Syst. (ICPADS)*, Dec. 2014, pp. 671–676.
[114] F. Hu, Q. Hao, and K. Bao, "A survey on software-defined network and OpenFlow: From concept to implementation," *IEEE Commun. Surveys Tuts.*, vol. 16, no. 4, pp. 2181–2206, 4th Quart., 2014.
[115] D. Pliatsios, P. Sarigiannidis, S. Goudos, and G. K. Karagiannidis, "Realizing 5G vision through cloud RAN: Technologies, challenges, and trends," *EURASIP J. Wireless Commun. Netw.*, vol. 2018, no. 1, pp. 1–15, Dec. 2018.
[116] S. Sun, M. Kadoch, L. Gong, and B. Rong, "Integrating network function virtualization with SDR and SDN for 4G/5G networks," *IEEE Netw.*, vol. 29, no. 3, pp. 54–59, May/Jun. 2015.
[117] T. Ismail and H. H. M. Mahmoud, "Optimum functional splits for optimizing energy consumption in V-RAN," *IEEE Access*, vol. 8, pp. 194333–194341, 2020.
[118] A. A. Barakabitze and R. Walshe, "SDN and NFV for QoE-driven multimedia services delivery: The road towards 6G and beyond networks," *Comput. Netw.*, vol. 214, Sep. 2022, Art. no. 109133.
[119] A. Gudipati, D. Perry, L. E. Li, and S. Katti, "SoftRAN: Software defined radio access network," in *Proc. 2nd ACM SIGCOMM Workshop Hot Topics Softw. Defined Netw.*, Aug. 2013, pp. 25–30.
[120] I. F. Akyildiz, P. Wang, and S.-C. Lin, "SoftAir: A software defined networking architecture for 5G wireless systems," *Comput. Netw.*, vol. 85, pp. 1–18, Jul. 2015.
[121] K. Sundaresan, M. Y. Arslan, S. Singh, S. Rangarajan, and S. V. Krishnamurthy, "FluidNet: A flexible cloud-based radio access network for small cells," in *Proc. 19th Annu. Int. Conf. Mobile Comput. Netw.*, 2013, pp. 99–110.
[122] C.-Y. Chang, N. Nikaein, R. Knopp, T. Spyropoulos, and S. S. Kumar, "FlexCRAN: A flexible functional split framework over Ethernet fronthaul in cloud-RAN," in *Proc. IEEE Int. Conf. Commun. (ICC)*, May 2017, pp. 1–7.
[123] A. Garcia-Saavedra and X. Costa-Perez, "O-RAN: Disrupting the virtualized RAN ecosystem," *IEEE Commun. Standards Mag.*, vol. 5, no. 4, pp. 96–103, Dec. 2021.
[124] T. Pfeiffer, "Next generation mobile fronthaul and midhaul architectures," *J. Opt. Commun. Netw.*, vol. 7, no. 11, p. B38, 2015.
[125] S. Iezekiel, *Microwave Photonics: Devices and Applications*. Hoboken, NJ, USA: Wiley, 2009.
[126] L. Li, M. Bi, H. Xin, Y. Zhang, Y. Fu, X. Miao, A. M. Mikaeil, and W. Hu, "Enabling flexible link capacity for eCPRI-based fronthaul with load-adaptive quantization resolution," *IEEE Access*, vol. 7, pp. 102174–102185, 2019.
[127] A. Checko, H. L. Christiansen, Y. Yan, L. Scolari, G. Kardaras, M. S. Berger, and L. Dittmann, "Cloud RAN for mobile networks—A technology overview," *IEEE Commun. surveys Tuts.*, vol. 17, no. 1, pp. 405–426, 1st Quart., 2014.
[128] *100GbE CPRI QSFP28 MMF Transceiver*, MMA1B00-C100C-Datasheet, Mellanox Technologies, Sunnyvale, CA, USA, 2018.
[129] X. Zhang, D. Shen, and T. Liu, "Review of linearization techniques for fiber-wireless systems," in *Proc. IEEE Int. Wireless Symp. (IWS)*, Mar. 2014, pp. 1–4.
[130] S. Yao, Y.-W. Chen, S.-J. Su, Y. Alfadhli, S. Shen, R. Zhang, Q. Zhou, and C. Hang, "Non-orthogonal uplink services through co-transport of D-RoF/A-RoF in mobile fronthaul," *J. Lightw. Technol.*, vol. 38, no. 14, pp. 3637–3643, Mar. 12, 2020.
[131] S. Shen, J.-H. Yan, P.-C. Peng, C.-W. Hsu, Q. Zhou, S. Liu, S. Yao, R. Zhang, K.-M. Feng, J. Finkelstein, and G.-K. Chang, "Polarization-tracking-free PDM supporting hybrid digital-analog transport for fixed-mobile systems," *IEEE Photon. Technol. Lett.*, vol. 31, no. 1, pp. 54–57, Jan. 1, 2018.
[132] X. Hu, C. Ye, and K. Zhang, "Converged mobile fronthaul and passive optical network based on hybrid analog-digital transmission scheme," in *Proc. Opt. Fiber Commun. Conf.*, 2016, pp. 3–5.
[133] C. Browning, A. Farhang, A. Saljoghei, N. Marchetti, V. Vujicic, L. E. Doyle, and L. P. Barry, "5G wireless and wired convergence in a passive optical network using UF-OFDM and GFDM," in *Proc. IEEE Int. Conf. Commun. Workshops (ICC Workshops)*, May 2017, pp. 386–392.
[134] N. Argyris, G. Giannoulis, K. Kanta, N. Iliadis, C. Vagionas, S. Papaioannou, G. Kalfas, D. Apostolopoulos, C. Caillaud, H. Debregeas, N. Pleros, and H. Avramopoulos, "A 5G mmWave fiber-wireless IFoF analog mobile fronthaul link with up to 24-Gb/s multiband wireless capacity," *J. Lightw. Technol.*, vol. 37, no. 12, pp. 2883–2891, Jun. 15, 2019.
[135] M. Morant, A. Trinidad, E. Tangdiongga, T. Koonen, and R. Llorente, "Experimental demonstration of mm-wave 5G NR photonic beamforming based on ORRs and multicore fiber," *IEEE Trans. Microw. Theory Techn.*, vol. 67, no. 7, pp. 2928–2935, Jul. 2019.
[136] M. Sung, S.-H. Cho, J. Kim, J. K. Lee, J. H. Lee, and H. S. Chung, "Demonstration of IFoF-based mobile fronthaul in 5G prototype with 28-GHz millimeter wave," *J. Lightw. Technol.*, vol. 36, no. 2, pp. 601–609, Jan. 15, 2018.
[137] Z. Cao, X. Zhao, F. M. Soares, N. Tessema, and A. M. J. Koonen, "38-GHz millimeter wave beam steered fiber wireless systems for 5G indoor coverage: Architectures, devices, and links," *IEEE J. Quantum Electron.*, vol. 53, no. 1, pp. 1–9, Feb. 2017.
[138] P. T. Dat, F. Rottenberg, A. Kanno, N. Yamamoto, and T. Kawanishi, "3×3 MIMO fiber–wireless system in W-band with WDM/PDM RoF transmission capability," *J. Lightw. Technol.*, vol. 39, no. 24, pp. 7794–7803, Dec. 15, 2021.
[139] A. O. Mufutau, F. P. Guiomar, M. A. Fernandes, A. Lorences-Riesgo, A. Oliveira, and P. P. Monteiro, "Demonstration of a hybrid optical fiber–wireless 5G fronthaul coexisting with end-to-end 4G networks," *J. Opt. Commun. Netw.*, vol. 12, no. 3, pp. 72–78, 2020.
[140] K. Kanta, A. Pagano, E. Ruggeri, M. Agus, I. Stratakos, R. Mercinelli, C. Vagionas, P. Toumasis, G. Kalfas, G. Giannoulis, A. Miliou, G. Lentaris, D. Apostolopoulos, N. Pleros, D. Soudris, and H. Avramopoulos, "Analog fiber-wireless downlink transmission of IFoF/mmWave over in-field deployed legacy PON infrastructure for 5G fronthauling," *J. Opt. Commun. Netw.*, vol. 12, no. 10, p. D57, 2020.
[141] E. S. Lima, R. M. Borges, L. A. M. Pereira, H. R. D. Filgueiras, A. M. Alberti, and A. C. Sodre, "Multiband and photonically amplified fiber-wireless Xhaul," *IEEE Access*, vol. 8, pp. 44381–44390, 2020.
[142] L. C. D. Souza, E. S. Lima, and A. C. S. Junior, "Implementation of a full optically-powered 5G NR fiber-wireless system," *IEEE Photon. J.*, vol. 14, no. 1, pp. 1–8, Feb. 2022.
[143] M. Xu, F. Lu, J. Wang, L. Cheng, D. Guidotti, and G.-K. Chang, "Key technologies for next-generation digital RoF mobile fronthaul with statistical data compression and multiband modulation," *J. Lightw. Technol.*, vol. 35, no. 17, pp. 3671–3679, Sep. 15, 2017.
[144] M. Noweir, Q. Zhou, A. Kwan, R. Valivarthi, M. Helaoui, W. Tittel, and F. M. Ghannouchi, "Digitally linearized radio-over fiber transmitter architecture for cloud radio access network's downlink," *IEEE Trans. Microw. Theory Techn.*, vol. 66, no. 7, pp. 3564–3574, 2018.
[145] X. Zhang, "Broadband linearization for 5G fronthaul transmission," *Frontiers Optoelectron.*, vol. 11, no. 2, pp. 107–115, Jun. 2018.
[146] I. Romdhane and G. Kaddoum, "A reinforcement-learning-based beam adaptation for underwater optical wireless communications," *IEEE Internet Things J.*, vol. 9, no. 20, pp. 20270–20281, Oct. 2022.
[147] T. Q. Duong, J. A. Ansere, B. Narottama, V. Sharma, O. A. Dobre, and H. Shin, "Quantum-inspired machine learning for 6G: Fundamentals, security, resource allocations, challenges, and future research directions," *IEEE Open J. Veh. Technol.*, vol. 3, pp. 375–387, 2022.
[148] L. A. M. Pereira, L. L. Mendes, and C. J. A. Bastos-Filho, "Machine learning-based linearization schemes for radio over fiber systems," *IEEE Photon. J.*, vol. 14, no. 6, pp. 1–10, Dec. 2022.
[149] S. Liu, X. Wang, W. Zhang, G. Shen, and H. Tian, "An adaptive activated ANN equalizer applied in millimeter-wave RoF transmission system," *IEEE Photon. Technol. Lett.*, vol. 29, no. 22, pp. 1935–1938, Nov. 15, 2017.
[150] E. Liu, Z. Yu, C. Yin, and K. Xu, "Nonlinear distortions compensation based on artificial neural networks in wideband and multi-carrier systems," *IEEE J. Quantum Electron.*, vol. 55, no. 5, pp. 1–5, Oct. 2019.
[151] L. A. M. Pereira, L. L. Mendes, C. J. A. Bastos-Filho, and S. A. Cerqueira, "Linearization schemes for radio over fiber systems based on machine learning algorithms," *IEEE Photon. Technol. Lett.*, vol. 34, no. 5, pp. 279–282, Mar. 1, 2022.

[152] H. Henniger and O. Wilfert, "An introduction to free-space optical communications," *Radioengineering*, vol. 19, no. 2, pp. 1–10, 2010.

[153] S. A. Al-Gailani, A. B. Mohammad, and R. Q. Shaddad, "Enhancement of free space optical link in heavy rain attenuation using multiple beam concept," *Optik*, vol. 124, no. 21, pp. 4798–4801, Nov. 2013.

[154] A. Jahid, M. H. Alsharif, and T. J. Hall, "A contemporary survey on free space optical communication: Potentials, technical challenges, recent advances and research direction," *J. Netw. Comput. Appl.*, vol. 200, Apr. 2022, Art. no. 103311.

[155] S. Bloom, E. Korevaar, J. Schuster, and H. Willebrand, "Understanding the performance of free-space optics," *J. Opt. Netw.*, vol. 2, pp. 178–200, Jun. 2003.

[156] Y. Kaymak, R. Rojas-Cessa, J. Feng, N. Ansari, M. Zhou, and T. Zhang, "A survey on acquisition, tracking, and pointing mechanisms for mobile free-space optical communications," *IEEE Commun. Surveys Tuts.*, vol. 20, no. 2, pp. 1104–1123, 2nd Quart., 2018.

[157] X. Liu, "Free-space optics optimization models for building sway and atmospheric interference using variable wavelength," *IEEE Trans. Commun.*, vol. 57, no. 2, pp. 492–498, Feb. 2009.

[158] S. A. Al-Gailani, M. F. M. Salleh, A. A. Salem, R. Q. Shaddad, U. U. Sheikh, N. A. Algeelani, and T. A. Almohamad, "A survey of free space optics (FSO) communication systems, links, and networks," *IEEE Access*, vol. 9, pp. 7353–7373, 2021.

[159] E. Leitgeb, M. S. Awan, P. Brandl, T. Plank, C. Capsoni, R. Nebuloni, and T. Javornik, "Current optical technologies for wireless access," in *Proc. 10th Int. Conf. Telecommun.*, 2009, pp. 7–17.

[160] M. A. Khalighi and M. Uysal, "Survey on free space optical communication: A communication theory perspective," *IEEE Commun. Surveys Tuts.*, vol. 16, no. 4, pp. 2231–2258, 4th Quart., 2014.

[161] J. Bohata, M. Komanec, J. Spacil, Z. Ghassemlooy, S. Zvanovec, and R. Slavik, "24–26 GHz radio-over-fiber and free-space optics for fifth-generation systems," *Opt. Lett.*, vol. 43, no. 5, pp. 1035–1038, 2018.

[162] M. A. Esmail, A. M. Ragheb, H. A. Fathallah, M. Altamimi, and S. A. Alshebeili, "5G-28 GHz signal transmission over hybrid all-optical FSO/RF link in dusty weather conditions," *IEEE Access*, vol. 7, pp. 24404–24410, 2019.

[163] L. Vallejo, M. Komanec, B. Ortega, J. Bohata, D.-N. Nguyen, S. Zvanovec, and V. Almenar, "Impact of thermal-induced turbulent distribution along FSO link on transmission of photonically generated mmW signals in the frequency range 26–40 GHz," *IEEE Photon. J.*, vol. 12, no. 1, pp. 1–9, Feb. 2020.

[164] P. T. Dat, A. Kanno, K. Inagaki, F. Rottenberg, J. Louveaux, N. Yamamoto, and T. Kawanishi, "High-speed radio-on-free-space optical mobile fronthaul system for ultra-dense radio access network," in *Proc. Opt. Fiber Commun. Conf. (OFC)*, 2020, pp. 1–3.

[165] D.-N. Nguyen, L. Vallejo, V. Almenar, B. Ortega, P. T. Dat, S. T. Le, J. Bohata, and S. Zvanovec, "Full-duplex transmission of multi-Gb/s subcarrier multiplexing and 5G NR signals in 39 GHz band over fiber and space," *Appl. Opt.*, vol. 61, no. 5, pp. 1183–1193, 2022.

[166] C. H. D. S. Lopes, E. S. Lima, L. A. M. Pereira, R. M. Borges, A. C. Ferreira, M. Abreu, W. D. Dias, D. H. Spadoti, L. L. Mendes, and A. C. S. Junior, "Non-standalone 5G NR fiber-wireless system using FSO and fiber-optics fronthauls," *J. Lightw. Technol.*, vol. 39, no. 2, pp. 406–417, Jan. 15, 2021.

[167] A. Jovicic, J. Li, and T. Richardson, "Visible light communication: Opportunities, challenges and the path to market," *IEEE Commun. Mag.*, vol. 51, no. 12, pp. 26–32, Dec. 2013.

[168] A.-M. C ilean and M. Dimian, "Current challenges for visible light communications usage in vehicle applications: A survey," *IEEE Commun. Surveys Tuts.*, vol. 19, no. 4, pp. 2681–2703, 4th Quart., 2017.

[169] P. H. Pathak, X. Feng, P. Hu, and P. Mohapatra, "Visible light communication, networking, and sensing: A survey, potential and challenges," *IEEE Commun. Surveys Tuts.*, vol. 17, no. 4, pp. 2047–2077, 4th Quart., 2015.

[170] A. T. Hussein, M. T. Alresheedi, and J. M. H. Elmirghani, "20 Gb/s mobile indoor visible light communication system employing beam steering and computer generated holograms," *J. Lightw. Technol.*, vol. 33, no. 24, pp. 5242–5260, Dec. 15, 2015.

[171] H. Chun, S. Rajbhandari, G. Faulkner, D. Tsonev, E. Xie, J. J. D. McKendry, E. Gu, M. D. Dawson, D. C. O'Brien, and H. Haas, "LED based wavelength division multiplexed 10 Gb/s visible light communications," *J. Lightw. Technol.*, vol. 34, no. 13, pp. 3047–3052, Jul. 15, 2016.

[172] H. Sifaou, A. Kammoun, K.-H. Park, and M.-S. Alouini, "Robust transceivers design for multi-stream multi-user MIMO visible light communication," *IEEE Access*, vol. 5, pp. 26387–26399, 2017.

[173] R. K. Vs and I. B. Djordjevic, "MIMO-WDM visible light communications based on commercial RGBA LEDs," in *Proc. 20th Int. Conf. Transparent Opt. Netw. (ICTON)*, Jul. 2018, pp. 1–5.

[174] C. E. Mejia and C. N. Georghiades, "Coding for visible light communication using color-shift keying constellations," *IEEE Trans. Commun.*, vol. 67, no. 7, pp. 4955–4966, Jul. 2019.

[175] L. C. Mathias, J. C. M. Filho, and T. Abrao, "Predistortion and pre-equalization for nonlinearities and low-pass effect mitigation in OFDM-VLC systems," *Appl. Opt.*, vol. 58, no. 19, pp. 5328–5338, Jul. 2019. [Online]. Available: http://opg.optica.org/ao/abstract.cfm?URI=ao-58-19-5328

[176] Z. Na, Y. Wang, M. Xiong, X. Liu, and J. Xia, "Modeling and throughput analysis of an ADO-OFDM based relay-assisted VLC system for 5G networks," *IEEE Access*, vol. 6, pp. 17586–17594, 2018.

[177] S. Baig, H. Muhammad, S. Mumtaz, M. Shafiq, J.-G. Choi, and T. Umer, "High data rate discrete wavelet transform-based PLC-VLC design for 5G communication systems," *IEEE Access*, vol. 6, pp. 52490–52499, 2018.

[178] A. M. Vegni and M. Biagi, "Optimal LED placement in indoor VLC networks," *Opt. Exp.*, vol. 27, no. 6, pp. 8504–8519, Mar. 2019. [Online]. Available: http://opg.optica.org/oe/abstract.cfm?URI=oe-27-6-8504

[179] H.-H. Chou and C.-Y. Tsai, "Demonstration of micro-projection enabled short-range communications for 5G," in *Proc. 21st OptoElectron. Commun. Conf. (OECC) Int. Conf. Photon. Switching (PS)*, 2016, pp. 1–3.

[180] L. Shi, W. Li, X. Zhang, Y. Zhang, G. Chen, and A. Vladimirescu, "Experimental 5G new radio integration with VLC," in *Proc. 25th IEEE Int. Conf. Electron., Circuits Syst. (ICECS)*, Dec. 2018, pp. 61–64.

[181] S. P. Valluri, V. Kishore, and V. M. Vakamulla, "A new selective mapping scheme for visible light systems," *IEEE Access*, vol. 8, pp. 18087–18096, 2020.

[182] F. T. Monteiro, W. S. Costa, J. L. C. Neves, D. M. I. Silva, H. R. O. Rocha, E. O. T. Salles, and J. A. L. Silva, "Experimental evaluation of pulse shaping based 5G multicarrier modulation formats in visible light communication systems," *Opt. Commun.*, vol. 457, Feb. 2020, Art. no. 124693. [Online]. Available: https://www.sciencedirect.com/science/article/pii/S0030401819308946

[183] M. A. de Oliveira, E. S. Lima, M. S. P. Cunha, and M. Abreu, "RGB-based VLC system using 5G NR standard," *Opt. Commun.*, vol. 481, Feb. 2021, Art. no. 126542. [Online]. Available: https://www.sciencedirect.com/science/article/pii/S0030401820309603

[184] N. Chi, *LED-Based Visible Light Communications*. Cham, Switzerland: Springer, 2018.

[185] J. Grubor, S. Randel, K.-D. Langer, and J. W. Walewski, "Broadband information broadcasting using LED-based interior lighting," *IEEE J. Lightw. Technol.*, vol. 26, no. 24, pp. 3883–3892, Dec. 15, 2009.

[186] D. Karunatilaka, F. Zafar, V. Kalavally, and R. Parthiban, "LED based indoor visible light communications: State of the art," *IEEE Commun. Surveys Tuts.*, vol. 17, no. 3, pp. 1649–1678, 3rd Quart., 2015.

[187] L.-Y. Wei, Y. Liu, C.-W. Chow, G.-H. Chen, C.-W. Peng, P.-C. Guo, J.-F. Tsai, and C.-H. Yeh, "6.915-Gbit/s white-light phosphor laser diode-based DCO-OFDM visible light communication (VLC) system with functional transmission distance," *Electron. Lett.*, vol. 56, no. 18, pp. 945–947, Sep. 2020.

[188] O. Alsulami, A. T. Hussein, M. T. Alresheedi, and J. M. H. Elmirghani, "Optical wireless communication systems, a survey," 2018, *arXiv:1812.11544*.

[189] L. E. M. Matheus, A. B. Vieira, L. F. Vieira, M. A. Vieira, and O. Gnawali, "Visible light communication: Concepts, applications and challenges," *IEEE Commun. Surveys Tuts.*, vol. 21, no. 4, pp. 3204–3237, 4th Quart., 2019.

[190] G. Pan, H. Lei, Z. Ding, and Q. Ni, "3-D hybrid VLC-RF indoor IoT systems with light energy harvesting," *IEEE Trans. Green Commun. Netw.*, vol. 3, no. 3, pp. 853–865, Sep. 2019.

[191] Z. Huang and Y. Ji, "Design and demonstration of room division multiplexing-based hybrid VLC network," *Chin. Opt. Lett.*, vol. 11, no. 6, 2013, Art. no. 060603.

[192] S. Shao, A. Khreishah, M. Ayyash, M. B. Rahaim, H. Elgala, V. Jungnickel, D. Schulz, T. D. Little, J. Hilt, and R. Freund, "Design and analysis of a visible-light-communication enhanced WiFi system," *J. Opt. Commun. Netw.*, vol. 7, no. 10, pp. 960–973, 2015.

[193] P. Botsinis, D. Alanis, S. Feng, Z. Babar, H. V. Nguyen, D. Chandra, S. X. Ng, R. Zhang, and L. Hanzo, "Quantum-assisted indoor localization for uplink mm-wave and downlink visible light communication systems," *IEEE Access*, vol. 5, pp. 23327–23351, 2017.

[194] M. T. Alresheedi, A. T. Hussein, and J. M. H. Elmirghani, "Uplink design in VLC systems with IR sources and beam steering," *IET Commun.*, vol. 11, no. 3, pp. 311–317, Feb. 2017.

[195] O. Z. Aletri, M. T. Alresheedi, and J. M. H. Elmirghani, "Infrared uplink design for visible light communication (VLC) systems with beam steering," in *Proc. IEEE Int. Conf. Comput. Sci. Eng. (CSE) IEEE Int. Conf. Embedded Ubiquitous Comput. (EUC)*, Aug. 2019, pp. 57–60.

[196] S. Iezekiel, M. Burla, J. Klamkin, D. Marpaung, and J. Capmany, "RF engineering meets optoelectronics: Progress in integrated microwave photonics," *IEEE Microw. Mag.*, vol. 16, no. 8, pp. 28–45, Sep. 2015.

[197] D. Marpaung, J. Yao, and J. Capmany, "Integrated microwave photonics," *Nature Photon.*, vol. 13, no. 2, pp. 80–90, Feb. 2019.

[198] W. Zhang and J. Yao, "Silicon-based integrated microwave photonics," *IEEE J. Quantum Electron.*, vol. 52, no. 1, pp. 1–12, Jan. 2016.

[199] S. Sung, E. R. Brown, W. S. Grundfest, Z. D. Taylor, S. Selvin, N. Bajwa, S. Chantra, B. Nowroozi, J. Garritano, J. Goell, A. D. Li, and S. X. Deng, "THz imaging system for in vivo human cornea," *IEEE Trans. THz Sci. Technol.*, vol. 8, no. 1, pp. 27–37, Jan. 2018.

[200] S. Movassaghi, M. Abolhasan, J. Lipman, D. Smith, and A. Jamalipour, "Wireless body area networks: A survey," *IEEE Commun. Surveys Tuts.*, vol. 16, no. 3, pp. 1658–1686, 3rd Quart., 2014.

[201] J. Yao, "Microwave photonics," *J. Lightw. Technol.*, vol. 27, no. 3, pp. 314–335, Feb. 1, 2009.

[202] J. Capmany and D. Novak, "Microwave photonics combines two worlds," *Nature Photon.*, vol. 1, no. 6, pp. 319–330, Jun. 2007.

[203] M. Smit et al., "An introduction to InP-based generic integration technology," *Semicond. Sci. Technol.*, vol. 29, no. 8, Jun. 2014, Art. no. 083001, doi: 10.1088/0268-1242/29/8/083001.

[204] T. Barwicz, Y. Taira, T. W. Lichoulas, N. Boyer, Y. Martin, H. Numata, J.-W. Nah, S. Takenobu, A. Janta-Polczynski, E. L. Kimbrell, R. Leidy, M. H. Khater, S. Kamlapurkar, S. Engelmann, Y. A. Vlasov, and P. Fortier, "A novel approach to photonic packaging leveraging existing high-throughput microelectronic facilities," *IEEE J. Sel. Topics Quantum Electron.*, vol. 22, no. 6, pp. 455–466, Nov. 2016.

[205] Z. Wang et al., "Novel light source integration approaches for silicon photonics," *Laser Photon. Rev.*, vol. 11, no. 4, 2017, Art. no. 1700063, doi: 10.1002/lpor.201700063.

[206] J. Yao and J. Capmany, "Microwave photonics," *Sci. China Inf. Sci.*, vol. 65, no. 12, pp. 1–15, Aug. 2022.

[207] D. J. Blumenthal et al., "Integrated photonics for low-power packet networking," *IEEE J. Sel. Topics Quantum Electron.*, vol. 17, no. 2, pp. 458–471, Mar. 2011.

[208] L. Augustin, M. Smit, N. Grote, M. Wale, and R. Visser, "Standardized process could revolutionize photonic integration," *Euro Photon.*, vol. 18, pp. 30–34, Sep. 2013.

[209] P. Kaur, A. Boes, G. Ren, T. G. Nguyen, G. Roelkens, and A. Mitchell, "Hybrid and heterogeneous photonic integration," *APL Photon.*, vol. 6, no. 6, Jun. 2021, Art. no. 061102, doi: 10.1063/5.0052700.

[210] S. Zeng, X. Zhao, L. Sweatt, and L. Zhu, "Photonic integrated circuits based hybrid integration for wavelength beam combining," *Opt. Lett.*, vol. 45, no. 22, pp. 6338–6341, Nov. 2020. [Online]. Available: http://www.osapublishing.org/ol/abstract.cfm?URI=ol-45-22-6338

[211] Z. Zhang et al., "Hybrid photonic integration on a polymer platform," *Photonics*, vol. 2, no. 3, pp. 1005–1026, Sep. 2015.

[212] M. Smit, X. Leijtens, E. Bente, J. Tol, H. Ambrosius, D. Robbins, M. Wale, N. Grote, and M. Schell, "Generic foundry model for InP-based photonics," *IET Optoelectron.*, vol. 5, no. 5, pp. 187–194, 2011.

[213] F. M. Soares, M. Baier, T. Gaertner, N. Grote, M. Moehrle, T. Beckerwerth, P. Runge, and M. Schell, "InP-based foundry PICs for optical interconnects," *Appl. Sci.*, vol. 9, no. 8, p. 1588, Apr. 2019. [Online]. Available: https://www.mdpi.com/2076-3417/9/8/1588

[214] G. N. Tzintzarov, S. G. Rao, and J. D. Cressler, "Integrated silicon photonics for enabling next-generation space systems," *Photonics*, vol. 8, no. 4, p. 131, Apr. 2021. [Online]. Available: https://www.mdpi.com/2304-6732/8/4/131

[215] A. Ayazi, T. Baehr-Jones, Y. Liu, A. E.-J. Lim, and M. Hochberg, "Linearity of silicon ring modulators for analog optical links," *Opt. Exp.*, vol. 20, no. 12, pp. 13115–13122, Jun. 2012. [Online]. Available: http://www.osapublishing.org/oe/abstract.cfm?URI=oe-20-12-13115

[216] K. Shang, S. Pathak, C. Qin, and S. J. B. Yoo, "Low-loss compact silicon nitride arrayed waveguide gratings for photonic integrated circuits," *IEEE Photon. J.*, vol. 9, no. 5, pp. 1–5, Oct. 2017.

[217] S. Gundavarapu, M. Belt, T. A. Huffman, M. A. Tran, T. Komljenovic, J. E. Bowers, and D. J. Blumenthal, "Interferometric optical gyroscope based on an integrated Si_3N_4 low-loss waveguide coil," *J. Lightw. Technol.*, vol. 36, no. 4, pp. 1185–1191, Feb. 15, 2018.

[218] M. Li, J. Ling, Y. He, U. A. Javid, S. Xue, and Q. Lin, "Lithium niobate photonic-crystal electro-optic modulator," *Nature Commun.*, vol. 11, no. 1, p. 4123, Aug. 2020.

[219] S. Sun, M. He, M. Xu, S. Gao, S. Yu, and X. Cai, "Hybrid silicon and lithium niobate modulator," *IEEE J. Sel. Topics Quantum Electron.*, vol. 27, no. 3, pp. 1–12, May 2021.

[220] S. Yokoyama, G.-W. Lu, X. Cheng, and F. Qiu, "Long-term stable electro-optic polymer for hybrid integration," in *Proc. Opt. Fiber Commun. Conf. (OFC)*, 2019, pp. 1–4.

[221] D. de Felipe, M. Kleinert, C. Zawadzki, A. Polatynski, G. Irmscher, W. Brinker, M. Moehrle, H. G. Bach, N. Keil, and M. Schell, "Recent developments in polymer-based photonic components for disruptive capacity upgrade in data centers," *J. Lightw. Technol.*, vol. 35, no. 4, pp. 683–689, Sep. 16, 2016.

[222] S. Nellen, S. Lauck, E. Peytavit, P. Szriftgiser, M. Schell, G. Ducournau, and B. Globisch, "Coherent wireless link at 300 GHz with 160 Gbit/s enabled by a photonic transmitter," *J. Lightw. Technol.*, vol. 40, no. 13, pp. 4178–4185, Jul. 1, 2022.

[223] S. Jia, M.-C. Lo, L. Zhang, O. Ozolins, A. Udalcovs, D. Kong, X. Pang, R. Guzman, X. Yu, S. Xiao, S. Popov, J. Chen, G. Carpintero, T. Morioka, H. Hu, and L. K. Oxenløwe, "Integrated dual-laser photonic chip for high-purity carrier generation enabling ultrafast terahertz wireless communications," *Nature Commun.*, vol. 13, no. 1, pp. 1–8, Mar. 2022.

[224] M. Burla, D. A. I. Marpaung, L. Zhuang, M. R. Khan, A. Leinse, W. Beeker, M. Hoekman, R. G. Heideman, and C. G. H. Roeloffzen, "Multiwavelength-integrated optical beamformer based on wavelength division multiplexing for 2-D phased array antennas," *J. Lightw. Technol.*, vol. 32, no. 20, pp. 3509–3520, Jun. 23, 2014.

[225] D. J. Kebort, G. B. Morrison, H. Garrett, J. N. Campbell, S. B. Estrella, R. H. Banholzer, J. B. Sherman, L. A. Johansson, D. Renner, and M. L. Mashanovitch, "Monolithic four-channel (QUAD) integrated widely tunable transmitter in indium phosphide," *IEEE J. Sel. Topics Quantum Electron.*, vol. 24, no. 1, pp. 1–7, Jan. 2018.

[226] W. Yao, B. Smalbrugge, M. K. Smit, K. A. Williams, and M. J. Wale, "A 6 × 30 Gb/s tunable transmitter PIC with low RF crosstalk from an open-access InP foundry," *IEEE J. Sel. Topics Quantum Electron.*, vol. 25, no. 5, pp. 1–10, Sep. 2019.

[227] S. H. Oh, O. K. Kwon, K. S. Kim, Y. T. Han, C. W. Lee, Y. A. Leem, J. W. Shin, and E. S. Nam, "A multi-channel etched-mesa PBH DFB laser array using an SAG technique," *IEEE Photon. Technol. Lett.*, vol. 27, no. 24, pp. 2567–2570, Dec. 15, 2015.

[228] S. Kanazawa, W. Kobayashi, Y. Ueda, T. Fujisawa, K. Takahata, T. Ohno, T. Yoshimatsu, H. Ishii, and H. Sanjoh, "30-km error-free transmission of directly modulated DFB laser array transmitter optical sub-assembly for 100-Gb application," *J. Lightw. Technol.*, vol. 34, no. 15, pp. 3646–3652, Aug. 1, 2016.

[229] N. Andriolli, P. Velha, M. Chiesa, A. Trifiletti, and G. Contestabile, "A directly modulated multiwavelength transmitter monolithically integrated on InP," *IEEE J. Sel. Topics Quantum Electron.*, vol. 24, no. 1, pp. 1–6, Jan. 2018.

[230] C. Liu, J. Wang, L. Cheng, M. Zhu, and G.-K. Chang, "Key microwave-photonics technologies for next-generation cloud-based radio access networks," *J. Lightw. Technol.*, vol. 32, no. 20, pp. 3452–3460, Oct. 15, 2014.

[231] M. S. B. Cunha, E. S. Lima, N. Andriolli, D. H. Spadoti, G. Contestabile, and A. Cerqueira, "5G NR RoF system based on a monolithically integrated multi-wavelength transmitter," *IEEE J. Sel. Topics Quantum Electron.*, vol. 27, no. 2, pp. 1–8, Mar. 2021.

[232] M. S. B. Cunha, E. S. Lima, N. Andriolli, D. H. Spadoti, G. Contestabile, and A. Cerqueira, "Non-standalone 5G NR FiWi system based on a photonic integrated multi-wavelength transmitter," *IEEE Wireless Commun. Lett.*, vol. 10, no. 5, pp. 1001–1004, May 2021.

[233] M. S. B. Cunha, E. S. Lima, N. Andriolli, D. H. Spadoti, F. B. Fidéles, G. Contestabile, and J. Oliveira, "RoF/FSO system based on a monolithically integrated multi-wavelength transmitter," in *Proc. SBFoton Int. Opt. Photon. Conf. (SBFoton IOPC)*, 2021, pp. 1–4.

[234] J.-G. Werthen, S. Widjaja, T.-C. Wu, and J. Liu, "Power over fiber: A review of replacing copper by fiber in critical applications," *Opt. Technol. Arming, Safing, Fuzing, Firing*, vol. 5871, Jan. 2005, Art. no. 58710C.
[235] J.-G. Werthen, "Powering next generation networks by laser light over fiber," in *Proc. Conf. Opt. Fiber Commun./Nat. Fiber Optic Eng. Conf.*, Feb. 2008, pp. 1–3.
[236] M. Dumke, G. Heiserich, S. Franke, L. Schulz, and L. Overmeyer, "Power transmission by optical fibers for component inherent communication," *Systemics Cybern. Informat.*, vol. 8, no. 1, pp. 55–60, 2010.
[237] M. Matsuura, "Recent advancement in power-over-fiber technologies," *Photonics*, vol. 8, no. 8, p. 335, Aug. 2021.
[238] M. Matsuura, H. Nomoto, H. Mamiya, T. Higuchi, D. Masson, and S. Fafard, "Over 40-W electric power and optical data transmission using an optical fiber," *IEEE Trans. Power Electron.*, vol. 36, no. 4, pp. 4532–4539, Apr. 2021.
[239] C. Vazquez, J. D. Lopez-Cardona, P. C. Lallana, D. S. Montero, F. M. A. Al-Zubaidi, S. Perez-Prieto, and I. P. Garcilopez, "Multicore fiber scenarios supporting power over fiber in radio over fiber systems," *IEEE Access*, vol. 7, pp. 158409–158418, 2019.
[240] M. Matsuura, N. Tajima, H. Nomoto, and D. Kamiyama, "150-W power-over-fiber using double-clad fibers," *J. Lightw. Technol.*, vol. 38, no. 2, pp. 401–408, Jan. 15, 2020.
[241] I. A. Alimi, A. M. Abdalla, A. O. Mufutau, F. P. Guiomar, I. Otung, J. Rodriguez, P. P. Monteiro, and A. L. Teixeira, "Energy efficiency in the cloud radio access network (C-RAN) for 5G mobile networks: Opportunities and challenges," in *Optical and Wireless Convergence for 5G Networks*, 2019, pp. 225–248.
[242] T. Umezawa, P. T. Dat, K. Kashima, A. Kanno, N. Yamamoto, and T. Kawanishi, "100-GHz radio and power over fiber transmission through multicore fiber using optical-to-radio converter," *J. Lightw. Technol.*, vol. 36, no. 2, pp. 617–623, Jan. 15, 2018.
[243] J. D. L. Cardona, P. Lallana, R. Altuna, A. Fresno-Hernandez, X. Barreiro, and C. Vazquez, "Optically feeding 1.75 W with 100 m MMF in efficient C-RAN front-hauls with sleep modes," *J. Lightw. Technol.*, vol. 39, no. 24, pp. 7948–7955, Dec. 15, 2021.
[244] F. M. A. Al-Zubaidi, J. D. Lopez-Cardona, D. S. Montero, and C. Vazquez, "Optically powered radio-over-fiber systems in support of 5G cellular networks and IoT," *J. Lightw. Technol.*, vol. 39, no. 13, pp. 4262–4269, Jul. 1, 2021.
[245] H. Yang, D. Peng, Y. Qin, J. Li, M. Xiang, O. Xu, and S. Fu, "10-W power light co-transmission with optically carried 5G NR signal over standard single-mode fiber," *Opt. Lett.*, vol. 46, no. 20, pp. 5116–5119, 2021.
[246] J. López-Cardona, S. Rommel, E. Grivas, D. Montero, M. Dubov, D. Kritharidis, I. Tafur-Monroy, and C. Vázquez, "Power-over-fiber in a 10 km long multicore fiber link within a 5G fronthaul scenario," *Opt. Lett.*, vol. 46, pp. 5348–5351, Nov. 2021.
[247] S. Wang, H. Yang, Y. Qin, D. Peng, and S. Fu, "Power-over-fiber in support of 5G NR fronthaul: Space division multiplexing versus wavelength division multiplexing," *J. Lightw. Technol.*, vol. 40, no. 13, pp. 4169–4177, Jul. 1, 2022.
[248] *5G Power White Paper*, Huawei Technologies Co., HiSilicon, HI, USA, 2019.
[249] *Alcatel-Lucent 9362 Enterprise Cell V2.2 2100 MHz*, Alcatel-Lucent, Colombes, France, 2012.

HUGO RODRIGUES DIAS FILGUEIRAS (Associate Member, IEEE) received the B.Sc., M.Sc., and Ph.D. degrees in telecommunications from the Laboratory Wireless and Optical Convergent Access (WOCA), National Telecommunications Institute (Inatel). He acted as a Researcher Engineer of fifth and sixth generation mobile communications networks (5G and 6G) at the Radiocommunications Reference Center (CRR), Inatel, and a Consultant at the Inatel Competence Center (ICC) Training and Consulting Team. He has a teaching experience for being a Monitor and a Professor in several subjects of the telecommunications engineering graduation by means of the Teaching Internship Program. He acts as an Invited Professor of the propagation discipline of Lato Sensu Postgraduate Courses in Network Engineering and Telecommunications Systems, Inatel. He worked on research and development projects in the area of antenna development, analysis of high-intensity radiated fields for aeronautical applications, and coexistence between IMT and satellite systems. He is currently a 5G and Information Security Innovation Manager with VS Telecom, São Paulo. He has more than 30 publications in national and international magazines and conferences of high scientific impact factor and one patent pending. His research interests include the development of antennas, propagation, mobile communication systems, digital modulation schemes and topologies of optical, and wireless access networks stand out.

EDUARDO SAIA LIMA received the B.Sc. and M.Sc. degrees in telecommunications engineering from the National Institute of Telecommunications (Inatel), Brazil, in 2017 and 2019, respectively, where he is currently pursuing the Ph.D. degree in telecommunications. Also, he acts as a Researcher with the Laboratory WOCA, Inatel. His research interest includes microwave photonics applied to 5G and 6G systems.

MATHEUS SÊDA BORSATO CUNHA received the bachelor's and master's degrees in telecommunications from the National Telecommunications Institute (Inatel), Brazil, in 2015 and 2018, respectively, and the Ph.D. degree in electrical engineering from the Federal University of Itajubá (UNIFEI), Brazil, in March 2022. Currently, he is a Research Engineer with the Radiocommunications Reference Center (CRR), Inatel. His research interests include the optical communications, microwave photonics, integrated optics, and optical wireless networks applied to fifth and sixth generation mobile communications networks (5G and 6G) stand out.

CELSO HENRIQUE DE SOUZA LOPES received the B.Sc. degree in electrical engineering from FAINOR, Brazil, in 2016, and the master's degree in telecommunications engineering from the National Institute of Telecommunications (Inatel), Brazil, in 2018, where he is currently pursuing the Ph.D. degree in telecommunications. Also, he acts as a Researcher with the Laboratory WOCA, Inatel. His research interest includes optical wireless communications applied to communication systems.

LETÍCIA CARNEIRO DE SOUZA received the B.Sc. and M.Sc. degrees in telecommunications engineering from the National Institute of Telecommunications (Inatel), Brazil, in 2020 and 2022, respectively, where she is currently pursuing the Ph.D. degree in telecommunications. Also, she acts as a Researcher with the Laboratory WOCA, Inatel. Her research interests include optical communications, mobile communication systems, wireless systems, microwave photonics, and power-over-fiber systems.

RAMON MAIA BORGES received the B.Sc. degree in electrical engineering and the M.Sc. degree in telecommunications from the National Institute of Telecommunications (Inatel), Brazil, in 2012 and 2015, respectively, and the Ph.D. degree in electrical engineering from the Federal University of Itajubá (UNIFEI), Brazil, in 2020. From 2015 to 2022, he worked as a Researcher and a Professor with Inatel, where he is acting on research and development projects at the Radiocommunications Reference Center and Brazil 6G. He is currently a Professor with UNIFEI. His research interests include embrace diverse areas of telecommunications, including 5G and 6G networks, optical-wireless systems, and microwave photonics.

LUIZ AUGUSTO MELO PEREIRA received the B.Sc. and M.Sc. degrees in telecommunications engineering from the National Institute of Telecommunications (Inatel), Brazil, in 2017 and 2020, respectively, where he is currently pursuing the Ph.D. degree in telecommunications. Also, he acts as a Researcher with the Laboratory WOCA, Inatel. His research interests include optical communications, mobile communication systems, wireless systems, microwave photonics, and machine learning-based techniques applied to communication systems.

TIAGO HENRIQUE BRANDÃO received the degree in mathematics from UNIVAS, Brazil, in 2009, and the B.Sc. and M.Sc. degrees in telecommunications engineering from Inatel, Brazil, in 2016 and 2019, respectively, where he is currently pursuing the Ph.D. degree in telecommunication. He has experience in teaching for being a Physics, Digital Transmission and Stochastics Process Tutor on undergraduate courses in the Teaching Internship Program at Inatel, from 2012 to 2018. He acted as an Antenna Developer at Ideal Antennas Company, from 2018 to 2019. Also, he acts as a Researcher with the Wireless and Optical Convergent Access (WOCA) Laboratory, Inatel. His research interests include antennas, advanced antenna systems for mobile networks, and mobile networks.

TOMÁS POWELL VILLENA ANDRADE received the B.Sc. degree in engineering physics from the National University of Engineering (UNI), Lima, Peru, and the M.Sc. degree from Unicamp, Brazil, in 2011. He is currently pursuing the Ph.D. degree in telecommunications engineering with the National Institute of Telecommunications (Inatel), Brazil. His research interests include embedded electronics, microwave photonics, and integrated photonics for telecommunications applications.

LUCIANO CAMILO ALEXANDRE received the M.Sc. degree in telecommunications from Inatel, Brazil, where he is currently pursuing the Ph.D. degree. He is also acting as a Spectrum Engineering Consultant, performing sharing and compatibility studies between space and terrestrial communications systems. He participates in ITU-R Study Groups and the Inter-American Telecommunications Commission (CITEL) meetings. He is also a member of the Brazilian Communication Commission–Radiocommunication Sector (CBC-2).

GERALDO NETO received the M.Sc. degree from San Francisco State University, San Francisco, CA, USA, in 2016. In 2016, he joined at TMG, where he is currently the Director of technical and policy. He actively participates in meetings of the ITU and the Inter-American Telecommunications Commission (CITEL), representing companies at different study groups and committees on issues related to mobile services, spectrum, the IoT, OTT, ICTs, and holding leadership roles.

AGOSTINHO LINHARES received the Ph.D. degree. He is currently an Advisor with the Secretary of Telecommunications, Brazilian Ministry of Communications. Before that, he was a Manager of spectrum, orbit, and broadcasting at Brazilian Telecommunications Regulatory Agency (Anatel) and a Coordinator of the Brazilian Communication Commission, Radiocommunication Sector (CBC-2). He has authored or coauthored more than 30 scientific papers published in specialized journals, magazines, and conferences. He was responsible for the Brazilian preparation for the World Radiocommunication Conference 2023 (WRC-23). He was the Head of the Brazilian Delegation at the WRC-15 and WRC-19 and the Vice-Chair of the Radiocommunication Assembly 2019 (RA-19). He is also the Vice-Chairperson of PCC.II/Citel, from 2018 to 2022.

LUCIANO LEONEL MENDES (Member, IEEE) received the B.Sc. and M.Sc. degrees in electrical engineering from Inatel, Brazil, in 2001 and 2003, respectively, and the Ph.D. degree in electrical engineering from Unicamp, Brazil, in 2007. Since 2001, he has been a Professor with Inatel, where he acted as the Technical Manager of the Hardware Development Laboratory, from 2006 to 2012. From 2013 to 2015, he was a Visiting Researcher with the Vodafone Chair Mobile Communications Systems, Technical University of Dresden, where he has developed his postdoctoral research. In 2017, he was elected as a Research Coordinator of the 5G Brazil Project, an association involving industries, telecom operators, and academia which aims for funding and build an ecosystem toward 5G in Brazil. He is also the Technical Coordinator of the Brazil 6G Project.

MURILO ARAUJO ROMERO (Senior Member, IEEE) received the Electrical Engineering and M.S. degrees from the Pontifical Catholic University of Rio de Janeiro, Brazil, in 1988 and 1991, respectively, and the Ph.D. degree from Drexel University, Philadelphia, PA, USA, in 1995. He joined at the University of São Paulo, São Carlos, in 1995, as a Faculty Member, where he became an Associate Professor, in 2001, and a Full Professor, in 2008. He was the Head of the Electrical Engineering Department, EESC-USP, from 2009 to 2013. From 2014 to 2017, he was the Head of electrical engineering area at CAPES, an accreditation agency of the Brazilian Government, established to regulate and carry out quality control of graduate studies in Brazil. His research interests include semiconductor devices, optical communications, and microwave-photonics. Samples of his research work can be found in more than 50 journal articles. He served as the Chair for the Electrical and Biomedical Engineering Committee, Brazilian Research Council (CNPq), from 2011 to 2013. He is also an Associate Editor for *Terahertz and Microwave Photonics* and the newly launched journal *Frontiers in Photonics*.

ARISMAR CERQUEIRA S. JR. received the B.Sc. degree in electrical engineering from the Federal University of Bahia, Brazil, in 2001, the M.Sc. degree from Unicamp, Brazil, in 2002, and the Ph.D. degree from Scuola Superiore Sant'Anna, Italy, in 2006. He was an Invited Researcher and a Professor for many world-recognized universities, such as the University of Oulu, in 2017; Scuola Superiore Sant'Anna, in 2015, 2017, and 2019; Danish Technical University, Denmark, in 2013; Max-Planck Institute, Germany, in 2010; and University of Bath, U.K., in 2004, 2005, and 2007. He was an Associate Professor at Unicamp, from March 2009 to August 2011. He joined as an Associate Professor with the Brazilian National Institute of Telecommunications (Inatel). Since 2009, he has been acting as a Coordinator of research and development projects on diverse areas of telecommunications, including 5G, 6G, antennas, radars, and microwave photonics. He is a holder of 11 patents, transferred 25 products to the industry, and published more than 300 scientific papers.

Capítulo 4

Conclusões e Trabalhos Futuros

Foi proposto neste trabalho a investigação experimental de diferentes arquiteturas de redes móveis baseadas em A-RoF e FSO para o transporte de sinais 5G operando de forma simultânea. Resultados experimentais comprovaram que as tecnologias podem coexistir utilizando a mesma infraestrutura de rede, se devidos parâmetros forem levados em conta, estes são: deslocamento de frequência mínimo entre as portadoras de RF dos sinais; níveis de potência óptica na recepção e níveis de potência de RF transmitidas. Propõe-se também a implementação híbrida utilizando as tecnologias A-RoF, FSO, VLC e ondas milimétricas com objetivo de atender possíveis soluções para diferentes cenários de atuação do 5G e 6G.

A primeira investigação propõe a integração de uma rede óptica híbrida baseada em A-RoF operando na faixa de ondas milimétricas em uma rede WDM-PON. A técnica específica utilizada no *fronthaul* no enlace óptico é conhecida como CS-DSB e emprega dois estágios em cascata de modulação externa usando moduladores MZM. Através da otimização dos parâmetros operacionais do modulador, é possível alcançar uma multiplicação de frequência de RF em duas vezes no domínio elétrico. A solução proposta permite a geração e transporte de um sinal 5G NR na frequência de 60 GHz com uma largura de banda de 400 MHz e um esquema de modulação por QPSK. Com base nos resultados obtidos, a solução proposta demonstrou sua viabilidade para atender às demandas de densificação de células das redes 5G/6G, alcançando uma taxa de transferência de dados de aproximadamente 11,8 Gbit/s.

A segunda configuração experimental converge para uma arquitetura de rede unificada que combina soluções baseadas em FiWi, FSO e VLC para atender aos requisitos das redes 5G e 6G. Para isso, a arquitetura implementada é baseada no conceito X-HAUL, utilizando 20 km de fibra óptica seguido por um enlace FSO como *fronthaul* da rede, considerando aplicações de última milha. Na seção de acesso, um link 5G NR em ondas milimétricas a 39 GHz foi implementado a uma distância de 2 m, e simultaneamente, uma transmissão VLC utilizando um sinal M-QAM, a 550 MHz foi avaliada para aplicações em ambientes internos. Resultados experimentais demonstraram uma coexistência satisfatória entre as tecnologias utilizadas, alcançando uma taxa total de transferência de dados de 4,8 Gbit/s.

As duas arquiteturas propostas foram avaliadas de acordo com os requisitos de EVM_{RMS} estabelecidos pelo 3GPP *Release* 18.

Como trabalhos futuros, o principal foco é no aumento no tamanho dos links FSO e mm-wave, para isso o objetivo de propor soluções com transceptores FSO comerciais, com possibilidade de estender o link em até 1,5 km.

Referencias

[1] R. Wenzlhuemer, "The dematerialization of telecommunication: communication centres and peripheries in Europe and the world, 1850–1920," *Journal of Global History*, vol. 2, no. 3, pp. 345–372, 2007.

[2] G. Madden and S. J. Savage, "Telecommunications and economic growth," *International Journal of Social Economics*, 2000.

[3] W. F. Brinkman, D. E. Haggan, and W. W. Troutman, "A history of the invention of the transistor and where it will lead us," *IEEE journal of solid-state circuits*, vol. 32, no. 12, pp. 1858–1865, 1997.

[4] T. Dunnewijk and S. Hultén, "A brief history of mobile communication in Europe," *Telematics and Informatics*, vol. 24, no. 3, pp. 164–179, 2007.

[5] R. Ling and R. McEwen, "Mobile communication and ethics: implications of everyday actions on social order," *Etikk i praksis-Nordic Journal of Applied Ethics*, no. 2, pp. 11–26, 2010.

[6] A. Fehske, G. Fettweis, J. Malmodin, and G. Biczok, "The global footprint of mobile communications: The ecological and economic perspective," *IEEE communications magazine*, vol. 49, no. 8, pp. 55–62, 2011.

[7] C. S. Inc, "Cisco Annual Internet Report (2018–2023)," 2020.

[8] S. Henry, A. Alsohaily, and E. S. Sousa, "5G is real: Evaluating the compliance of the 3GPP 5G new radio system with the ITU IMT-2020 requirements," *IEEE Access*, vol. 8, pp. 42 828–42 840, 2020.

[9] U. Equipment, "Group Radio Access Network; NR; User Equipment (UE) Radio Transmission and Reception; Part 1: Range 1 Standalone."

[10] A. Dogra, R. K. Jha, and S. Jain, "A survey on beyond 5G network with the advent of 6G: Architecture and emerging technologies," *IEEE Access*, vol. 9, pp. 67 512–67 547, 2020.

[11] R. M. Borges, C. H. de Souza Lopes, E. S. Lima, M. A. de Oliveira, M. S. B. Cunha, L. C. Alexandre, L. G. da Silva, L. A. M. Pereira, D. H. Spadoti, M. A. Romero *et al.*, "Integrating optical and wireless techniques towards novel fronthaul and access architectures in a 5G NR framework," *Applied Sciences*, vol. 11, no. 11, p. 5048, 2021.

[12] W. Chen, X. Lin, J. Lee, A. Toskala, S. Sun, C. F. Chiasserini, and L. Liu, "5G-Advanced Toward 6G: Past, Present, and Future," *IEEE Journal on Selected Areas in Communications*, vol. 41, no. 6, pp. 1592–1619, 2023.

[13] J. Yu, G.-K. Chang, Z. Jia, A. Chowdhury, M.-F. Huang, H.-C. Chien, Y.-T. Hsueh, W. Jian, C. Liu, and Z. Dong, "Cost-effective optical millimeter technologies and field demonstrations for very high throughput wireless-over-fiber access systems," *Journal of Lightwave Technology*, vol. 28, no. 16, pp. 2376–2397, 2010.

[14] Y. Wang, L. Pei, J. Li, and Y. Li, "Millimeter-wave signal generation with tunable frequency multiplication factor by employing UFBG-based acousto-optic tunable filter," *IEEE Photonics Journal*, vol. 9, no. 1, pp. 1–10, 2017.

[15] J. Capmany and D. Novak, "Microwave photonics combines two worlds," *Nature photonics*, vol. 1, no. 6, p. 319, 2007.

[16] J. Yao, "Microwave photonics," *Journal of lightwave technology*, vol. 27, no. 3, pp. 314–335, 2009.

[17] C. Lim, Y. Tian, C. Ranaweera, T. A. Nirmalathas, E. Wong, and K.-L. Lee, "Evolution of radio-over-fiber technology," *Journal of Lightwave Technology*, vol. 37, no. 6, pp. 1647–1656, 2019.

[18] A. Pizzinat, P. Chanclou, F. Saliou, and T. Diallo, "Things you should know about fronthaul," *Journal of Lightwave Technology*, vol. 33, no. 5, pp. 1077–1083, 2015.

[19] C. Liu, J. Wang, L. Cheng, M. Zhu, and G.-K. Chang, "Key microwave-photonics technologies for next-generation cloud-based radio access networks," *Journal of Lightwave Technology*, vol. 32, no. 20, pp. 3452–3460, 2014.

[20] S. Yao, Y.-W. Chen, S.-J. Su, Y. Alfadhli, S. Shen, R. Zhang, Q. Zhou, and G.-K. Chang, "Non-orthogonal uplink services through co-transport of D-RoF/A-RoF in mobile fronthaul," *Journal of Lightwave Technology*, vol. 38, no. 14, pp. 3637–3643, 2020.

[21] M. A. Khalighi and M. Uysal, "Survey on free space optical communication: A communication theory perspective," *IEEE communications surveys & tutorials*, vol. 16, no. 4, pp. 2231–2258, 2014.

[22] F. Nadeem, V. Kvicera, M. S. Awan, E. Leitgeb, S. S. Muhammad, and G. Kandus, "Weather effects on hybrid FSO/RF communication link," *IEEE journal on selected areas in communications*, vol. 27, no. 9, pp. 1687–1697, 2009.

[23] M. A. Esmail, A. M. Ragheb, H. A. Fathallah, M. Altamimi, and S. A. Alshebeili, "5G-28 GHz signal transmission over hybrid all-optical FSO/RF link in dusty weather conditions," *IEEE Access*, vol. 7, pp. 24 404–24 410, 2019.

[24] R. Li, H. Shi, H. Tian, Y. Li, B. Liu, Y. Song, and M. Hu, "All-polarization-maintaining dual-wavelength mode-locked fiber laser based on Sagnac loop filter," *Optics Express*, vol. 26, no. 22, pp. 28 302–28 311, 2018.

[25] K. Balakier, M. J. Fice, F. van Dijk, G. Kervella, G. Carpintero, A. J. Seeds, and C. C. Renaud, "Optical injection locking of monolithically integrated photonic source for generation of high purity signals above 100 GHz," *Optics Express*, vol. 22, no. 24, pp. 29 404–29 412, 2014.

[26] J.-P. Zhuang and S.-C. Chan, "Tunable photonic microwave generation using optically injected semiconductor laser dynamics with optical feedback stabilization," *Optics letters*, vol. 38, no. 3, pp. 344–346, 2013.

[27] L. Johansson and A. Seeds, "Millimeter-wave modulated optical signal generation with high spectral purity and wide-locking bandwidth using a fiber-integrated optical injection phase-lock loop," *IEEE Photonics Technology Let-*

ters, vol. 12, no. 6, pp. 690–692, 2000.

[28] C.-T. Lin, P.-T. Shih, J. Chen, W.-J. Jiang, S.-P. Dai, P.-C. Peng, Y.-L. Ho, and S. Chi, "Optical millimeter-wave up-conversion employing frequency quadrupling without optical filtering," *IEEE Transactions on Microwave Theory and Techniques*, vol. 57, no. 8, pp. 2084–2092, 2009.

[29] W. Li and J. Yao, "Microwave and terahertz generation based on photonically assisted microwave frequency twelvetupling with large tunability," *IEEE Photonics Journal*, vol. 2, no. 6, pp. 954–959, 2010.

[30] A. B. Dar and F. Ahmad, "Optical millimeter-wave generation techniques: An overview," *Optik*, p. 168858, 2022.

[31] T. Fortier and E. Baumann, "20 years of developments in optical frequency comb technology and applications," *Communications Physics*, vol. 2, no. 1, p. 153, 2019.

[32] V. Torres-Company and A. M. Weiner, "Optical frequency comb technology for ultra-broadband radio-frequency photonics," *Laser & Photonics Reviews*, vol. 8, no. 3, pp. 368–393, 2014.

[33] H. A. Haus, "Mode-locking of lasers," *IEEE Journal of Selected Topics in Quantum Electronics*, vol. 6, no. 6, pp. 1173–1185, 2000.

[34] A. Martinez and S. Yamashita, "Multi-gigahertz repetition rate passively mode-locked fiber lasers using carbon nanotubes," *Optics express*, vol. 19, no. 7, pp. 6155–6163, 2011.

[35] A. C. S Jr, J. C. Boggio, A. Rieznik, H. Hernandez-Figueroa, H. Fragnito, and J. Knight, "Highly efficient generation of broadband cascaded four-wave mixing products," *Optics Express*, vol. 16, no. 4, pp. 2816–2828, 2008.

[36] J. Pfeifle, V. Brasch, M. Lauermann, Y. Yu, D. Wegner, T. Herr, K. Hartinger, P. Schindler, J. Li, D. Hillerkuss *et al.*, "Coherent terabit communications with microresonator Kerr frequency combs," *Nature photonics*, vol. 8, no. 5, pp. 375–380, 2014.

[37] M. Imran, P. M. Anandarajah, A. Kaszubowska-Anandarajah, N. Sambo, and

L. Potí, "A survey of optical carrier generation techniques for terabit capacity elastic optical networks," *IEEE Communications Surveys & Tutorials*, vol. 20, no. 1, pp. 211–263, 2017.

[38] Y. Yoshida, "Mobile Xhaul evolution: enabling tools for a flexible 5G Xhaul network," in *2018 Optical Fiber Communications Conference and Exposition (OFC)*. IEEE, 2018, pp. 1–85.

[39] I. Chih-Lin, H. Li, J. Korhonen, J. Huang, and L. Han, "RAN revolution with NGFI (xHaul) for 5G," *Journal of Lightwave Technology*, vol. 36, no. 2, pp. 541–550, 2018.

[40] A. Tzanakaki, M. Anastasopoulos, I. Berberana, D. Syrivelis, P. Flegkas, T. Korakis, D. C. Mur, I. Demirkol, J. Gutiérrez, E. Grass *et al.*, "Wireless-optical network convergence: enabling the 5G architecture to support operational and end-user services," *IEEE Communications Magazine*, vol. 55, no. 10, pp. 184–192, 2017.

[41] N. Chen and M. Okada, "Toward 6G internet of things and the convergence with RoF system," *IEEE Internet of Things Journal*, vol. 8, no. 11, pp. 8719–8733, 2020.

[42] L. A. M. Pereira, L. L. Mendes, C. J. A. Bastos Filho, and A. C. Sodré, "Amplified radio-over-fiber system linearization using recurrent neural networks," *Journal of Optical Communications and Networking*, vol. 15, no. 3, pp. 144–154, 2023.

[43] Y. Tian, K.-L. Lee, C. Lim, and A. Nirmalathas, "60 GHz analog radio-over-fiber fronthaul investigations," *Journal of Lightwave Technology*, vol. 35, no. 19, pp. 4304–4310, 2017.

[44] R. M. Borges, T. R. R. Marins, M. S. B. Cunha, H. R. D. Filgueiras, I. F. da Costa, R. N. da Silva, D. H. Spadoti, L. L. Mendes, and A. C. Sodré, "Integration of a GFDM-based 5G transceiver in a GPON using radio over fiber technology," *Journal of Lightwave Technology*, vol. 36, no. 19, pp. 4468–4477, 2018.

[45] G. Hasanuzzaman, A. Kanno, P. T. Dat, and S. Iezekiel, "Self-oscillating optical frequency comb: Application to low phase noise millimeter wave generation and radio-over-fiber link," *Journal of Lightwave Technology*, vol. 36, no. 19, pp. 4535–4542, 2018.

[46] D.-N. Nguyen, J. Bohata, J. Spacil, D. Dousek, M. Komanec, S. Zvanovec, Z. Ghassemlooy, and B. Ortega, "M-QAM transmission over hybrid microwave photonic links at the K-band," *Optics express*, vol. 27, no. 23, pp. 33 745–33 756, 2019.

[47] R. M. Borges, L. A. M. Pereira, H. R. D. Filgueiras, A. C. Ferreira, M. S. B. Cunha, E. R. Neto, D. H. Spadoti, L. L. Mendes, and A. Cerqueira, "DSP-based flexible-waveform and multi-application 5G fiber-wireless system," *Journal of Lightwave Technology*, vol. 38, no. 3, pp. 642–653, 2019.

[48] K. Kanta, A. Pagano, E. Ruggeri, M. Agus, I. Stratakos, R. Mercinelli, C. Vagionas, P. Toumasis, G. Kalfas, G. Giannoulis *et al.*, "Analog fiber-wireless downlink transmission of IFoF/mmWave over in-field deployed legacy PON infrastructure for 5G fronthauling," *Journal of Optical Communications and Networking*, vol. 12, no. 10, pp. D57–D65, 2020.

[49] L. Vallejo, J. Mora, D.-N. Nguyen, J. Bohata, V. Almenar, S. Zvanovec, and B. Ortega, "On the 40 GHz remote versus local photonic generation for DML-based C-RAN optical fronthaul," *Journal of Lightwave Technology*, vol. 39, no. 21, pp. 6712–6723, 2021.

[50] C. H. de Souza Lopes, E. S. Lima, L. A. M. Pereira, R. M. Borges, A. C. Ferreira, M. Abreu, W. D. Dias, D. H. Spadoti, L. L. Mendes, and A. C. S. Junior, "Non-standalone 5G NR fiber-wireless system using FSO and fiber-optics fronthauls," *Journal of Lightwave Technology*, vol. 39, no. 2, pp. 406–417, 2020.

[51] J. Bohata, D. Nguyen, J. Spáčil, M. Komanec, B. Ortega, L. Vallejo, Z. Ghassemlooy, and S. Zvánovec, "Experimental comparison of DSB and CS-DSB mmW formats over a hybrid fiber and FSO fronthaul network for 5G," *Optics Express*, vol. 29, no. 17, pp. 27 768–27 782, 2021.

[52] L. Vallejo, J. Mora, and B. Ortega, "Harmonic and Intermodulation Distortion

Analysis in Directly Modulated Lasers Over Local and Remote Photonically Generated Millimeter-Wave Signals," *Journal of Lightwave Technology*, vol. 40, no. 15, pp. 5128–5140, 2022.

[53] F. Shi, Y. Fan, X. Wang, W. Zhang, and Y. Gao, "High-performance dual-band radio-over-fiber link for future 5G radio access applications," *Journal of Optical Communications and Networking*, vol. 14, no. 4, pp. 267–277, 2022.

[54] E. Ruggeri, C. Vagionas, R. Maximidis, G. Kalfas, D. Spasopoulos, N. Terzenidis, R. M. Oldenbeuving, P. W. van Dijk, C. G. Roeloffzen, N. Pleros *et al.*, "Reconfigurable Fiber Wireless fronthaul with A-RoF and D-RoF co-existence through a Si3N4 ROADM for Heterogeneous mmWave 5G C-RANs," *Journal of Lightwave Technology*, vol. 40, no. 16, pp. 5514–5521, 2022.

[55] Z. Htay, C. Guerra-Yánez, Z. Ghassemlooy, S. Zvanovec, M. M. Abadi, and A. Burton, "Experimental real-time GbE MIMO FSO under fog conditions with software defined GNU Radio platform-based adaptive switching," *Journal of Optical Communications and Networking*, vol. 14, no. 8, pp. 629–639, 2022.

[56] E. S. Lima, R. M. Borges, N. Andriolli, E. Conforti, G. Contestabile, and A. C. Sodré Jr, "Integrated optical frequency comb for 5G NR Xhauls," *Scientific Reports*, vol. 12, no. 1, p. 16421, 2022.

[57] T. P. Andrade, L. C. De Souza, E. S. Lima, and A. C. Sodré, "Demonstration of a hybrid A-RoF/VLC system for beyond 5G applications," *Applied Optics*, vol. 62, no. 8, pp. C115–C121, 2023.

[58] C. Vagionas, R. Maximidis, I. Stratakos, A. Margaris, A. Mesodiakaki, M. Gatzianas, K. Kanta, P. Toumasis, G. Giannoulis, D. Apostolopoulos *et al.*, "End-to-End Real-Time Service Provisioning over a SDN-controllable analog mmWave Fiber-Wireless 5G X-haul Network," *Journal of Lightwave Technology*, 2023.

[59] M. Series, "IMT Vision–Framework and overall objectives of the future development of IMT for 2020 and beyond," *Recommendation ITU*, vol. 2083, no. 0, 2015.

[60] D. 3GPP, "Study on new radio access technology physical layer aspects," *Tech-*

nical Report (TR) 38.802, V14. 2.0, 2017.

[61] I. Rahman, S. M. Razavi, O. Liberg, C. Hoymann, H. Wiemann, C. Tidestav, P. Schliwa-Bertling, P. Persson, and D. Gerstenberger, "5G evolution toward 5G Advanced: An overview of 3GPP releases 17 and 18," *Ericsson Technology Review*, vol. 2021, no. 14, pp. 2–12, 2021.

[62] G. Liu, Y. Huang, Z. Chen, L. Liu, Q. Wang, and N. Li, "5G deployment: Standalone vs. non-standalone from the operator perspective," *IEEE Communications Magazine*, vol. 58, no. 11, pp. 83–89, 2020.

[63] Y. Qi, M. Hunukumbure, H. Nam, H. Yoo, and S. Amuru, "On the phase tracking reference signal (pt-rs) design for 5g new radio (nr)," in *2018 IEEE 88th Vehicular Technology Conference (VTC-Fall)*. IEEE, 2018, pp. 1–5.

[64] H. Holma, A. Toskala, and T. Nakamura, *5G technology: 3GPP new radio*. John Wiley & Sons, 2020.

[65] P. K. Korrai, E. Lagunas, A. Bandi, S. K. Sharma, and S. Chatzinotas, "Joint power and resource block allocation for mixed-numerology-based 5G downlink under imperfect CSI," *IEEE Open Journal of the Communications Society*, vol. 1, pp. 1583–1601, 2020.

[66] A. K. Bairagi, M. S. Munir, M. Alsenwi, N. H. Tran, S. S. Alshamrani, M. Masud, Z. Han, and C. S. Hong, "Coexistence mechanism between eMBB and uRLLC in 5G wireless networks," *IEEE Transactions on Communications*, vol. 69, no. 3, pp. 1736–1749, 2020.

[67] M. Kottkamp, A. Pandey, D. Raddino, A. Rosessler, and R. Stuhlfauth, *5G New Radio: Fundamentals, procedures, testing aspects*. Rohde & Schwarz GmbH & Company KG, 2019.

[68] R. Schmogrow, B. Nebendahl, M. Winter, A. Josten, D. Hillerkuss, S. Koenig, J. Meyer, M. Dreschmann, M. Huebner, C. Koos *et al.*, "Error vector magnitude as a performance measure for advanced modulation formats," *IEEE Photonics Technology Letters*, vol. 24, no. 1, pp. 61–63, 2011.

[69] J. G. dos Santos, "Radio over fibre techniques for backhaul and fronthaul," Ph.D.

dissertation, Technische Universität Berlin, 2017.

[70] M. A. Habibi, M. Nasimi, B. Han, and H. D. Schotten, "A comprehensive survey of RAN architectures toward 5G mobile communication system," *IEEE Access*, vol. 7, pp. 70 371–70 421, 2019.

[71] A. Checko, H. L. Christiansen, Y. Yan, L. Scolari, G. Kardaras, M. S. Berger, and L. Dittmann, "Cloud RAN for mobile networks—A technology overview," *IEEE Communications surveys & tutorials*, vol. 17, no. 1, pp. 405–426, 2014.

[72] C. Mobile, "C-ran: the road towards green ran," *White paper, ver*, vol. 2, no. 5, pp. 15–16, 2011.

[73] Z. Corporation, "Green technology innovations."

[74] G. Kalfas, C. Vagionas, A. Antonopoulos, E. Kartsakli, A. Mesodiakaki, S. Papaioannou, P. Maniotis, J. S. Vardakas, C. Verikoukis, and N. Pleros, "Next generation fiber-wireless fronthaul for 5G mmWave networks," *IEEE Communications Magazine*, vol. 57, no. 3, pp. 138–144, 2019.

[75] D. Novak, R. B. Waterhouse, A. Nirmalathas, C. Lim, P. A. Gamage, T. R. Clark, M. L. Dennis, and J. A. Nanzer, "Radio-over-fiber technologies for emerging wireless systems," *IEEE Journal of Quantum Electronics*, vol. 52, no. 1, pp. 1–11, 2016.

[76] G. P. Agrawal, *Fiber-optic communication systems*. John Wiley & Sons, 2012.

[77] D. Wake, A. Nkansah, and N. J. Gomes, "Radio over fiber link design for next generation wireless systems," *Journal of lightwave Technology*, vol. 28, no. 16, pp. 2456–2464, 2010.

[78] C. Specification, "V2. 0,"common public radio interface (cpri)," *interface specification," Tech. Rep*, 2004.

[79] A. De la Oliva, J. A. Hernandez, D. Larrabeiti, and A. Azcorra, "An overview of the cpri specification and its application to c-ran-based lte scenarios," *IEEE Communications Magazine*, vol. 54, no. 2, pp. 152–159, 2016.

[80] G.-K. Chang and L. Cheng, "The benefits of convergence," *Philosophical Transactions of the Royal Society A: Mathematical, Physical and Engineering Sci-*

ences, vol. 374, no. 2062, p. 20140442, 2016.

[81] I. Series and G. Sup, "55,"transmission systems and media, digital systems and networks-radio-over-fibre (rof) technologies and their applications9,"," Tech. Rep., July, Tech. Rep., 2015.

[82] A. Nirmalathas, P. A. Gamage, C. Lim, D. Novak, and R. Waterhouse, "Digitized radio-over-fiber technologies for converged optical wireless access network," *Journal of Lightwave Technology*, vol. 28, no. 16, pp. 2366–2375, 2010.

[83] J. Ribeiro, "Comunicações ópticas, érica," *São Paulo*, 2003.

[84] G. Smith, D. Novak, and Z. Ahmed, "Technique for optical SSB generation to overcome dispersion penalties in fibre-radio systems," *Electronics letters*, vol. 33, no. 1, pp. 74–75, 1997.

[85] X. Li, X. Xiao, Y. Xu, K. Wang, L. Zhao, J. Xiao, and J. Yu, "Real-time demonstration of over 20Gbps V-and W-band wireless transmission capacity in one OFDM-RoF system," in *Optical Fiber Communication Conference*. Optica Publishing Group, 2017, pp. M3E–3.

[86] P. Cao, X. Hu, J. Wu, L. Zhang, X. Jiang, and Y. Su, "Reconfigurable uwb pulse generation based on a dual-drive mach–zehnder modulator," *IEEE Photonics Journal*, vol. 6, no. 5, pp. 1–6, 2014.

[87] A. J. Seeds and K. J. Williams, "Microwave photonics," *Journal of lightwave technology*, vol. 24, no. 12, pp. 4628–4641, 2006.

[88] R. A. Linke, "Optical heterodyne communications systems," *IEEE Communications Magazine*, vol. 27, no. 10, pp. 36–41, 1989.

[89] V. J. Urick, K. J. Williams, and J. D. McKinney, *Fundamentals of microwave photonics*. John Wiley & Sons, 2015.

[90] A. Hurtado, I. D. Henning, M. J. Adams, and L. F. Lester, "Generation of tunable millimeter-wave and THz signals with an optically injected quantum dot distributed feedback laser," *IEEE Photonics Journal*, vol. 5, no. 4, pp. 5 900 107–5 900 107, 2013.

[91] X.-H. Huang, C.-Y. Li, H.-H. Lu, C.-R. Chou, H.-M. Hsia, and Y.-H. Chen, "A bidirectional FSO communication employing phase modulation scheme and remotely injection-locked DFB LD," *Journal of Lightwave Technology*, vol. 38, no. 21, pp. 5883–5892, 2020.

[92] C.-Y. Li, H.-H. Lu, C.-R. Chou, H.-M. Hsia, C.-Y. Feng, Y.-H. Chen, Y.-T. Huang, and A. Nainggolan, "A flexible bidirectional fiber-FSO-5G wireless convergent system," *Journal of Lightwave Technology*, vol. 39, no. 5, pp. 1296–1305, 2021.

[93] R. Ramos and A. Seeds, "Fast heterodyne optical phase-lock loop using double quantum well laser diodes," *Electronics letters*, vol. 1, no. 28, pp. 82–83, 1992.

[94] K. Balakier, M. J. Fice, L. Ponnampalam, A. J. Seeds, and C. C. Renaud, "Monolithically integrated optical phase lock loop for microwave photonics," *Journal of Lightwave Technology*, vol. 32, no. 20, pp. 3893–3900, 2014.

[95] H. R. Rideout, J. S. Seregelyi, S. Paquet, and J. Yao, "Discriminator-aided optical phase-lock loop incorporating a frequency down-conversion module," *IEEE Photonics Technology Letters*, vol. 18, no. 22, pp. 2344–2346, 2006.

[96] F. Fan and M. Dagenais, "Optical generation of a megahertz-linewidth microwave signal using semiconductor lasers and a discriminator-aided phase-locked loop," *IEEE Transactions on Microwave Theory and Techniques*, vol. 45, no. 8, pp. 1296–1300, 1997.

[97] S. Rommel, D. Dodane, E. Grivas, B. Cimoli, J. Bourderionnet, G. Feugnet, A. Morales, E. Pikasis, C. Roeloffzen, P. van Dijk *et al.*, "Towards a scaleable 5G fronthaul: Analog radio-over-fiber and space division multiplexing," *Journal of Lightwave Technology*, vol. 38, no. 19, pp. 5412–5422, 2020.

[98] L. Johansson and A. Seeds, "Generation and transmission of millimeter-wave data-modulated optical signals using an optical injection phase-lock loop," *Journal of Lightwave Technology*, vol. 21, no. 2, p. 511, 2003.

[99] G. Qi, J. Yao, J. Seregelyi, S. Paquet, C. Belisle, X. Zhang, K. Wu, and R. Kashyap, "Phase-noise analysis of optically generated millimeter-wave sig-

nals with external optical modulation techniques," *Journal of Lightwave Technology*, vol. 24, no. 12, pp. 4861–4875, 2006.

[100] C.-T. Lin, J. J. Chen, S.-P. Dai, P.-C. Peng, and S. Chi, "Impact of nonlinear transfer function and imperfect splitting ratio of mzm on optical up-conversion employing double sideband with carrier suppression modulation," *Journal of Lightwave Technology*, vol. 26, no. 15, pp. 2449–2459, 2008.

[101] G. Ning, P. Shum, and J. Zhou, "Dispersion effect and compensation in optical-carrier-suppressed modulation transport systems," *JOSA A*, vol. 24, no. 11, pp. 3432–3436, 2007.

[102] C. Lim, A. Nirmalathas, M. Bakaul, P. Gamage, K.-L. Lee, Y. Yang, D. Novak, and R. Waterhouse, "Fiber-wireless networks and subsystem technologies," *Journal of Lightwave Technology*, vol. 28, no. 4, pp. 390–405, 2010.

[103] H. Haas, J. Elmirghani, and I. White, "Optical wireless communication," p. 20200051, 2020.

[104] M. Z. Chowdhury, M. K. Hasan, M. Shahjalal, M. T. Hossan, and Y. M. Jang, "Optical wireless hybrid networks: Trends, opportunities, challenges, and research directions," *IEEE Communications Surveys & Tutorials*, vol. 22, no. 2, pp. 930–966, 2020.

[105] M. Uysal and H. Nouri, "Optical wireless communications—An emerging technology," in *2014 16th international conference on transparent optical networks (ICTON)*. IEEE, 2014, pp. 1–7.

[106] S. A. Al-Gailani, M. F. M. Salleh, A. A. Salem, R. Q. Shaddad, U. U. Sheikh, N. A. Algeelani, and T. A. Almohamad, "A survey of free space optics (FSO) communication systems, links, and networks," *IEEE Access*, vol. 9, pp. 7353–7373, 2020.

[107] A. Jahid, M. H. Alsharif, and T. J. Hall, "A contemporary survey on free space optical communication: Potentials, technical challenges, recent advances and research direction," *Journal of Network and Computer Applications*, vol. 200, p. 103311, 2022.

[108] J. Bohata, M. Komanec, J. Spacil, R. Slavik, and S. Zvanovec, "Transmitters for combined radio over a fiber and outdoor millimeter-wave system at 25 GHz," *IEEE Photonics Journal*, vol. 12, no. 3, pp. 1–14, 2020.

[109] Z. Ghassemlooy, S. Arnon, M. Uysal, Z. Xu, and J. Cheng, "Emerging optical wireless communications-advances and challenges," *IEEE journal on selected areas in communications*, vol. 33, no. 9, pp. 1738–1749, 2015.

[110] D. Killinger, "Free space optics for laser communication through the air," *Optics and photonics news*, vol. 13, no. 10, pp. 36–42, 2002.

[111] S. Bloom, E. Korevaar, J. Schuster, and H. Willebrand, "Understanding the performance of free-space optics," *Journal of optical Networking*, vol. 2, no. 6, pp. 178–200, 2003.

[112] W.-S. Tsai, H.-H. Lu, C.-Y. Li, T.-C. Lu, C.-H. Liao, C.-A. Chu, and P.-C. Peng, "A 20-m/40-Gb/s 1550-nm DFB LD-based FSO link," *IEEE Photonics Journal*, vol. 7, no. 6, pp. 1–7, 2015.

[113] Z. Zhao, Z. Zhang, J. Tan, Y. Liu, and J. Liu, "200 Gb/s FSO WDM communication system empowered by multiwavelength directly modulated TOSA for 5G wireless networks," *IEEE Photonics Journal*, vol. 10, no. 4, pp. 1–8, 2018.

[114] J. Libich and S. Zvanovec, "Influences of turbulences in near vicinity of buildings on free-space optical links," *IET microwaves, antennas & propagation*, vol. 5, no. 9, pp. 1039–1044, 2011.

[115] K. Niachou, I. Livada, and M. Santamouris, "Experimental study of temperature and airflow distribution inside an urban street canyon during hot summer weather conditions. Part II: Airflow analysis," *Building and environment*, vol. 43, no. 8, pp. 1393–1403, 2008.

[116] H. Kaushal and G. Kaddoum, "Optical communication in space: Challenges and mitigation techniques," *IEEE communications surveys & tutorials*, vol. 19, no. 1, pp. 57–96, 2016.

[117] D. K. Borah and D. G. Voelz, "Pointing error effects on free-space optical communication links in the presence of atmospheric turbulence," *Journal of*

Lightwave Technology, vol. 27, no. 18, pp. 3965–3973, 2009.

[118] M. A. Esmail, A. Ragheb, H. Fathallah, and M.-S. Alouini, "Investigation and demonstration of high speed full-optical hybrid fso/fiber communication system under light sand storm condition," *IEEE Photonics Journal*, vol. 9, no. 1, pp. 1–12, 2017.

[119] S. A. Al-Gailani, M. F. Mohd Salleh, A. A. Salem, R. Q. Shaddad, U. U. Sheikh, N. A. Algeelani, and T. A. Almohamad, "A survey of free space optics (fso) communication systems, links, and networks," *IEEE Access*, vol. 9, pp. 7353–7373, 2021.

[120] L. C. Andrews, R. L. Phillips, and C. Y. Hopen, *Laser beam scintillation with applications*. SPIE press, 2001, vol. 99.

[121] A. Malik, P. Singh *et al.*, "Free space optics: current applications and future challenges," *International journal of optics*, vol. 2015, 2015.

[122] A. K. Majumdar and J. C. Ricklin, *Free-space laser communications: principles and advances*. Springer Science & Business Media, 2010, vol. 2.

[123] Z. Ghassemlooy, W. Popoola, and S. Rajbhandari, *Optical wireless communications: system and channel modelling with Matlab®*. CRC press, 2019.

[124] H. Parikh, J. Chokshi, N. Gala, and T. Biradar, "Wirelessly transmitting a grayscale image using visible light," in *2013 international conference on advances in technology and engineering (ICATE)*. IEEE, 2013, pp. 1–6.

[125] N. Bardsley, S. Bland, L. Pattison, M. Pattison, K. Stober, F. Welsh, and M. Yamada, "Solid-state lighting research and development multi-year program plan," *US Department of Energy*, 2014.